TAMPEREEN TEKNILLINEN YLIOPISTO
TAMPERE UNIVERSITY OF TECHNOLOGY

Jennika Karvinen

Hydrazone Crosslinked Polysaccharide-based Hydrogels for Soft Tissue Engineering

Julkaisu 1578 • Publication 1578

Tampere 2018

Tampereen teknillinen yliopisto. Julkaisu 1578
Tampere University of Technology. Publication 1578

Jennika Karvinen

Hydrazone Crosslinked Polysaccharide-based Hydrogels for Soft Tissue Engineering

Thesis for the degree of Doctor of Philosophy to be presented with due permission for public examination and criticism in Tietotalo Building, Auditorium TB109, at Tampere University of Technology, on the 2nd of November 2018, at 12 noon.

Tampereen teknillinen yliopisto - Tampere University of Technology
Tampere 2018

Doctoral candidate: Jennika Karvinen
Biomaterials and Tissue Engineering Group
Faculty of Biomedical Sciences and Engineering
Tampere University of Technology
Finland

Supervisor: Minna Kellomäki, Prof., Dr. Tech
Biomaterials and Tissue Engineering Group
Faculty of Biomedical Sciences and Engineering
Tampere University of Technology
Finland

Pre-examiners: Anna-Lena Kjøniksen, Prof., Dr. Scient
Faculty of Engineering
Østfold University College
Norway

Sanjukta Deb, Prof., Ph.D
Department of Tissue Engineering & Biophotonics
King's College London
United Kingdom

Opponent: Jukka Seppälä, Prof., Dr.Sc.Tech.
Department of Chemical and Metallurgical Engineering
Aalto University
Finland

ISBN 978-952-15-4208-4 (printed)
ISBN 978-952-15-4222-0 (PDF)
ISSN 1459-2045

Abstract

Soft tissue engineering (TE) aims to generate new soft tissue by combining cells with a porous scaffold in order to replace or repair lost or diseased tissues. Soft TE and stem cell therapy can be used, for example, to replace damaged corneal stroma or to treat a damaged central nervous system (CNS). Blindness due to corneal dysfunction is currently treated by the transplantation of a donor cornea. However, alternative treatment methods are needed due to the limitations of the procedure. In order to mimic the functions of the cornea, scaffold material should at the minimum provide protection, transparency, and adequate refractive power. The human CNS suffers from low inbuilt regenerative capacity. Therefore, healing the damaged CNS with traditional medicine is insufficient and better treatment options, such as cell therapy combined with a supportive biomaterial scaffold, are needed. In addition to the general requirements, brain-mimicking mechanical properties and injectability, which enables minimally invasive surgery, are desired properties for neural applications. Hydrogels are considered to be the most attractive soft TE scaffolds due to their functional and structural similarities with the natural extracellular matrix (ECM). Hydrogels crosslinked with hydrazone chemistry are especially promising due to their advantageous characteristics, such as mild reaction conditions, versatility, simplicity, reversibility, and absence of toxic reagents and side products.

The main aim of this thesis was to find an optimal hydrazone crosslinked hydrogel material for soft TE, especially for corneal and neural applications, and to characterize the hydrogels thoroughly using several methods. Different polysaccharides, i.e., hyaluronan (HA), alginate (AL), and gellan gum (GG), and synthetic polymer polyvinyl alcohol (PVA) were modified with complementary reactive aldehyde- and hydrazide-groups to enable hydrazone crosslinking. Different HA-PVA-, AL-PVA-, GG-HA-, and HA-HA-based hydrogels were fabricated by varying the gel parameters, i.e., the degree of substitution and molecular weight of the gel components, the ratio of components, and the polymer concentration of the hydrogels. The mechanical, rheological, swelling/deswelling, enzymatic degradation, and diffusion properties of the hydrogels were characterized. Since microstructure plays an essential role in the control of hydrogel properties, the microstructure of the hydrogels was also characterized using rheology- and diffusion (fluorescence recovery after photobleaching, FRAP)-based methods. More precisely, the structural parameters, i.e., the mesh size, the average molecular weight of the polymer chain between neighboring crosslinks, and crosslinking density were evaluated. HA-HA-based hydrogels were intended for the regeneration of the corneal stroma. Therefore, their suitability for the delivery of human adipose stem cells (hASCs) was studied. The addition of collagen I, which is the main ECM component in the corneal stroma, was also tested. In addition, the suitability of HA-PVA- and AL-PVA-based hydrogels to serve as 3D supportive and biomimicking materials for human pluripotent stem cell-derived neuronal cells was tested. GG-HA-based

hydrogels were not intended for any specific application, but their potential applicability as scaffold material for soft TE was tested in terms of their material properties.

Results showed that the fabrication of hydrazone crosslinked HA-PVA-, AL-PVA-, GG-HA-, and HA-HA-based hydrogels from complementary reactive polymers was successful. The traditional crosslinking methods of GG were replaced with this method, and variable mechanical and physical properties were obtained by varying the gel parameters described earlier. These GG-HA-based hydrogels showed ionic nature of deswelling in the presence of cations. This means that the physical properties of the hydrogels can be controlled in different solution environments. They also showed that their stiffness was similar to that of soft tissues at low strains. It should be noted that due to the non-linear elastic behavior of the hydrogels (and tissues), the stiffness was also presented as a function of strain, instead of only giving the second-order elastic constants. Overall, the properties and injectability of GG-HA-based hydrogels supported their potential use in soft TE.

For the fabrication of the HA-HA-based hydrogels, two different types of aldehyde- and hydrazide-modifications were tested. In order to promote hASC attachment and survival, collagen I was added to the hydrogel with better stability. This led to a reduced swelling ratio and increased hydrogel stiffness. Good optical properties (transparency and refractive index) were obtained with both gel types. However, even though all HA-HA-based hydrogels showed good hASC survival directly after encapsulation, only in the collagen-containing hydrogel were cells with elongated morphology found. Furthermore, the cornea organ culture model suggested that these hydrogels could be used as injectable cell delivery vehicles to corneal stromal defects. The biodegradability of HA, the favorable characteristics of hydrazone crosslinking, and the results described above all support the use of these hydrogels as potential materials for hASC delivery in the treatment of corneal stromal defects.

To the best of our knowledge, this is the first time that the polymerization and properties of the hydrazone crosslinked AL-PVA hydrogel has been reported. The AL-PVA hydrogel, together with HA-PVA-based hydrogels, were fabricated and their properties were changed by varying the gel parameters described earlier. When the effect of the gel parameters on the growth of human pluripotent stem cell-derived neuronal cells was tested, the results showed that the most supportive hydrogels had brain-mimicking mechanical properties at low strains, and that they contained a high molecular weight HA component. In addition, the lowering of the polymer concentration (softer hydrogels) resulted in enhanced neuronal growth. The AL-PVA hydrogel was shown to be similarly supportive. The neuronal spreading and 3D network formation were enhanced inside the softest hydrogels. Based on these results, the HA-PVA- and AL-PVA-based hydrogels were considered to be potential supportive biomaterials for 3D neural cell cultures.

The microstructures of the previously described hydrogels were evaluated thoroughly for the first time using rheology- and FRAP-based methods. With these methods, the microstructure can be determined from wet samples, with no need to use destructive drying. The obtained results supported each other, i.e., diffusivity decreased when larger dextran sizes (500 kDa and 2000 kDa) were used, and those molecule sizes were equivalent to the mesh sizes of hydrogels (15 nm to 47 nm) determined by the rheological method. This size range allows the transportation of small molecules, peptides, and most of the proteins. The results also showed a proportionality between the structural parameters and storage moduli (and second order elastic constants). In summary, the results showed that hydrazone crosslinking offers an easy way to produce polysaccharide-based hydrogels with tunable properties that are suitable for soft TE applications.

Preface

This study was carried out at Tampere University of Technology (TUT) in the doctoral programme of the Faculty of Biomedical Sciences & Engineering. This work was financially supported by the Finnish Funding Agency for Technology and Innovation (TEKES) Human spare parts project, and by the supplementary dissertation funding provided by TUT graduate school.

I would like to express my sincere gratitude to my supervisor, Prof. Minna Kellomäki, for your help and support throughout this thesis and for giving me an opportunity to continue my work under your guidance. I would also like to thank my former supervisor, Prof. Tuula Pakkanen from the University of Eastern Finland, for introducing me to the field of biomaterials and hydrogels.

I would like to thank all the co-authors, Tiina Joki, Laura Koivusalo, Eetu Sorsa, Janne Koivisto, Teresa Calejo, Teemu Ihalainen, Jari Väliaho, Laura Ylä-Outinen, Ilari Jönkkäri, Tanja Ilmarinen, Pasi Kallio, Susanna Miettinen and Susanna Narkilahti for your contributions to my research and for sharing your expertise with me. I would also like to thank our "hydrogel group", Jenny Parraga and Janne Koivisto, for nice work atmosphere and help during these years. I will also express my gratitude to entire Biomaterials and Tissue Engineering Group (former and present colleagues), and laboratory and technical personnel of the department (especially Suvi Heinämäki and Heikki Liejumäki) for your help. I also thank Alexander Efimov and Anne-Maarit Tikkanen from the Chemistry department of TUT for your help with NMR and FTIR measurements. I am also very grateful to Peter Heath for language editing.

I owe my deepest gratitude to my parents, Kaija and Eero, for your support and love. You have always believed in me and encouraged me.

Finally, I will express my deepest gratitude to my dear beloved Ville. You have helped me numerous times and encouraged me to continue. I cannot thank you enough!

Pirkkala, September 2018

Jennika Karvinen

Contents

List of Publications

This thesis is based on the following publications that are later referred in the text as Studies I-III. The publications are reprinted with the kind permission of the publishers.

I Karvinen J., Koivisto J.T., Jönkkäri I., Kellomäki M., "The production of injectable hydrazone crosslinked gellan gum-hyaluronan-hydrogels with tunable mechanical and physical properties", *Journal of the Mechanical Behavior of Biomedical Materials*, 71(2017) 383-391.

II Koivusalo L.*, Karvinen J.*, Sorsa E., Jönkkäri I., Väliaho J., Kallio P., Ilmarinen T., Miettinen S., Skottman H., Kellomäki M., "Hydrazone crosslinked hyaluronan-based hydrogels for therapeutic delivery of adipose stem cells to treat corneal defects", *Materials Science and Engineering C: Materials for Biological Applications*, 85 (2018), 68-78.

III Karvinen J., Joki T., Ylä-Outinen L., Koivisto J.T., Narkilahti S., Kellomäki M., "Soft hydrazone crosslinked hyaluronan- and alginate-based hydrogels as 3D supportive matrices for human pluripotent stem cell-derived neuronal cells", *Reactive and Functional Polymers*, 124 (2018), 29-39.

* Authors contributed equally.

Unpublished manuscripts

This thesis is also based on the following unpublished manuscript that is later referred in the text as Study IV.

IV Karvinen J., Ihalainen T., Calejo T., Jönkkäri I., Kellomäki M., "Characterization of the microstructure of hydrazone crosslinked polysaccharide-based hydrogels through rheological and diffusion studies", submitted on 22.01.2018.

Author's contribution

The author's contribution to the publications was the following:

I The author was the principal author of this paper. The author was responsible for planning the work together with the co-authors, synthesizing and characterizing the polymers, preparing and characterizing the hydrogels (other than compression test measurements), and analyzing all the data.

II The author was the principal co-author of this paper. The author was responsible for planning the work together with the co-authors, synthesizing and characterizing the polymers, preparing and characterizing the hydrogels (other than cell tests) together with the third co-author, and analyzing all the data related to the characterization of materials (other than cell tests).

III The author was the principal author of this paper. The author was responsible for planning the work together with the co-authors, synthesizing and characterizing the polymers, preparing and characterizing the hydrogels (other than compression test measurements and cell tests), and analyzing all the data related to the characterization of materials (other than cell tests).

IV The author was the principal author of this paper. The author was responsible for planning the work together with the co-authors, preparing the hydrogels and characterizing the hydrogels (other than FRAP-imaging), and analyzing all the data.

Abbreviations

2D	Two-dimensional
3D	Three-dimensional
ADH	Adipic acid dihydrazide
AL	Alginate
ALALD	Aldehyde-modified alginate (oxidized)
ASCs	Adipose-derived stem cells
ASTM	American Society for Testing and Materials
AP	Hydrazone crosslinked alginate-polyvinyl alcohol hydrogel
Ba^{2+}	Barium
Ca^{2+}	Calcium
$CaCl_2$	Calcium chloride
CDI	1,1'-carbonyldiimidazole
CDH	Carbodihydrazide
CEC-l-OSA	N-carboxyethyl chitosan-l-oxidized sodium alginate
CESCs	Corneal epithelial cells
CNS	Central nervous system
col I	Collagen type-I
CT	Microcomputed tomography
DDS	Drug delivery system
DMEM/F12	Dulbecco's Modified Eagle Medium: Nutrient Mixture F-12
DMSO	Dimethyl sulfoxide
DS%	Degree of substitution
ECM	Extracellular matrix
EDC	1-Ethyl-3-[3-(dimethylamino) propyl]carbodiimide
EWC	Equilibrium water content
FDA	Food and Drug Administration
FITC	Fluorescein isothiocyanate
FRAP	Fluorescence recovery after photobleaching
FTIR	Fourier-transform infrared (spectroscopy)
GG	Gellan gum
GGALD	Aldehyde-modified gellan gum (oxidized)
GG-Ca	Ca-crosslinked gellan gum

GH1,GH2,GH3,GH4	Hydrazone crosslinked gellan gum-hyaluronan-based hydrogel
HA	Hyaluronan
HAADH	Hydrazide-modified hyaluronan (modified using ADH)
HAADH-H	High molecular weight-version of HAADH
HAADH-L	Low molecular weight-version of HAADH
HAALD	Aldehyde-modified hyaluronan (selective oxidation of diol-modified hyaluronan)
HAALD-L	Low molecular weight-version of HAALD
HACDH	Hydrazide-modified hyaluronan (modified using CDH)
HACDH-L	Low molecular weight-version of HACDH
HALD	Aldehyde-modified hyaluronan (oxidized)
HALD-H	High molecular weight-version of HALD
HALD-L	Low molecular weight-version of HALD
hASC	Human adipose stem cell
hESC	Human embryonic stem cell
HH1,HH2	Hydrazone crosslinked hyaluronan-based hydrogel
HH2C	Hydrazone crosslinked hyaluronan-collagen I hydrogel
HOBt	1-hydroxybenzotriazole
HP1,HP2,HP3,HP4	Hydrazone crosslinked hyaluronan-polyvinyl alcohol-based hydrogel
HP1a, HP1b	Hydrazone crosslinked hyaluronan-polyvinyl alcohol-based hydrogel, reduced polymer concentration
iPSC	Induced pluripotent stem cell
iPSC-NPCs	Induced pluripotent stem cell-derived neural progenitor cells
Ks	Keratocytes
LESCs	Limbal epithelial stem cells
LVR	Linear viscoelastic region
Ma^{2+}	Magnesium
NaOH	Sodium hydroxide
NMR	Nuclear magnetic resonance (spectroscopy)
^{1}H-NMR	Proton nuclear magnetic resonance (spectroscopy)
NPCs	Neural progenitor cells
NSCs	Neural stem cells
PBS	Phosphate buffered saline
PDMS	Polydimethylsiloxane
PEG	Polyethylene glycol
PLGA	Poly(lactic-co-glycolide)
PVA	Polyvinyl alcohol
PVAHY	Hydrazide-modified polyvinyl alcohol
RET	Rubber elastic theory
RM	Regenerative medicine
RT	Room temperature
SCI	Spinal cord injury
SD	Degree of swelling
SPD^{3+}	Spermidine
SPM^{4+}	Spermine
SPR	Surface plasmon resonance

SR	Swelling ratio
SR^{2+}	Strontium
TBC	t-butyl carbazate
TBI	Traumatic brain injury
TE	Tissue engineering
TNBS	Picrylsulfonic acid solution (also called 2,4,6-Trinitrobenzenesulfonic acid solution)
UV-VIS-NIR	Ultraviolet-Visible-Near Infrared (spectroscopy)

Symbols

A	Area
c	(Polymer) concentration
c	Velocity of light in vacuum
c_{k-1}	kth-order elastic constant
d	Deformation (in Fourier-transform infrared spectroscopy)
F	Force
G'	Storage modulus
G"	Loss modulus
G*	Complex modulus
G_e	Plateau value of storage modulus
M_c	Average molecular weight of the polymer chain between neighboring crosslinks
M_w	Molecular weight
N_A	Avogadro constant (6.022×10^{23})
n	Refractive index
n_1, n_2	Refractive indices of different media
n_e	Crosslinking density
n_{gel}	Refractive index of hydrogel
n_{glass}	Refractive index of glass
R	Universal gas constant (8.314 J/K $\cdot$ mol)
R^2	Coefficient of determination
$\tan\delta$	Loss tangent
α	Angle of incidence
δ	Phase angle between stress and strain
ϵ	Strain
γ	Strain
γ_0	Strain amplitude
ν	Stretching (in Fourier-transform infrared spectroscopy)
ν	Velocity of propagation of light
ρ	Density
σ	Stress
σ_0	Stress amplitude
τ	Stiffness
$\tau_{1/2}$	Half maximum
θ_1	Angle of incidence
θ_2	Angle of refraction
ω	Frequency
ξ	Average mesh size

1 Introduction

The aim of tissue engineering (TE) is to generate new tissue to replace or repair lost or diseased tissues. In TE, cells and a porous scaffold are combined and, under suitable conditions, they are organized into tissues. The success of these engineered tissues depends on the cell types, scaffolds, and the *in vitro* culture methods used. [1] For example, the scaffolds used in TE have many functions; they not only provide three-dimensional (3D) structural support for the cells, but also regulate cell functions and promote tissue growth. [1, 2] Hydrogels have many structural and functional properties similar to the native extracellular matrix (ECM), and therefore they are considered to be the most attractive TE scaffolds [2]. In general, scaffolds that are ECM-mimicking as a result of their composition, structure, and mechanical properties are the most desired [3]. When hydrogels are designed for TE applications, their mechanical, physical, and degradation properties should be known thoroughly. Sometimes certain properties need to be altered without affecting others, which can be difficult [4].

The hydrogels presented in this thesis are mainly intended for use in soft TE applications, and in particular to replace damaged corneal stroma or to treat a damaged central nervous system (CNS). Blindness is a worldwide problem that is caused by various diseases as well as trauma and burns. Currently, blindness due to corneal dysfunction is treated by transplantation of donor corneas. [5] However, alternative treatment options are needed due to the limitations of the treatment, such as a shortage of suitable donor tissue, immune reactions, or graft failure. TE and stem cell therapy therefore are great alternative options for the treatment of blindness. In order to mimic the functions of the cornea, there are at least three primary requirements for the material. The material should offer protection and transparency in addition to providing an optical interface with sufficient refractive power. [6] Trauma and deficits in the CNS may have a permanent effect on the functionality of a patient. Healing with traditional medicine is insufficient due to the low inbuilt regenerative capacity of the human CNS. [7] Therefore, alternative treatment options are needed. For example, TE, or more specifically, cell therapy combined with a supportive biomaterial scaffold is one such promising strategy. For this application, the scaffolds need to be soft and have a suitable degradation rate [8]. Injectability would allow minimally invasive surgery [9].

This thesis comprises a literature review, an experimental part, and four original publications. The literature review provides an overview of the hydrogels and their diverse characteristics as well as their characterization methods. It also provides a short overview of the crosslinking method used in this thesis. The final part of the literature review presents two soft TE applications, corneal and neural TE, and collects some hydrogel materials used for these applications. In the experimental part, the fabrication and characterization of hydrazone crosslinked polysaccharide-based hydrogels intended for soft TE applications are introduced. More specifically, the modification of hyaluronan

(HA), alginate (AL), gellan gum (GG), and polyvinyl alcohol (PVA) with complementary reactive aldehyde- and hydrazide-groups is presented, and the fabrication of HA-PVA-, AL-PVA-, GG-HA-, and HA-HA(-col I)-based hydrogels is shown. Different methods are used to study the characteristics of the produced hydrogels. The mechanical, rheological, swelling, degradation, and diffusion properties of hydrogels in addition to their microstructure are studied. The suitability of HA-HA(-col I)-based hydrogels for the delivery of human adipose stem cells (hASCs) for the regeneration of corneal stroma is also studied. Furthermore, the suitability of HA-PVA- and AL-PVA-based hydrogels to serve as a 3D supportive and biomimicking material for human pluripotent stem cell-derived neuronal cells is tested.

2 Literature review

2.1 Hydrogels – definition, forms and applications

Hydrogel, as a term, first appeared in 1894 describing a colloidal gel of inorganic salts. In 1960, Wichterle and Lim were the first to report hydrogels as we know them today, when they introduced polyhydroxyethylmethacrylate (poly-HEMA)-based hydrogels used for contact lens applications. A more detailed history of hydrogels is reviewed by Buwalda et al. [10].

According to IUPAC, hydrogel is "*a gel in which the swelling agent is water*" and "*the network component of a hydrogel is usually a polymer network*" [11]. In general, hydrogels are considered to be three-dimensional (3D) water-containing polymeric crosslinked networks that can absorb a large amount of water (swell, Fig. 2.1)[10]. For a material to be classed as a hydrogel, at least 10% of the total weight (or volume) must be water. When the water content is higher than 95%, the hydrogel is considered to be superabsorbent [12]. Moreover, hydrogels are insoluble in water [3]. Hydrogels behave like viscoelastic solids, and they can hold their shape like a solid, despite being mostly liquid [13].

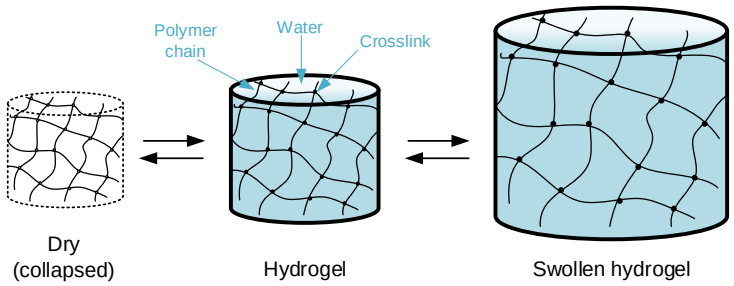

Figure 2.1: Dry and wet forms of hydrogels.

Hydrogels can be used in either their wet or dry form. It should be noted, however, that the drying (method) affects the structure of hydrogel and at worst can even destroy it. For example, traditional air drying is not able to keep the gel structure (*xerogels*), whereas freeze drying can lead to a damaged structure and cracks (*cryogels*). Supercritical drying serves as an alternative drying technique because it does not damage the structure as much (*aerogels*). [14] Depending on the application, hydrogels can exist in different physical forms, such as 3D scaffolds, coatings, films, and nano- or microparticles [15]. Hydrogels are widely used in different applications, e.g., in tissue engineering (TE), as drug delivery systems, wound healing, soft contact lenses, hygiene products, breast implants, in

environmental applications (purifying water), or as electrophoresis gels, medical electrodes, and biosensors. [16–18]

2.2 Classification of hydrogels

Fig. 2.2 shows different ways to classify hydrogels. The following sections present them in more detail.

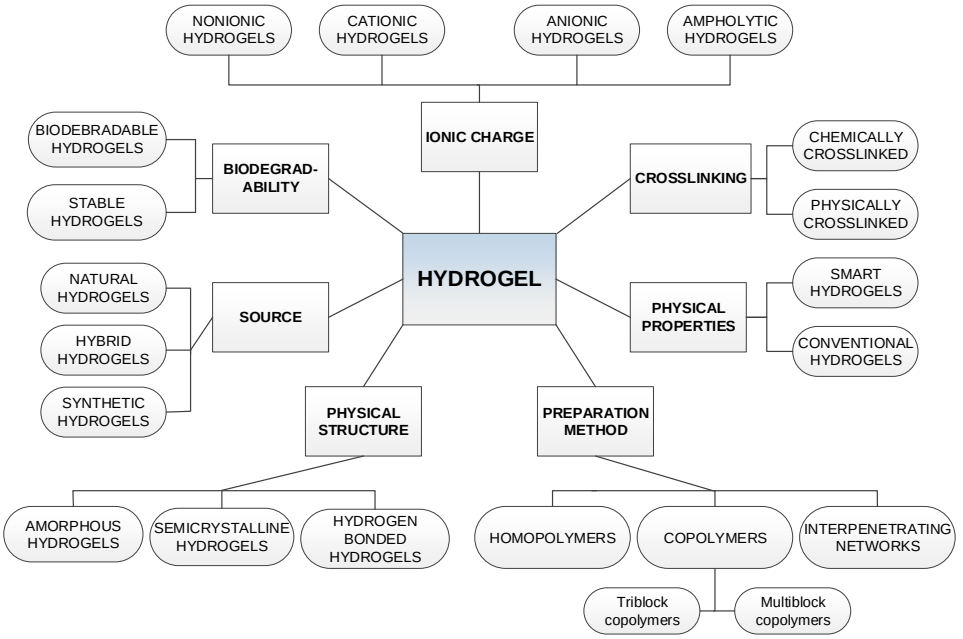

Figure 2.2: Classification of hydrogels.

2.2.1 Polymer source

Hydrogels can be classified according to the polymer source into natural, synthetic, or hybrid hydrogels [3]. They are each presented in the following sections.

2.2.1.1 Natural hydrogels

There are three classes of naturally derived biopolymers: 1) polysaccharides, 2) proteins, and 3) microbial polymers. *Polysaccharides*, such as alginate, hyaluronan, and gellan gum, are composed of monosaccharides that are linked by glycosidic linkages. [19] Polysaccharides can be further divided into homo- or hetero-polysaccharides based on their number of monosaccharide units. Polysaccharides can be obtained either from plants, marine algae, animals, or bacteria. [20] Polysaccharides have many advantageous properties. For example, they are water soluble and biodegradable, and they have low toxicity. However, their polydispersity (molecular weight can vary from a single source), low cell adhesion (if there are no specific cell binding receptors), and low mechanical strength may limit their use. [20] *Proteins*, such as collagen and gelatin, are large molecules

that are composed of one or more long chains of amino acid residues [19]. Proteins are also biodegradable and biocompatible, but their use can be limited by batch-to-batch variation, high cost, and antigenicity [21]. The third type of natural biopolymer is *microbial polymers*. Polysaccharides, such as bacterial cellulose and dextran, polyamines, such as poly-γ-glutamic acid (PGA)), and polyesters, such as polyhydroxy-alkanoate, can all be produced by micro-organisms [19]. The following examples give more information on the natural polymers used in this thesis.

Alginate (AL) is an anionic and hydrophilic polysaccharide that is composed of 1,4-linked β-D-mannuronic acid (M) and α-L-guluronic acid (G) residues (Fig. 2.3 (a)). AL is obtained from brown algae, and it is structurally similar to ECM matrices. AL is inherently non-biodegradable, but can be made degradable, for example, by replacing the divalent cations with monovalent cations or by oxidation. [22, 23] AL gels are biocompatible, transparent, non-toxic, and relatively biologically inert [19, 20]. The carboxyl and hydroxyl groups of AL not only allow specific modification, but also the introduction of functional groups for crosslinking [24]. AL can be crosslinked physically by using multivalent cations ($Mg^{2+} << Ca^{2+} < SR^{2+} < Ba^{2+}$) [19, 23, 25], or by using various crosslinkers (e.g., adipic acid dihydrazide, lysine) [23], hydrazone crosslinking [26], or photocrosslinking [27]. When hydrogels are formed with a high D-mannuronic acid content, they have high flexibility but poor rigidity, whereas more rigid hydrogels are obtained when they are formed with a high L-guluronic acid content [20]. AL has been widely used for different biomedical applications [20, 23].

Hyaluronan (HA) is an anionic, hydrophilic, non-sulphated polysaccharide that is composed of β-1,4-D-glucuronic acid and β-1,3-N-acetyl-D-glycosamine residues (Fig. 2.3 (b)). HA is a major glucosaminoglucan component of the ECM that is found in various mammalian tissues. HA is produced by animals as well as certain members of the streptococci species (*Streptococcus equi* and *Streptococcus zooepidemicus*) [28]. HA has a strong ability to retain water due to its strong anionic nature (the structure of the HA chains acts to trap water between the coiled chains). A high number of hydroxyl groups resulting in hydrogen bonding ability can also explain its water retention properties. [28] HA is degraded by hyaluronidase enzymes as well as by reactive oxygen species [23]. Only high molecular weight HA has muco-adherence and anti-inflammatory properties [19]. The carboxyl and hydroxyl groups not only allow specific modification, but also allow the introduction of functional groups for crosslinking [2]. HA can be crosslinked in many ways, such as by using Schiff base crosslinking, click chemistry, hydrazone crosslinking, Michael-type addition, enzymatic crosslinking, or photocrosslinking [2, 23, 29]. Due to its two signal-transducing cell-surface HA-receptors (CD44 and RHAMM), HA plays an important role in different cellular events [20]. HA has been widely used for different biomedical applications [20, 23].

Gellan gum (GG) is an anionic polysaccharide that is composed of tetrasaccharide repeating units of 1,3-β-D-glucose, 1,4-β-D-glucuronic acid, 1,4-β-D-glucose, and 1,4-$\alpha\beta$-L-rhamnose, containing one carboxyl side group (Fig. 2.3 (c)). *Sphingomonas elodea* bacteria produces GG. [30] GG can be used in two different forms to form thermoreversible gels. Deacetylated GG forms hard and brittle gels, whereas acetylated GG forms soft and elastic gels. [20] GG exists as a disordered coil at higher temperatures ($\geq 40\ ^oC$), whereas it forms a double-helix structure on cooling

(weak gel characteristics, but not a true gel). When the helices associate through cations (monovalent or divalent cations), a true gel is formed. By using divalent cations, such as Ca^{2+} and Mg^{2+}, a stronger gel is formed (a bridge is formed between pairs of carboxyl groups), whereas weaker gels are formed when monovalent cations, such as K^+ or Na^+, are used (cations suppress electrostatic repulsions that induce an aggregation). [30] However, this crosslinking method has some downsides that include the weakening of the mechanical properties and a loss of stability that occur when the divalent cations are exchanged with monovalent cations (for example, in the physiological environment). Ionically crosslinked GG hydrogels can also be produced by using polyamines, such as spermidine (SPD^{3+}) and spermine (SPM^{4+}) [31, 32]. Chemical crosslinking using methacrylate derivatives followed by photocrosslinking with UV-light is also possible [33], although the downsides of this method are the reactivity of the photoinitiator and the phototoxicity of UV-light. Human enzymes, such as lysozyme, trypsin, and amylase, can degrade GG [30]. GG is a relatively inert biomaterial, like many other polysaccharides. GG has been approved by the Food and Drug Administration (FDA) in the US and by the European Medicines Agency (EMA) in the EU for use in food and medical products for use as a gelling, stabilizing, and suspending agent [34, 35]. Since GG is structurally and functionally similar to alginate, which is widely used in tissue engineering, it has also been proposed as a scaffold material for TE applications [36].

Collagen (col) is the main structural protein in the ECM in the various connective tissues in animals [37]. There exist many types of collagen in various tissues. Types I, II, and III are the most abundant in the human body. [25] Type I, which is used in this thesis, can be found from the skin, tendon, bone, cornea, fibrocartilage, dentin, dermis, intestine, uterus, and large vessels [38]. Collagen is composed of amino acids that are wound together to form triple-helices that further form fibrils (Fig. 2.4). The most common motifs in the amino acid sequence are glycine-proline-X and glycine-hydroxyproline-X, where X is any other amino acid. Each collagen type has a unique triple-helix configuration of α-chains. For example, type I comprises two α1(I) and one α2(I) chains, type III of three α1(III) chains, and type IV of two α1(IV) and one α2(IV) chains. [38] Collagen is non-toxic, biocompatible, and possesses low immunogenicity [5, 39]. As a natural ECM protein, it contains signals that promote cell adhesion and function [37]. Collagen is degraded by collagenase or serine proteases [37]. Collagen can be crosslinked, for example, using chemical crosslinkers (e.g., glutaraldehyde, carbodiimides, genipin), temperature-responsive gelation, or photocrosslinking [40]. Different types of collagen have been widely used for various biomedical applications [23].

2.2.1.2 Synthetic hydrogels

Synthetic polymers, such as polyvinyl alcohol (PVA), polyethylene glycol (PEG), and poly(N-isopropylacrylamide)(PNIPAAm), offer an easily controlled structure with adjustable mechanical properties, a reliable source of raw materials, and no batch-to-batch variation. They can also be considered non-immunogenic. Synthetic polymers, however, have low biodegradability, may not support cell adhesion, and can include toxic substances. All of the above drawbacks can limit their use. [1, 23] The following gives more information on the synthetic polymer used in this thesis.

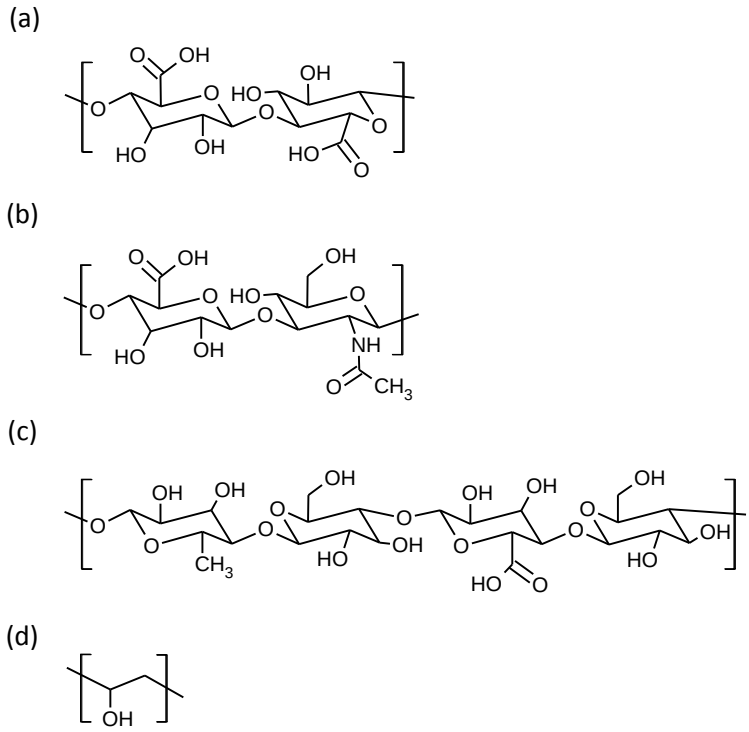

Figure 2.3: Chemical structures of a) alginate (AL), b) hyaluronan (HA), c) gellan gum (GG), and (d) polyvinyl alcohol (PVA).

Polyvinyl alcohol (PVA) is a synthetic, hydrophilic polymer with good chemical, thermal, and mechanical stability. The partial or complete hydrolysis of polyvinyl acetate produces PVA. PVA degrades by hydrolysis. It has a low protein adsorption and good biocompatibility. [23] Hydroxyl groups in the structure (Fig. 2.3 (d)) provide a chemical versatility that enables further modification and functionalization [41]. PVA can be crosslinked either chemically (e.g., click chemistry, radial polymerization, Schiff base reaction), or physically (e.g., cryogenic gelation, hydrogen bonding) [23]. PVA has also been approved by the FDA and Conformité Européenne (CE) for clinical use in humans. [42] PVA hydrogels have been quite widely studied in several biomedical applications [23, 43].

2.2.1.3 Hybrid hydrogels

Hybrid hydrogels are a mixture of synthetic and natural polymers. The properties of hybrid hydrogels can be more specific and versatile compared to materials based on only natural or synthetic polymers. [3] In this thesis, HA was combined with PVA in order to form hybrid hydrogels with improved and widened properties.

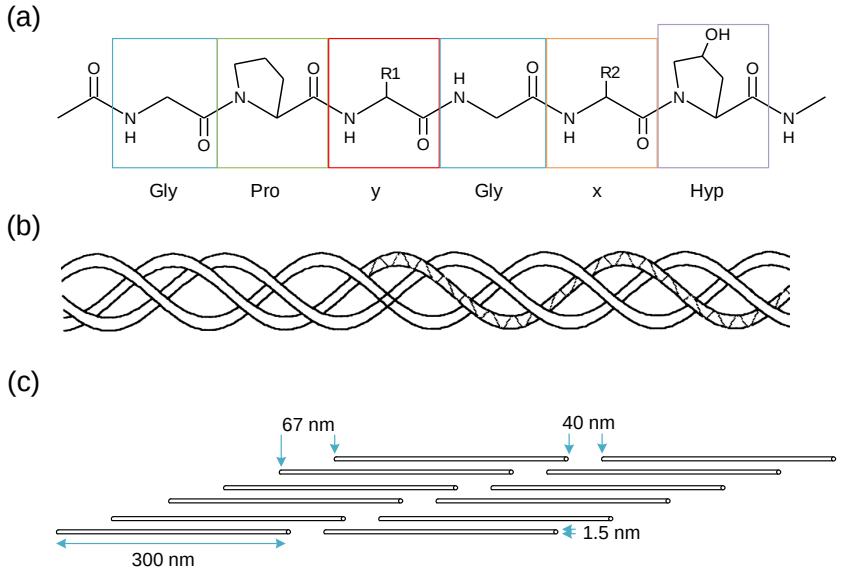

Figure 2.4: Chemical structure of collagen type I. a) Primary amino acid sequence, b) secondary left-handed helix and tertiary right-handed triple-helix structure, and c) staggered quaternary structure. Modified from [38].

2.2.2 Crosslinking

Hydrogels can be classified into physically and chemically crosslinked hydrogels (Fig. 2.5). A combination of these hydrogel types (or just single types) is also possible. An interpenetrating network structure is formed, and this type of gel is called a double (or dual)-network hydrogel (Fig. 2.5 (c)). It has been designed to overcome the disadvantages of single crosslinking types and to widen the properties of hydrogels, such as sensitivity or swelling ability. [44, 45]

Physically crosslinked hydrogels are held together with non-covalent bonds, i.e., molecular entanglements, electrostatic interactions, hydrogen bonding, and hydrophobic interactions, and they can respond to physical, chemical, or biochemical changes of environment (e.g., temperature, pH, ionic strength, pressure, electric or magnetic field, light, glucose, enzymes). Physical hydrogels are reversible due to the conformational changes. [44] Physical crosslinking can be attained by using thermal, ionic (divalent cations) or pH sensitive crosslinking, or freeze-thawing. [46]

Chemically crosslinked hydrogels are held together with covalent bonds, and they have higher stability. Furthermore, they can absorb water until they reach equilibrium swelling. Chemically crosslinked hydrogels are irreversible and permanent due to configurational changes. [44] Chemical crosslinking can be attained by using, for example, Michael addition, aldehyde-hydrazide coupling, click reactions, nucleophilic substitution reaction, chemical crosslinkers (e.g., glutaraldehyde, calcium chloride), gelling agents (e.g., glycophosphate, 1,2-propanediol, mannitol), or enzymatic crosslinking (e.g., horseradish peroxidases, transglutaminases) [46].

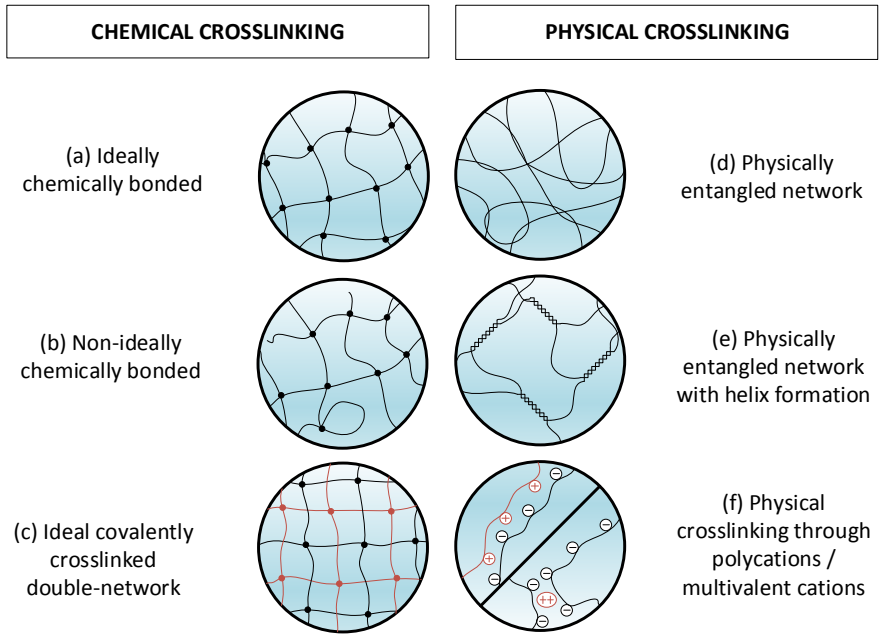

Figure 2.5: Microstructures of hydrogels defining different crosslinking types. a) Ideally chemically bonded, b) non-ideally chemically bonded (molecular ends and loops), c) ideal covalently crosslinked double-network gel, d) physically entangled network, e) physically entangled network with helix formation, and f) physical crosslinking through polycations or multivalent cations. Modified from [45].

The following gives more information on the chemical crosslinking method used in this thesis.

2.2.2.1 Hydrazone crosslinking

One of the most promising chemical methods used in recent years has been click chemistry due to its mild reaction conditions, high reactivity, and selectivity. Hydrogels prepared in this way are highly compatible with encapsulated living cells, proteins, peptides, and drugs due to the bio-orthogonal nature of the reaction ("*bio-orthogonal reactions are reactions that do not interfere with biological processes*" [47]). [48] Click chemistry reactions can be divided into three categories: 1) Cu(I) catalyzed azide-alkyne cycloaddition (CuAAC), 2) copper-free click reactions, and 3) pseudo-click reactions. [48] Reaction examples are shown in Fig. 2.6. Copper ions have been found to be cytotoxic (the toxicity is due to oxidative damage from reactive oxygen species formed by the copper catalysts, and also copper complexes have been found to induce changes in cellular metabolism and are taken up by cells). Therefore, the first reaction type is not suitable for use with live cells, and thus copper-free reactions have been created. Reactions with a similar nature to click reactions have been included third in this list and they are called pseudo click reactions that include thiol-Michael additions and aldehyde-hydrazide coupling. These reactions offer high reactivity and yield as well as simple and mild reaction conditions. [48]

The aldehyde-hydrazide coupling reaction, also called hydrazone crosslinking, is a widely

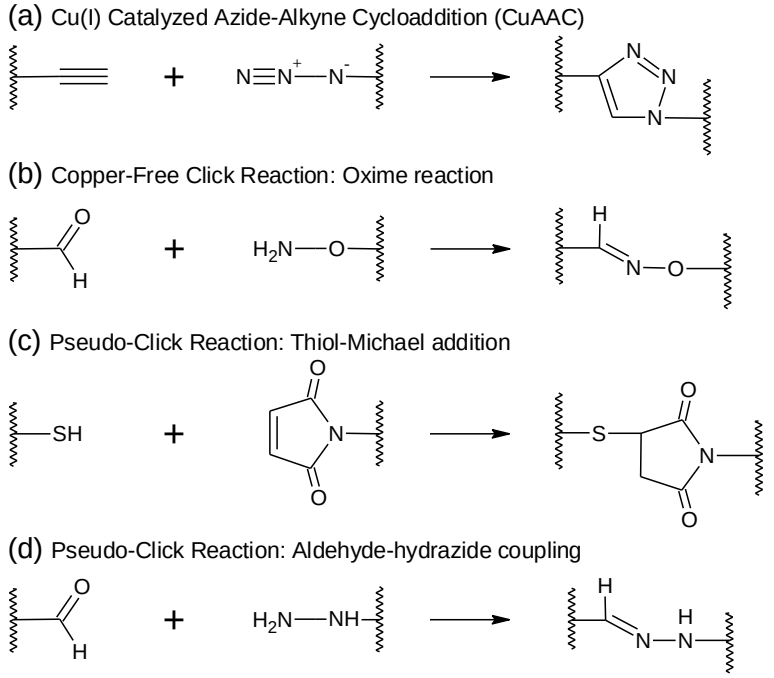

Figure 2.6: Examples of click chemistry and pseudo click chemistry reactions. a) Cu(I) catalyzed azide-alkyne cycloaddition (CuAAC), b) oxime reaction (copper-free click reactions), c) thiol-Michael addition (pseudo-click reaction), and d) aldehyde-hydrazide coupling (pseudo-click reaction).

used reaction that was first introduced in the 1880s, and it is especially attractive for use in tissue regeneration due to its favorable properties, such as versatility, simplicity, reversibility, and absence of toxic reagents and side products [48]. Furthermore, injectable hydrogels can also be formed with this crosslinking method, making it even more desirable. Hydrazone linkage (C=N-NH) is formed from the α-nucleophile (hydrazide) and a carbonyl compound (aldehyde or ketone). Water is the only by-product of this reaction. [49] The reaction mechanism is shown in Fig. 2.7. Briefly, the reaction starts with a proton-catalyzed attack of the hydrazide (1) on the carbonyl atom of aldehyde (2). The hemiaminal (the tetrahedral intermediate, 3) is obtained after proton transfer. It can further undergo dehydration, so that first the hydroxyl function is protonated and then the water is eliminated. Two resonance forms of protonated intermediate (4a and 4b) exist. After the final deprotonation, hydrazone (5) is obtained. The hydrolysis reaction is obtained by reversing the reaction steps. [49]

The reaction is advantageous in pH of around 4.5, whereas under physiological conditions (neutral pH) the reaction rate is slower. The reaction rate can be enhanced by using nucleophilic catalysts, such as aniline. The bond is stable when it is formed with ketone, but somewhat labile when formed with aldehyde, although the reaction rate is typically faster with aldehyde. The hydrazone linkage is considered more stable than the easily reversible Schiff base interaction (imine) between the amine and aldehyde group due to the negative inductive effect of the additional heteroatom (NH). It is possible to further

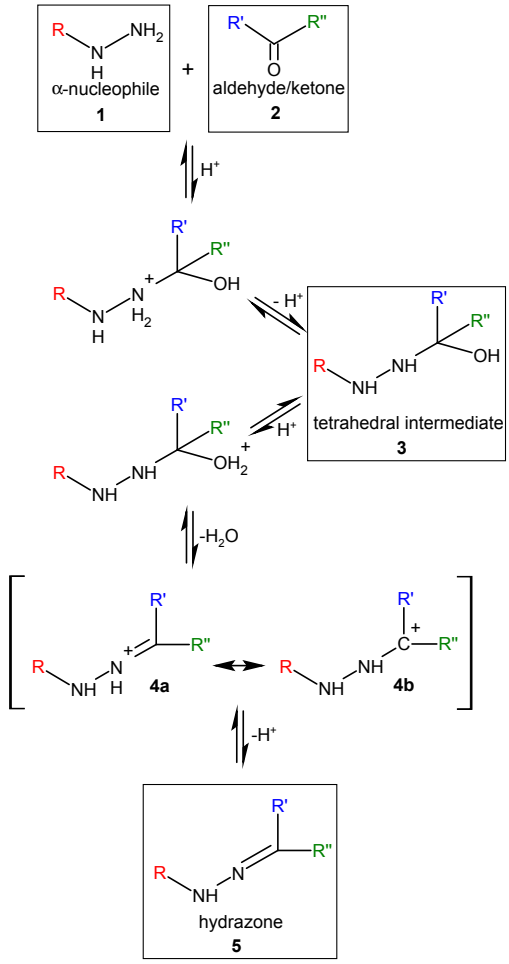

Figure 2.7: Mechanism for the formation of hydrazone.

stabilize the bond with sodium cyanoborohydride to reduce the C=N double bond. [49, 50] The reaction environment affects the stability of hydrazone, meaning that under acidic conditions it undergo more rapid hydrolysis, whereas under physiological pH it is more stable [49].

Hydrazone crosslinking is termed a "pseudo click reaction", where pseudo refers to moderate orthogonality. [48] The use of this term should, however, be treated with caution since the bio-orthogonality of the hydrazone reaction is not unconditional. Aldehydes (and ketones) are common in nature, unlike α-effect nucleophiles that are rarely found. Furthermore, strongly nucleophilic hydrazides can readily react with a wide range of electrophiles, whereas aldehydes (and ketones) can form imines with various amines (although in a reversible manner, which explains potential toxicity). Regardless, hydrazone conjugation can be considered effectively bio-orthogonal, if there are only low concentrations of aldehydes (or ketones) and highly reactive electrophiles, which is the case in many biological environments. [49]

As previously mentioned, the polymer must contain either aldehyde (or ketone) or hydrazide groups in order to undergo hydrazone reaction. If not, they need to be introduced. There are different ways to do this. For example, in the case of HA, periodate oxidation can be used to generate aldehyde groups from vicinal diol groups of HA [51]. Alternatively, aldehyde groups can be generated by incorporating an amino-glycerol side chain via an amidation reaction and the selective oxidation of the pendent group of HA [52]. This method actually offers a less invasive polymer modification. Hydrazide groups, on the other hand, can be generated, for example, via reaction with adipic acid dihydrazide (ADH) [53] or carbodihydrazide (CDH) [54].

Hydrazone crosslinked hydrogels have been formed between different polymers and used for different applications: HA-HA- [54], HA-AL- [26], HA-PVA- [55, 56], HA-PEG-hydrogels [57].

2.2.3 Physical structure

Based on their physical structure, hydrogels can be divided into *amorphous*, *semicrystalline*, and *hydrogen-bonded* hydrogels. The macromolecular chains of amorphous hydrogels are randomly arranged, whereas in semicrystalline hydrogels there are crystallites (dense regions of ordered macromolecular chains). The network of hydrogen-bonded hydrogels is held together by hydrogen bonds. [44, 58]

The physical structure of the polymer network is considered strong when it is chemically crosslinked (permanent and cannot be reformed if broken), and weak when the crosslinks can be broken and reformed. Pseudo gels, on the other hand, are entangled polymer systems with gel-like properties, meaning that the physical entanglements mimic chemical crosslinks, but the gels flow like a fluid in response to a constant applied stress. [13]

2.2.4 Preparation method

Hydrogels can be classified according to preparation method into *homopolymers*, *copolymers* (tri- or multiblock copolymers), and *interpenetrating networks*. Homopolymer hydrogels are produced by one type of hydrophilic monomer unit, whereas copolymer hydrogels consist of two co-monomer units (at least one unit is hydrophilic). Interpenetrating network hydrogels (IPNs) consist of two polymers, where at least one is crosslinked in the immediate presence of the other, leading to two intermeshing network structures. The term "*semi-interpenetrating network*" is used when a linear polymer penetrates another crosslinked network, so that there are no chemical bonds between them. [44, 58]

2.2.5 Physical properties

On the basis of their physical properties, hydrogels can be classified into *smart* (environmentally sensitive) and *conventional* hydrogels. Smart hydrogels differ from inert conventional hydrogels in that they can respond to environmental stimuli, so that their mechanical strength, permeability, and network structure can change. These environmental stimuli can be divided into physical (temperature, electric fields, light, pressure, ultrasound, magnetic fields, mechanical stress), chemical (pH, ions, chemical agents), and biochemical (glucose level, antigen, enzyme, ligand) stimuli. [44]

2.2.6 Biodegradability

Hydrogels can be classified into *biodegradable* and *stable* (non-biodegradable) hydrogels [44]. The term biodegradation means that the biological system mediates the degradation (at least partially) [59]. Even though no polymer is completely inert to the chemical processes and mechanical action of the body [60], non-biodegradable polymers are considered stable because they require a longer time to degrade than what is needed for the application they are used for [59]. The biodegradability of hydrogels is discussed in more detail in Section 2.3.7.

2.2.7 Ionic charge

Hydrogels can be classified according to ionic charge into *neutral* (non-ionic, no charge), *anionic* (negative charge), *cationic* (positive charge), and *ampholytic* (positive and negative charges) hydrogels. The swelling behavior of neutral hydrogels has no pH dependency. Cationic and anionic hydrogels, on the other hand, show superior swelling in low and high pH, respectively. Since the charges of ampholytic hydrogels are balanced at their iso-electric point (at a certain pH), the ionic properties of hydrogels can be changed by changing the pH. [61]

2.3 Hydrogel properties and their characterization

Standard guide F2900-11 [62] provides an overview of the test methods that are suitable for characterizing hydrogels. Based on the standard, some key elements that should be considered in the characterization of hydrogels are collected in Fig. 2.8.

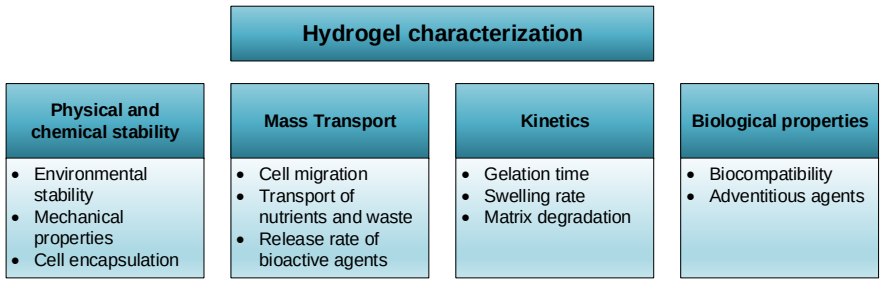

Figure 2.8: Key elements that should be considered in the characterization of hydrogels according to Standard guide F2900-11 [62].

The following sections describe some of the characteristics of the hydrogels and how to characterize them and focus on the properties characterized in this thesis.

2.3.1 Gelation time

Gelation is the transition from a liquid to a solid state [13]. Gelation point is the point in time at which this transition happens. The gelation time of hydrogels is especially important for *in situ* gelling systems. There are a few test methods that can be used to assess the gelation time of hydrogels. These include, for example, the tube tilt test and the falling ball test. In the tube tilt test, a tube containing the solution is tilted and the gelation time is the point when the system stops to flow. In the falling ball test, the

gel point is determined by recording the time it takes for the ball to sink to the bottom of the hydrogel-containing tube. Alternative methods, such as monitoring changes in optical turbidity or dynamic and static light scattering, are also applicable, since turbidity and scattering often increase when the gelation point is reached. These methods are especially suitable for rapidly gelling samples. The gelation time can also be determined by monitoring the time-dependent changes in rheological properties. The gelation time can be determined in many ways. For example, it can be considered the point in time when storage modulus becomes greater than loss modulus, or alternatively, the frequency independence of tan delta can indicate network formation. Other less common methods used are dielectric spectroscopy and the ultrasonic method. [62]

2.3.2 Swelling behavior

A hydrogel network starts to swell due to the thermodynamic compatibility of the water and polymer chains [63]. When dry hydrogel is immersed in water, it starts to absorb the water. First, the most polar, hydrophilic groups are hydrated by the first water molecules entering the matrix. This type of water is called *primary bound water*. The network swells after the completion of the hydration of the hydrophilic groups and the polar groups. The hydrophobic groups are then exposed, and they start to interact with the water. This type of water is called *secondary bound water* (or hydrophobically-bound water). When both types of water are together, they are called *total bound water*. After the interaction of water with the hydrophobic and hydrophilic sites, additional water is absorbed by the network. This is caused by the osmotic driving force of the network chains towards infinite dilution. This additional swelling force is counterbalanced by the elastic network retraction force (induced by the covalent or physical crosslinks). The balance of these forces establishes an equilibrium swelling level. The imbibed additional water is called *free water* (or *bulk water*). It is expected to fill the space between the network chains as well as the center of larger pores, macropores, or voids. It should be noted that even if dry gels may never be used as a TE matrix, the total water is still composed of *free* and *bound* water. [64] The different types of water in hydrogels are illustrated in Fig. 2.9.

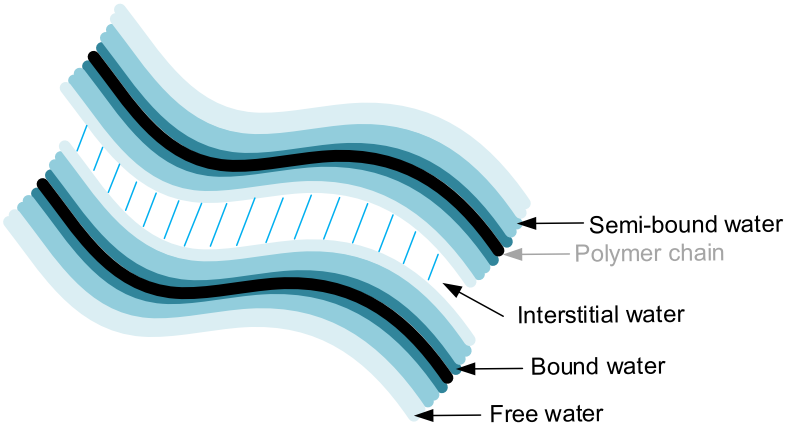

Figure 2.9: Different types of water in hydrogel: *free water*, *interstitial water* (not attached to the network, physically trapped), *bound water*, and *semi-bound water* (properties of free and bound water). Modified from [61].

The size of the chemically crosslinked hydrogel sample can either increase (swelling), decrease (deswelling) or remain constant, when it is immersed in an excess of liquid, and it is allowed to equilibrate. This is because the swelling is dependent upon the "thermodynamic quality" of the solvent and the degree of crosslinking. [65] Hydrogels with a lower degree of crosslinking swell more than highly crosslinked hydrogels. Crosslinking hinders the mobility of the polymer chains and leads to a lower swelling ratio. The chemical structure of the hydrogels can also affect swelling. Hydrogels with hydrophobic groups swell less compared with those having hydrophilic groups because in the presence of water the hydrophobic groups minimize their exposure to the water molecules by collapsing. [61] Based on these facts, some assumptions can be made. For example, the lower the degree of crosslinking, the lower the number of crosslinks, and further, the larger the chain between the network junctions, the higher the degree of swelling. It should also be noted that swelling is isotropic, meaning that the hydrogel retains its original shape during the swelling [66].

Swelling can be characterized by determining the so-called *swelling ratio* (SR) (sometimes also called the *degree of swelling* (SD)). The primary method for the determination of the SR is the quantification of water content as a function of time (swelling is a thermodynamic and kinetic process). The degree of swelling is usually quantified by calculating the ratio of sample volume in the swollen state to the volume in the dry state, or by calculating the weight degree of swelling, which is the ratio of the weight of the swollen sample to that of the dry sample. The actual measurement is usually done by immersing a pre-weighed dry or wet hydrogel sample in distilled water, phosphate buffered saline (PBS), or cell culture medium. The sample is then kept at 37 ^{o}C. The degree of swelling can be followed by weighing the sample at specific time points. This is continued until the equilibrium has been reached. [62] The drawback of using initially dry samples is the possibility that the drying process damages the hydrogel structure, and thus distorts the results [14]. There are also alternative methods, where the changes in the shape of the hydrogel are monitored over time with no need to remove the sample from the solution. [62]

2.3.3 Microstructure

The suitability of hydrogels as biomaterials for a specific application is dependent on their structure [67]. Therefore, it is important to know the network parameters of the hydrogels, e.g., mesh size, crosslinking density, and the average molecular weight of the polymer chain between neighboring crosslinks. *Mesh size* is defined as the distance (Å) between the crosslinking points in the hydrogel, and indicates the maximum size of the molecules that can diffuse in the hydrogel (passive diffusion). The mesh size of hydrogels usually varies between 10 Å to 150 Å. [68] Mesh size can be altered, for example, by modifying the degree of crosslinking or the chemical structure of the gel components, or with external stimuli (e.g., pH, temperature, ions). Mesh size should not, however, be confused with pore size. Pores are larger voids in the structure that typically have a diameter of μm scale. However, pore size positively correlates with mesh size. [68–70] The difference between pore and mesh size is illustrated in Fig. 2.10. Pores can occur naturally based on the chemistry of hydrogel, or they can be created deliberately, for example, by incorporating faster degrading regions or particles, gas foaming, or particulate leaching [68].

Porosity, as a term, is described with the mesh size [68], whereas *pore structure* is determined by the pore size, size distribution, and continuity of the individual pores within the hydrogel [69]. Porous hydrogels can be classified as macroporous (diameter

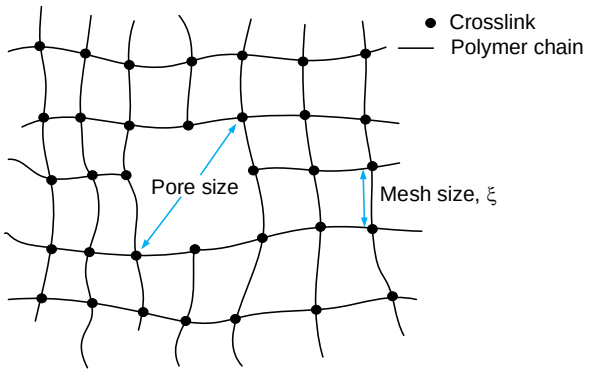

Figure 2.10: Differences in the pore and mesh size of crosslinked hydrogel.

d > 50 nm), mesoporous (2 nm < d < 50 nm), microporous (d < 2 nm), or nonporous materials. Microporous materials only allow the penetration of small molecules, such as gases, aminoacids, small peptides, and sugars, whereas mesoporous materials allow the transportation of larger molecules, such as small proteins. Large molecules (i.e., large proteins) are capable of freely penetrating macroporous materials, and even cells can migrate through the pores if the pores are large enough. [71]

Porosity indicates whether the structure will provide a suitable 3D environment for the cells, as well as providing information on the diffusion, swelling, degradation and mechanical properties of the hydrogel. [70, 72] In tissue engineering (TE), the mesh size of the hydrogel plays a critical role in modulating the cellular phenotype, proliferation and the production of the ECM, since cells (size typically between 7 μm to 15 μm) may encounter physical constraints if the mesh size (or pore size) is too small [73, 74]. Moreover, a large mesh size is extremely important for the proper exchange of nutrients and waste products across the polymer and with the external environment. Therefore, mesh size should be considered when cells are encapsulated inside the hydrogel. In consistency, when hydrogels are used as drug delivery systems (DDS), mesh size can significantly affect the loading capacity and the release kinetics of the bioactive species.

The mesh size of hydrogels can be determined using different methods. For example, the swelling-based method is widely used [75], but mesh size can also be evaluated by using the rheology-based method presented in Section 2.3.5. This method allows the estimation of the average mesh size of hydrogels [67]. Mesh size can also be estimated by studying the diffusion of molecules inside the hydrogel by using, for example, the fluorescence recovery after photobleaching (FRAP) measurement shown in Section 2.3.4, since it has been shown that mesh size correlates with the diffusivity of molecules in hydrogels [73].

In addition to mesh size, the pore size may also be determined. Nowadays, there are several methods to evaluate the porous structure of hydrogels, such as theoretical calculation, scanning electron microscopy (SEM), mercury and flow porosimetry, gas pycnometry, gas adsorption, and microcomputed tomography (CT). [69, 72] For effective evaluation, the method used should be fast, accurate, and non-destructive. The drawback of many of these methods is the need for drying, which can be very destructive for the structure of the hydrogel.

2.3.4 Mass transport

Hydrogels are ideal systems for tissue matrices due to their ECM-mimicking nature and mass transport properties [76]. How successful a hydrogel scaffold is for TE depends on the sufficient transport of nutrients, gases, waste products, proteins, and cells within, into, and out of the scaffold. *Diffusion* is the primary mass transport property of interest. [77] Understanding the diffusion processes in hydrogel systems not only helps to design an ideal material, but also enhances the basic understanding of ECMs [76].

The material and solute (molecule) characteristics and interactions dictate the rate and distance the solute diffuses. For example, material properties, such as water content, crosslinker concentration (or density), polymer size, polymer fraction, pore and mesh size, and charge as well as solute parameters, such as solute size (defined by Stokes radii), molecular weight, shape and charge, hydrophilic and hydrophobic character, and the hydration of the solute molecules, all affect the diffusion rate. On the other hand, physical (e.g., obstruction) and chemical (e.g., hydrogen bonding, electrostatic effects, van der Waals interactions) interactions between the diffusion solutes and the hydrogel material also have an effect. [77, 78]

The network crosslinking density is a key structural parameter dictating the diffusional characteristics of hydrogels. [79] The mesh size of the hydrogel, which is dependent on the crosslinking density, has been used to correlate the diffusivity of solutes inside the hydrogel [73]. In theory, a mesh size larger than the hydrodynamic radii of the solute is required for diffusion [67]. Otherwise, a smaller mesh size leads to a greatly reduced diffusion rate. Therefore, the smaller the mesh size, the slower the diffusion. [68] In addition to porosity, the size of the pore interconnections also influences the ease at which a solute or fluid can flow through the network (active transport (due to fluid flow), or passive transport (by diffusion)) [72].

Geometrical constraints and possible binding events can retain the diffusion of solutes. Therefore, the solutes should be chosen so that they do not show any binding interactions with the hydrogel components (it is expected that any possible retained diffusion would be due to a steric hindrance, rather than actual binding between the solutes and hydrogel). The crosslinking sites can form microregions in the structure (polymer is precipitated in certain areas), and these heterogeneities can also distort the diffusion results. In addition, because the solute transport within the hydrogel occurs within the water-filled regions delineated by the polymer chains, a reduction in the size of these spaces will have an effect on the movement of the solute. The size of the solute in relation to the size of the openings between the polymer chains, polymer chain mobility, and the existence of groups able to bind the solute molecule can all reduce the size of these spaces. [80]

As previously mentioned, suitable diffusivity is an important parameter especially for TE applications, since it enables the transportation of molecules, such as nutrients, gases, drugs, and cells. Therefore, mesh size also plays an important role in modulating the cellular phenotype, proliferation, and ECM production [68, 73]. Ultimately, the scaffold application will dictate the diffusion requirements and material choice [77].

Diffusion can be studied in different ways; either the passage through or movement within the hydrogel can be detected. Such methods are, for example, twin chambered devices (diffusion chambers) for nutrients and waste, electrical conductivity measurements for the diffusion of ions, optical methods using dyes for nutrient movements, or advanced methods, such as pulsed-field gradient spin-echo nuclear magnetic resonance (PFG-SE-

NMR) and fluorescence recovery after photobleaching (FRAP). [62] The following gives more information about the FRAP method used in this thesis.

2.3.4.1 Fluorescence Recovery After Photobleaching (FRAP)

One advanced technique used to study the diffusion within hydrogels is called fluorescence recovery after photobleaching (FRAP). With this technique, the diffusion of fluorescent molecules is quantified by following the recovery of the fluorescence in a photobleached region in the sample. Figure 2.11 shows the different phases of a FRAP experiment. Briefly, a short light pulse is used to bleach the fluorescence in a certain region in the sample. This is followed by the measurement of the recovery of the fluorescence due to the exchange of fluorescent and non-fluorescent molecules between the bleached region and its surroundings. Finally, the diffusion rates can be measured based on the fluorescence recovery kinetics [81].

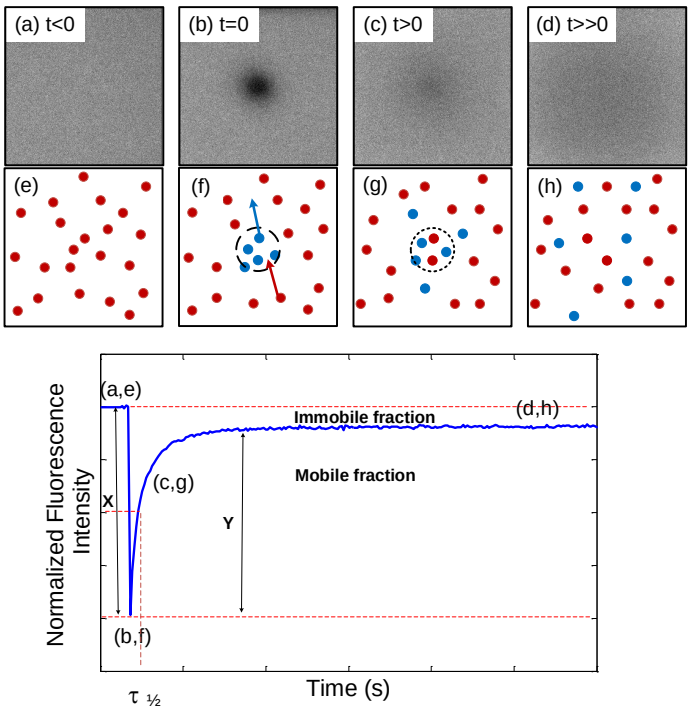

Figure 2.11: Different phases of a FRAP experiment. (a, e) A baseline of fluorescence (before the photobleaching), (b, f) the amount of fluorescence is reduced significantly (after the photobleaching), (c, g) over time, the amount of fluorescence in the photobleached area increases as the unbleached molecules diffuse into this area, (d, h) stabilization of the amount of fluorescence recovery. The fraction of molecules that contribute to the recovery are called the *mobile fraction* and those that do not are called the *immobile fraction*.

Using a suitable FRAP model, the diffusion coefficient can be determined, since the rate of fluorescence recovery is proportional to the rate of diffusion of the fluorescently labeled molecules [82]. In the case of hydrogels, the diffusion rate depends on the mesh size of the hydrogel. Thus, FRAP also enables the estimation of the mesh size of the hydrogels.

In addition, the half maximum ($\tau_{1/2}$) and percent recovery can be determined from the FRAP-curves.

$\tau_{1/2}$ can be considered as the index for the speed of recovery and it is defined as the time it takes for the curve to reach 50% of the plateau fluorescence intensity level (Fig. 2.11). The shorter the $\tau_{1/2}$, the faster the recovery. Since the use of this parameter in FRAP quantification has been criticized (because it also depends on the geometry and the size of the bleached region) [83], a more accurate method, for example Virtual Cell (VCell) modeling, is needed to stimulate the fluorescence recovery kinetics. A more detailed description of the modeling is shown in Study IV.

The FRAP recovery curve does not always reach the original level of fluorescence intensity. Some of the bleached molecules are immobile within the FRAP ROI; they neither contribute to the recovery nor give away sites for incoming un-bleached molecules. The curve can therefore be divided into immobile and mobile fractions (Fig. 2.11). Percent recovery indicates how much light returns relative to the amount of light that was there before the photobleaching. [83] Percent recovery can be determined from the following equation:

$$\%recovery = \left(\frac{Y}{X}\right) \times 100\%, \tag{2.1}$$

where Y is the amount of fluorescence that returns to the bleached area and X is the amount of fluorescence lost due to photobleaching (Fig. 2.11).

2.3.5 Rheological properties

Hydrogels behave like viscoelastic solids [13]. Viscoelastic material shows both viscous and elastic behavior. The viscoelastic behavior of hydrogels can be measured using a rheological technique called small-amplitude oscillatory shear (SAOS). In this technique, a sample is placed either between a cone and a plate or between two parallel plates (Fig. 2.12 (a)), and a small-amplitude torsional oscillation generates shear flow in the sample. [84] In the linear viscoelastic region (LVR) (Fig. 2.12 (b)), the viscoelastic character of the material can be described. At low amplitude values in this region, both storage modulus (G')- and loss modulus (G")-curves show constant plateau values, whereas outside this region G' decreases, indicating a breakdown of structure caused by large deformations. [85]

Amplitude and frequency sweeps can be measured to determine the rheological properties of the materials. An amplitude sweep is an oscillatory test that is performed at variable amplitudes, while keeping the frequency constant. The LVR limit of a sample can be determined by conducting a strain sweep, for example, from 0.1% to 100% strain at a frequency of 1 Hz (typically used for gels). A frequency sweep, on the other hand, is an oscillatory test that is performed at variable frequencies (0.01 Hz to 10 Hz), while keeping the amplitude constant (chosen based on the LVR). It can be used to examine the behavior of G' and G" in the LVR. [85] There are different parameters that are given as a result of the oscillatory tests. Some of these are presented below.

Storage modulus (G') represents the elastic behavior of the material, and it is a measure of the deformation energy stored by the material during the shear. After the removal of load, the energy is completely available, and acts as a driving force for reformation or it compensates the previous deformation. Thus, the material shows reversible deformation behavior. [85] G' describes how the material responds to shearing strains and can be

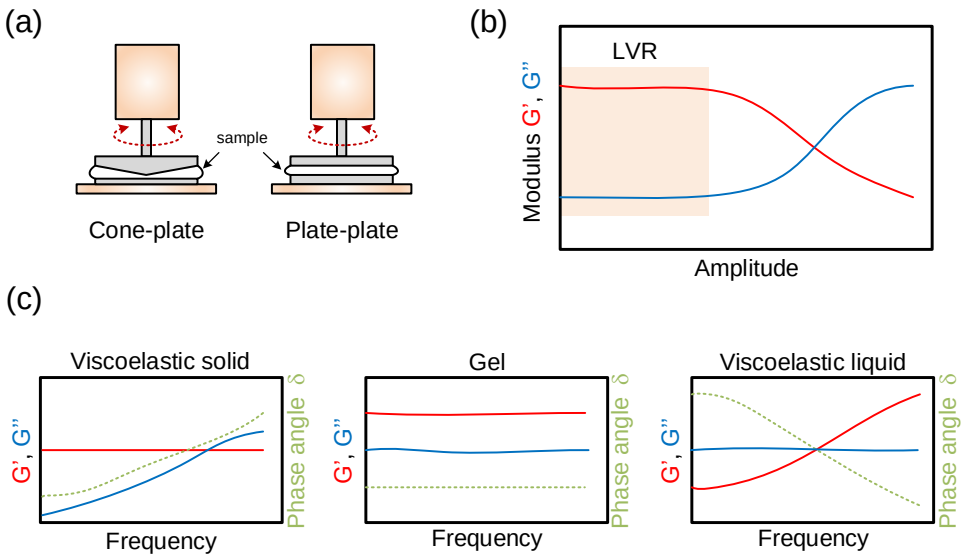

Figure 2.12: Rheology of hydrogels. (a) Schematic presentation of a typical rheometer setup. The sample is placed either between a cone and a plate or between two plates. (b) Amplitude dependence of moduli. Within the LVR, the material's response is independent of the magnitude of deformation. (c) Frequency dependence of moduli and phase angle δ. Viscoelastic solid, gel, and viscoelastic liquid all behave differently.

calculated using the following equation:

$$G' = \frac{\sigma_0}{\gamma_0}\cos(\delta), \tag{2.2}$$

where σ_0 is the stress, γ_0 is the strain amplitude, and δ is the phase angle between stress and strain.

Loss modulus (G") represents the viscous behavior of the material, and it is a measure of the deformation energy used by the material during shear (for changing the material structure). Energy losing materials show irreversible deformation behavior. [85] G" can be calculated using the following equation:

$$G'' = \frac{\sigma_0}{\gamma_0}\sin(\delta). \tag{2.3}$$

Complex modulus (G*) results from the storage and loss modulus, and therefore it characterizes the complete viscoelastic behavior containing both the elastic and viscous portion. [85] G* can be calculated using the following equation:

$$|G^*| = \sqrt{(G')^2 + (G'')^2}. \tag{2.4}$$

The loss tangent ($\tan\delta$) indicates the overall viscoelasticity of the material, and it is the ratio of lost energy to stored energy during deformation [86]. $\tan\delta$ can be calculated from the following ratio:

$$\tan\delta = \frac{G''}{G'}. \tag{2.5}$$

When $\tan\delta$ is smaller than 0.1, the gel structure is considered to be strong, whereas if $\tan\delta$ is larger than 0.1, the gel structure is considered to be weak. [58]

Fig. 2.12 (c) shows the typical behavior of viscoelastic solid, gel and viscoelastic liquid. For gels, the G' and G" exhibit a plateau in the range of 0.01 Hz to 10 Hz and are parallel to each other, whereas at higher frequencies the G' usually increases. This happens because, as the frequency increases, the polymer chains have less time for greater movement, and their rearranging fails at a given time scale. This leads to a more solid-like behavior and stiffening. [86]

The viscoelastic properties of hydrogels correlate strongly with their microstructures. Hydrogel, as a natural rubber, is assumed to fully recover rapidly into its original dimension after being subjected to a small deformation (< 20%). The so-called rubber elastic theory (RET) enables the study of the network structure of hydrogels. Average mesh size and crosslinking density can be approximated based on the affine network model from the storage modulus of the hydrogel. [67]

2.3.5.1 Calculation of the structural parameters

The average *mesh size* of the hydrogels (ξ, nm) can be calculated based on RET from the following equation:

$$\xi = (\frac{G'N_A}{RT})^{-1/3}, \tag{2.6}$$

where G' is the storage modulus, N_A is the Avogadro constant (6.022×10^{23}), R is the gas constant (8.314 J/K $\cdot$ mol), and T is the temperature (in this thesis T= 310 K) [67, 87].

The *crosslinking density* of the hydrogels (n_e, mol/m^3), which describes the number of elastically active junctions in the network per unit of volume, can be calculated based on RET using the following equation:

$$n_e = \frac{G_e}{RT}, \tag{2.7}$$

where G_e is the plateau value of storage modulus measured by frequency sweep test, and T is the temperature (in this thesis T= 310 K). [88]

The average *molecular weight of the polymer chain between neighboring crosslinks* (M_c, kg/mol) in the hydrogel can be calculated from the following equation:

$$M_c = \frac{c\rho RT}{G_e}, \tag{2.8}$$

where c is the polymer concentration (0.0375-1.5% w/v), ρ is the density of water at 310 K (993 kg/m^3), and T is the temperature (in this thesis T= 310 K). [89]

2.3.6 Mechanical properties

The mechanical properties of hydrogels play an important role when designing hydrogels for biomedical applications. The most common ways to measure their mechanical elastic properties are tension, compression, indentation testing, and frequency-based tests. [90] In this section, mainly compression-based tests are discussed because only they were studied in this thesis. Tensile-based tests, where a strip of material is held between two grips and the applied force and elongation of the material are measured to give a stress-strain curve, would also provide valuable information about the mechanical properties of the

material under tensile forces [91]. Local properties, which are not detected by the bulk measurements (e.g., compression or tensile testing), can be tested, for example, by using indentation-based tests because there are local regions in biological systems where the stiffness is higher than in the regions beside them. The ongoing remodeling of the ECM and the composite character cause these heterogeneities, and cells respond to these spatial variations. [92]

There are two ways to perform compression tests: unconfined and confined. In an unconfined test, the specimen is compressed by using two non-porous plates (Fig. 2.13 (a)), whereas in a confined test the specimen, which is kept within a vessel, is compressed by using a porous plate that allows the fluid to flow through. (Fig. 2.13 (b)). [90]

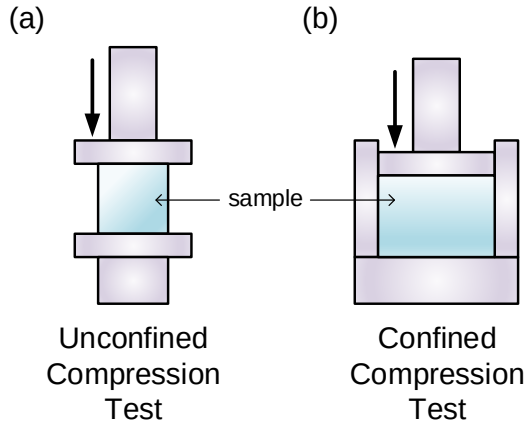

Figure 2.13: Mechanical testing of hydrogels. (a) Unconfined compression testing and (b) confined compression testing.

As the name of the compression stress-strain test implies, the force is compressive. The contraction of the specimen occurs along the direction of the stress. The size of the specimen determines the load-deformation characteristics. [93]

Compressive stress (σ) is a stress that tends to compress the material and acts perpendicular to the stressed area. It is defined as follows:

$$\sigma = \frac{F}{A_0}, \tag{2.9}$$

where F is the applied load (force, N), and A_0 is the original cross-sectional area (m^2) (before the load is applied). The unit is Pascals (1 Pa= N/m^2). Compressive force is negative, yielding a negative stress. [93]

Compressive strain (ϵ) is the deformation of the specimen that is caused by a compressive stress. It is the relative change in a single dimension of the object:

$$\epsilon = \frac{l_i - l_0}{l_0} = \frac{\Delta l}{l_0}, \tag{2.10}$$

where l_0 is the original length (before load is applied), and l_i is the length at some time. Sometimes $l_i - l_0$ is denoted as Δl (the change in length at some time). Compressive

strains are negative, since l_0 is greater than l_i. Strain is unitless. Sometimes strain is also denoted as a percentage (strain value $\times$ 100). [93]

When the specimen is subjected to a stress, its shape changes. [94]. How much the structure deforms depends on the magnitude of an applied stress [93]. There exists a so-called elastic limit for the stress, below which the strain is recoverable (when the stress is removed, the specimen returns to its original shape) [94]. The stress-strain curve can be divided into two deformation regions: *elastic deformation* and *plastic deformation* (Fig. 2.14). The elastic deformation (in which stress and strain are proportional) is non-permanent. This means that when the load is removed, the specimen fully recovers to its original shape. Plastic deformation, on the other hand, is permanent. The specimen cannot recover, and this leads finally to fracture of the specimen. [93] For sufficiently small stresses, the strain is proportional to the applied stress as follows:

$$\sigma = c_1 \epsilon. \tag{2.11}$$

This relationship is called *Hooke's law*, and c_1 is the constant of proportionality (Pa), also called *Young's modulus*, stiffness, elastic stiffness constant, or second-order elastic constant as in this thesis. [93, 94] At this point, it would be good to clarify the use of the terms related to mechanical properties. *Compliance* is the inverse of stiffness (1/Pa), and is sometimes also called elastic modulus [94]. *Strength*, as a term, is different from stiffness, and refers to the resistance of a material against fracture or failure that results from an excessive deformation [90].

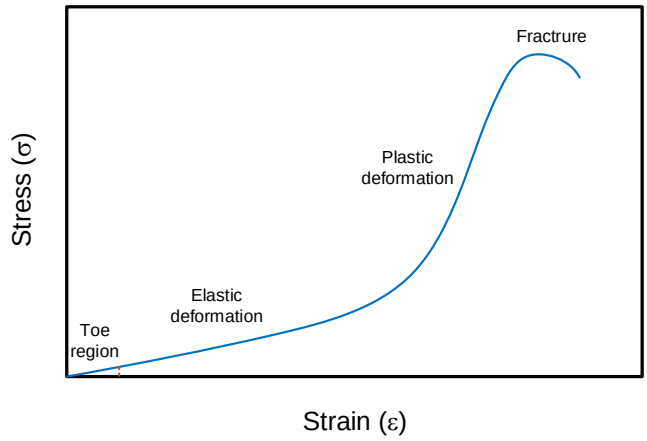

Figure 2.14: Stress-strain curve.

For many materials, such as steel, carbon fiber, and glass, the proportionality of stress and strain is linear. As a result, the slope of this linear segment corresponds to the c_1 (*stiffness* or the resistance of material to elastic deformation). The greater the c_1, the stiffer the material. [93] For hydrogels, however, the elastic portion of the stress-strain curve is non-linear, meaning that the c_1 cannot be determined as described earlier. The method used in this thesis (presented in Study I) is presented next.

Determination of the stiffness of non-linear materials: The data obtained from a stress-strain curve can be used to estimate the so-called stiffness of the material.

Here, the stiffness τ is defined as the derivative of stress σ with respect to strain ϵ (or second derivative of energy density with respect to strain). Therefore, if the measured stress-strain data are represented by a polynomial

$$\sigma(\epsilon) = \sum_{k=0}^{n} c_k \epsilon^k, \tag{2.12}$$

the stiffness may be defined as

$$\frac{d\sigma}{d\epsilon} \equiv \tau(\epsilon) = \sum_{k=1}^{n} k c_k \epsilon^{k-1}, \tag{2.13}$$

where the coefficients of the polynomial c_k are the so-called elastic constants [94, 95]. For example, c_1 in Eq. (2.13) is the second-order elastic constant (sometimes called elastic constant, Young's modulus or elastic stiffness constant) [93–95], while the coefficient c_{k-1} is the kth-order elastic constant. At relatively small strains, the so-called Hooke's law is usually expected to hold [94] and in this case one puts $n = 1$ and writes for Eq. (2.12) $\sigma(\epsilon) \approx c_1\epsilon$, which is Eq. 2.11. Here we assumed that $c_0 = 0$, that is, $\sigma(0) = 0$ (stress vanishes at zero strain). Due to the characteristic non-linear elastic behavior of hydrogels and tissues, the stress-strain curve cannot be described appropriately by Hooke's law except at low strains. Therefore, 6th-order polynomials [in Eq. (2.12) $n = 6$] were used in all cases to represent the measured stress-strain data, and the coefficients were obtained by using least square fitting optimizing the coefficient of determination R^2 (sometimes also called correlation coefficient). The stiffness describes the same quantity as the second-order elastic constant, the latter being the stiffness at zero strain $\tau(0) = c_1$. The stress polynomial was fitted at strains between 0% and 60%. To compare the $\tau(\epsilon)$ values for different hydrogels and tissues, the stiffness [Eq. (2.13)] values as a function of strain obtained from the polynomials were plotted.

As is customary, estimates for the second-order elastic constants are given. One way to obtain the second-order elastic constant is to use a linear fit at the small strains of the stress-strain data, the second-order elastic constant being the slope of this linear fit. However, the result may depend rather strongly on the strain interval chosen for the fit, which was also verified in the present work. As previously mentioned, the elastic constants of different order can be obtained, in principle, from the polynomial coefficients. However, the polynomial coefficients, when fitting such experimental data, can behave in a rather unpredictable way, even when the polynomial fit itself describes the measured data quite accurately when measured with R^2. Such instability of the polynomial coefficients can follow from the problem of collinearity [96], and this was found to be the case in the present work. In order to give some estimates for the second-order elastic constants, the following method was used. The mean and standard deviation of stiffness polynomials for parallel samples were taken at 0 to 0.15 strain. Within this interval, estimates for the second-order elastic constants were chosen to be the mean values for which the standard deviations have their minimum. By using the preceding procedure, the exclusion of initial measurement disruption was enabled. The upper limit for the strain (0.15) was a compromise in that the initial disruption (toe region) is taken into account, and that the non-linear elasticity of the materials at this strain is rather weak. The preceding procedure only gives a rather rough estimate for the second-order elastic constants, and it is probably more beneficial to study the elasticity in these materials by considering the stiffness as a function of strain.

There are many ways to affect the mechanical properties of hydrogels. Softer hydrogels can be achieved by increasing the space between the crosslinks by, for example, diluting the hydrogel with a liquid, or by increasing the molecular weight of the polymer chain between the crosslinks. Overall, a lower degree of crosslinking produces softer hydrogels, whereas a higher crosslinking density makes more rigid hydrogels. [13, 68] Hydrogels can also be reinforced by adding particles, such as carbon nanotubes, ceramic materials, or polymeric microspheres [97]. Stiffness is also related to other properties of the material. For example, stiffness decreases during the degradation process as the crosslinks are lost [68]. Porosity and mechanical properties are also linked, as already discussed in Section 2.3.3.

The importance of mechanical properties arises from the nature of native ECM. ECM and soluble factors strongly affect cellular behavior in tissue microenvironments. ECM, which is composed of fibrous proteins (e.g., collagen, laminin, fibronectin, and elastin), provides sufficient stiffness for the matrix *in vivo* (1 kPa to hundreds kPa). The cells sense the matrix stiffness while interacting with the proteins via binding proteins. [90] Material stiffness (mechanical environment) can affect cell viability and behavior [92]. There have also been suggestions that stiffness could influence cell sensitivity to other microenvironmental signals [98]. When cells are cultured on material with a similar stiffness to their native ECM, they are better able to maintain their functional phenotype. Matrix mechanics is not only important for mechanically active cell types (e.g., cardiomyocytes, muscle cells), but also for less active ones (e.g., neuronal cells). [98] Not all cells respond similarly to matrix stiffness. In some cases, chemical stimuli can be overridden by matrix stiffness, whereas in other cases an adhesive ligand together with substrate stiffness can direct specific processes. [99]

2.3.7 Biodegradability

Together with the previously mentioned properties, biodegradability plays an important role in the design of hydrogels intended for TE or drug release applications. As previously stated in Section 2.2.6, hydrogels can be classified into biodegradable and non-biodegradable (stable) hydrogels [44]. Biodegradability is a desired property because the surrounding tissues in the body can absorb the scaffold with no need for the surgical removal of the scaffold. Usually, the idea of the scaffold is first to support the growth of cells and then to degrade as subsequent repair takes place. For an ideal scaffold, the by-products should be non-toxic and easily disposed. [7] During the biodegradation process, polymer molecules may break down into fragments that can move away from their target site, but not always from the body [100]. Only biodegradation leads to the complete elimination of the original polymer from the body, resulting in only carbon dioxide, water, and biomass [101]. It should be noted that the degradation by-products may not only affect the degradation rate, but also the biocompatibility of the material. A suitable degradation rate is also important. A slower rate would be beneficial for a scaffold because it gives the cells time to develop their own ECM and to extend processes. Faster degradation, however, would be beneficial *in vivo*, since quick degradation can contribute to a reduced immune response. [68]

A biological system mediates at least partially the biodegradation [59]. Biodegradation can be defined in different ways, such as changes in the surface properties, loss of mechanical strength, backbone chain breakage, degradation by enzymes, or reduction in the average molecular weight of the polymer. Degradation can occur in combination with the above mechanisms or alone. [100]

There are two ways to cleave the polymer bonds: passively by hydrolysis and actively by enzymatic reaction [59]. In hydrolysis, water causes the scission of covalent bonds [102]. Functional groups, such as amides, anhydrides, carbonates, esters, orthoesters, ureas, and urethanes, are susceptible to hydrolysis. [103]. Enzymatic degradation is associated with the number of enzymes, hydrolases, and oxidoreductases. There are two different forms of enzymatic degradation: exo and endo. Exo depolymerases cleave small oligomer fragments from the chain ends, whereas endo depolymerases perform random scission along the chain, which leads to a more dramatic loss of properties. [102] Natural polymers degrade mainly by enzymatic degradation; for example, HA is degraded by hyaluronidase [23] and collagen by collagenases [37].

The degradation of a hydrogel can occur via bulk or surface erosion. In surface degradation, the surface or exterior bonds are cleaved first because the water and enzymes cannot penetrate the interior of the hydrogel. This can happen to hydrogels with a high crosslinking density or if there is limited access to cleavage points. In bulk erosion, on the contrary, the degradation takes place homogeneously throughout the hydrogel. This is actually more common for hydrogels due to their high water content and fast diffusion. [68] Bulk erosion begins with the entering of water to the polymer bulk (accompanied by swelling), where it triggers the chemical polymer degradation, and oligomers and monomers are created. As the degradation progresses, the microstructure of the bulk will change through the formation of pores. At this point, the degradation products (with some acid-base functionality) start to control the pH inside the pores. This can lead to a faster degradation inside the material compared with the surface, since the degradation products can be dissolved into the surrounding fluid from the surface. Oligomers and monomers are released via pores, which leads to the weight loss of the polymer, as well as a loss of physical properties. [59, 104]

The *in vitro* and *in vivo* degradation of hydrogels differ from each other. *In vitro* degradation is dependent on hydrolysis, because there is unlimited access to water. Also, the degradation is usually based on a single enzyme (e.g., hyaluronidase). *In vivo*, however, there is limited access to water. There are also multiple enzymes present that can degrade the hydrogel. [68]

Factors that influence the degradation behavior of polymers are the chemical composition and structure, molecular weight, the distribution of repeating units in multimers, polydispersity, the presence of low M_w compounds, the presence of chain defects and ionic groups, configurational structure, morphology (i.e., crystallinity, the presence of microstructure, orientation, and residue stress), storage history, sterilization method, processing methods and conditions, site of implantation, physiochemical factors (i.e., shape, size), absorbed compounds, and mechanism of hydrolysis (enzymes or water). [60, 104] For example, polymer degradation is accelerated by a more hydrophilic backbone or monomer, a more hydrophilic and acidic endgroups, a more reactive hydrolytic group in the backbone, less crystallinity, smaller size, and sometimes being under mechanical stress. [104]

Degradation can be followed, for example, by monitoring the molecular weight changes (e.g., using dilute solution viscosity, size exclusion chromatography (SEC), gel permeation chromatography (GPC) or MALDI mass spectroscopy), loss of mechanical strength, morphological changes (e.g., swelling, deformation, bubbling, disappearance), bulk mass loss, change in chemistry (e.g., infrared spectroscopy (IR), Nuclear Magnetic Resonance Spectroscopy (NMR), TOF-SIMS), oxygen uptake, evolution of CO_2 or CH_4, or changes in crystallinity. [59, 101, 102]

2.3.8 Injectability

Cell-based therapeutic approaches that are based on the delivery of living cells to the target location are considered important tools in TE. Commonly, high-density single-cell suspensions are injected directly to the site of the injury, although many times these approaches lead to a large and rapid loss of cell viability, reduced entanglement of delivered cells, and limited control over cell fate. Thus, more effective cell transplantation methods are needed. One method is to deliver the transplanted cells with a biocompatible material that serves as a temporary support. This method offers protection for the cells, a more physiological 3D environment, and prolonged retention at the injury site. Injectable materials offer a more desirable approach over traditional scaffold-based systems because the technique is minimally invasive, improves patient compliance, and leads to faster recovery and lower health care costs. Further, injectable materials allow an easy incorporation of therapeutic agents (e.g., proteins, cells) and their localized delivery, and they offer a simple implantation technique as well as high contourability (fills defects of irregular sizes and shapes). They also offer site specificity and confined delivery. [27, 105]

A cell delivery vehicle should maintain the cell viability throughout the injection process. The cells can experience three types of mechanical forces that may lead to cell disruption when they flow through the needle of a syringe. These include pressure drops across the cell, shearing forces (due to linear shear flow), and stretching forces (due to extensional flow). Thus, the material to be injected should have suitable mechanical properties in order to protect and ensure the survival of the injected cells. [27]

There are different types of injectable cell-based systems, such as surface immobilization, micro-encapsulation, matrix-entrapment, and multicellular aggregation. Due to the scope of this thesis, only the matrix entrapment-type is discussed here. In this system, the cells (and growth factors, drugs) are embedded in a hydrogel matrix that provides a 3D environment. It can be formed *in situ* or *ex situ*. [27] For example, the cells can be loaded in the hydrogel precursor, and then injected into the injury site, where *in situ* gelation occurs. [105] It should be noted that the gelation should start or be completed shortly after injection. [27]

Injectable *in situ* formed hydrogels can be fabricated from natural and/or synthetic polymers using different crosslinking techniques, such as physical self-assembly, ionic interaction, thermal gelation, photopolymerization (limited by the injection depth), as well as many chemical crosslinking methods, such as Michael-type addition, Schiff base crosslinking, click chemistry, and gelation agents (e.g., genipin, glutaraldehyde), although covalent crosslinking methods are considered more advantageous over the non-covalent ones. [105]

2.3.9 Optical properties

2.3.9.1 Transparency

Optical transparency is beneficial for many applications. For example, optical clarity is an obvious requirement for contact lenses to achieve maximal visual performance, but it would also be desirable in ocular prostheses or in sensors based on fluorescent markers embedded in hydrogel as well as in wounds that are dressed with hydrogels (e.g., ocular wounds). [106] Optical transparency is not always necessary for the application. It is worth considering, however, because optical transparency might be needed for *in situ* microscopy and non-invasive optical assays of cell behaviors [20].

Polymeric materials, including hydrogels, can be considered transparent, translucent, or opaque. You can see through transparent materials, whereas translucent materials allow the light to pass through, but you cannot see through them. Opaque materials, on the contrary, neither allow the light to pass through, nor allow you to see through them. [107] The thinness of the hydrogel as well as the size and shape of the its constituents and their refractive indices all determine the transparency of hydrogels [108].

The optical clarity (or transparency) is usually represented as the percentage of transmission of the visible electromagnetic spectrum (wavelengths between 400 nm to 700 nm) [107, 109]. The transmittance of hydrogels can be measured using an ultraviolet-visible (UV-Vis) spectrophotometer, or an optical fiber spectrometer [109]. A photography-based optical measurement and calculation has also been developed to evaluate the transparency and blurriness of hydrogels [110]. The optical clarity can also be visually evaluated by taking an image of a hydrogel with some text in the background. However, since this method is based only on visual inspection and the use of image editing programs is possible, it is highly subjective.

2.3.9.2 Refractive index

Suitable refractive power is needed for a material intended for ophthalmic applications [6]. For example, for the corneal application presented in this thesis, the refractive index of a hydrogel should be similar to that of the cornea (n= 1.376) [111, 112].

Refractive index (n) of a medium is defined as:

$$n = \frac{c}{\nu}, \tag{2.14}$$

where ν is the velocity of the propagation of light in a particular medium and c is the velocity of light in a vacuum [113]. Consider the situation presented in Fig. 2.15. In this situation, a beam of light propagates from one medium with refractive index n_1 to another medium with refractive index n_2 with the angle of incidence θ_1 and the angle of refraction θ_2 (see Fig. 2.15). According to the so-called Snell's law, these quantities are related as follows [113]:

$$n_1 \sin\theta_1 = n_2 \sin\theta_2. \tag{2.15}$$

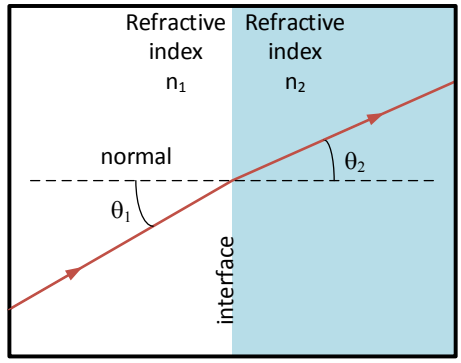

Figure 2.15: Refraction of a ray of light.

The refractive index of hydrogels can be measured with a refractometer [114] or, as in this thesis, with surface plasmon resonance (SPR) equipment using the device's goniometer and light source to scan the critical angle of total internal reflection between glass and hydrogel. The refractive indices of the hydrogels can be determined from the curves where the reflection coefficient is shown as a function of the angle of incidence by utilizing Snell's law with the critical angle condition (see Section 4.2.4.8).

The refractive indices of conventional hydrogels can be tuned by changing the water content (for water n= 1.333 [115]). Refractive indices show a relationship with the equilibrium water content (EWC) of hydrogel, meaning that the refractive index decreases with increasing water content. [112]

2.3.10 Biocompatibility

Biocompatibility has been defined in many ways. According to Williams [116], it is defined as: "*the ability of a biomaterial to perform with an appropriate host response in the specific application*". Later, the definition was modified to the following by Kohane and Langer [117]: "*an expression of the benignity of the relation between a material and its biological environment*". Various natural-, synthetic- and hybrid-based biomaterials are used for TE. These materials should have certain functional properties if they are intended to be used *in vivo*. For example, they should restore the tissue so that it possesses an appropriate function and cellular phenotypic expression. They should also inhibit the macrophage and foreign body giant cell responses (degrades the material) as well as inhibit scar formation and immune responses. Today, creating materials that give better control over inflammatory and immune responses, and thereby reducing the chance of rejection, is more desirable than creating only bioactive materials. The body responds with one or more negative and/or positive reactions after the implantation of biomaterial. These are, for example, foreign body reaction, wound healing, stem cell interactions, temporary inflammation, blood interactions, provisional matrix formation, oxidative stress, and the formation of granulation tissue. Preliminary biomaterial tests using non-human tissues may also trigger species-specific immune responses, which could possibly be prevented by using cells/components from one species and testing them with that same species. [37]

When evaluating the biocompatibility of material, the goal is to determine the toxic effects on the body. The biological responses, such as wound healing, inflammation, and the immunological reaction/immunotoxicity, should at least be evaluated. Because the Standard Practice for "Evaluation of Immune Responses in Biocompatibility Testing of ASTM" (American Society for Testing and Materials) had some limited protocols, it was withdrawn in 2011. Currently, there is no all-inclusive standard for biological evaluation. [37] Overall, *in vitro* tests (e.g., MTT assay, measures of DNA synthesis and proliferation, and dye-based cell membrane integrity tests) provide a rough estimation of how the relevant cell types can survive in the presence of the biomaterial, whereas *in vivo* tests help to understand the biocompatibility. The *in vitro-in vivo* correlation should also be considered. [117]

The cells are structurally supported by the ECM, which is composed of a mixture of proteins and polysaccharides. Since the native ECM contains all the components of the tissue from where it was derived, it can be considered to be an ideal biological scaffold. [37] Even though inert materials have been previously used as scaffolds for many applications, nowadays the biocompatibility of biomaterials can be defined as follows: "*the biocompatibility of a scaffold or matrix for a tissue engineering (TE) product refers to the ability to perform as a substrate that will support the appropriate cellular activity,*

including the facilitation of molecular and mechanical signaling systems, in order to optimize tissue regeneration, without eliciting any undesirable local or systemic response in the eventual host" [118]. Biocompatible scaffolds should, therefore, directly influence cells, as well as support cell signaling. Controllable degradation with non-toxic degradation by-products are also desired. [37] More specific goals for biocompatible scaffolds are presented in Section 2.4.1.

Hydrogels can be used as a TE scaffold due to their favorable and controllable properties, but above all, due to their natural ECM-mimicking nature in terms of structure and composition. [37] The chemistry and mechanical properties of hydrogels affect their biocompatibility. For example, toxic degradation by-products can limit their use, whereas the addition of signaling effects, such as peptides or proteins, can favor their use with encapsulated cells. Most of the cell types also favor materials with a tissue-mimicking mechanical environment. [68] In addition, material variables, such as bulk material composition, microstructure, water content, hydrophobic-hydrophilic balance, porosity, and different surface properties can influence the host response. [118]

2.4 Hydrogels for tissue engineering

2.4.1 Tissue engineering

In tissue engineering (TE), the normal biological functions of the tissues or organs are replaced or regenerated. This can be done by combining the cells with biomimetic matrices (scaffolds), biological signals, and biophysical cues. Fig. 2.16 represents the basic principle of TE. In *in vitro* TE, a tissue-like implantable construct is generated in order to re-create the microenvironment *ex vivo*, whereas in *in vivo* TE, endogeneous cells are recruited by the scaffold materials for tissue repair. [2]

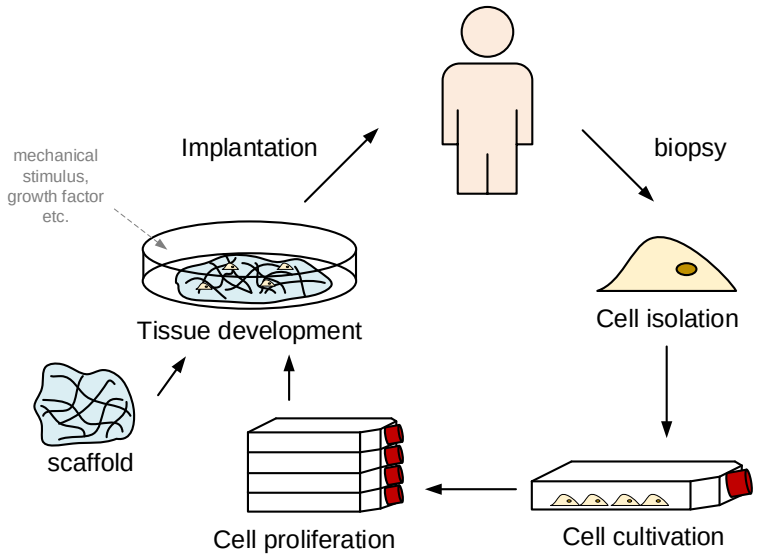

Figure 2.16: The principle of tissue engineering.

The terms TE and regenerative medicine (RM) are sometimes used synonymously. RM is a broad field that includes tissue engineering as well as cell therapies and gene therapy. Rather than replace the diseased tissue with synthetic material, the main aim of RM has been to regenerate the diseased tissue. [118]

2.4.2 General requirements for the hydrogel scaffolds

Scaffolds have many functions in TE. For example, they not only provide physical support, but they also actively regulate cell functions and promote tissue growth. [2] Hydrogels can be considered the most attractive TE scaffolds because they are structurally and functionally similar to ECM [2]. In fact, materials that mimic natural ECM in terms of composition, structural character, and mechanical properties are desired. [37] The main requirements for the scaffold have already been mentioned in Section 2.3.10. Fig. 2.17 presents some general requirements for TE scaffolds.

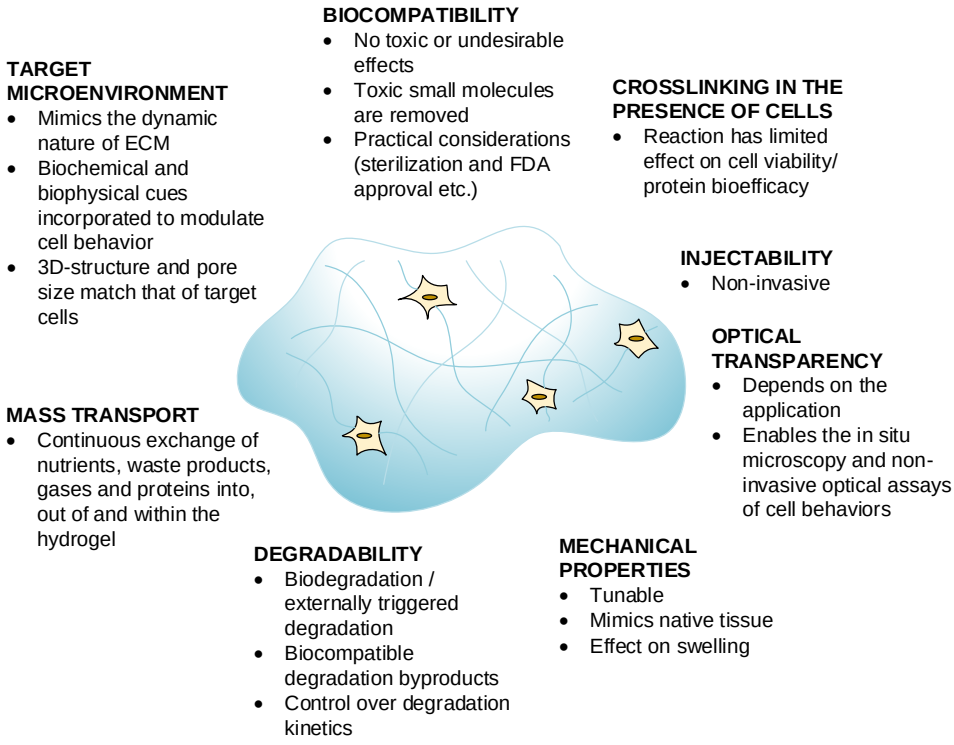

Figure 2.17: General requirements for the hydrogel scaffolds used for tissue engineering. Modified from [23].

It is important that the hydrogels can be formed in the presence of cells (and/or molecules to be delivered) *in vitro* and *in vivo*. *In vivo*, this enables the molding of the gel into any shape and minimally invasive delivery. The crosslinking reaction itself can affect cell function/viability (or activity of cargo molecules). Therefore, the gelation method should avoid sudden changes in pH, temperature, and free radicals. In addition, instead

of using organic solvents, water-based methods with mild conditions should be preferred. [23, 69, 119]

The pore size, as well as the 3D structure of the hydrogel, should be suitable for the target cells. Subsequently, cells would have space to migrate and there would be space for vascularization. A large enough pore size also keeps the cells viable inside the scaffold because it allows the continuous exchange of proteins, gases, nutrients, and waste products within, out of, and into the hydrogel. [23, 37]

The degradation by-products of scaffolds should be biocompatible and non-cytotoxic, and they should be able to excrete from the body after the cells have populated the scaffold and produced their own ECM. The degradation process should not induce any inflammatory or immune response from the body. The degradation kinetics should also be stable and controllable. Degradation provides space for the migrating and proliferating cells, and for vascularization. [23, 37]

The mechanical properties are also important because it has been shown that in applications where the cells are encapsulated, the mechanical properties can influence cellular responses (cell migration, proliferation, and differentiation). [23] The mechanical properties of a scaffold should match those of native tissue in order to mimic the natural cellular microenvironment. This is also important because the mechanical properties will change over time due to degradation and during the formation of new tissue. [120]

One unaddressed challenge in scaffold design is how to mimic the dynamic nature of ECM. The matrices should make the bidirectional crosstalk between the resident cells and the microenvironment possible. [23] The scaffold should also be bioactive, meaning that by adding some biological cues, such as adhesion ligands or growth factors, the regeneration of the tissue could be enhanced as it mimics the native cellular microenvironment. [23, 37]

Even though optical transparency might not be necessary for the application, it should be taken into consideration, since *in situ* microscopy and non-invasive optical assays of cell behaviors might require optical transparency. [20]

2.4.3 Soft tissue engineering applications

This thesis mainly focuses on corneal and neural TE applications. Therefore, only those applications are briefly reviewed here.

2.4.3.1 Corneal tissue engineering

Blindness is a worldwide problem. It is caused by corneal dysfunction due to various inherited or acquired diseases, or by trauma or burns. Annually, there are over 1 million new cases reported [5, 121]. Currently, corneal dysfunction is treated by transplantation of donor corneas, although this method can suffer from graft failure and immune reactions. There is also a continuous shortage of suitable donor tissue [6]. Therefore, alternative treatment options are needed, such as TE and stem cell therapy. For example, since mesenchymal stem cells (MSCs) have antiangiogenic and immunomodulatory properties, as well as the capability to inhibit corneal scarring, they have attained a great interest in corneal regeneration [122, 123]. The 3D bioengineering corneal tissues can be constructed *in vitro* in many ways, for example, by using prefabricated matrices, decellularized corneal tissues, or, as in this thesis, by using a hydrogel technique [124].

The cornea is a transparent, avascular, collagen-rich connective tissue, and it forms the front of the eye [6, 125]. It provides mechanical protection for the eye and protection from infections [6]. The cornea can be considered to be the window to the eye. It not only provides transparency and protects the retina from damaging UV light [6], but it is also mainly responsible for its refractive power [5]. The cornea is anisotropic, meaning that its properties are not uniform in every direction. The properties of the cornea are both non-linear elastic and viscoelastic. [126] There are three distinct cellular layers in the cornea (Fig. 2.18): endothelium, stroma, and epithelium. These layers are separated by an acellular and collagenous Bowman's layer and Descemet's membrane. [5, 6] Epithelium is a stratified non-keratinized squamous layer that regulates the transfer of water and other soluble components out of and into the stroma. It also provides protection for layers below from infections and chemical injuries. Together with the tear film, epithelium also allow the refraction of light (as it enters the cornea). [5, 6] The stroma makes up around 90% of the overall thickness of the cornea, and is composed of layers of highly organized collagen fibrils (lamellae, mainly heterotypic hybrids of types I and V) that together with some small leucine-rich proteoglycans (e.g., decorin, lumican, keratocan decorated with dermatan sulfate and keratan sulfate) provide mechanical support and suitable biophysical properties that transparency requires. The stroma also contains keratocytes that maintain the matrix components. [5, 6] A monolayer of specialized endothelial cells form the endothelium [5]. Endothelium serves as a metabolic pump that maintains a suitable level of stromal hydration by removing the water from the stroma. This is important for corneal transparency [6].

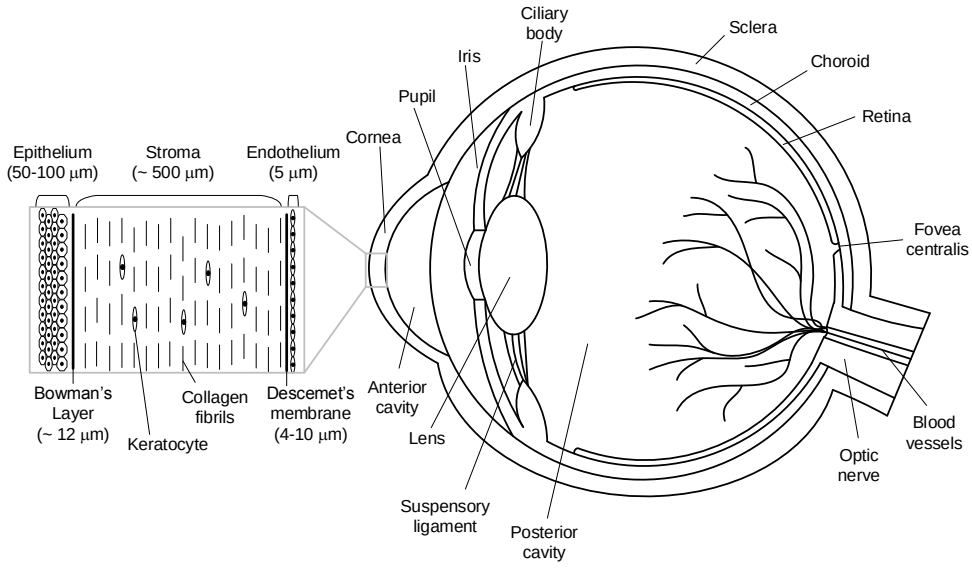

Figure 2.18: Human eye anatomy. The specific anatomy of the cornea is magnified.

In order to mimic the functions of the cornea, there are at least three main requirements for corneal substitute material. It should provide transparency, protection, and suitable

refractive power. [6] It is difficult to rebuild corneal stroma due to its complicated structure and properties, such as transparency (light transmittance within the visible wavelength $> 87\%$ [127]) and mechanical properties (tensile strength 3.81 ± 0.40 MPa, Young's modulus 3 MPa to 13 MPa [127]) [6]. The substitute material should be strong enough to be able to protect the cornea, and it should also withstand handling during the surgical procedure [128]. The refractive index of the cornea is n= 1.376 [111]. Although the cornea provides the strongest refractive power of the eye, it may not be necessary to replicate its exact refractive index, since refractive errors can be adjusted with spectacles. Therefore, transparency is more important. The transparency should mimic that of native tissue. A substitute material that can support the growth of an epithelial layer and serve as a vehicle for the transplantation of keratocytes would also be desired. [129] More general requirements for the hydrogel scaffold, such as suitable permeability and biodegradability have already been discussed in Section 2.4.2.

HA- and collagen-based hydrogels were studied in this thesis. Therefore, only studies related to HA- and collagen-based hydrogels used for corneal repair were chosen to be listed in Table 2.1. As previously mentioned, collagen I is the main ECM component in the corneal stroma. It provides high transparency and mechanical strength for the cornea [130]. Collagen hydrogels have many advantageous properties, such as low immunogenicity, biodegradability, and biocompatibility. Also, conventional collagen hydrogels can be chemically crosslinked or plastically compressed in order to improve their mechanical properties. [39] The feasibility of collagen-based hydrogels for use as regenerative scaffolds has already been demonstrated in many pre-clinical studies [5]. Subsequently, collagen, especially type I, is an obvious material choice for this application. Although HA is found in the eye from the vitreous, corneal epithelium, lacrimal gland, and conjunctiva, it is not normally found in the stroma [28, 131]. The benefits of HA include its anti-inflammatory properties and its ability to stimulate corneal epithelial cell migration (corneal wound healing) [28, 131]. HA also acts as a natural lubricant as it increases the corneal wettability by retaining water on the surface of the cornea. All these properties make HA suitable for ophthalmic applications. [28] At the moment, HA-based hydrogels are not as widely studied for this application as collagen hydrogels. Other hydrogels that have been used as scaffolds for corneal repair are, for example, fibrin, alginate, chitosan, gelatin, silk fibroin, and silicone hydrogels, as reviewed by Wright et al. [39] and Nguyen et al. [5].

Table 2.1: Some collagen- and HA-based materials used for corneal TE, and HA- and AL-based materials used for neural TE. Abbreviations: LESCs= limbal epithelial stem cells, CESCs= corneal epithelial cells, Ks= keratocytes, ASCs= adipose-derived stem cells, NPCs= neural progenitor cells, iPSC-NPCs= induced pluripotent stem cell-derived neural progenitor cells, NSCs= neural stem cells, PLGA=poly (lactic-co-glycolide), HA= hyaluronan, AL= alginate, PEG= polyethylene glyco, CEC-l-OSA= N-carboxyethyl chitosan-l-oxidized sodium alginate, PC= Plastic Compressed. Extracel-SS, HyStem-HP, and HyStem-CSS are commercially provided by Glycosan BioSystem Inc. (Salt Lake City, UT, USA). GMHA (thiolated hyaluronic acid) and Gelin-S (thiolated porcine gelatin) are commercially provided by BioTime Inc. (Alameda, CA, USA), GSSG (oxidized glutathione, sodium salt).

Application	Polymer-basis	Material	Cell type	Results	Reference
Corneal	Collagen	EDC-NHS cross-linked collagen I	Human CESCs	Material supported confluent human epithelial and stromal-derived mesenchymal stem cell populations.	[132]
		Collagen I (high concentration)	Human LESCs	The matrices stood culture of epithelial cells coming from a human limbal explant and remained transparent during the culture.	[133]
		Collagen I gel (PC) + electrospun PLGA mats	Human CESCs and Ks	The cells adhered, proliferated, and maintained their phenotype well on the material.	[124]
	Hyaluronan	Extracel-SS, HyStem-HP, and HyStem-CSS hydrogels	Human ASCs	h-ASCs were successfully grown on hydrogels *in vivo* and could express human cornea-specific proteins.	[134]
		CMHA/Gelin/GSSG hydrogels	Human ASCs	Supported the 3D culture of ASCs *in vitro*, and was biocompatible in preliminary intracutaneous and subconjunctival experiments *in vivo*.	[135]
		HyStem-C hydrogel	Human CESCs	The hydrogel scaffold-based xeno-free culture system supported the expansion of regenerative CESCs.	[136]
Neural	Hyaluronan	Methacrylate-modified HA hydrogel, UV-crosslinked	Mouse ventral midbrain-derived NPCs	Softer hydrogels caused mostly neuronal differentiation, and stiffer hydrogels astrocyte differentiation.	[137]
		Methacrylate-modified HA hydrogel, UV-crosslinked	Human iPSC-derived NPCs	Layered hydrogel of different moduli influenced migration and differentiation.	[138]
		Methacrylate-modified HA hydrogel, UV-crosslinked	Human iPSC-derived NPCs	Lower hydrogel stiffness promoted differentiation and robust neurite outgrowth was observed.	[139]
		RGD-heparin-HA hydrogel crosslinked with PEG-diazide crosslinkers	Human PSC-derived neural progenitors	Enhanced cell survival both during and post-transplantation.	[140]
	Alginate	Ionically cross-linked AL hydrogel	Rat NSCs	The rate of cell proliferation was lower with higher hydrogel modulus, the expression of the neuronal marker b-tubulin III was enhanced within the softest hydrogels.	[141]
		Ionically cross-linked AL hydrogel	Rat embryonic cortical neurons	Cells encapsulated within the softest hydrogels showed excellent viability, extensive formation of axons and dendrites, and long-term activity.	[142]
		CEC-l-OSA hydrogels	Rat NSCs	Self-healing hydrogels with brain-mimicking stiffness supported the proliferation and neuronal differentiation of NSCs.	[143]

2.4.3.2 Neural tissue engineering

Traumas and deficits in the human central nervous system (CNS), such as traumatic brain injuries (TBI), spinal cord injuries (SCI), Parkinson's disease, Alzheimer's, Multiple Sclerosis, Retinitis Pigment, and Age-related Macular degeneration, may have a permanent effect on the functionality of the patient, and the prognosis in many cases is poor. At the same time, human CNS suffers from a low inbuilt regenerative capacity, which makes healing with traditional medicine (drugs and surgical procedures) insufficient. [7] As a result, TE or more specifically regenerative medicine is considered to be a potential treatment for CNS deficits because it aims to restore normal functionality by enhancing the regeneration of tissue or by replacing the damaged parts with engineered biological transplants. One such strategy is cell therapy combined with a supportive biomaterial scaffold, such as hydrogel.

The central nervous system (CNS) (Fig. 2.19 (a)) is a part of the nervous system, and it comprises the brain, spinal cord, and retina. [7, 144]. The skull and vertebrae protect the brain and spinal cord, respectively. The nervous system is composed of neurons, and non-neuronal glial cells (e.g., astrocytes, oligodentrocytes) that mainly support and protect neurons. The cell body of a neuron is called a soma (plural somata) (Fig. 2.19 (b)). A neuron also consists of some processes, i.e., dendrites (extend the receiving surface of neuron) and an axon (conducts nerve impulses). Many axons are surrounded by a myelin sheath. The nervous tissue can be divided into white and gray matter. White matter contains axons and no neuronal somata (color due to myelin), whereas gray matter contains somata and dendrites. Both white and gray matter also contain glial cells. [144] Hyaluronan, proteoglycans (lecticans) and tenascins are the main constituents of healthy brain tissue [8]. HA is a major glycosaminoglucan component in the ECM of the brain. Since HA increases the hydration of brain tissue, it has been hypothesized to be the reason for the low stiffness of brain tissue (compressive moduli for brain tissue ranges from 2 kPa to 5 kPa, whereas for spinal cord it is around 8 kPa [137]). [8] HA also plays a vital role in the development of the CNS. During the differentiation of the spinal cord, HA surrounds the immature neurons, whereas it is also abundant in the fetal brain [137]. The CNS has limited spontaneous regenerative capacity [7, 145].

Hydrogels should fulfill specific criteria when they are used for neural TE. For example, they should have similar mechanical properties to those of the brain or spinal cord, since soft matrices (stiffness < 1 kPa) have been shown to improve axon length and cell attachment and survival [8, 148]. In addition, hydrogels should also allow the infiltration of cells and axons and enable the transportation of nutrients and metabolites (suitable porosity and pore size, and diffusion properties). Hydrogels should also integrate with the host tissue so that there is no inflammatory reaction or glial scar formation. [148] A suitable degradation rate together with non-toxic degradation products are also desired [8, 148]. Optical clarity might be needed for the imaging of cell cultures. The electrical conductance of materials would be beneficial in order to deliver an electrical current to the cells. [8] Injectability, together with a suitable gelation time, would allow minimally invasive surgery [145]. More general requirements for the hydrogel material have already been discussed in Section 2.4.2.

Based on the polymer-basis of the hydrogels used in this thesis, only examples of studies related to HA- and AL-based hydrogels used for neural TE (especially for the 3D *in*

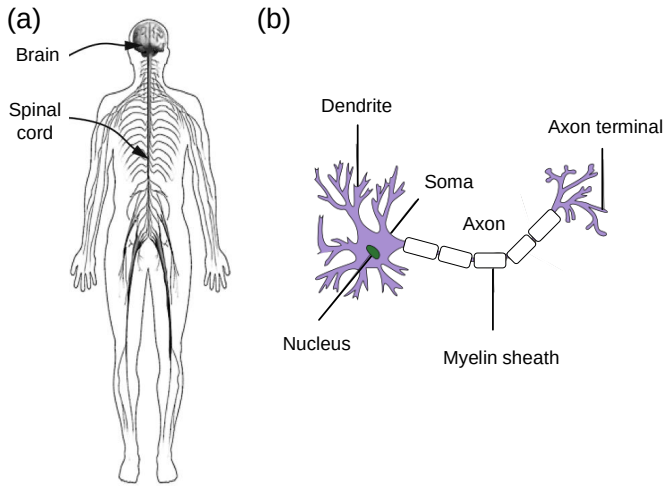

Figure 2.19: (a) The central nervous system (CNS) and (b) the anatomy of a neuron. Modified from [146] and [147].

vitro culture of neural lineage cells) were chosen to be listed in Table 2.1. The role of HA in the native CNS was discussed earlier. In addition, there are also many favorable properties discussed in Section 2.2.1.1 that explain why HA-based hydrogels are widely used for neural applications. AL-based hydrogels are also used for neural applications. AL is structurally similar to the ECM. As a natural hydrogel, it has many favorable properties (Section 2.2.1.1), which make it suitable for these applications. In addition, collagen type-I, Matrigel (mixture of ECM proteins), PuraMatrix (synthetic peptide hydrogel), chitosan, fibrin, IKVAV/RADA16 self-assembling peptides, and polyethylene glycol (PEG) hydrogels have all been successfully used for 3D *in vitro* culture of neural lineage cells, as reviewed by Murphy et al. [149].

3 Aims of the study

The primary aim of this thesis was to find optimal hydrazone crosslinked hydrogel material for soft TE applications, especially for corneal and neural applications, and to investigate their detailed properties using suitable characterization methods. It was hypothesized that the chemical, physical and mechanical properties of the hydrogel would affect their usability in different biological applications. Further, it was hypothesized that by choosing mainly natural-based gel components as well as a mild and simple crosslinking method, bio-mimicking materials with suitable characteristics for the soft TE applications could be achieved.

The specific objectives of the studies were:

Study I:

- To create GG-HA-based hydrogels that would be suitable for soft TE applications based on their physical and mechanical properties, and replace the traditional crosslinking methods of GG-based hydrogels with hydrazone crosslinking to improve their properties as well as enable the injectability of the hydrogel, and to improve the method used to analyze the mechanical compression test data.

Study II:

- To create transparent HA-based hydrogels (with suitable physical and mechanical properties) that would be suitable for the delivery of hASCs for regeneration of the corneal stroma, to incorporate collagen I into these hydrogels in order to promote hASC attachment and survival, and to use an organ culture model with excised porcine corneas to show the clinical relevance of the HA-based hydrogels for hASC delivery to stromal defects.

Study III:

- To create injectable HA- and AL-based hydrogels (with suitable physical and mechanical properties) that would serve as a 3D supportive and biomimicking material for neural cell culture (human pluripotent stem cell-derived neuronal cells).

Study IV:

- To evaluate the microstructure of previously studied hydrazone crosslinked HA-, AL-, and GG-based hydrogels (Studies I-III) using rheology- and FRAP-based methods in order to show their suitability as biomaterial for soft TE applications, and to show how different gel parameters have an effect on the viscoelastic and diffusion properties, and further on the microstructure of these hydrogels.

4 Materials and methods

4.1 Materials

Hyaluronic acid sodium salt (HA, M_w= 1.5 × 10^5 g/mol) was purchased from Lifecore (Chaska, MN, USA). Acetic acid, adipic acid dihydrazide (ADH), alginic acid sodium salt from brown algae (AL, low viscosity), 3-amino-1,2-propanediol, boric acid, carbodihydrazide (CDH), 1,1'- carbonyldiimidazole (CDI), collagen type I from human placenta, deuterium oxide (99.9 atom % D, contains 0.05 wt.% 3-(trimethylsilyl)-propionic-2,2,3,3-d4 acid, sodium salt), dimethyl sulfoxide (DMSO), 1-Ethyl-3-[3-(dimethylamino) propyl]carbodiimide (EDC), ethylene glycol, gellan gum (GG, Gelzan^{TM}, M_w= 1,000 kg/mol), glycine ethyl ester hydrochloride, hyaluronic acid sodium salt from streptococcus equi (HA, M_w= 1.5-1.8 × 10^6 g/mol), hyaluronidase from bovine testes (Type I-S, 400-1000 units/mg solid), hydrazine solution (35 wt.% in H_2O), 1-hydroxybenzotriazole (HOBt), hydroxylamine hydrochloride, picrylsulfonic acid solution (5-% (w/v) in H_2O, TNBS), polyvinyl alcohol (PVA, M_w= 27000 g/mol, 98.0-98.8% hydrolyzed), sodium acetate, sodium cyanoborohydride ($NaBH_3CN$), sodium periodate, sodium tetraborate decahydrate, sucrose and t-butyl carbazate (TBC) were purchased from Sigma-Aldrich (St. Louis, MO, USA). Sodium chloride and triethylamine were purchased from J.T. Baker (The Netherlands). Dulbecco's Modified Eagle Medium: Nutrient Mixture F-12 (DMEM/F12) was purchased from Thermo Fisher Scientific (Waltham, MA, USA). Acetate buffer was prepared from sodium acetate and acetic acid, and borate buffer was prepared from sodium tetraborate decahydrate and boric acid. All solvents used were of analytical quality. Milli-Q water was used in synthesis and determinations. Dialysis membranes (Spectra/Por cut-off 1000, 3500, 12000-14000 and 25000 g/mol) were purchased from Spectrum Laboratories, Inc. (Rancho Dominguez, CA, USA).

FITC-dextrans with average molecular weight of 20, 150, 500 and 2000 kDa were purchased from TdB Consultancy AB (Uppsala, Sweden). Table 4.1 shows the hydrodynamic radii of the FITC-dextrans given by the supplier and those calculated based on the equation provided by Hadjiev and Amsden [150],

$$R_h = 0.0163 M_w^{0.52}, \tag{4.1}$$

where R_h is the hydrodynamic radius, and M_w is the molecular weight of solute (dextran).

4.2 Methods

4.2.1 Spectroscopic methods (Studies I-III)

Nuclear Magnetic Resonance (NMR) spectroscopy experiments were performed with a Varian Mercury 300 MHz NMR Spectrometer (Palo Alto, USA). Samples (5 mg)

Table 4.1: Hydrodynamic radii of the FITC-dextrans according to the supplier (R_{h1}), and as calculated based on the equation provided by Hadjiev and Amsden [150] (R_{h2}).

Solute	M_w kDa	R_{h1} nm	R_{h2} nm
FD20	20	3.3	2.8
FD150	150	8.5	8.0
FD500	500	14.7	15.0
FD2000	2000	27.0	30.8

were dissolved in deuterium oxide (600 μL) containing an internal standard (0.05 wt.% 3-(trimethylsilyl)-propionic-2,2,3,3-d4 acid, sodium salt). ^{1}H-NMR spectra of polymer components are shown in Studies I-III. Fourier Transform Infrared (FTIR) spectroscopy experiments were collected on a Perkin Elmer Spectrum One ATR-FTIR Spectrometer (Waltham, MA, USA) in the spectral range of 400 cm^{-1} to 4000 cm^{-1}. Samples (1 mg to 2 mg) were either pressed into KBr (200 mg) tablets or measured with the ATR-unit.

4.2.2 Modification of polymers

4.2.2.1 Introducing aldehyde-groups to hyaluronan, alginate, and gellan gum (Studies I-III)

Synthesis of aldehyde-modified hyaluronan and alginate – method I (Studies II, III)

Aldehyde groups were generated from the vicinal diol groups of HA and AL by using periodate oxidation (Fig. 4.1(a), (b)) according to a previously reported method [51] that was slightly modified. Detailed descriptions of the methods are shown in Studies II and III. Purified polymers were lyophilized to obtain white cotton-like products, HALD and ALALD. ^{1}H-NMR (D_2O, 300 MHz, ppm): HALD: δ 4.47 (m, 1H, H1 of glucose unit), 3.82-3.35 (m, 5H, H2-5 of glucose unit), 2.03 (s, 3H, -NHC(O)CH_3). ALALD: 5.72 (s, 1H, H4-G), 5.26 and 5.18 (s, 1H, hemiacetal protons), 5.00 (s, 1H, H1-G), 4.59 (s, 1H, H1-M and H5-GM), 4.39 (s, 1H, H5-GG). FTIR (Fig. 5.1 (a), Fig. 5.3 (a), KBr pellet, cm^{-1}): HALD: 1721 (ν(C=O) of -C(O)H), 1633 (ν(C=O) of -NHC(O)- and –C(O)OH), 1618 (d(N-H) of -NHC(O)-). FTIR (Fig. 5.1 (b), KBr pellet, cm^{-1}): ALALD: 1732 (ν(C=O) of -C(O)H)), 1634 (ν(C=O) of –C(O)OH).

The DS% of HALD was determined using a method based on a reaction with t-butyl carbazate (TBC) followed by $NaCNBH_3$ [55]. A detailed description of the method is shown in Studies II and III. The DS% of ALALD was determined using a TNBS-based aldehyde assay [151]. A detailed description of the method is shown in Study III.

Synthesis of aldehyde-modified hyaluronan – method II (Study II)

Aldehyde groups were introduced to HA by using selective oxidation of diol-modified HA (Fig. 4.1 (a)), according to a previously reported method [52]. A detailed description of the method is shown in Study II. Purified polymer was lyophilized to obtain a white cotton-like product, HAALD. ^{1}H-NMR (D_2O, 300 MHz, ppm) 2,3-dihydroxypropyl amide derivative of HA: δ 4.53 (br s, 1H), 3.83-3.34 (m, 10H), 2.00 (s, 3H). HAALD (D_2O, 300

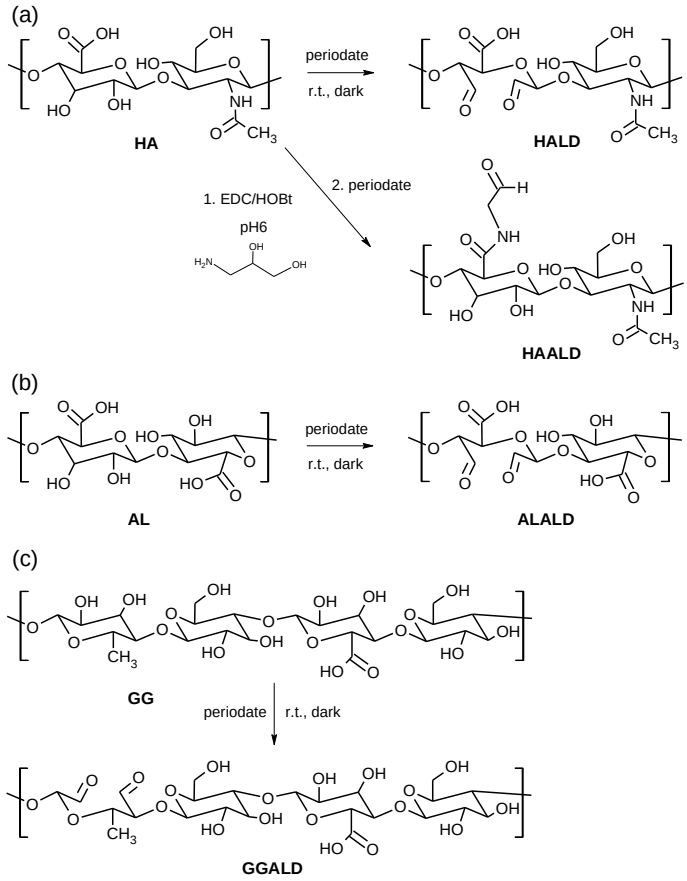

Figure 4.1: Reaction schemes of the aldehyde-modification of (a) HA (HALD and HAALD), (b) AL (ALALD), and (c) GG (GGALD).

MHz, ppm): δ 9.57 (s, 1H), 4.53 (br s, 1H), 3.65 (sharp s, 1H), 3.83-3.34 (m, 10H), 2.01 (s, 3H). FTIR (Fig. 5.3 (b), cm^{-1}): 1732 (ν(C=O) of -C(O)H), 1643 (ν(C=O) of sec. amide), 1617 (d(N-H) of -NHC(O)-), 1558 (d(N-H) of sec. amide).

The DS% of HAALD was determined using a TBC-based method described earlier.

Synthesis of aldehyde-modified gellan gum (Study I)

GG was modified with aldehyde groups using periodate oxidation (Fig. 4.1 (c)) according to a previously reported method [152] that was slightly modified. A detailed description of the method is shown in Study I. Purified polymer was lyophilized to obtain white cotton-like product, GGALD. ^{1}H-NMR (D_2O, 300 Hz, ppm): δ 5.15 (s, 1H, CH-1 of rhamnose unit), 4.72 (s, 1H, CH-1 of glucose unit), 4.56 (s, 1H, CH-1 of glucuronic acid unit), 4.07-3.43 (m, 5H, CH-2-5 of units), 1.3 (s, 3H, CH_3 of rhamnose unit). FTIR (Fig. 5.2, KBr pellet, cm^{-1}): 1733 (ν(C=O) of -C(O)H), 1615 (ν(C=O) of -C(O)OH).

The DS% of GGALD was determined using a previously reported method [9]. A detailed description of the method is shown in Study I.

4.2.2.2 Introducing hydrazide-groups to hyaluronan and poly(vinyl alcohol) (Studies I-III)

Synthesis of hydrazide-modified hyaluronan – method I (Studies I, II)

HA was modified with hydrazide groups by using homobifunctional ADH (10-atom bridge) as a source of the hydrazide unit (Fig. 4.2 (a)) according to a previously reported method [51, 53]. A detailed description of the method is shown in Study I. Purified polymer was lyophilized to obtain white cotton-like product, HAADH. ^{1}H-NMR (D_2O, ppm, 300 MHz, ppm): δ 2.42 (m, 2H, $NHNHCOCH_2$), 2.26 (m, 2H, $CH_2CONHNH_2$), 1.66 (m, 4H, $CH_2CH_2CH_2CH_2$). FTIR (Fig. 5.2, Fig. 5.3 (a), KBr pellet, cm^{-1}): 1706 (ν(C=O) of sec. amide), 1652 (d(N-H) of prim. amine and amide), 1559 (d(N-H) of sec. amine and amide), 1410 (d(CH_2-C=O) of -CH_2), 1078 (ν(C-N) of amine).

The DS% of HAADH components were determined from integration of the ^{1}H-NMR peaks according to [122]. A detailed description of the method is shown in Study I.

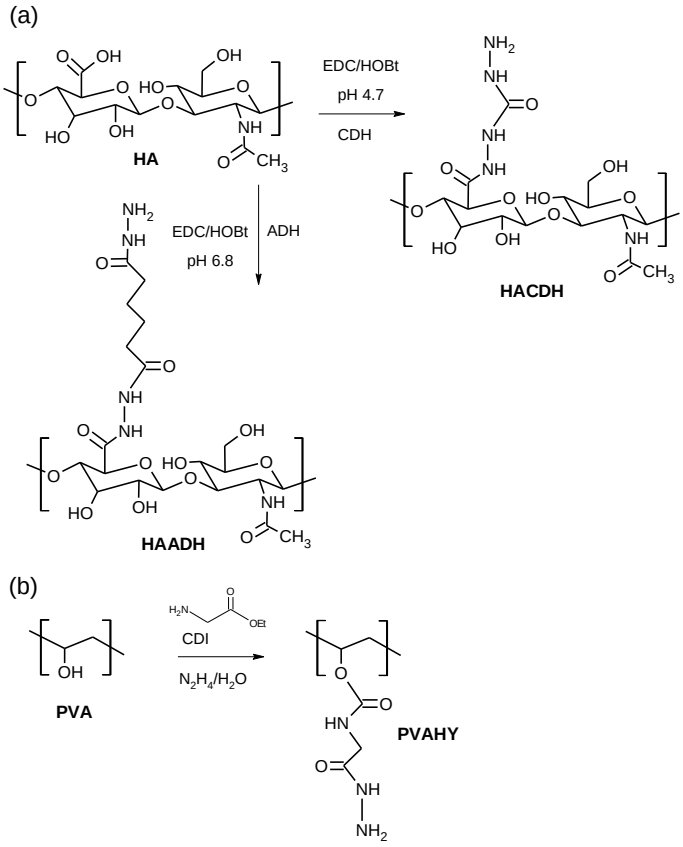

Figure 4.2: Reaction schemes of the hydrazide-modification of (a) HA (HAADH and HACDH), and (b) PVA (PVAHY).

Synthesis of hydrazide-modified hyaluronan – method II (Study II)

Hydrazide groups were introduced to HA by using homobifunctional CDH (5-atom bridge) as a source of the hydrazide unit (Fig. 4.2 (a)) according to previously reported method [54]. A detailed description of the method is shown in Study II. Purified polymer was lyophilized to obtain a white cotton-like product, HACDH. ^{1}H-NMR (D_2O, 300 MHz, ppm): δ 4.54 (br s, 1H), 3.84-3.34 (m, 10H), 2.02 (s, 3H). FTIR (Fig. 5.3 (b), cm^{-1}): 1722 and 1648 (νC=O) of sec. amide), 1611 (d(N-H) of prim. amine), 1557 (d(N-H) of prim. amide), 1415 (d(N-H) of sec. amide), 1028 (ν(C-N) of amine).

The DS% of HACDH was determined with TNBS assay similarly to [54].

Synthesis of hydrazide-modified polyvinyl alcohol (Study III)

PVA was modified with hydrazide groups by using glycine ethyl ester and hydrazine as a source of the hydrazide unit (Fig. 4.2 (b)) according to a previously reported method [41]. A detailed description of the method is shown in Study III. Purified polymer was lyophilized to obtain a white cotton-like product, PVAHY. ^{1}H-NMR (D_2O, 300 MHz, ppm): δ 4.90 (m, 1H, polymer backbone CH of the modified unit), 4.00-3.72 (m, 3H, polymer backbone CH of the unmodified unit + $CH_2CONHNH_2$), 1.92-1.60 (m, 2H, polymer backbone CH_2). FTIR (Fig. 5.1, KBr pellet, cm^{-1}): 1710 (ν(C=O) of –C(O)O-), 1634 (d(N-H) of prim. amine), 1520 (d(N-H) of sec. amine), 1280 (ν(C-O) of –C(O)O-).

The DS% of PVAHY was determined using a spectrophotometric method based on the reaction between TNBS and the primary amines of PVAHY according to [41]. A detailed description of the method is shown in Study III.

4.2.3 Formation of hydrazone crosslinked hydrogels (Studies I-IV)

The chemical structures of hydrogels are shown in Fig. 4.4. Hydrazone crosslinked hydrogels were formed according to Table 4.2 and Fig. 4.3. Briefly, the freeze dried polymer components of hydrogels 1 to 12 were dissolved in 10% sucrose, whereas the polymer components of hydrogels 13 and 14 were dissolved in PBS (pH 7.4). GGALD components were dissolved at 50 ^{o}C, whereas other components were dissolved at room temperature (RT). All solutions were sterilized prior to gelation using Whatman FP 30/0.2 CA-s 0.2 μm (Whatman plc, Little Chalfont, UK) filters. Components A and B (volume ratio of 1:1) were mixed together at RT and the hydrogels were allowed to gelate for at least 1 hour (depending on the characterization method). In the case of HA-HA-based hydrogels, the gelation was shown to occur at RT, as well as at 37 ^{o}C. In this work, the components were allowed to gel at 37 ^{o}C for at least 30 minutes. Additionally, collagen I (col I) was introduced as a third gel component in the HH2 hydrogel. Briefly, col I solution (5 mg/mL in acetic acid, pH $\approx$ 3) was sonicated and then neutralized using 1M NaOH. After neutralization, col I was mixed with HAALD1 component followed by mixing with HACDH component, so that the volume ratio of HA:HA:col I was 2:2:1. For different characterizations, cut syringes were used as molds to ease pushing the sample out. The final polymer concentrations of the hydrogels were from 0.375% to 3% (Table 4.2). Only well gelated samples were chosen for further characterization. For example, all the tested compositions of GG-HA-based hydrogels are collected in Study I, but only those listed in Table 4.2 were chosen for further characterization.

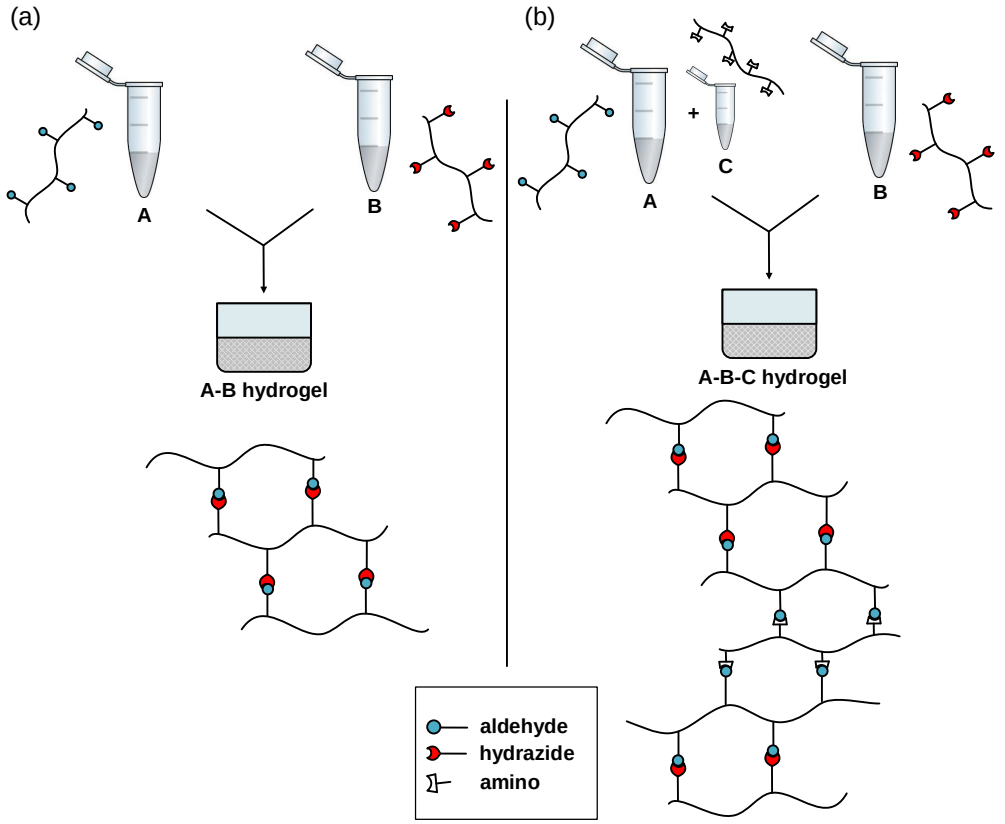

Figure 4.3: Fabrication of hydrazone crosslinked hydrogels. (a) Hydrazone crosslinked HA-PVA-, AL-PVA-, GG-HA- and HA-HA-based hydrogels are fabricated by mixing components A and B together, so that the volume ratio of components A:B is 1:1. (b) Hydrazone crosslinked HA-HA-col I hydrogel is fabricated by first mixing components A and C together, and then mixing them with component B, so that the volume ratio of components A:B:C is 2:2:1. Imine (Shiff base) interactions are also expected to be formed between the amino-groups of component C and aldehyde-groups of component A.

Ca-crosslinked GG gel (GG-Ca) was used as control for GG-based hydrogels, and it was prepared similarly to [32]. Briefly, GG (0.5% w/v) and $CaCl_2$ (10 mM) were dissolved in 10% sucrose and the solutions were heated in a water bath to 37 ^oC prior to gelation. The components were then mixed together at a volume ratio of 3:1 (GG:$CaCl_2$) with a final crosslinker concentration of 2.5 mM.

Table 4.2: Compositions and gelation times of hydrazone-crosslinked HA-PVA-, AL-PVA-, GG-HA- and HA-HA-based hydrogels. The number in the name of the components A is related to the variable DS% of the polymer, and H or L at the end of the name is related to the different molecular weight (H= high M_w= 1.5-1.8 x 10^6 g/mol and L= low M_w= 1.5 x 10^5 g/mol) of the polymer.

Gel #	Gel code	Component A	DS%	Conc. mg/mL	Component B	DS%	Conc. mg/mL	Component C	Conc. mg/mL	Mass ratio A:B(:C)	Vol. ratio A:B(:C)	Polymer conc. %	Gelation Time
1	HP1	HALD1-H	5	20	PVAHY	13	10	-	-	2:1	1:1	1.5	seconds
2	HP1a	HALD1-H	5	10	PVAHY	13	5	-	-	2:1	1:1	0.75	1-5 min
3	HP1b	HALD1-H	5	5	PVAHY	13	2.5	-	-	2:1	1:1	0.375	5 min
4	HP2	HALD2-H	9	25	PVAHY	13	5	-	-	5:1	1:1	1.5	seconds
5	HP3	HALD1-L	5	20	PVAHY	13	10	-	-	2:1	1:1	1.5	seconds
6	HP4	HALD2-L	9	20	PVAHY	13	10	-	-	2:1	1:1	1.5	seconds
7	AP	ALALD	7	20	PVAHY	13	10	-	-	2:1	1:1	1.5	1-5 min
8	GH1	GGALD3	20	20	HAADH-H	30	10	-	-	2:1	1:1	1.5	5 min
9	GH2	GGALD3	20	20	HAADH-L	50	10	-	-	2:1	1:1	1.5	5 min
10	GH3	GGALD4	25	15	HAADH-H	30	15	-	-	1:1	1:1	1.5	5 min
11	GH4	GGALD4	25	15	HAADH-L	50	15	-	-	1:1	1:1	1.5	5 min
12	HH1	HALD2-L	9	20	HAADH-L	50	10	-	-	2:1	1:1	1.5	5 min
13	HH2	HAALD1-L	15	30	HACDH-L	17	30	-	-	1:1	1:1	3	5 min
14	HH2C	HAALD1-L	15	30	HACDH-L	17	30	Collagen I	5	12:12:1	2:2:1	2.5	5 min

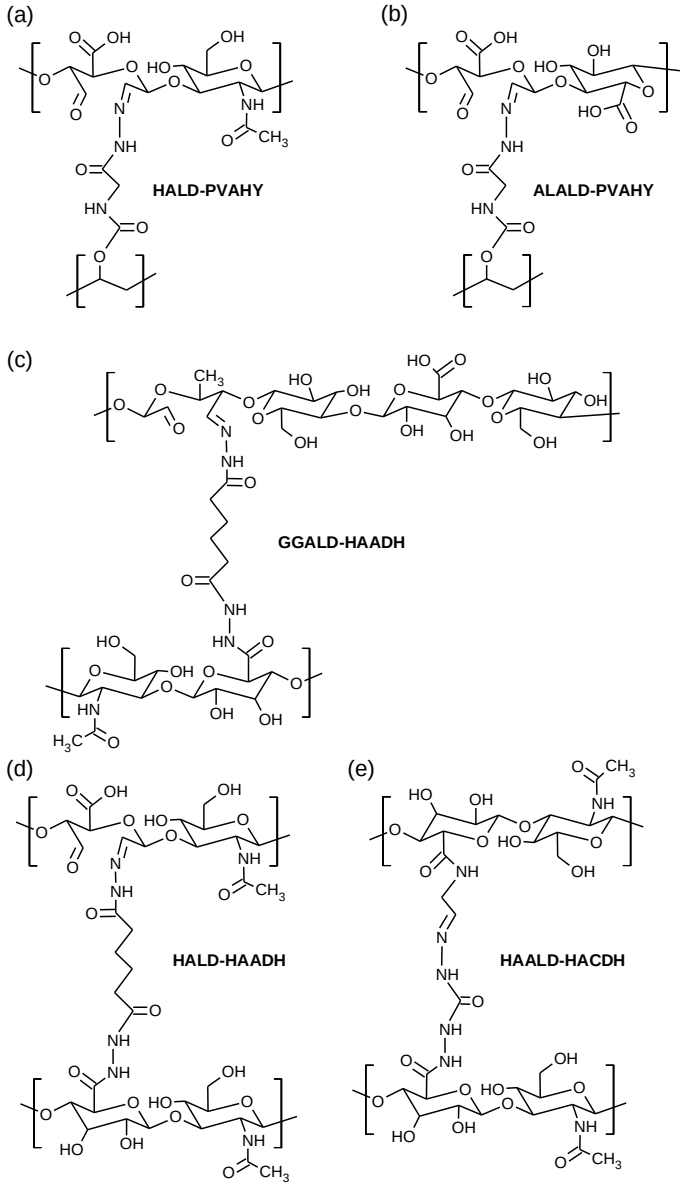

Figure 4.4: Chemical structures of (a) HA-PVA- (HALD-PVAHY), (b) AL-PVA- (ALALD-PVAHY), (c), GG-HA- (GGALD-HAADH), and (d,e) HA-HA-based (HALD-HAADH and HAALD-HACDH) hydrogels.

4.2.4 Characterization of hydrogels

All the methods used to characterize the hydrogels in this thesis are presented in Table 4.3. The table shows in which Study (I-IV) the methods have been presented and used.

Table 4.3: Characterization methods used for hydrazone crosslinked hydrogels (Studies I-IV).

Gel #	Gel code	Gelation time	Chemical structure analysis	Swelling kinetics	Diffusion studies	Rheological studies	Mechanical studies	Enzymatic degradation	Optical properties	*In vitro* cell culture (cornea)	*In vitro* cell culture (neural)
1	HP1	III	III	III	IV	IV	III, IV	III			III
2	HP1a	III	III	III	IV	IV	III, IV	III			III
3	HP1b	III	III	III	IV	IV	III, IV	III			III
4	HP2	III	III	III	IV	IV	III, IV	III			III
5	HP3	III	III	III	IV	IV	III, IV	III			III
6	HP4	III	III	III	IV	IV	III, IV	III			III
7	AP	III	III	III	IV	IV	III, IV	III			III
8	GH1	I	I	I	IV	I, IV	I	I			
9	GH2	I	I	I	IV	I, IV	I	I			
10	GH3	I	I	I	IV	I, IV	I	I			
11	GH4	I	I	I	IV	I, IV	I	I			
12	HH1	II	II	II	IV	II, IV	II	II	II	II	
13	HH2	II	II	II	IV	II, IV	II	II	II	II	
14	HH2C	II	II	II	IV	II, IV	II	II	II	II	

4.2.4.1 Gelation time (Studies I-III)

A tube tilt test [62] was used to determine the gelation time of the hydrogels. The gel solution was put into a tube that was tilted until the solution stopped flowing (gel point).

4.2.4.2 Chemical structure (Studies I-III)

FTIR was used to determine the chemical structure of the hydrogels. Hydrogel samples were freeze dried and they were either pressed into KBr tablets and measured with a FT-IR spectrometer (a Perkin Elmer Spectrum One FT-IR Spectrometer, Waltham, MA, USA) in the spectral range of 400 cm^{-1} to 4000 cm^{-1}, or measured with the ATR-unit.

4.2.4.3 Swelling kinetics (Studies I-III)

The swelling kinetics of the HA-PVA-, AL-PVA- and HA-HA-based hydrogels were studied in cell culture medium (DMEM/F12). Freshly made hydrogel samples were (100 μL, 3 parallel samples) weighed and placed into DMEM at 37 ^{o}C. The samples were weighed at specific time points, and the swelling ratio (SR) was calculated from the following equation:

$$SR = \frac{W_{swollen} - W_{initial}}{W_{initial}} \times 100\%, \tag{4.2}$$

where $W_{swollen}$ is the mass of swollen hydrogel (at a given time point), and $W_{initial}$ is the mass of freshly made wet hydrogel. When the hydrogel mass remained constant, the equilibrium was considered to have been reached.

The swelling-deswelling kinetics of GG-HA-based and GG-Ca (control) hydrogels were studied in deionized water and in PBS (osmolarity and ion concentrations of the solutions match those of the human body (isotonic)). The studies were carried out as described above. Furthermore, the ionic nature of GG-HA-based hydrogel shrinking was tested similarly to [33]. Briefly, the hydrogel was first immersed in water for 30 minutes, then in PBS for 20 hours, and again immersed in water for 30 minutes. Hydrogel mass variation (%) was illustrated at different time points.

4.2.4.4 Diffusion properties (Study IV)

Diffusion within the hydrogels was studied using FRAP experiments, where the uptake of the fluorescence labeled dextran molecules of different sizes (20, 150, 500, and 2000 kDa) into the hydrogels was studied. FRAP experiments were performed using a Zeiss LSM780 Laser Scanning Confocal Microscope (Carl Zeiss, Germany) and a Plan-Apochromat 63x/1.2 water immersion objective (Carl Zeiss, Germany). A more detailed description of the experiment is shown in Study IV. Five parallel FRAP experiments were conducted with each hydrogel containing different sized dextrans. ImageJ was used to construct an average shape and intensity profile of the circular region of interest (ROI). The FRAP data were then exported to Excel (Microsoft, Redmond, USA). The normalization of the data was performed according to [153]. FRAP recoveries were modeled with Virtual Cell (VCell) software [154]. A more detailed description of the modeling is shown in Study IV. In addition to the specified diffusion coefficients, the half maximum ($\tau_{1/2}$, Fig. 2.11) and percent recovery (Eq. 2.1, Fig. 2.11) were determined from the FRAP-curves.

4.2.4.5 Rheological properties (Studies I, II, IV)

Rheological measurements of the hydrogels were performed using a rotational Haake RheoStress RS150 rheometer equipped with Rheowizard 4.3 software (ThermoHaake, Germany) with cone-plate geometry (20 mm diameter) and a gap of 0.8 mm. Hydrogel samples (500 μL, 3 parallel samples) were prepared into molds (20 mL cut syringe) covered with Parafilm and allowed to gelate for 24 hours to obtain uniform hydrogels. All rheological experiments were performed at 37 ^{o}C in the oscillatory mode. Amplitude sweep (γ= 0.01 to 10, ω= 1 Hz) and frequency sweep (ω= 0.1 Hz to 10 Hz, γ= 0.03 or 0.1 chosen from the linear viscoelastic region (LVR) based on the amplitude sweep measurement) were used.

4.2.4.6 Mechanical properties (Studies I-III)

Compression measurements were performed using a BOSE Electroforce Biodynamic 5100 machine equipped with a 225 N load sensor and Wintest 4.1 software (Bose Corporation, Eden Prairie, Minnesota, USA). Hydrogel samples (875 μL, 5 parallel samples) were prepared into molds (5 mL cut syringe) covered with Parafilm and allowed to gelate for 24 hours to obtain uniform hydrogels. New Zealand white rabbit (age 10 weeks, male) midbrain and heart samples (obtained from the animal experiments conducted at Tampere University Medical School, University of Tampere) of the same size were tested as a reference. The surface of the platens was covered with Parafilm to avoid slipping of the sample. The samples were compressed using unconfined compression at a rate of 10 mm/min to at least 65% to 70% strain in the air at RT.

The measuring data were imported to MS Excel and plotted as stress-strain curves. The data obtained from a stress-strain curve were used to estimate the stiffness of the hydrogel according to the method described in Section 2.3.6.

4.2.4.7 Enzymatic degradation (Studies I-III)

The enzymatic degradation of the HA-containing hydrogels was studied using hyaluronidase-enzyme (HAse). Hydrogel samples (100 μL, 3 parallel samples) were weighed, placed into HAse solution (20 U/mL to 50 U/mL, in PBS), and incubated at 37 ^{o}C until the hydrogels were completely degraded (visually no gel left to weigh). The hydrogels were weighed at specific time points, and their residual masses (%) were determined. The data were plotted as mass loss curves. Control samples, without HAse, were used to show that the degradation was not only due to simple hydrolysis.

4.2.4.8 Optical properties (Study II)

Refractive indices of the HA-HA(-col I) hydrogels were determined using surface plasmon resonance equipment Navi 210A (BioNavis, Tampere, Finland). The goniometer and light source of the device were used to scan the critical angle of total internal reflection between glass and hydrogel. A glass slide (BK7 glass) with a known refractive index was used for device calibration and measurements. After calibration, the flow cell of the device was filled with a hydrogel sample. A curve that shows the reflection coefficient as a function of the angle of incidence was obtained from the measurement. The refractive indices of the hydrogels were determined from the curves by using Snell's law with the critical angle condition:

$$n_{gel} = n_{glass} \sin(\alpha), \tag{4.3}$$

where n_{gel} and n_{glass} are the refractive indices of the hydrogel and glass slide (n_{glass}= 1.514 [155]), respectively, and α is the angle of incidence determined from the curve.

The optical transparency of the hydrogels was evaluated using a spectrophotometer (UV-VIS-NIR Spectrophotometer UV-3600Plus, Shimadzu, Kyoto, Japan) operating at the visible wavelength range (400 nm to 700 nm). Hydrogel samples (900 μL, thickness 10 mm) were prepared directly into the 1.5 mL semi-micro cuvettes. The hydrogel films (diameter 10 mm $\times$ thickness 1 mm) were also photographed to show visually their optical clarity and transparency.

4.2.5 *In vitro* cell culture

4.2.5.1 *In vitro* cell culture studies using human adipose stem cells (Study II)

The cell culture experiments with HA-HA-based hydrogels were conducted using human adipose stem cells (hASCs, isolated from adipose tissue samples from a female donor undergoing elective plastic surgery at Tampere University Hospital (Tampere, Finland)). The studies were conducted in collaboration with the Eye group from the University of Tampere (BioMediTech Institute and Faculty of Medicine and Life Sciences). Cells were encapsulated in hydrogels at passages 4-6. Prior to encapsulation, hASCs were detached from cell culture flasks and collected by centrifugation. Cells were resuspended in cell culture medium, counted, and the appropriate number of cells required for each hydrogel were centrifuged to a pellet. Supernatant was removed, and cell pellets were mixed by thorough pipetting into the HALD or HAALD component at a concentration of 4×10^6 cells/mL, with final hydrogel volume of 100 μL. The hydrogels were then formed in PDMS molds as described in Section 4.2.3. The cell-laden hydrogels were transferred onto tissue culture plates for further *in vitro* culture. Fresh hASC medium was changed three times a week. The viability of the hydrogel-encapsulated hASCs was assessed at time points 1 day, 3 days, 7 days, and 10 days after encapsulation. Resazurin-based measurement of metabolic activity was performed using PrestoBlue Cell Viability Reagent, and qualitative analysis of viable cells using LIVE/DEAD viability/cytotoxicity kit for mammalian cells (both from Thermo Fisher Scientific). A more detailed descriptions of the cell culture experiment and cell viability measurements are shown in Study II.

For implantation of hydrogels to porcine corneas, the corneas were mounted on a Barron artificial anterior chamber (Katena products Inc., Denville, NJ, USA) where the operation was performed. Stromal cavities were formed, where the hydrogels with hASCs (n = 5) and without any cells (n = 2) were then cast as described above and in Section 4.2.3 with a final hydrogel volume of 50 μL. After gelation, the corneas were removed from the artificial anterior chamber, placed back into culture plates and covered with silicone contact lenses (EyeQ One-Day Premium, Cooper Vision, Hamble, UK). To evaluate hASC incorporation into the corneal stroma, immunohistochemical staining for the pan-human marker TRA-1-85 was performed. A more detailed descriptions of the cornea organ culture experiment is shown in Study II.

4.2.5.2 *In vitro* cell culture studies using human pluripotent stem cell-derived neuronal cells (Study III)

The cell culture experiments with HA-PVA- and AL-PVA-based hydrogels were conducted using human pluripotent stem cell derived neuronal cells. The studies were conducted in collaboration with the Neuro group from the University of Tampere (BioMediTech

Institute and Faculty of Medicine and Life Sciences). Human embryonic stem cell (hESC) lines Regea08/023 and Regea11/013, and human induced pluripotent stem cell (iPCS) lines HEL 24.3 (kindly donated by Prof. Timo Otonkoski, University of Helsinki, Finland), and 04511.WT were used. The cells were plated as previously described [156, 157]. Briefly, pre-differentiated neuronal cell aggregates were mechanically cut into small cell clusters. These freshly cut small clusters were then plated either on top of the hydrogel surface or encapsulated inside the hydrogel. 2D growth controls were plated on top of mouse laminin (10 μg/mL) coated cell culture plastic. When culturing cells on top of the hydrogel surfaces, the gelation was performed directly into the cell culture well similarly as described in Section 4.2.3 and mixed using a pipette tip. After complete gelation, the cells were plated on top of the hydrogel. When preparing 3D cultures with cells encapsulated inside the hydrogel, the cell clusters were mixed into PVAHY component prior to gelation. The cells were then cultured for two weeks either on top of or encapsulated inside the hydrogel. Cell culture media (NDM without FGF) was changed three times a week and cells were monitored during the culturing. After two weeks in culture, the cells underwent viability analysis and immunocytochemical analysis as previously described [157]. Detailed descriptions of the cell culture experiment and molecular biology analysis are shown in Study III.

4.2.6 Statistical analysis (Studies I-IV)

Statistical data analyses were performed with MATLAB (Statistics and Machine Learning Toolbox^{TM}). All the quantitative data are presented as mean and standard deviation. A non-parametric Kruskal-Wallis test was used to determine whether there were statistically significant differences within the mechanical, rheological, and FRAP data set. A Wilcoxon rank sum test (equivalent to Mann-Whitney U test) was used to analyze the specific sample pairs for statistically significant differences. Due to a relatively low n, the assumption of normally distributed data would be unjustifiable, and therefore non-parametric testing was chosen. When more than two groups were compared, the resulting p values were multiplied by the number of comparisons performed (Bonferroni correction). A p-value of < 0.05 was considered significant.

5 Results

5.1 Modification of polymers with complementary reactive groups

Complementary reactive aldehyde- and hydrazide-groups were introduced to polymers. The modifications were confirmed with ^{1}H-NMR and FTIR analysis.

Aldehyde-modification of hyaluronan, alginate, and gellan gum

HA, AL, and GG were periodate oxidized by cleaving the C2-C3 bond from the polysaccharide chain to obtain aldehyde-groups containing HALD, ALALD, and GGALD components with variable DS% and molecular weight (Table 4.2). In the ^{1}H-NMR spectra of HALD (Study III) and GGALD (Study I), the aldehyde peak (9 ppm to 10 ppm) was invisible. One explanation for this can be that in water aldehydes exist in equilibrium with their hydrated forms. They may also form reversible hemiacetals when reacting with some hydroxyl groups of polymers [158]. Furthermore, the DS% of the components were rather low, which made it more difficult to observe the aldehyde signal. In the FTIR spectra of HALD (Fig. 5.1 (a), Fig. 5.3 (a)) and GGALD (Fig. 5.2), the aldehyde shoulder (HALD: 1720 cm^{-1}, GGALD: 1733 cm^{-1}) was observed. The signal partly overlaps with the carboxyl and amide C=O stretching (HALD: 1633 cm^{-1}, GGALD: 1615 cm^{-1}) signal, which makes observation more difficult. In the ^{1}H-NMR spectrum of the ALALD component (Study III), two new peaks at 5.26 ppm and 5.19 ppm were found. Those corresponded to a hemiacetalic proton that is formed when aldehyde reacts with neighboring hydroxyl groups of alginate. In the FTIR spectrum of ALALD (Fig. 5.1 (b)), a new peak appeared at 1147 cm^{-1} (C-O-C), whereas the peaks at 879 cm^{-1} and 818 cm^{-1} (C-O-C) weakened. The aldehyde shoulder at 1732 cm^{-1} was also found.

In addition, the aldehyde-groups were introduced in HA using an alternative method, where selective oxidation of diol-modified HA was used. The modification was conformed as previously described. In the ^{1}H-NMR spectrum of HAALD (Study II), a barely observable aldehyde peak (9.57 ppm) was detected. The presence of aldehyde-groups was confirmed based on the FTIR-spectrum (Fig. 5.3), where the typical aldehyde shoulder (1732 cm^{-1}) was detected.

Hydrazide-modification of hyaluronan and polyvinyl alcohol

HA was modified with hydrazide-groups using either homobifunctional ADH (10-atom bridge) or CDH (5-atom bridge) as a source of the hydrazide unit. Two HAADH components (different DS% and molecular weight), as well as one HACDH component

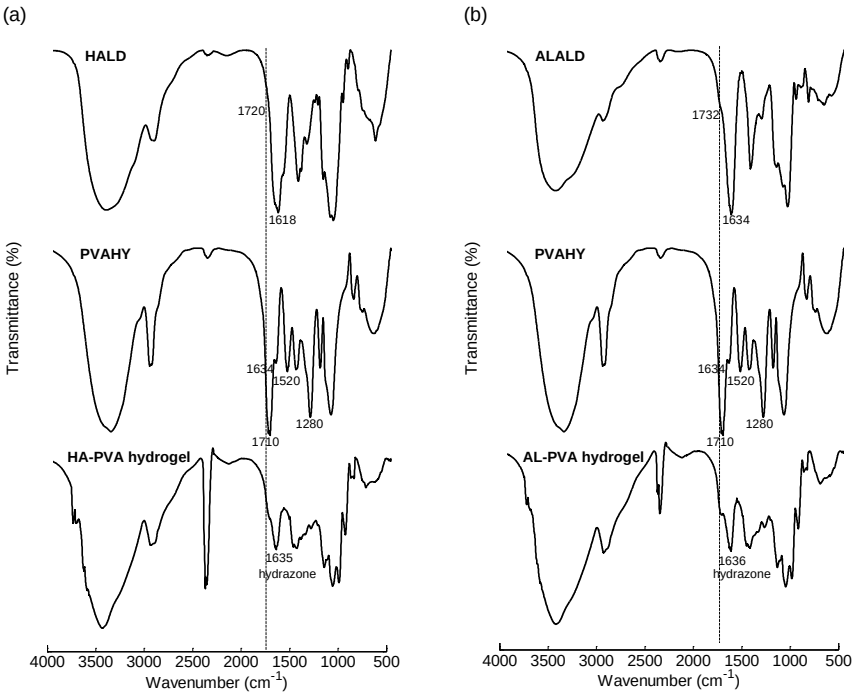

Figure 5.1: Chemical structure analysis of HA-PVA- and AL-PVA-based hydrogels and their polymer components. FTIR spectra of (a) HA-PVA-, and (b) AL-PVA-based hydrogels, including their components HALD, PVAHY, and ALALD. The peak of 2300 cm^{-1} was caused by a CO_2 problem with the Spectrometer and was not related to the samples.

were obtained (Table 4.2). In the ^{1}H-NMR spectrum of HAADH (Study I), new CH_2 peaks of the modified hydrazide unit were observed at 2.42 ppm, 2.26 ppm, and 1.66 ppm, whereas the ^{1}H-NMR spectrum (Study II) of HACDH hardly differed from that of non-modified HA, since there were no CH_2 groups in the hydrazide unit of HACDH. In the FTIR spectrum of HAADH (Fig. 5.2, Fig. 5.3 (a)), strong amide C=O stretching (1706 cm^{-1}) and amine/amide N-H deformation (1652 cm^{-1} and 1559 cm^{-1}) signals from the hydrazide unit were observed. In the FTIR-spectrum of HACDH (Fig. 5.3 (b)), signals from the hydrazide unit were detected that included strong amide C=O stretching (1722 cm^{-1}) and amide N-H deformation (1611 cm^{-1} and 1557 cm^{-1}) signals.

PVA was modified with hydrazide-groups by using glycine ethyl ester and hydrazine as a source of hydrazide unit. The ^{1}H-NMR spectrum of PVAHY (Study III) showed new CH peaks of the polymer backbone and the CH_2 of the modified hydrazide unit around 4.90 ppm and 4.00 ppm to 3.72 ppm. In the FTIR spectrum (Fig. 5.1, the carbonyl C=O and C-O stretching signals (1710 cm^{-1} and 1280 cm^{-1}) and the amine N-H deformation signals (1634 cm^{-1} and 1520 cm^{-1}) of the modified unit were observed. There was also a C=O stretching signal in the spectrum of the unmodified PVA, but this was due to the acetate groups left over from the manufacturing process.

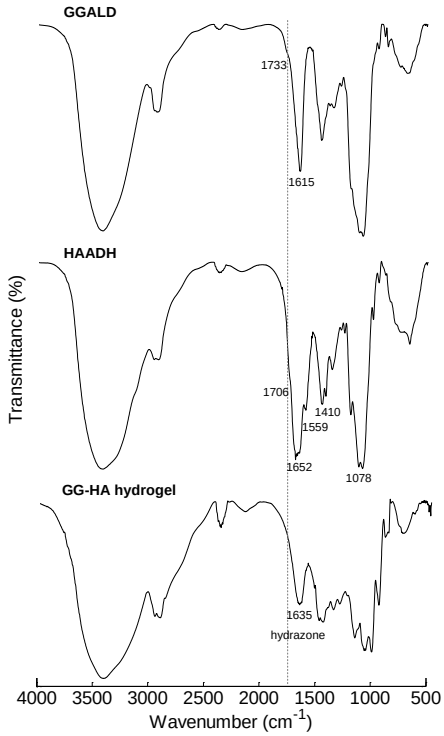

Figure 5.2: Chemical structure analysis of GG-HA-based hydrogels and their polymer components. FTIR spectra of GG-HA-based hydrogel, including its components GGALD and HAADH.

5.2 Formation of hydrazone crosslinked polysaccharide-based hydrogels

Hydrazone crosslinked HA-PVA-, AL-PVA-, GG-HA- and HA-HA-based hydrogels were formed from complementary reactive polymer components according to Table 4.2. Hydrogels with variable properties were obtained by varying the DS%, molecular weight, or the ratio of the polymer components, as well as the polymer concentration of the hydrogel. A decrease in the polymer concentration of HP1-based hydrogels led to softer hydrogels and less constant shape due to a higher water content and a lower number of crosslinkable groups. AL-PVA hydrogel and other HA-PVA-based hydrogels had a stronger gel structure with better shape constancy that was presumably due to a higher crosslinking density of HP2, HP3, and HP4 hydrogels. In fact, HP3 and HP4 hydrogels looked more crystalline and fragile when compared with AP, HP1, and HP2 hydrogels. In order to find the best GG-HA-based hydrogel formulations, several gelation tests were made by changing the molecular weight of the HAADH component, the DS% of polymers, and the ratio of the polymer components (Study I). The four GG-HA-based hydrogels that were chosen for characterization were transparent and looked the same as the ionically crosslinked control GG-Ca gel. The only drawback was the high viscosity of the HAADH component solution, which made it more difficult to filter and handle. This could have been avoided by filtering the polymer solution prior to lyophilization and working aseptically afterwards, or by using other safe sterilization methods that do not

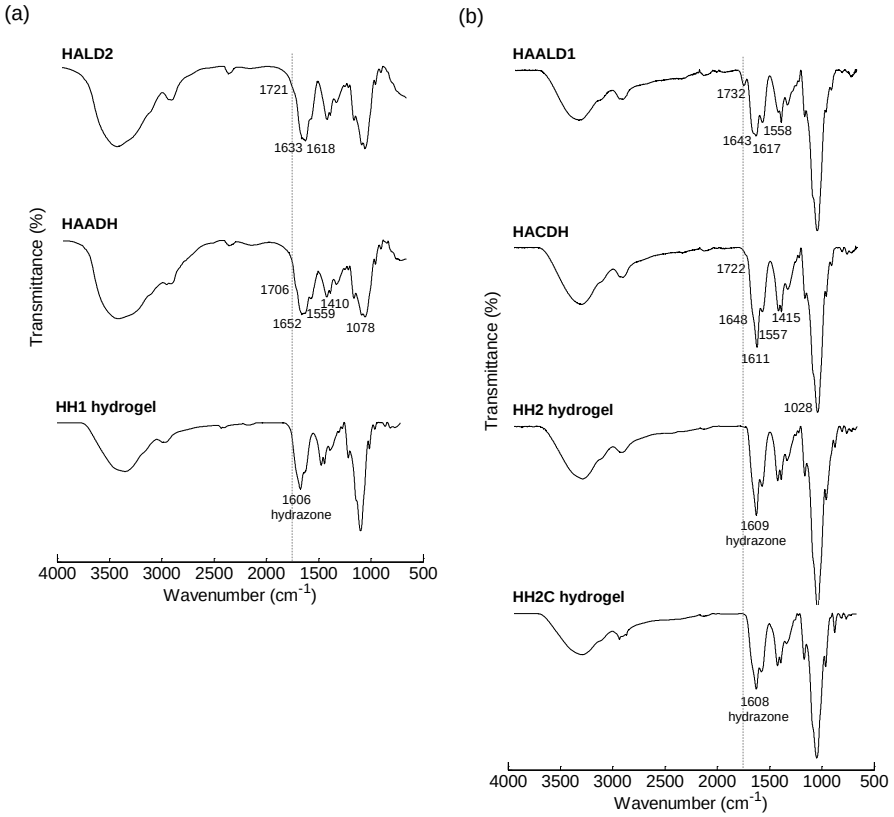

Figure 5.3: Chemical structure analysis of HA-HA-based hydrogels and their polymer components. (a) FTIR spectra of HH1 and (b) HH2, and HH2C hydrogels, including their components HALD2, HAADH, HAALD1, and HACDH.

degrade the polymer structure. The HA-HA-based hydrogels looked similar to previous gels. The HH2 hydrogel was preferred due to its more stable structure and less invasive modification of HAALD component, and thus the effect of col I addition was only tested with this hydrogel. The gelation of HH2 hydrogels was successful only when PBS or cell culture medium solutions were used, whereas HH1 hydrogel gelated only in deionized water or in 10% sucrose. Sucrose was used to make the osmotic pressure more suitable for the cells in cell culture experiments. Therefore it was used in other experiments too.

A stickiness to different surfaces, such as plastic or glass, and a clear and transparent appearance was common for all tested hydrogels, except for control GG-Ca gel. The hydrogels presented in Table 4.2 were chosen based on a preliminary gelation study, which showed, for example, that HA-PVA- and AL-PVA-based hydrogels containing PVAHY component with lower DS%, or ALALD component with higher DS% did not gelate well. Moreover, the gelation of GG-HA-based hydrogels was poor or there was no gelation with GGALD1 or GGALD2 components (lower DS%). The gelation was more successful with higher DS% components (Study I).

5.3 Characterization of hydrazone crosslinked hydrogels

5.3.1 Gelation time of hydrogels

The gelation times of the hydrogels (Table 4.2) were determined using a tube tilt test, which is a simple method, although the drawback is that it only gives estimated results. The gelation time of HA-PVA-based hydrogels varied from seconds to minutes, and the time taken depended on the polymer concentrations and the properties of the gel components. The gelation time of the AP hydrogel was around 30 seconds. GG-HA- and HA-HA-based hydrogels gelated in 3 minutes to 5 minutes with no clear difference between them. The control GG-Ca gel started to gelate in a few minutes, but it took a longer time to fully gelate compared with the GG-HA-based hydrogels. Since GG-HA- and HA-HA-based hydrogels had reasonable gelation times, it was possible to prepare them either by pipetting the gel solution a few times back and forth in the tip or by using a double syringe system. This enhances the mixing of the gel components, and hence a more homogeneous gel structure can be achieved.

5.3.2 Chemical structure of hydrogels

The chemical structures of the hydrogels were determined using FTIR. The FTIR spectra of the HA-PVA- and AL-PVA-based hydrogels (Fig. 5.1) showed the disappearance of an aldehyde signal (HALD: 1720 cm^{-1}, ALALD: 1732 cm^{-1}), and the appearance of a hydrazone C=N stretching signal at 1635 cm^{-1} for the HA-PVA-based hydrogels and 1636 cm^{-1} for AL-PVA-based hydrogel. The change in the amine/amide signal (PVAHY: 1634 cm^{-1}) is not easily detected because it overlaps with the hydrazone signal. Similarly, the FTIR spectrum of the GG-HA-based hydrogel (Fig. 5.2) showed the disappearance of an aldehyde signal at 1733 cm^{-1} and the appearance of a new signal at 1635 cm^{-1}, indicating hydrazone crosslinking (C=N stretching). The change of this signal is not so easy to verify, since the amide signal at 1652 cm^{-1} overlaps with the hydrazone signal. The appearance of a hydrazone C=N stretching signal at 1609 cm^{-1}, 1608 cm^{-1}, and 1606 cm^{-1} for HH2, HH2C, and HH1 hydrogels, respectively, and the disappearance of an aldehyde signal at 1732 cm^{-1} for HH2 and HH2C hydrogels, and at 1721 cm^{-1} for HH1 hydrogel confirmed the presence of hydrazone crosslinking (Fig. 5.3).

5.3.3 Swelling and deswelling kinetics of hydrogels

5.3.3.1 Swelling and deswelling kinetics of HA-PVA-, AL-PVA-, and HA-HA-based hydrogels in cell culture medium

The swelling kinetics of the HA-PVA-, AL-PVA-, and HA-HA-based hydrogels were determined by quantifying the swelling ratio as a function of time. The swelling tests were conducted in cell culture medium (DMEM/F-12) in order to determine hydrogel swelling behavior in the cell culture environment. The swelling ratios (SR, %) of the hydrogels are shown in Fig. 5.4. The results showed that in cell culture medium AL-PVA- and some HA-PVA-based hydrogels started to shrink in the presence of divalent ions (Fig. 5.4 (a)). The HP1 and HP3 hydrogels (HALD: DS%= 5) slightly swelled in cell culture medium, whereas other hydrogels shrank. The lower the polymer concentrations of the hydrogel were, the more the hydrogels shrank. The SR was higher with hydrogels containing a lower molecular weight HALD component when compared with similar gels containing a higher molecular weight HALD component. The AP hydrogel shrank the most. Similar behavior was also observed during the cell culture experiments. With

HA-HA-based hydrogels, the results revealed a difference in the stability of the hydrogels. Both HH2 and HH2C hydrogels were stable even after 48 hours, whereas HH1 hydrogel degraded in hours, and after 24 hours there was no gel left to weigh. Both HH2 and HH2C hydrogels swelled considerably. After 48 hours, the SR of the HH2 hydrogel was over 200%, whereas that of the HH2C hydrogel was approximately 150%. However, the addition of col I lowered the SR by approximately 20% at each data point. Overall, HA-HA-based hydrogels swelled considerably more in cell culture medium than HA-PVA- and AL-PVA-based hydrogels.

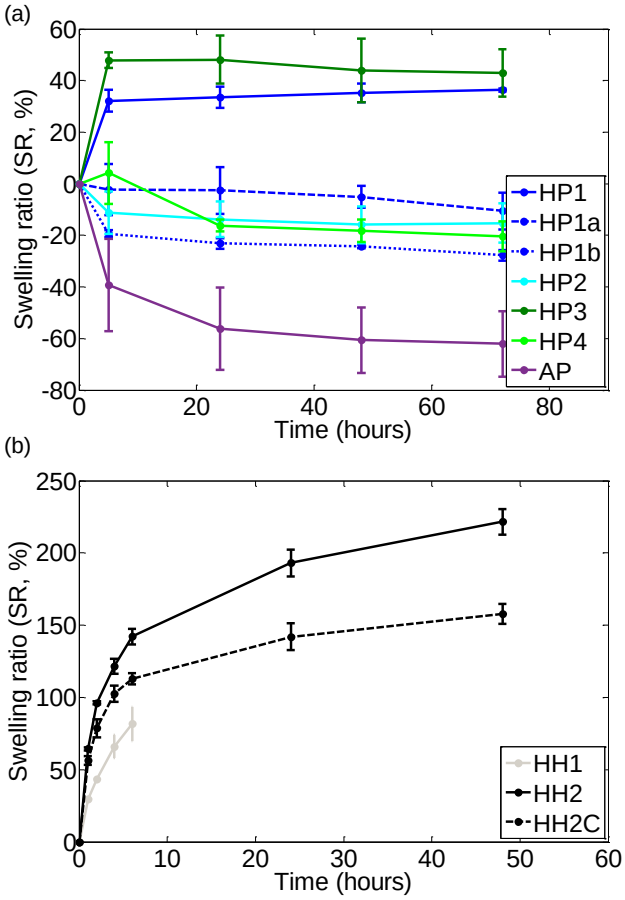

Figure 5.4: Swelling kinetics of HA-PVA-, AL-PVA- and HA-HA-based hydrogels. Swelling ratios (SR,%) of the initially wet (a) HA-PVA- and AL-PVA-based hydrogels and (b) HA-HA-based hydrogels in cell culture medium (DMEM/F12). The mean (n= 3) and standard deviation bars are shown.

5.3.3.2 Swelling and deswelling kinetics of GG-HA-based hydrogels in PBS and deionized water, and ionic nature of hydrogel shrinking

The swelling and deswelling kinetics of the GG-HA-based hydrogels in deionized water and PBS are presented in Fig. 5.5. The results showed that in water GH2 and GH4 hydrogels (contain a HAADH-L component) swelled only slightly, leading quickly to the

degradation of the structure, whereas GH1 and GH3 hydrogels (contain a HAADH-H component) swelled more without degrading. On the other hand, in PBS, GH1 and GH3 hydrogels shrank instead of swelling, whereas GH2 and GH4 hydrogels slightly swelled instead of shrinking. However, no significant difference between the GGALD3 and GGALD4 component-containing hydrogels was observed in water or PBS. A control GG-Ca gel shrank the most in PBS, but in water it hardly swelled.

PBS can form ionical crosslinks with GG, since it contains cations. The ionic nature of GG-HA-based hydrogel shrinking was confirmed by immersing the hydrogels by turns in water and PBS. The results (Fig. 5.6) showed a swelling-deswelling-swelling behavior for all the GG-HA hydrogels. A control GG-Ca gel was tested similarly. However, due to the degradation of the gel between timepoints 2 and 3, it was not included in Fig. 5.6.

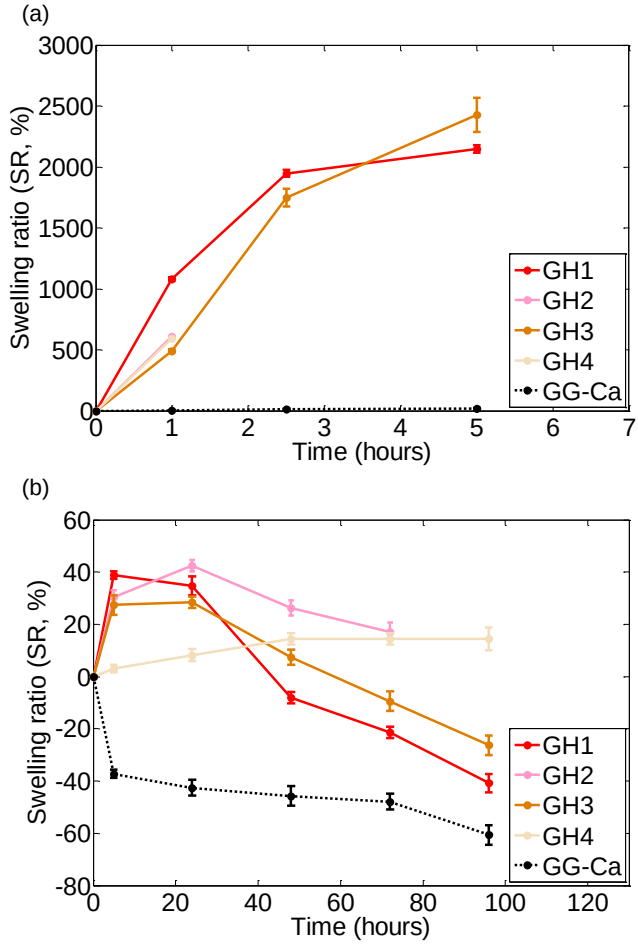

Figure 5.5: Swelling and deswelling kinetics of GG-HA-based hydrogels. Swelling ratios of hydrogels (a) in deionized water and (b) in PBS. The mean (n = 3) and standard deviation bars are shown.

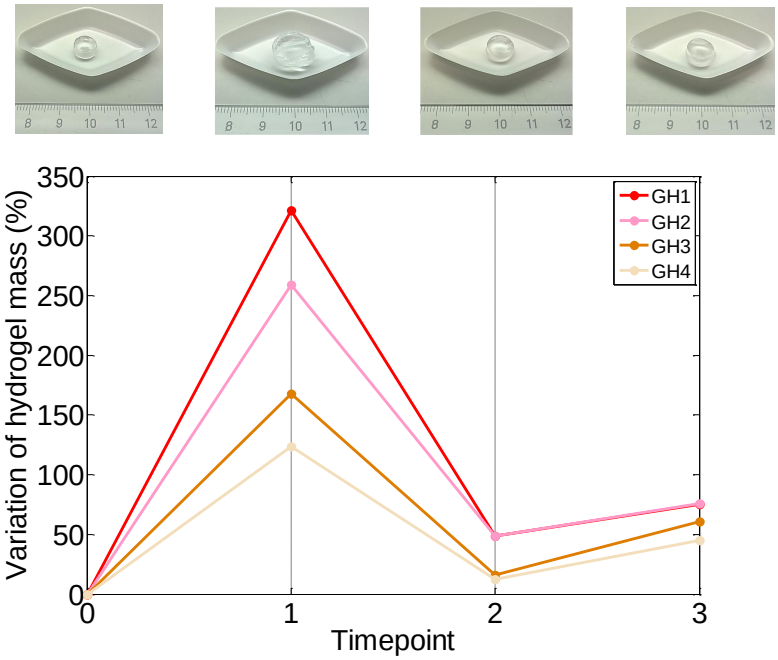

Figure 5.6: The ionic nature of the GG-HA-based hydrogel shrinking. Timepoint 1 was taken after swelling in water for 30 minutes, timepoint 2 after shrinking in PBS for 20 hours, and timepoint 3 after swelling in water for 30 minutes. The GH1 hydrogel is shown here as an example.

5.3.4 Diffusion properties of hydrogels

Diffusion within the hydrogels was studied by FRAP. Normalized fluorescence recovery curves of different sized FITC-dextrans (20, 150, 500, and 2000 kDa) in hydrazone crosslinked HP1, AP, GH4, and HH2C hydrogels are shown in Fig. 5.7. Different phases of the FRAP experiment are presented next to the curves. The normalized fluorescence recovery curves of other HA-PVA-, GG-HA-, and HA-HA-based hydrogels are shown in the Supplementary Material of Study IV.

The half maximums ($\tau_{1/2}$) were determined from the FRAP curves, and they are presented in Fig. 5.8. Shorter $\tau_{1/2}$ indicates faster recovery. In the case of HA-PVA-based hydrogels (Fig. 5.8 (c)), the recovery was faster with HP1-based hydrogels compared with the others. Also, the recovery was faster when the polymer concentration of HP1-hydrogel decreased, whereas it was slower when the M_w of the HALD-component decreased (HP3 and HP4 hydrogels), or when the DS% of the HALD-component increased (HP2 and HP4 hydrogels). With GG-HA hydrogels (Fig. 5.8 (d)), the recovery was slower when the DS% of the HAADH- or GGALD-component increased (GH2 and GH4 hydrogels). In the case of HA-HA-based hydrogels (Fig. 5.8 (b)), the recovery was slower when the polymer concentration increased (HH2-based hydrogels), as well as when collagen was added (HH2C hydrogel). When the HH1 hydrogel was compared with similar HP4 and GH2 hydrogels, the recovery in the HP4 hydrogel was faster, whereas in the GH2 hydrogel it was the opposite. The recovery in the AP hydrogel (Fig. 5.8 (c)) was faster than in HP2, HP3, HP4, GG-HA-, HA-HA-based hydrogels, but slower than in HP1-

based hydrogels. The recovery in GG-HA-based hydrogels was slower compared with HA-PVA-based and AP-hydrogels, but faster compared with HA-HA-based hydrogels. The recovery in HA-HA-based hydrogels was slower compared with HA-PVA-based and AP hydrogels.

Since the use of half maximum in the FRAP quantification has been criticized (because it also depends on the geometry and the size of the bleached region) [83], more accurate Virtual Cell (VCell) modeling was used to simulate the fluorescence recovery kinetics. The diffusion coefficients were determined by fitting the simulated recovery kinetics with the measured FRAP data. The diffusion coefficients of FITC-dextrans in different hydrogels are collected in Table 5.1. Overall, the diffusion coefficient decreased with larger dextran size. With 20 kDa dextrans, the diffusion coefficients in certain HA-PVA hydrogels (HP1a and HP1b hydrogels) were close to that of water. When the dextran size was larger, the diffusion coefficients decreased significantly and were far from that of water (Table 5.1). The following results are based on the diffusion coefficients determined for the larger dextran sizes, since those sizes were more interesting considering the possible restrictions. When HA-PVA-based hydrogels were compared, the diffusion coefficients increased when the polymer concentration of the hydrogel was lower (HP1a and HP1b hydrogels). The change in the M_w or DS% of the HALD-component did not significantly affect the diffusion coefficient. The change in the DS% of the HAADH- or GGALD-component of GG-HA-based hydrogels did not affect the diffusion coefficient either. In HA-HA hydrogels, the diffusion coefficient was lower when the polymer concentration of the hydrogel increased (HH2-based hydrogels), whereas the diffusion coefficient remained almost unchanged when collagen was added. When the HH1 hydrogel was compared with similar HP4 and GH2 hydrogels, the diffusion coefficients of dextrans in the HH1 hydrogel were higher in both cases. Similar diffusion coefficient values were found for dextrans in HA-PVA, HA-HA, and GG-HA hydrogels, whereas in AP hydrogel the diffusion coefficient was the highest among all the hydrogels. Overall, the difference between the hydrogels became less pronounced when the size of the dextrans increased because the hydrogels started to restrict the diffusion of dextran molecules.

The percent recoveries are shown in Fig. 5.8 (a, b). Higher percent recovery indicates larger mobile fraction. In the case of HA-PVA-based hydrogels (Fig. 5.8 (a)), the mobile fraction was larger when the polymer concentration of the HP1-hydrogel or the M_w of the HALD-component decreased (HP3 hydrogel). When the DS% of the high molecular weight HALD-component increased (HP2 hydrogel), or when the DS% of the low molecular weight HALD-component decreased (HP3 hydrogel), the mobile fraction was larger. In GG-HA-based hydrogels (Fig. 5.8 (b)), the mobile fraction was smaller when the DS% of HAADH- or GGALD-component increased (GH2 and GH4 hydrogels). In the case of HA-HA-based hydrogels (Fig. 5.8 (b)), the mobile fraction was smaller when the polymer concentration increased (HH2-based hydrogels), whereas the addition of collagen slightly decreased the mobile fraction (HH2C hydrogel). Compared with similar HP4 and GH2 hydrogels, the mobile fraction in the HH1 hydrogel was larger. The mobile fraction in the AP hydrogel was close to that in GG-HA and HA-HA hydrogels, but slightly larger than that in HA-PVA hydrogels. Overall, the difference between the hydrogels was not so prominent when the size of the dextrans increased. The recovery was almost 100% when smaller dextran sizes were used, but as the dextran size increased, the curves failed to reach the original level.

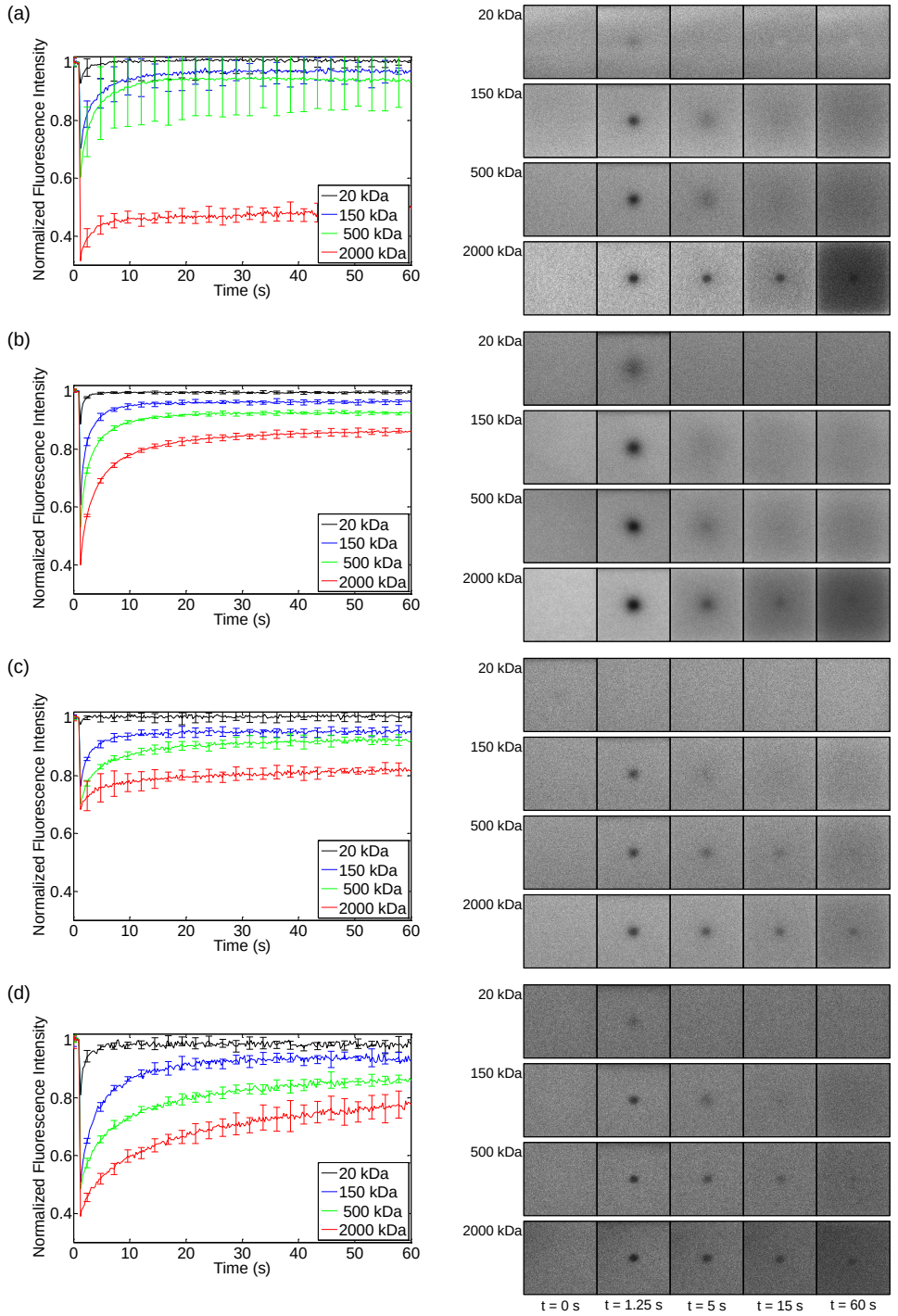

Figure 5.7: FRAP experiments of hydrazone crosslinked hydrogels. Normalized fluorescence recovery curves of different sized FITC-dextrans (20, 150, 500, and 2000 kDa) in (a) HP1, (b) AP, (c) GH4, and (d) HH2C hydrogels. Different phases of the FRAP experiment are presented next to the curves. The curves of other hydrogels are shown in the Supplementary Material of Study IV. The mean (n = 5) and standard deviation bars are shown.

Table 5.1: Diffusion coefficients of FITC-dextrans incorporated inside the hydrazone crosslinked hydrogels determined based on FRAP analysis and VCell modeling. Comparable theoretical values of diffusion coefficients of FITC-dextrans in water are calculated according to Brandl et al. [159]. The mean (n = 5) and standard deviation are shown. The p-values are shown in the Supplementary Material of Study IV.

Sample #	Gel code	Diffusion coefficient $\mu m^2/s$			
		20 kDa	**150 kDa**	**500 kDa**	**2000 kDa**
1	HP1	30 ± 4	2.0 ± 0.4	0.75 ± 0.18	0.05 ± 0.03
2	HP1a	75 ± 2	8.0 ± 1.2	1.50 ± 1.00	0.25 ± 0.04
3	HP1b	80 ± 4	10.0 ± 1.4	2.00 ± 0.13	0.25 ± 0.05
4	HP2	50 ± 1	2.0 ± 0.5	0.75 ± 0.18	0.10 ± 0.07
5	HP3	60 ± 8	2.0 ± 0.4	0.75 ± 0.04	0.10 ± 0.01
6	HP4	50 ± 4	2.0 ± 0.4	1.00 ± 0.18	0.10 ± 0.02
7	AP	45 ± 5	10.0 ± 0.4	2.00 ± 0.22	0.50 ± 0.01
8	GH1	40 ± 1	3.0 ± 0.7	0.50 ± 0.05	0.25 ± 0.01
9	GH2	40 ± 4	2.0 ± 0.6	0.25 ± 0.18	0.10 ± 0.01
10	GH3	40 ± 4	3.0 ± 0.1	0.75 ± 0.01	0.10 ± 0.06
11	GH4	40 ± 4	2.0 ± 0.1	0.25 ± 0.01	0.10 ± 0.04
12	HH1	55 ± 3	5.0 ± 0.1	1.00 ± 0.25	0.25 ± 0.01
13	HH2	40 ± 5	1.0 ± 0.5	0.20 ± 0.06	0.05 ± 0.02
14	HH2C	35 ± 4	0.8 ± 0.1	0.10 ± 0.02	0.05 ± 0.01
	Water	81	28	15	7

5.3.5 Rheological properties of hydrogels

The viscoelastic properties of the hydrogels were determined using rheological tests. Some structural parameters (ξ, M_c and n_e) were also determined for the hydrogels.

5.3.5.1 Storage, loss and complex moduli, and loss tangent

Amplitude frequency sweep measurements were performed at variable (strain) amplitudes by keeping the frequency constant in order to determine the LVR of the hydrogels. The amplitude dependence of the moduli of hydrogels are presented in Fig. 5.9. A fairly linear behavior of G' up to about 10% strain was seen for all hydrogels, whereas outside the LVR the decrease of G' indicated structure breakdown.

The frequency sweep measurements were performed at variable frequencies at the LVR strain amplitude determined earlier. The frequency dependence of modulus of HA-PVA- and AL-PVA-based hydrogels are presented in Fig. 5.9 (b,d), whereas the corresponding curves for GG-HA- and HA-HA-based hydrogels are presented in 5.9 (f) and (h), respectively. The phase angle $\tan\delta$ of the hydrogels are presented in Study IV. For all hydrogels, the G' was higher than G" (elastic response is stronger than the viscous one) and independent of frequency (for the measuring range 0.1 Hz to 10 Hz). G' was also parallel to G". The ratio of G" to G' ($\tan\delta$) was < 0.1 for all hydrogels, and therefore their structures were considered to be strong. Results also showed that, for some gels, such as HP3, AP, and GH1 hydrogels, the G' increased at higher frequencies.

The storage moduli (G'), loss moduli (G"), and complex moduli (G^*) of the hydrogels are presented in Table 5.2. The results showed that the G' (and G^*) of HA-PVA-based

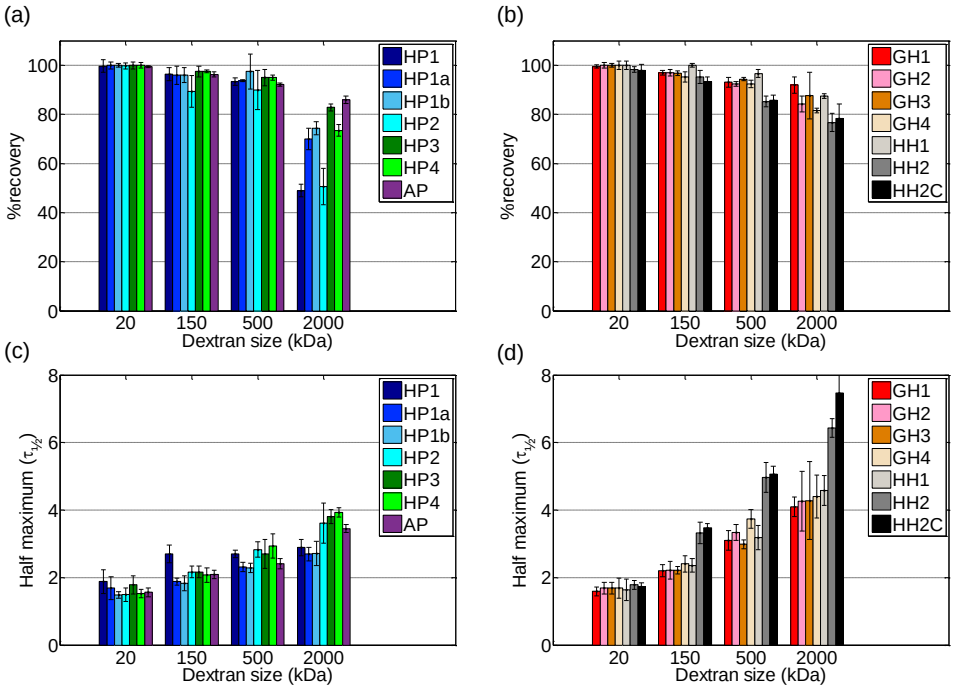

Figure 5.8: (a, b) Percent recoveries and (c, d) half maximums ($\tau_{1/2}$) determined in HA-PVA- and AL-PVA-, GG-HA-, and HA-HA-based hydrogels based on the normalized fluorescence recovery curves of different sized FITC-dextrans (20, 150, 500, and 2000 kDa).

hydrogels decreased when the polymer concentration of hydrogel (HP1a and HP1b hydrogels) and the DS% of the HALD-component decreased (HP1 and HP3 hydrogels), or when the molecular weight of HA increased (HP1 and HP2 hydrogels). With GG-HA-based hydrogels, the G' (and G*) increased when the DS% of the HAADH-component increased (GH2 and GH4 hydrogels), or when the mass ratio was 1:1 (GH3 and GH4 hydrogels) compared with a mass ratio of 2:1. The G' (and G*) of HA-HA-based hydrogels were close to previous values. The G' (and G*) increased when the polymer concentration of HA-HA hydrogel increased (HH2-based hydrogels). The addition of collagen into the hydrogel further increased the G' (and G*) and led to the highest G' (and G*) of all the hydrogels (HH2C hydrogel). The AP hydrogel differed significantly from others and showed the lowest G' (and G*) of all. The hydrogels arranged according to decreasing G' (and G*): HHAC>HP4>HH2>HP2>GH4>HH1>HP3>HP1>GH2>GH3>GH1>HP1a>HP1b>AP. The G" followed this order with some minor exceptions. For some hydrogels, such as the HH1 hydrogel, the G" showed some non-linear behavior that indicates possible non-homogeneity in the structure. Complex moduli (G*) were equal to G', which indicates that the elastic response dominates the properties of hydrogels over the viscous response.

GG-Ca gel was used as a control for GG-HA-based hydrogels. Unfortunately, the rheological measurement of the GG-Ca gel was not possible. There were measuring problems that were caused by a water layer existing near the plates. The rheological measurements of brain and heart tissues could not be performed either.

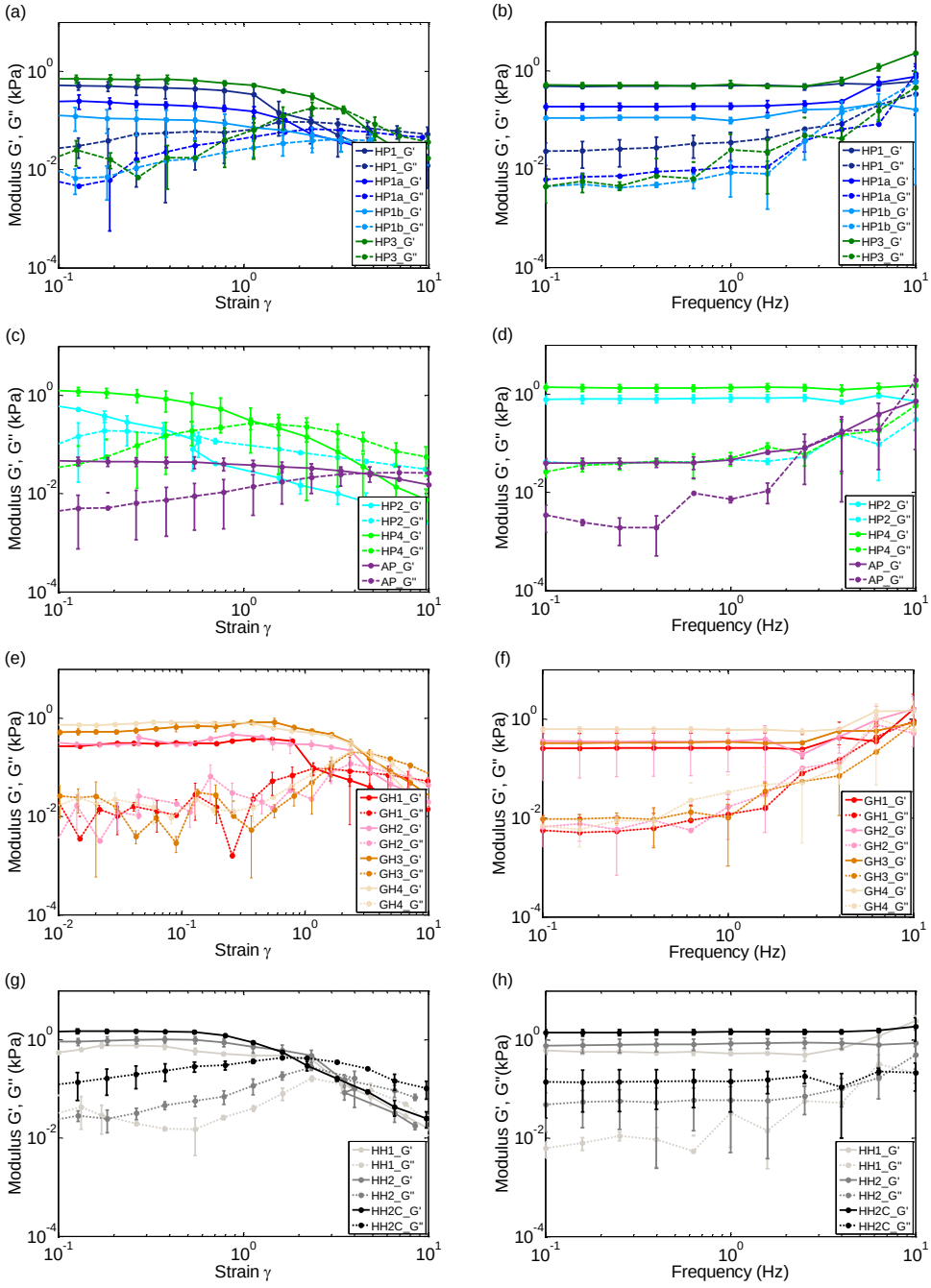

Figure 5.9: Rheological properties of hydrazone crosslinked hydrogels. Amplitude and frequency dependence of moduli of (a-d) HA-PVA- and AL-PVA-, (e,f) GG-HA-, and (g,h) HA-HA-based hydrogels. The mean (n = 3) and standard deviation bars are shown.

Table 5.2: Parameters of hydrazone crosslinked hydrogels determined based on the rheological frequency sweep analysis and mechanical compressive test. Storage moduli (G'), loss moduli (G"), complex moduli (G^*), average mesh sizes (ξ), average crosslinking densities (n_e), and average molecular weights of the polymer chain between neighboring crosslinks (M_c) and second-order elastic constants of the hydrazone crosslinked HA-PVA-, AL-PVA-, GG-HA-, and HA-HA-based hydrogels. The mean (rheological: n = 3, mechanical: n = 5) and standard deviation are shown. The p-values of the mechanical properties (second-order elastic constants) are collected in Appendix I (Table 1.). Otherwise, there were no statistically significant differences between the hydrogels (p> 0.05).

Sample #	**Gel code**	**G' Pa**	**G" Pa**	**G^* Pa**	ξ **nm**	n_e **mol/m^3**	M_c **kg/mol**	**Second-order elastic constant kPa**
1	HP1	491 ± 5	28 ± 15	492 ± 5	20.6 ± 0.1	0.190 ± 0.002	78.2 ± 0.8	2.8 ± 0.8
2	HP1a	189 ± 29	8 ± 1	189 ± 29	28.4 ± 1.5	0.073 ± 0.011	206.4 ± 32.0	2.5 ± 0.8
3	HP1b	109 ± 11	5 ± 2	109 ± 11	34.0 ± 1.2	0.042 ± 0.004	354.6 ± 36.0	0.9 ± 0.4
4	HP2	804 ± 15	42 ± 3	805 ± 15	17.5 ± 0.1	0.312 ± 0.006	47.8 ± 0.9	5.1 ± 1.2
5	HP3	514 ± 71	9 ± 1	514 ± 72	20.3 ± 0.9	0.199 ± 0.028	75.7 ± 10.5	3.3 ± 0.9
6	HP4	1355 ± 219	39 ± 11	1355 ± 218	14.7 ± 0.8	0.526 ± 0.085	28.8 ± 4.7	4.9 ± 0.7
7	AP	41 ± 2	4 ± 3	41 ± 3	47.1 ± 0.8	0.016 ± 0.001	937.9 ± 45.8	1.0 ± 0.5
8	GH1	259 ± 2	7 ± 3	259 ± 2	25.5 ± 0.1	0.100 ± 0.001	148.2 ± 1.1	2.5 ± 0.1
9	GH2	352 ± 4	9 ± 4	352 ± 4	23.0 ± 0.1	0.137 ± 0.002	109.1 ± 1.2	3.5 ± 0.2
10	GH3	335 ± 7	10 ± 10	335 ± 7	23.4 ± 0.2	0.130 ± 0.003	114.6 ± 2.4	2.4 ± 0.7
11	GH4	618 ± 10	14 ± 11	619 ± 10	19.1 ± 0.1	0.240 ± 0.004	62.1 ± 1.0	6.6 ± 0.1
12	HH1	568 ± 59	12 ± 4	569 ± 59	19.6 ± 0.7	0.220 ± 0.023	68.1 ± 7.1	5.4 ± 1.1
13	HH2	805 ± 232	56 ± 45	809 ± 223	17.5 ± 1.8	0.312 ± 0.090	47.7 ± 15.2	6.7 ± 1.0
14	HH2C	1442 ± 197	142 ± 11	1418 ± 160	14.4 ± 0.7	0.559 ± 0.076	27.0 ± 3.7	11.6 ± 1.7
15	GG-Ca	–	–	–	–	–	–	6.6 ± 0.1
16	brain	–	–	–	–	–	–	2.1 ± 0.9
17	heart	–	–	–	–	–	–	12.2 ± 3.8

5.3.5.2 Evaluation of average mesh size, crosslinking density and average molecular weight of the polymer chain between neighboring crosslinks of hydrogels

The calculated average mesh sizes (ξ) and average molecular weight of the polymer chain between neighboring crosslinks (M_c) of the hydrogels are shown in Table 5.2. The ξ of the hydrogels varied from 14.7 ± 0.8 nm to 47.4 ± 3.4 nm, whereas the M_c of the hydrogels varied from 27.3 ± 1.3 kg/mol to 857.8 ± 146.8 kg/mol. The ξ and M_c of HA-PVA-based hydrogels increased when the polymer concentration of hydrogel (HP1a and HP1b hydrogels) or the DS% of the HALD-component decreased (HP1 and HP3 hydrogels), or when the molecular weight of HA increased (HP1 and HP2 hydrogels). With GG-HA-based hydrogels, the ξ and M_c slightly decreased when the DS% of the HAADH-component increased (GH2 and GH4 hydrogels), or when the mass ratio was 1:1 (GH3 and GH4 hydrogels) compared with a mass ratio of 2:1. The ξ and M_c of the HA-HA-based hydrogels were also close to previous gels. The comparison of HA-HA-based hydrogels was not easy due to the different compositions used, but overall the mesh size decreased with increased polymer concentration of the hydrogel (HH2-based hydrogels). Also, the addition of collagen into the gel further decreased the mesh size (HH2C hydrogel). This hydrogel showed the lowest ξ and M_c of all the hydrogels. When the HH1 hydrogel was compared with HP4 and GH2 hydrogels, the ξ and M_c of the HH1 hydrogel were higher than with the HP4 hydrogel, and lower than with the GH2 hydrogel. Compared with other hydrogels, the mesh size of the AP hydrogel differed significantly from others and showed the highest ξ and M_c of all. The hydrogels arranged according to increasing ξ and M_c: HHAC<HP4<HH2<HP2<GH4<HH1<HP3<HP1<GH2<GH3<GH1<HP1a<HP1b<AP.

The calculated crosslinking densities (n_e) of the hydrogels are presented in Table 5.2. The n_e of the hydrogels varied from 0.526 ± 0.085 mol/m^3 (5.26×10^{-19} mol/μm^3) to 0.016 ± 0.004 mol/m^3 (1.60×10^{-20} mol/μm^3). The n_e of HA-PVA-based hydrogels decreased when the polymer concentration of the hydrogel (HP1a and HP1b hydrogels) or the DS% of the HALD-component decreased (HP1 and HP3 hydrogels), or when the molecular weight of HA increased (HP1 and HP2 hydrogels). The n_e of GG-HA-based hydrogels slightly increased when the DS% of the HAADH-component increased (GH2 and GH4 hydrogels), or when the mass ratio was 1:1 (GH3 and GH4 hydrogels) compared with a mass ratio of 2:1. The n_e of HA-HA-based hydrogels were close to previous values. The n_e increased with the increased polymer concentration of HA-HA-based hydrogel (HH2-based hydrogels). The addition of collagen into the hydrogel further increased the n_e and led to the highest n_e of all the hydrogels (HH2C hydrogel). When the HH1 hydrogel was compared with HP4 and GH2 hydrogels, the n_e of the HH1 hydrogel was lower than with the HP4 hydrogel and higher than with the GH2 hydrogel. The AP hydrogel differed significantly from others and showed the lowest n_e of all. The hydrogels arranged according to decreasing n_e: HHAC>HP4>HH2>HP2>GH4>HH1>HP3>HP1>GH2>GH3>GH1>HP1a>HP1b>AP.

5.3.6 Mechanical properties of hydrogels

Since the stress-strain curve of hydrogels (and tissues) is non-linear in the elastic portion, even at low strains, a polynomial fit was used for the data, and the stiffness of materials was determined according to method described in Section 4.2.4.6. Moreover, instead of giving only the second-order elastic constants for the materials, the stiffness as a function of strain was shown in order to represent the material behavior in a wider strain range. The representative compressive stress as a function of the deformation strain curves, and the stiffness as a function of the strain curves of the HA-PVA- and AL-PVA-based

hydrogels (and midbrain tissue) are shown in Fig. 5.10 (a) and (b), respectively, whereas for GG-HA- (and GG-Ca, midbrain tissue, heart tissue) and HA-HA-based hydrogels are shown in Fig. 5.10 (c,e) and (d,f), respectively.

The stress-strain curves (Fig. 5.10 (a,c,e)) show that all the hydrogels were initially resistant to deformation, and when the load was increased, they became progressively stiffer, leading finally to the fracture of the hydrogels. The HP2 and AP hydrogels had the lowest fracture strains (50% to 57% strain) compared with the others (over 60% strain). The stress-strain curves of the HA-PVA- and AL-PVA-based hydrogels behaved similarly to midbrain tissue at lower strains, but at higher strains the curve of the midbrain tissue became steeper showing no clear fracture. In addition, it was noted that at lower strain values, HP4 hydrogel was stiffer than midbrain tissue, but at higher strains (over 20% strain) the opposite was the case. Altogether, the stress-strain curves of the brain tissue and the HA-PVA- and AL-PVA-based hydrogels were in the same range at lower strains and showed similar elastic behavior, whereas at higher strains in the fracture area the difference was clearer. The results of HA-HA-based hydrogels showed that the hydrogels fractured at 55% to 70% strain range. Due to a higher fracture strain, the HH2 hydrogel was considered to be more elastic compared with the HH2C and HH1 hydrogels, whereas the col I-containing HH2C hydrogel was the least elastic. The control GG-Ca hydrogel fractured at a lower strain (around 30% strain) compared with the GG-HA-based hydrogels (over 55% strain). When the stress-strain curves of GG-HA-based hydrogels and tissues were compared, the GG-HA-based hydrogels showed a similar elastic behavior to brain tissue at lower strains.

The stiffness-strain curves (Fig. 5.10 (b,d,f)) showed that the stiffness was strain dependent and quite constant at around 20% strain with all the hydrogels. After that, the stiffness increased more or less depending on the sample, and at a specific point started to drop. This drop occurred sooner for the HP2 and AP hydrogels when compared with the others. The stiffness decreased when the polymer concentration of the hydrogel decreased (HP1a and HP1b hydrogels). At low strain values, the stiffness of HA-PVA-based hydrogels was higher when the molecular weight of HALD-component was lower (HP3 and HP4 hydrogels) or its DS% was higher (HP2 and HP4 hydrogels). In addition, the stiffness of the AP hydrogel was similar to the lowest HP1b hydrogel. At lower strain values, the stiffness of the HP1 hydrogel was the most similar to midbrain tissue. The stiffness of GH2 and GH4 hydrogels was fairly constant up to 20% to 30% strain, after which it increased rapidly, leading eventually to the fracture of hydrogel. The stiffness of GH1 and GH3 hydrogels was fairly constant until 40% strain. Both hydrogels started to fracture at around 60% strain. For different hydrogels, the drop in the stiffness value (indicating fracture) occurred at different strains. The drop in stiffness value occurred sooner for the GH2 hydrogel and the control GG-Ca gel than the others. In general, GG-HA-based hydrogels can be considered more elastic when compared with the control GG-Ca gel. Brain tissue, on the contrary, showed constant stiffness until 20% strain, after which it increased with no clear fracture. The constant area of heart tissue was even shorter, after which the stiffness increased rapidly with no clear fracture. According to Fig. 5.10 (d), GH1, GH2 and GH3 hydrogels were shown to behave in a fairly similar way to brain tissue from 0% to 15% strain. After that, the stiffness of the brain tissue increased more steeply with no sign of a fracture, whereas the stiffness of hydrogels slowly increased, and they fractured. On the other hand, the stiffness of the hydrogels was shown to be too low at low strains to mimic heart tissue.

The second-order elastic constants for the hydrogels and midbrain and heart tissues are

presented in Table 5.2. The HP1b hydrogel showed a statistically significant difference $p< 0.01$ with respect to the HP1, HP1a, HP2, HP3, and HP4 hydrogels. The HP4 hydrogel showed significant difference $p< 0.05$ with respect to the HP1a, HP3 and AP hydrogels and midbrain, and $p< 0.01$ with respect to HP1 and HP1b hydrogels. Moreover, the AP hydrogel showed significant difference $p< 0.05$ with respect to the HP1, HP2, HP3, and HP4 hydrogels. No statistically significant differences were detected between the other HA-PVA- and AL-PVA-based hydrogels or with respect to midbrain tissue. Overall, the second-order elastic constants of HA-PVA- and AL-PVA-based hydrogels were relatively low (0.9 kPa to 5.1 kPa) and similar to midbrain tissue, which could indicate their suitability for neural application. In particular, the HP1 hydrogel showed the most similar elastic behavior (and second-order elastic constant) compared with midbrain tissue at lower strains. The HH2C hydrogel with the highest second-order elastic constant showed a significant difference ($p< 0.05$) with respect to the HH1 hydrogel. Otherwise, there were no statistically significant differences between the HA-HA-based hydrogels. GH3 hydrogels showed a significant difference ($p< 0.05$) with respect to the GH4 hydrogel, control GG-Ca gel, and heart tissue. Heart tissue showed a relatively significant difference ($p= 0.0571$) with respect to GH1 and GH2 hydrogels, control GG-Ca gel, and midbrain tissue. Otherwise, there were no statistically significant differences detected between the GG-based hydrogels or with respect to midbrain and heart tissues. All p-values (tested also between different gel types) are collected in Appendix I (Table 1.). The hydrogels (and tissues) arranged according to decreasing second-order elastic constant: (heart>)HH2C>HH2(>GG-Ca)>GH4>HH1>HP2>HP4>GH2>HP3>HP1>GH1≈HP1a>GH3(>brain)>AP>HP1b.

5.3.7 Biodegradability of hyaluronan-based hydrogels

The enzymatic biodegradation of the HA-PVA-, HA-HA- and GG-HA-based hydrogels was followed by monitoring the bulk mass loss. A higher amount of HAse (20 U/mL to 50 U/mL) was used compared with physiological conditions. The following degradation curves are shown in Fig. 5.11. It was notable that almost all the gels swelled first before any mass loss could be detected. The HA-PVA-based hydrogels were completely degraded in 21 hours to 25 hours, the HA-HA-based hydrogels in 24 hours to 48 hours, and the GG-HA-based hydrogels in 24 hours to 34 hours. Degradation was faster when the polymer concentration of the HA-PVA-based hydrogels decreased (HP1a and HP1b hydrogels), and when both the molecular weight and the DS% of the HALD component were lower (HP3 hydrogel). The results of HA-HA-based hydrogels showed that the degradation behavior of HH2 and HH1 hydrogels differed from each other. HH2 and HH2C hydrogels remained relatively stable for 28 hours, after which they were completely degraded by the enzyme by the 48-hour timepoint. The HH2 and HH2C control hydrogels did not exhibit significant degradation during the 48 hours (Study II). On the other hand, the HH1 hydrogel degraded in a matter of hours. After 24 hours, there was no gel left to weigh. Even the control hydrogel started to degrade at the same time. The results of GG-HA-based hydrogels showed that due to a HAADH component, all hydrogels first swelled before any degradation could be detected. Hydrogels containing a high molecular weight HAADH component (GH1 and GH3 hydrogels) degraded faster than similar hydrogels with a low molecular weight HAADH component (GH2 and GH4 hydrogels). On the other hand, hydrogels containing a GGALD4 component degraded faster (GH3 and GH4 hydrogels) than hydrogels with a GGALD3 component (GH1 and GH2 hydrogels).

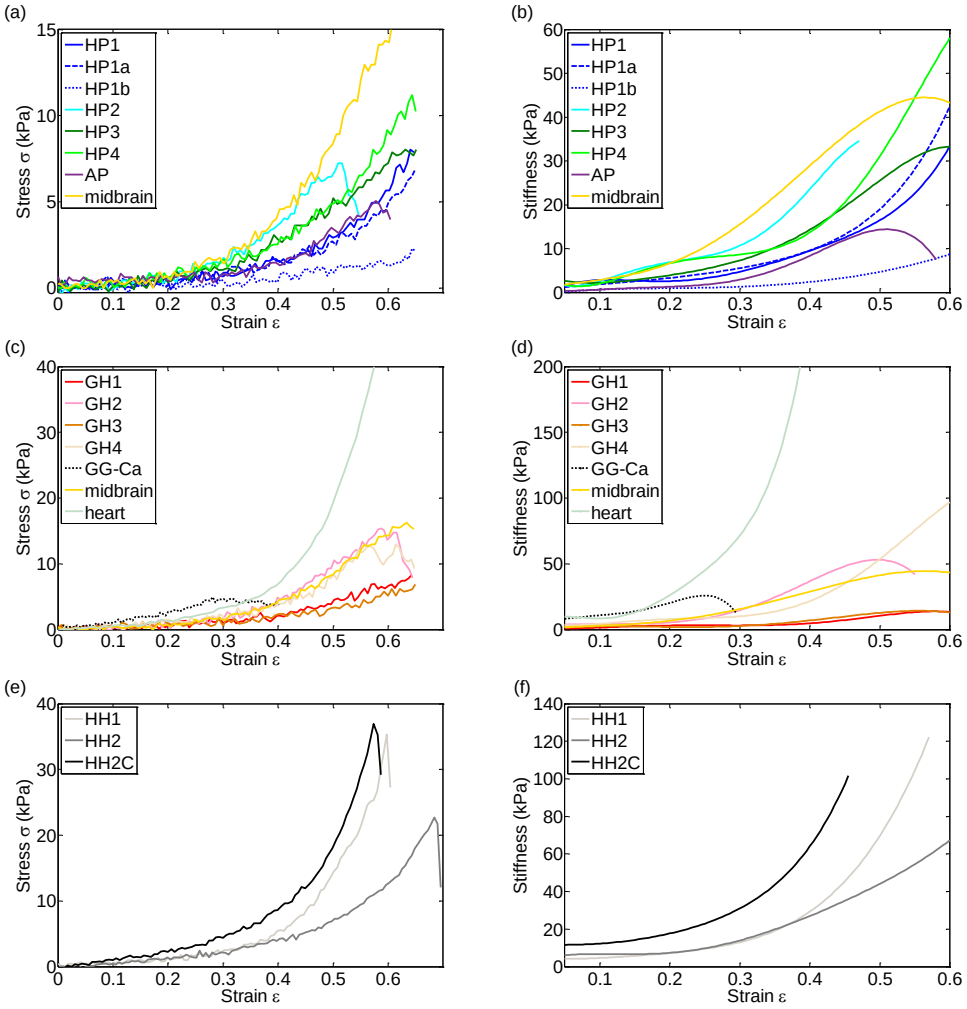

Figure 5.10: Stress as a function of strain (representative), and stiffness as a function of strain (average) curves of (a,b) HA-PVA- and AL-PVA-, (c,d) GG-HA-, and (e,f) HA-HA-based hydrogels and (a-d) rabbit midbrain and (c,d) heart tissue. The mean (n = 3 to 5) and standard deviation bars are shown.

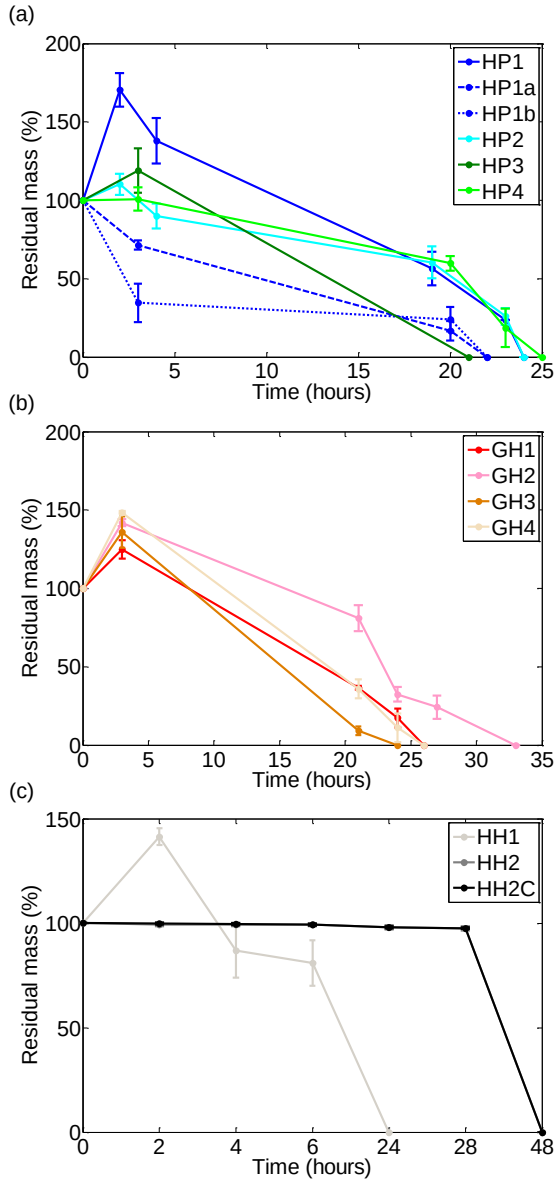

Figure 5.11: Enzymatic degradation of hydrogels. Enzymatic degradation profiles of the (a) HA-PVA-, (b) GG-HA-, and (c) HA-HA-based hydrogels in HAse enzyme (20 U/mL to 50 U/mL). The mean (n = 3) and standard deviation bars are shown.

5.3.8 Optical properties of hydrogels

5.3.8.1 Refractive index

The measurement data were presented as reflection coefficient, and they were plotted as a function of angle of incidence curves that are shown in Study II. The angle value was derived so that the tangent lines were first drawn on the vertical and horizontal parts of the curve, and then the angle at their intersection point was determined. The calculated refractive indices for HH1, HH2, and HH2C hydrogels were 1.332, 1.337, and 1.334, respectively. The results showed that the refractive index was higher when the polymer concentration of the hydrogel increased (HH2-based hydrogels).

5.3.8.2 Transparency

The visible light transmission spectra of hydrogels are shown in Fig. 5.12(a). The light transmittances for HH1, HH2, and HH2C hydrogels were 90 ± 1%, 85 ± 1%, and 82 ± 1%, respectively, in the 400 nm to 700 nm wavelength range. The results showed that the HH1 hydrogel was slightly more transparent than HH2-based hydrogels. Moreover, the addition of col I slightly lowered the transparency. The visible inspection of the samples inside the cuvettes also supported these findings. While the HH1 hydrogel looked visibly clear, the crosslinking was clearly seen inside the HH2-based hydrogels. This can be explained by the higher polymer concentration and higher crosslinking density of HH2-based hydrogels. The sample thickness used in the transparency measurements was significantly higher than the one intended for the final application. Therefore, thinner hydrogel films were photographed in order to show their optical clarity and transparency. As the photographic images presented in Fig. 5.12(b) (and (c)) show, all hydrogels were visibly transparent, even with the addition of col I.

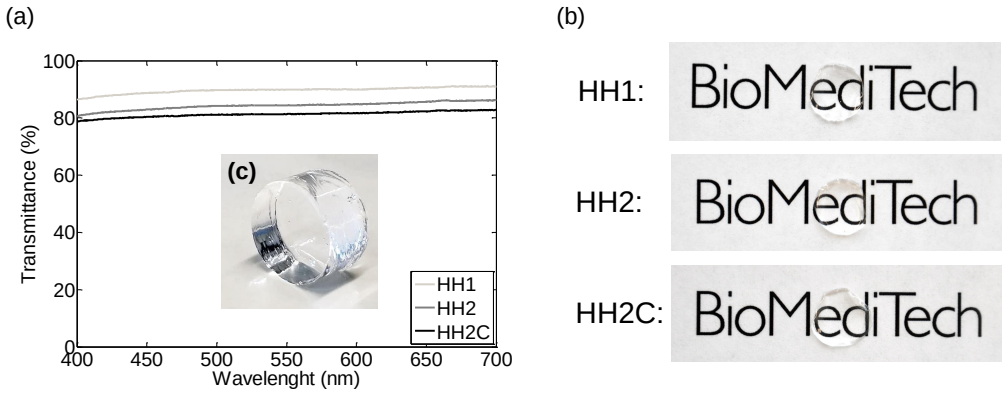

Figure 5.12: Transparency of HA-HA-based hydrogels. (a) Light transmission spectra of HH1, HH2, and HH2C hydrogels. (b) Photographic images of HH1, HH2, and HH2C hydrogels (diameter 10 mm x thickness 1 mm) showing their transparency. (c) Photographic image of HH2-based hydrogel (diameter 12 mm x thickness 7 mm) prepared for the compression testing.

5.4 *In vitro* cell culture studies

5.4.1 *In vitro* cell culture studies using human adipose stem cells

Human ASCs were encapsulated into the three HA-HA-based hydrogels. Their viability was assessed qualitatively using Live/Dead staining, and the relative metabolic activity in different hydrogels was analyzed with PrestoBlue. Both the Live/Dead staining (Fig. 5.13 (a)) and the PrestoBlue results (Fig. 5.13 (b)) showed that all HA-HA-based hydrogels were capable of sustaining short-term cell survival. However, the more unstable HH1 hydrogel samples degraded during the first three days of culture, making their handling for imaging and PrestoBlue analysis difficult. For this reason, no images could be obtained after the first time point.

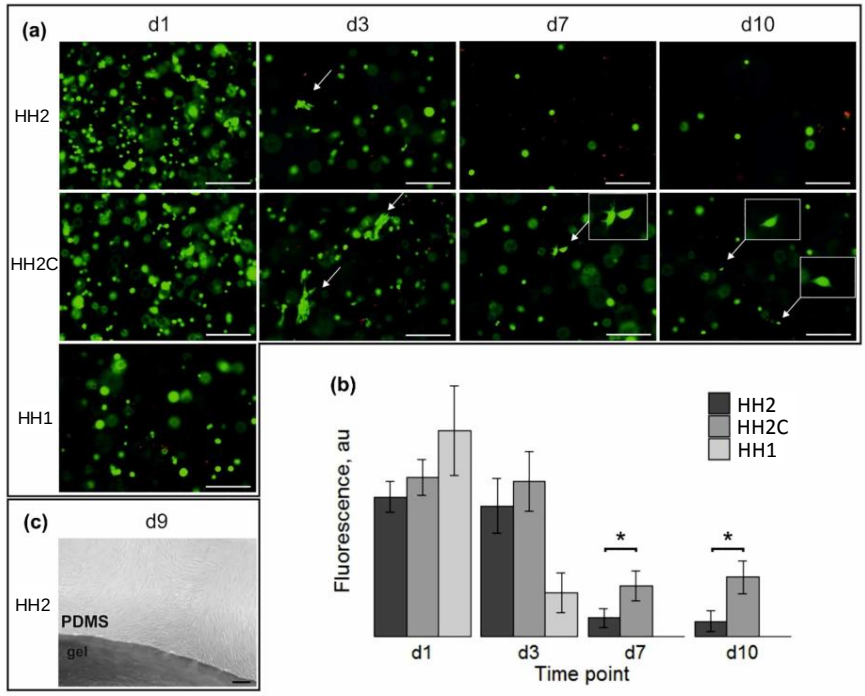

Figure 5.13: Cell viability and metabolic activity in HA-HA-based hydrogels. (a) Live-dead staining of hASCs encapsulated in HH1, HH2, and HH2C hydrogels at different time points (live cells in green and dead cells in red). Elongated cells are indicated by arrows. (b) Metabolic activity of hASCs encapsulated in hydrogels during *in vitro* culture (PrestoBlue analysis). The bars show the relative fluorescence values of cell-laden hydrogel samples with mean and standard deviation. The PrestoBlue analysis could not be performed after day 3 for the HH1 hydrogel (impossible to handle for imaging). $*$ significant difference at $p < 0.05$. (c) Representative image of the observed cell growth out of the hydrogels and under the PDMS mold at day 9. Scale bars in the images are 200 μm.

Live/Dead staining showed that the number of live cells seemed to decrease from the first time point onwards, although the number of dead cells did not increase. The major cause for this cell loss seemed to be the cell movement away from the hydrogels, which was observed during culture (Fig. 5.13 (c)). Based on the presence of more cells with

elongated morphology in the Live/Dead images, the col I-containing HH2C hydrogel seemed to support hASC attachment better than the purely HA-based HH2 hydrogel.

Cell metabolic activity seemed to decrease in all hydrogels after the first time point (Fig. 5.13 (b)). The trend was similar in all hydrogels, but the onset of the steep decline in metabolic activity varied; for the HH1 hydrogel, the drop occurred between day 1 and day 3, whereas for HH2 and HH2C it occurred between day 3 and day 7. The decline in cell metabolic activity correlated with the observed decrease of cells in the Live/Dead images, also indicating that cells escaped from the hydrogels. However, the remaining cells maintained their metabolic activity at a steady level for the rest of the culture period. Importantly, the HH2C hydrogel-encapsulated hASCs had significantly higher metabolic activity than those in the HH2 hydrogel in the two last time points, which indicates that addition of col I has a significant effect on promoting active cell metabolism and survival.

Excised porcine corneas were used to model the delivery of hASCs in the HA-HA-based hydrogels into stromal defects. As a proof-of-concept, large stromal wounds were inflicted, into which the hydrogels were implanted with and without hASCs. The immunohistological evaluation of the porcine corneas with hydrogel-delivered hASCs revealed cell migration into the corneal stroma after just one week of culture (Fig. 5.14). Successful integration of hASCs into the stroma was observed for all of the hydrogels, although the HH2C hydrogel samples seemed to show slightly less migrated hASCs in the stroma than HH2 and HH1.

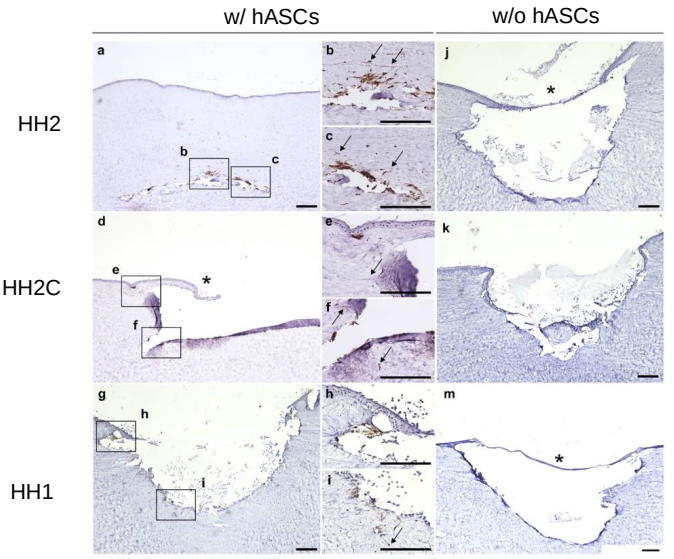

Figure 5.14: Immunohistochemical detection of hydrogel-delivered hASCs after 7 days in porcine corneal organ culture model using human cell marker TRA-1-85. Images (a−i) present HH1, HH2, and HH2C hydrogels with encapsulated hASCs, whereas images (j−m) present delivery of each gel vehicle only. All other sections present the central wound area, except that of HH2 w/ hASCs, which was sectioned near the wound edge. Successful hASC integration into the corneal stroma was seen for all hydrogels (examples marked with arrows), and epithelium growth on top of the transplanted gels was observed with all gels, even without hASCs (denoted by $*$ in images e, j and m). However, epithelial overgrowth could not be verified for all samples, as the gels were lost during histological processing. Scale bars in the images are 200 μm.

Despite the predominant loss of the hydrogels themselves during histological processing, re-epithelialization of the corneal surface was evident from the tissue sections. This was clearly seen in the vehicle-only controls of HH2 and HH1 in Fig. 5.14 (j) and (m), respectively. Fig. 5.14 (d) also implies epithelial outgrowth over the HH2C hydrogel sample, although the complete epithelium is not visible in the section. However, some sections showed epithelial growth at the edges of the wound rather than on top of the hydrogel (shown in Fig. 5.14 (k)), indicating that the gels were not always in good contact with the underlying tissue.

5.4.2 *In vitro* cell culture studies using human pluripotent stem cell derived neuronal cells

Hydrogel compositions were first tested as a growth surface for the cells. The human neuronal cells were cultured on top of the hydrogel surfaces and analyzed after two weeks of culturing. All tested hydrogel compositions supported cell growth and no cytotoxicity was observed (data not shown). The best compositions were the HA-PVA-based hydrogels containing a high molecular weight HALD component (HP1, HP2), as well as the AP hydrogel. Both compositions supported cell growth and neurite outgrowth along the hydrogel surface (Fig. 5.15(a), (c), (e)), whereas the HP3 and HP4 hydrogels containing a low molecular weight HALD component were less supportive (Fig. 5.15(b), (d)). Neurite outgrowth from cell aggregates was the highest in the HP1 hydrogel. The increase in the DS% of the HALD component in HA-PVA-based hydrogels had a negative effect on neurite outgrowth when the HP1 and HP2 hydrogels were compared (Fig. 5.15(f)). The effect of increasing the DS% was not as dramatic on the cells as the change in molecular weight. The most prominent compositions, HP1 and AL, had the lowest stiffness of all the tested hydrogels.

The most prominent hydrogel compositions, HP1 and AP, in terms of cell growth and neurite outgrowth support were selected for the following 3D culturing experiments where the cells were cultured as encapsulated in the hydrogel. First, the viability of neuronal cells inside the HP1 and AP hydrogels was analyzed after two weeks in culture. The cell viability in 3D was at a similar level as viability in 2D control cultures on top of laminin (Fig. 5.16 (a-c)). This indicates that the hydrogel was well tolerated as a culturing environment. Next, the effect of the decreased polymer concentration of the HP1 hydrogel was studied in order to see how the cells behaved in even softer hydrogels. Neuronal cells were cultured for two weeks as encapsulated inside the four soft hydrogel compositions (HP1, HP1a, HP1b, and AP). Cell growth was seen inside all the studied compositions and the cells were positive for the neuronal markers MAP-2 and β-tubulin III (Fig. 5.16 (d-g)). Slight differences were seen in the cell growth. In HP1 and HP1a hydrogels, for example, more cells stayed in clusters (Fig. 5.16(d), (e)), whereas inside the softest HP1b and AP hydrogels the cell outgrowth from the aggregates into the hydrogel was more robust (Fig. 5.16(f), (g)).

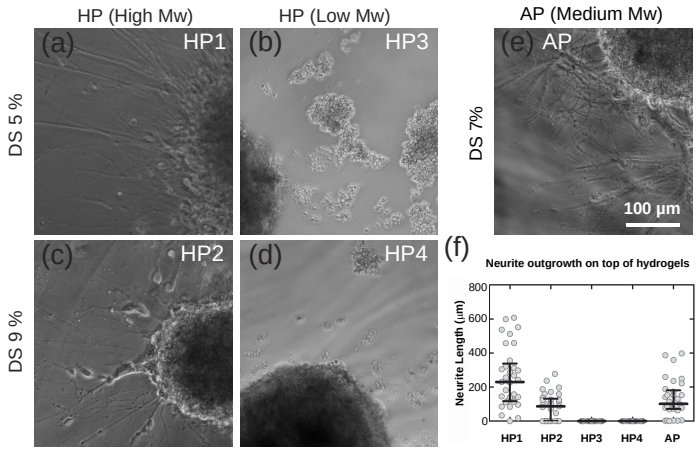

Figure 5.15: Representative images of neural cells growing on top of HA-PVA- and AL-PVA-based hydrogel surfaces: the high molecular weight HA-containing hydrogels (a) HP1 and (b) HP2, the low molecular weight HA-containing hydrogels (c) HP3 and (d) HP4, and (e) the alginate-based AP hydrogel. (f) Neurite outgrowth measured from cultures on top of the hydrogels. Median with inter-quartile range of the measured neurites is shown as line and whiskers whereas individual values are presented as gray dots. The scale bar in all images is 100 μm.

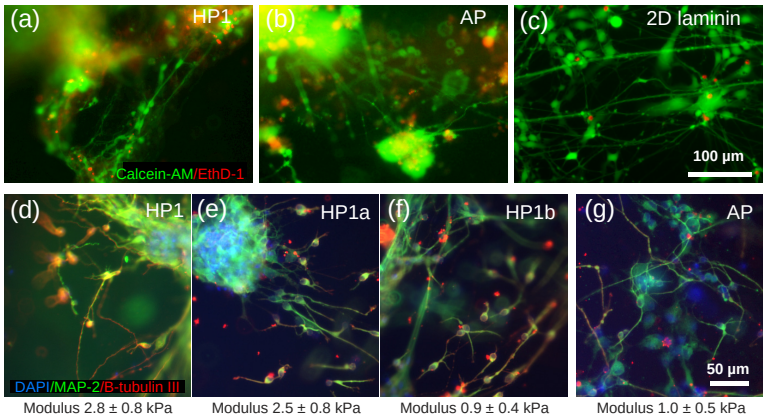

Figure 5.16: Live/dead labeling of the neurons cultured two weeks inside HP1 (a) and AP (b) hydrogels, and on top of laminin coated plastic (c). Living cells are labeled with Calcein-AM (green) and dead cells with EthD-1 (red). Neurons grown for two weeks encapsulated inside the HP1 (d), HP1a (e), HP1b (f), and AP (g) hydrogels labeled with neuron specific immunocytochemical markers MAP-2 (green) and B-tubulin III (red), co-labeled with nuclear marker DAPI (blue). The second-order elastic constants of each hydrogel are shown under the images. The scale bars in images (a-c) is 100 μm and 50 μm in (d-g).

6 Discussion

6.1 Fabrication of fast gelling *in situ* formed hydrazone crosslinked hydrogels from modified polymers

The choice of the fabrication method is important, especially when living cells are encapsulated. Mild reaction conditions, such as water-based methods, should be preferred, whereas any extreme conditions, such as extreme temperatures, free radicals, toxic components, or organic solvents, should be avoided. [69, 119] Injectable materials, on the other hand, offer a less invasive implantation process. Ideally, the cells would be premixed with the liquid precursors of the hydrogels, and then injected and gelated *in situ*. [27, 105] To meet these requirements, hydrazone crosslinking was chosen as a fabrication method for the hydrogels presented in this thesis. Hydrazone crosslinked (mainly HA-based) hydrogels have previously been studied, for example, for wound healing [57] and for cartilage and myocardial TE [26, 54–56]. However, for neural or corneal applications these hydrogel types have not really been studied before. Therefore, hydrazone crosslinked HA-PVA- (Study III), AL-PVA- (Study III), GG-HA- (Study I), and HA-HA(-col I) (Study II)-based hydrogels were fabricated and studied. HA, AL, GG, and PVA were chemically modified with complementary reactive aldehyde- and/or hydrazide-groups to allow their gelation. Overall, the DS% were kept as low as possible so as not to lose the original advantageous properties of the polymers.

Aldehyde-groups were introduced to HA, AL, and GG either through periodate oxidation by cleaving the C2-C3 bond from the polysaccharide chain (Studies I, III), or through selective oxidation of diol-modified polymer (only HA, Study II). Based on the ^{1}H-NMR and FTIR-analysis, the modifications were successful, although some things need to be considered with regard to the reaction used. For example, periodate oxidation can lead to the loss of native backbone structure and the molecular weight of a polymer can be reduced, which might have an effect on the ability of cells to recognize it. The benefit of using selective oxidation of diol-modified HA instead of periodate oxidation is that it keeps the ring-structure of HA intact, and therefore the cells can recognize the HA more easily. Thus, this modification method is usually preferred over the simple periodate oxidation method.

Mutually, hydrazide-groups were introduced to HA and PVA. Hydrazide-groups were introduced to PVA by using glycine ethyl ester and hydrazine as a source of hydrazide unit (Study III). HA, on the other hand, was modified either using homobifunctional ADH or CDH as a source of hydrazide unit (Studies I, II). ^{1}H-NMR and FTIR-analysis confirmed the success of these modifications. It should be noted, however, that when using ADH, it can act as a crosslinker if both of its hydrazide groups manage to react. Even when a large excess of ADH is used, the crosslinking effect can still be significant.

[158] The benefit of using CDH instead of ADH is discussed more deeply next. In the case of HA-HA-based hydrogels, the HH2 hydrogel was considered more stable than the HH1 hydrogel due to a resonance stabilization effect of CDH. As Oommen et al. [54] state, in the CDH-based hydrazone (C^1=N^1-N^2H-(C=O)N^3H), the neighboring heteroatom (N^3) of CDH can provide resonance stabilization to the developing N^2 positive charge. Thus, due to its urea-type structure, the N^2 positive charge can be delocalized. Instead, there is no stabilization effect with ADH. [54]

Successful gelation and hydrogels with variable properties were obtained by optimizing and varying the gel parameters, i.e., DS%, molecular weight and the ratio of polymer components, as well as the polymer concentration of hydrogel. The effect of these parameters on the properties of hydrogels is summarized in Section 6.8. The gelation time of the hydrogels varied from seconds to five minutes (Studies I-III), which should be enough for the proper mixing and injection of the cell-polymer solutions. However, it should be noted that injecting a large amount of fast-gelling material has the potential to damage the surrounding tissue. This might be avoided by injecting smaller amounts of gel over a longer period of time. The gelation time was not significantly affected by the gel parameters, only the decrease in polymer concentration of the hydrogel increased the gelation time (from seconds to minutes, Study III). The FTIR-based structure analysis confirmed the success of hydrazone crosslinking with all the gel types as the appearance of hydrazone C=N stretching signal was shown with all of them (Studies I-III).

6.2 Swelling and deswelling kinetics of hydrogels

The swelling ratio (SR) of hydrogels is usually estimated by quantifying the water content as a function of time. Generally, the SR is determined by studying the water uptake of dry hydrogels, or the water uptake of wet hydrogels that are dehydrated after the swelling. The drawback with the first method is that the drying process can be harmful to the hydrogel structure and cause distortions to the swelling results (that was also noted in this thesis, data not shown). Moreover, these methods do not describe how an initially wet hydrogel behaves in studied conditions, for example, during the cell culture experiments, since the gel is not dehydrated at any point of the experiment. For these reasons, in this thesis the swelling kinetics of the wet hydrogels in deionized water and cell culture medium (DMEM/F12) were studied without drying the sample at any stage of the experiment.

The swelling of HA-PVA-, AL-PVA-, and HA-HA(-col I)-based hydrogels was shown to be dependent on the solvent and its ionic strength (Studies II, III). Unlike in water, in cell culture medium most hydrogels shrank instead of swelling. This was expected because in the presence of salts hydrogel networks lose their hydrophilic-hydrophobic balance and shrink due to ex-osmosis. As counter ions (Na^+) condense around the fixed carboxylate ion charges of HA or AL, they cause a decrease in repulsive forces among the carboxylate groups. This leads to a decrease in swelling (internal network collapses). The cell culture medium and body fluids also contain divalent cations. [160] Therefore, it can be expected that when placed into such media or fluids, the AP hydrogel may also form ionic crosslinks that lead to a more crosslinked structure and reduced swelling, as was also reported, for example, by Kuo and Ma [161].

In water, the hydrogels swelled many times to that of cell culture medium (Studies II, III). The amount of hydrogel swelling depends on the degree of crosslinking and the chemical structure of the hydrogel. Hence, the more hydrophilic the structure, the stronger the

polymer-water interaction becomes. [61] Due to the large number of hydrophilic groups of HA-based hydrogels, they swelled more in water. It was also noted that the swelling ratio of HA-PVA-based hydrogels increased when the molecular weight of HA or the DS% of HALD-component decreased, whereas the swelling ratio decreased when the polymer concentration of the hydrogel decreased. Furthermore, as the crosslinking density increased, the swelling ratio decreased. The AP hydrogel was less stable in water and degraded in just a few hours. The addition of collagen into the HA-HA-based hydrogel decreased the swelling ratio by approximately 20% at each data point. One possible explanation for this is the imine formation between the aldehyde groups of HA and the amino groups of collagen that increases the crosslinking density. Collagen may also form gel itself. It should be also noted that there is a marked difference in the swelling behavior of the components themselves; HA is susceptible to swelling, whereas collagen is not.

The swelling and deswelling behavior of GG-HA-based hydrogels was studied in deionized water and PBS. Similar to previous hydrogels, GG-HA-based hydrogels swelled in water, whereas in PBS they mainly shrank. The swelling ratio was shown to decrease when the DS% of HAADH-component was lower, but the ratio of gel components did not show any significant affect. The swelling ability of these hydrogels in water can be connected to the HA component, since the control GG-Ca gel without any HA (a control sample) hardly swelled in water, whereas it shrank the most in PBS. The shrinking of GG-based hydrogels in PBS can be explained by the ions of PBS being similar to cell culture medium, although PBS only contains monovalent cations. Due to these cations, PBS is able to form ionic crosslinks with GG (ions increase the formation of double helix and junction zones), and this leads to a more crosslinked structure [33]. The ionic nature of GG-HA-based hydrogel shrinking was confirmed by immersing the hydrogel by turns in water and PBS. Similar to Coutinho et al. [33], the results confirmed the ionic nature of the GG-HA-based hydrogels. Thus, by changing the solution environment, the control of the physical properties of these gels could be possible.

6.3 Microstructure of hydrogels determined through rheological and diffusion studies

Microstructure controls the properties of hydrogels [13, 67]. Moreover, structural parameters, such as crosslinking density and mesh size, dictate the diffusion and mechanical properties of hydrogels [70, 79]. Indeed, mesh size has been used to correlate the diffusivity of molecules inside the hydrogel. Suitable diffusivity, on the other hand, is important for TE applications (especially when cells or drugs are encapsulated), since it enables the transportation of small molecules, such as nutrients, waste, and drugs. [73]

The exact analysis of hydrogel microstructure using common imaging methods is difficult. For example, a Scanning Electron Microscope (SEM) requires dehydration of samples. Drying methods, such as freeze drying, may damage the hydrogel structure [14], and therefore the images are not representative of the actual microenvironment. Therefore, it was necessary to use more suitable techniques. In this thesis, the microstructure was successfully investigated by using rheology- and FRAP-based methods (Study IV). The structural parameters could be determined from wet samples without any destructive drying. Since the mesh size, which is dependent on the crosslinking density, has been used to correlate the diffusivity of molecules inside the hydrogel, it was possible to use FRAP to evaluate the mesh size of the hydrogels.

The rubber elastic theory (RET) allows us to investigate the network structure of these

hydrogels with rheology. The mesh size, crosslinking density, and M_c were calculated for the hydrogels. It should be noted, however, that these parameters only give a raw estimation of the structure [67, 89]. The results shown in Table 5.2 were in line with the expected outcome that the higher the G' (and the higher the second order elastic constant), the lower the mesh size and M_c, and the higher the crosslinking density. In the case of HA-PVA-based hydrogels, a smaller mesh size and M_c, and a higher crosslinking density were attained by lowering the molecular weight of HA component, or by increasing the DS% of HALD-component, or the polymer concentration of the hydrogel. With GG-HA-based hydrogels, a larger mesh size and M_c, and lower crosslinking density were achieved by lowering the DS% of HAADH-component or by using the mass ratio of 2:1 (compared with 1:1). With HA-HA-based hydrogels, a smaller mesh size and M_c, and a higher crosslinking density were attained by adding collagen.

The mesh size of hydrogels can also be estimated by studying the diffusion of fluorescently labeled molecules using a FRAP method. In this thesis, FRAP was used to measure the ability of fluorescently labeled FITC-dextrans of different sizes to move around the hydrogel over a period of time. It is known that both geometrical constraints and possible binding events can retain the diffusion of molecules. The FRAP results showed that the recovery was more complete with smaller dextran molecules (20 kDa and 150 kDa), whereas with larger dextran molecules (500 kDa and 2000 kDa) the recovery was only partial. The diffusion coefficients also supported previous findings. The diffusion coefficients decreased significantly as the dextran size increased. In this study, we used molecules that would not show any binding interactions with hydrogel components. Therefore, it was expected that the retained diffusion shown by the results was due to a steric hindrance, rather than actual binding between the molecules and the hydrogel. For example, the crosslinking sites can form microregions in the structure, where the polymer is precipitated in certain areas, and these heterogeneities can distort the diffusion results. Also, the size of the solute in relation to the size of the openings between polymer chains, as well as polymer chain mobility can also affect the movement of the solute [80]. In the case of HA-PVA-based hydrogels, the diffusion coefficients increased when the molecular weight of HA-component, DS% of HALD-component or the polymer concentration of the hydrogel decreased. The results are reasonable since these gel parameters lead to larger mesh sizes and decreased crosslinking densities. Similarly, in GG-HA-based hydrogels, higher diffusion coefficients were attained by lowering the DS% of HAADH-component. In HA-HA-based hydrogels, the addition of collagen decreased the diffusion coefficients presumably due to additional crosslinking.

The results from the FRAP experiment fit well to the mesh sizes evaluated by the rheological experiments. As expected, the diffusivity decreased significantly with larger dextran sizes (hydrodynamic radii of dextrans: 20 kDa = 2.8 nm, 150 kDa = 8.0 nm, 500 kDa = 15.0 nm, 2000 kDa = 30.8 nm), which were equivalent to the average mesh sizes of the hydrogels (15 nm to 47 nm) determined by the rheological method. The mesh sizes of these hydrazone crosslinked hydrogels are comparable with many other (biological) hydrogels, since most hydrogels have a mesh size ranging from 5 nm to 100 nm [162]. This size range allows the flow of small molecules, for example, nutrients, growth factors, and small-molecule drugs, whereas the release or penetration of non-covalently entrapped larger molecules may be hindered. Nevertheless, since the average protein size within human cells is about 50 kDa (a sphere with a diameter of less than 6 nm to 7 nm), most proteins should diffuse through the gel, not to mention peptides that are much smaller in size. How fluids and small molecules move inside the hydrogel depends on the diffusion, whereas degradation plays a larger role in the later movement of the cells

and large molecules. For example, because water (2 Å) can easily diffuse in and out of the hydrogels, it can increase the hydrolysis and contribute to the degradation of the hydrogel structure [68]. Mesh size or degradation are not the only factors that affect the release from the hydrogels. For example, the release is influenced by how the molecule is incorporated and its specific polarity and size [68].

Tests with human pluripotent stem cell-derived neuronal cells (Study III) showed that the neuronal spreading and 3D neural network formation is enhanced inside the softest HA-PVA and AL-PVA hydrogels (AP and HP1-based hydrogels) that had brain mimicking mechanical properties at low strains and contained a high molecular weight HA component. The calculated structural parameters and FRAP results support these findings. The most promising results were obtained with HA-PVA and AL-PVA hydrogels having the highest mesh sizes and M_cs, and the lowest crosslinking densities, as well as the highest diffusion coefficients. This indicates that the microenvironment is more suitable for the cells in terms of better small molecule transportation properties compared with the other gels tested. The HA-HA-based hydrogels that were tested with hASCs (Study II), and especially HH2-based hydrogels, were shown to be suitable for the delivery of hASCs for the regeneration of the corneal stroma. Directly after encapsulation, all gels were showing good hASC survival, but only the HH2C hydrogel showed cells with elongated morphology and significantly higher cell metabolic activity compared with the HH2 hydrogel. In this case, the addition of collagen seems to have more of an effect compared with the size of the structural parameters, although the inferior stability of the HH1 hydrogel (compared with the HH2-based hydrogels) affected the cell test results, making comparison more difficult.

The balancing of suitable mesh size and mechanical properties can be difficult since normally larger mesh sizes decrease the mechanical strength, whereas smaller mesh sizes increase the mechanical strength. This can further affect the behavior of the encapsulated cells because the mesh size can affect the transportation of nutrients and waste. For example, even though larger mesh sizes were achieved for HA-PVA-based hydrogels by reducing their polymer concentration, and those gels were fairly compatible with human pluripotent stem cell derived neuronal cells (Study III), their manageability was affected. In addition, the manageability and mechanical properties of HA-HA-based hydrogels (Study II)) may be improved if they are intended for corneal stroma application, but in a way that the mesh sizes are not reduced.

To the best of our knowledge, the structural parameters or diffusion properties of these particular types of hydrogels have not been studied thoroughly before. These gels are mainly comparable with the similarly crosslinked HA-HA-based hydrogels presented by Oommen et al. [54], for which they have determined the mesh sizes and M_cs using a similar rheological method. Even though the polymer concentrations or ratios of components are not the same, the results were in line with each other. Since the FRAP experiments have not been conducted with similar types of hydrogels, a direct comparison of results was not possible. Comparison, for example, with PEG-based hydrogels studied by Brandl et al. [159] shows, however, that the diffusion coefficients of similar sized FITC-dextrans are of the same magnitude.

Overall, the results successfully showed that rheology- and FRAP-based methods are appropriate tools to characterize the microstructure of these polysaccharide-based hydrazone crosslinked hydrogels. The results also showed that hydrazone crosslinking offers an easy way to produce polysaccharide-based hydrogels with variable microstructures, and hence also variable rheological and diffusion properties. These properties were attained

by altering the polymer component and the type of its modification, molecular weight, and degree of modification, as well as the polymer concentration of the hydrogel and the ratio of polymer components. In future, in addition to the mesh sizes, the pore sizes may also be studied since they have a great impact on the structure and behavior of hydrogels. The performance of the microrheology measurements may also be justified since the viscoelastic properties of hydrogels may alter at that scale too.

6.4 Viscoelastic properties of hydrogels

Hydrogels possess complex viscoelastic behavior as a result of their intricate polymeric network and high water content. The evaluation of their frequency dependent mechanical properties is important because within the physiological frequency ranges and at low strains, the viscoelastic properties are significant (even for hard tissues). [163]

Many biological materials stiffen with higher strains to prevent large deformations. The amplitude sweep measurements (Studies I, II, IV) of HA-PVA-, AL-PVA, GG-HA- and HA-HA-based hydrogels showed that with these hydrogels there was no stiffening observed, which is common for gels. Further, the frequency sweep measurements (Studies I, II, IV) indicated a true gel structure, meaning that G' was parallel to G". Moreover, for ideal gels, the G' is higher than G" and independent of frequency, which was also shown here. [164] The $\tan\delta$ was < 0.1 for all the hydrogels, and therefore their structures were considered to be strong. Overall, due to these observations, these hydrogels were considered to be stable and strong crosslinked gels. The results also showed that for some hydrogels, such as HP3, AP, GH1 hydrogels, the G' increased at higher frequencies. This was because at higher frequencies the longer polymer chains have less time to move and rearrange, leading finally to stiffening and more solid-like behavior [86]. In addition, the G" of some hydrogels, such as AP and HH1 hydrogels, was more non-linear compared with the others, indicating possible non-homogeneity of the structure. These non-homogeneities can cause changes in the structure during the measurement. Overall, higher G' (or G^*) indicates higher resistance to deformation and stiffer structure. Such hydrogels were, for example, the HH2C, HH2, HP4, HP2, and GH4 hydrogels. In the case of HA-PVA-based hydrogels, higher G' (and G^*) was attained by lowering the molecular weight of HA-component, or by increasing the DS% of HALD-component or the polymer concentration of the hydrogel. With GG-HA-based hydrogels, lower G' (and G^*) was obtained by lowering the DS% of HAADH-component or by using a mass ratio of 2:1 instead of 1:1. The addition of collagen into HA-HA-based hydrogel increased the G' (and G^*). Moreover, the rheological data of the studied hydrogels showed a fairly linear behavior of G' up to about 10% strain, which should be suitable for soft TE applications since cells and tissues in the human body are seldom subjected to strains larger than 5%.

In this thesis, the rheological properties of native tissues (cornea and brain) were not measured, but there are related studies found in the literature [165–168]. Unfortunately, due to differences in testing conditions, experimental procedures and samples, the results are not directly comparable with each other, or with the results shown in this thesis.

6.5 Elastic properties of hydrogels

Materials mimicking the mechanical properties of natural ECM are desired since they are able to mimic the natural cellular microenvironment and to directly support the cells and the surrounding tissue [120]. The fate of cells, especially stem cell differentiation, has

been suggested to be greatly affected by the stiffness and stresses generated from the cell-substrate strains [163].

Young's modulus (in this thesis called the second-order elastic constant) is a commonly used hydrogel property in the literature, even though it is known that the behavior of hydrogels is far from an elastic response [163]. Due to the main constituents of hydrogels and tissues (water, structural proteins, cells, ECM), they do not possess linear elasticity [163]. This means that the stress-strain curve is non-linear in the elastic portion (even at small strains). When linear fit is used for this kind of data, the interpretation of the second-order elastic constant can differ a lot, depending on where the slope is determined (also tested in this thesis, data not shown). Therefore, in this thesis, a polynomial fit was used for the stress-strain data obtained from the compression measurements, and the stiffness of hydrogels was determined as shown in Section 4.2.4.6. Moreover, instead of giving only the second-order elastic constants for the materials, and due to the previously mentioned reasons, the stiffness as a function of strain was shown in order to represent the material behavior in a wider strain range.

The deformation of the hydrogel depends on the structure of the hydrogel. The shape of the stress-strain curves (Studies I-III) showed that all hydrogels were initially resistant to deformation (polymer chains re-orientate) but became progressively stiffer when the load increased (strain hardening [169]). Finally, at certain strains all hydrogels fractured (due to permanent deformation). The results also showed that, for example, in the case of HA-PVA-based hydrogels and midbrain tissue, HP4 was stiffer than midbrain tissue at lower strains, but at higher strains (over 20% strain) the opposite was the case. This would mean that for midbrain tissue a greater force is required to fracture it. Altogether, the stress-strain curves of the brain tissue and the HA-PVA- and AL-PVA-based hydrogels were in the same range at lower strains and showed similar elastic behavior, whereas at higher strains in the fracture area of hydrogels the difference was clearer. Hydrogels with a higher fracture strain are considered to be more elastic. Accordingly, in the case of HA-PVA- and AL-PVA-based hydrogels, the HP2 and AP hydrogels were considered to be less elastic than the others, whereas with GG-HA-based hydrogels the GH2 and GH4 were less elastic. Overall, the GG-HA-based hydrogels were more elastic compared with control GG-Ca gel. With HA-HA-based hydrogels, the HH2 hydrogel was the most elastic, whereas the collagen-containing HH2C hydrogel was the least elastic. When stiffness was plotted as a function of strain (Studies I-III), again, a non-linear deformation characteristic under compression (the strain hardening [169]) was observed with all hydrogels. The stiffness of hydrogels dropped at a certain strain (irreversible changes in the structure). For hydrogels such as HP2, AP, GH2, and HH2C, the drop happened sooner, which indicates that they can withstand less deformation before the final fracture.

The second-order elastic constants of hydrogels, and midbrain and heart tissues were also determined. The second-order elastic constants of the midbrain and heart tissues were in the same range as reported in previous studies [137, 170, 171]. This was true even though the same data of brain tissue had been previously analyzed (using linear fit) by Koivisto et al. [157] showing that the constant, or as they call it, the compressive modulus was slightly higher, and thus deviated from the literature. The second-order elastic constants of HA-PVA- and AL-PVA-based hydrogels were relatively low (0.9 kPa to 5.1 kPa) and similar to midbrain tissue, which could indicate their suitability for neural application. In the case of HA-HA-based hydrogels, even though the mechanical properties of the studied hydrogels were not close to the native cornea (0.1 MPa to 57 MPa [172]), the hydrogel films were still fairly easy to handle during the cell culturing.

This was also one of the main requirements for the material, and not to just replicate the mechanical properties, which might be redundant for cell delivery applications. In general, GG-HA-based hydrogels were intended for soft tissue applications. With this in mind, their mechanical properties were compared with those of midbrain and heart tissue. Even though the second-order elastic constants of the hydrogels were slightly higher than midbrain, overall the stiffness was similar at low strains. On the other hand, even if the stiffness of the hydrogels was too low at small strains to mimic the heart tissue, there are some studies showing that the myoblasts or cardiomyocytes can differentiate and beat synchronously on a matrix with a stiffness of 8 kPa to 11 kPa [173]. Therefore, the GH4 hydrogel being close to that range might be suitable for heart application. Overall, the gel parameters were shown to affect the second-order elastic constants of hydrogels. In the case of HA-PVA-based hydrogels, higher second-order elastic constants were attained by lowering the DS% of HA-component, or by increasing the DS% of HALD-component or the polymer concentration of the hydrogel. With GG-HA-based hydrogels, lower second-order elastic constants were achieved by lowering the DS% of HAADH-component or by using a mass ratio of 2:1 (instead of 1:1). With HA-HA-based hydrogels, the addition of collagen increased the second-order elastic constant.

In this thesis, the bulk properties of hydrogels were tested. However, in biological tissues there are local regions with variable stiffness (due to the character of their constituents, and ongoing remodeling of the ECM) [92, 174]. It is known that cells respond to these variations, and therefore the local mechanical properties should also be measured. One such method would be AFM [92], although the drawback of this method is that it only measures the surface of the material (2D) and does not really represent the 3D environment.

6.6 Biodegradability of hyaluronan-based hydrogels

Polymer bonds can be cleaved either passively by hydrolysis or actively by the enzymatic reaction [59]. The hydrogels studied in this thesis were mainly HA-based (HA-PVA-, GG-HA-, and HA-HA(-col I)-based) hydrogels. Hyaluronidase (HAse) enzymes degrade HA by cleaving the β-N-acetyl-D-glucosaminidic linkages [175]. Since HA degrades sufficiently quickly, it can be covalently crosslinked in order to improve its resistance to enzymatic break down [176]. In this thesis, the HA-based hydrogels were covalently crosslinked; however, the amount of HAse used was higher than in physiological conditions. The degradation was followed by monitoring the bulk mass loss.

The gel parameters were shown to affect degradation times. In the case of HA-PVA-based hydrogels (Study III), the lower molecular weight of HA-component, the DS% of HALD-component, and the polymer concentration of hydrogel all resulted in faster degradation times. With GG-HA-based hydrogels (Study I), the degradation was faster when a lower DS% of HAADH-component or a mass ratio of 1:1 (instead of 2:1) were used. The addition of collagen into HA-HA-based hydrogels did not affect their degradation time significantly (Study II). Overall, higher crosslinking density was shown to delay the degradation of the hydrogels. In addition, most hydrogels showed swelling at the beginning before any mass loss could be detected. This can be related to the HA-component of the hydrogel, as previously discussed in Section 6.2. There was also a significant difference between the degradation behavior of the HA-HA-based HH1 and HH2 hydrogels (Study II). In the case of the HH1 hydrogel, even the control sample started to degrade at the same time as the enzyme-degrading sample, which referred to its tendency to simple hydrolysis

caused by the solution environment. Similar behavior was observed in the swelling tests. HH2 hydrogels were more stable. Their control samples did not exhibit significant degradation during the testing period, which indicated that the observed degradation was truly enzymatic rather than due to simple hydrolysis. As previously discussed in Section 6.1, the difference can be explained by the resonance stabilization effect of CDH (HH2-based hydrogels). Overall, the results (Study I-III) showed that HAse can recognize and degrade the modified HA-components. This indicates that these HA-based hydrogels could also be degradable *in vivo*, as has also been shown in the literature with similar HA-modifications [55, 158, 177–179].

The degradation products of HA are mainly metabolized in the lymph nodes and liver and locally in densely structured alymphatic tissues, such as the cornea [180]. If these hydrogels were used *in vivo*, their degradation rate should be tested more thoroughly in the actual conditions (HAse enzyme concentration can vary from the amount of enzyme used in this thesis) to find out if it matches with the regeneration rate of the native tissue. For example, in the case of corneal stroma, it should be noted that the remodeling process of the injured stroma can take months or even years to complete [181]. In addition, the degradation products, rather than the polymer itself, may have a critical influence on the biocompatibility of the material. Degradation products of HA, N-acetylglucosamine at the reducing end and glucuronic acid at the non-reducing end, are cleared from the body, but they have also been found to modulate wound healing [175, 182].

In this thesis, only the enzymatic degradation of HA-based hydrogels was tested. In the case of AL-PVA hydrogel, AL is known to be inherently non-degradable, because mammals lack the alginase enzyme [22, 23]. However, it has been reported that AL can be made degradable in physiological conditions by partial oxidation [183], which was also done in this thesis. In the case of the GG-HA-based hydrogel, GG is known to be degradable by some human enzymes, such as lysozyme, trypsin, and amylase [30], but they were not tested in this thesis, however.

6.7 Optical properties of HA-HA-based hydrogels

Suitable optical properties, including transparency and refractive index, are obvious requirements for ophthalmic applications. However, transparency may also be useful in *in situ* microscopy and the optical assays of cell behaviors [20]. Since HA-HA-based hydrogels were intended to be used as biomaterials to treat corneal stroma defects, their optical properties were characterized. The results (Study II) showed that the refractive indices of the hydrogels were close to that of water (n= 1.333 [115]) and PBS (n= 1.335 [115]), depending on whether the hydrogels were based on water or PBS. The HH2 hydrogel had the highest refractive index of the three hydrogels, bringing it closest to that of the native corneal stroma (n= 1.376 [111]). The results also showed that the refractive index was higher when the polymer concentration of the hydrogel increased (HH2-based hydrogels), although it should be noted that these hydrogels were PBS-based, and the refractive index of PBS should be about 0.002 higher than water anyway. The transparency of all hydrogels (transmittance 82% to 90%) was close to that of native cornea (transmittance > 87% [127]), even though the samples were significantly thicker than what was intended for the application (sample thickness 10 mm versus application thickness $\approx$ 0.5 mm). Overall, the results showed that even if the addition of collagen slightly decreased the transparency and refractive index, they were still tolerable. The decrease in the transparency and refractive index may be explained by the higher polymer concentration and crosslinking

density (and lower mesh size and M_c) of the HH2C hydrogel, as shown by the results.

Even though the cornea represents the strongest part of the refracting power of the eye, it may not be necessary for the clinically viable corneal biomaterials to imitate its refractive capacity because possible refractive errors can be adjusted with spectacles. Thus, transparency is more important. Degradable materials should promote the healing of healthy stromal tissue so that it ultimately regains the refraction power of the cornea, and therefore this is especially true for them.

The optical properties were measured solely from the hydrogel delivery vehicle. It should, however, be noted that when cells are encapsulated in the hydrogels, it causes light scattering, and thus affects their optical properties. The swelling and degradation of hydrogel as well as the proliferation and differentiation of the encapsulated cells may also alter the refractive index and transparency.

6.8 The effect of the gel parameters and addition of collagen on the properties of hydrogels

In summary of the characterization results (Studies I-IV), the gel parameters, i.e., DS%, molecular weight and the ratio of gel components, and the polymer concentration of the hydrogel as well as the addition of collagen were shown to have an effect on the properties and structural parameters of the hydrogels. The different gel parameters of HA-PVA-, GG-HA-, and HA-HA-based hydrogels, and their effect on the properties (gelation time, swelling ratio, degradation time, diffusion coefficients, G' and second-order elastic constant) and structural parameters (mesh size, M_c and crosslinking density) of the hydrogels are shown in Table 6.1. With HA-PVA-based hydrogels, variable properties were achieved by changing the M_w of HA-component, the DS% of HALD-component, and polymer concentration of the hydrogel. In the case of GG-HA-based hydrogels, their properties were changed by varying the DS% of HAADH-component or the ratio of gel components (mass ratio of 2:1 versus 1:1). With HA-HA-based hydrogels, the properties were changed by adding collagen.

Table 6.1: The effect of gel parameters and the addition of collagen on the properties of hydrogels.

	Gelation time	**Swelling ratio**	**Degradation time**	**Diffusion coefficients**	**G'**	**Second-order elastic constant**	**Mesh size & M_c**	**Crosslinking density**
HA-PVA-based hydrogels:								
Lower M_w of HA	-	higher	faster	higher	higher	higher	smaller	higher
Lower DS% of HALD	-	higher	faster	higher	lower	lower	larger	lower
Lower polymer concentration	longer	lower	faster	higher	lower	lower	larger	lower
GG-HA-based hydrogels:								
Lower DS% of HAADH	-	lower	faster	higher	lower	lower	larger	lower
Mass ratio of 2:1 (versus 1:1)	-	-	slower	-	lower	lower	larger	lower
HA-HA-based hydrogels:								
Addition of collagen	-	lower	-	lower	higher	higher	smaller	higher

6.9 HA-HA-based hydrogels for therapeutic delivery of ASCs to treat corneal defects

Corneal blindness is currently treated by transplantation of donor corneas, although due to the limitations of the procedure, alternative treatment options, such as TE and stem cell therapy, are needed [5, 6]. MSCs are interesting therapeutic options for corneal regeneration [122, 123]. The hASCs, that are an abundant and accessible source of adult MSCs, have been shown to differentiate towards corneal stromal keratocytes *in vivo* [134, 184, 185]. Instead of using a simple stromal injection of hASCs, hydrogel delivery has proven to be better option because it increases the survival of hASCs in the corneal stroma [134]. In this thesis, the ability of transparent HA-HA-based hydrogels to support hASC survival was tested (Study II). Since previous research has shown that the addition of ECM components, such as collagen I or laminin, to HA-based hydrogels is required to support cellular attachment and elongated morphology for different cell types [26, 51, 186], col I-containing HA-HA hydrogel was also tested. The Live/Dead and PrestoBlue results indicated that hASCs survived encapsulated in all of the HA-HA-based hydrogels. However, the addition of col I is required for cell attachment to the hydrogel matrix. During the Live/Dead staining tests, some cell loss was observed. This can be attributed to cell movement away from the hydrogel and hydrogel swelling which pulls the cells further away from each other. The possible wash-out of unattached cells may also contribute to the apparent cell loss from the hydrogels. The efficient loss of cells from the hydrogels composed of purely HA-components suggests they could be suitable as cell delivery vehicles, with either a rapid (HH1 hydrogel) or more delayed delivery (HH2 hydrogel) of hASCs to stromal defects. However, for the long-term tissue integration of the hydrogel matrix, cell attachment may be required for efficient cell proliferation and ECM synthesis [3].

Excised porcine corneas were also used to model the delivery of hASCs in the HA-HA-based hydrogels into stromal defects (Study II). A successful integration of hASCs into the stroma was observed for all of the hydrogels, although slightly fewer migrated hASCs in the stroma were seen in the HH2C hydrogel samples. With these hydrogels, the effect of collagen in improving hASC attachment may have delayed their migration to the stroma. The integration of hASCs to the corneal stroma in the organ culture model demonstrated the clinical feasibility of the hydrogels for the stromal delivery of hASCs. Despite the predominant loss of the hydrogels themselves during histological processing, re-epithelialization of the corneal surface was evident from the tissue sections. Previous research has also reported that HA can support corneal epithelial cell growth [187], which further validates its use in the repair of the underlying stroma. The organ culture model also revealed that the degradation rate of the hydrogels on the corneal surface is not directly comparable to the dilute medium environment of the swelling tests or *in vitro* culture. For example, the complete re-epithelialization and shape retention of the corneal surface indicated that the HH1 hydrogel remained stable for the entire culture period of seven days, whereas during *in vitro* culture the hydrogel could no longer be observed after three days.

The corneal organ culture model can be used in the fast and low-cost preliminary screening of corneal biomaterials. It is an excellent method for studying cellular interactions at the organ level in addition to evaluating the clinical feasibility of biomaterials for corneal applications [188, 189]. The corneal organ culture model has previously been used to mainly study re-epithelialization because the organ-cultured corneas retain their capability for epithelial regeneration for as long as two months in culture [190]. By using the corneal

organ culture model, the number of unnecessary animal tests can be significantly reduced, even though the results obtained from this model always require validation in an *in vivo* animal model.

6.10 HA-PVA- and AL-PVA-based hydrogels for therapeutic delivery of human pluripotent stem cell derived neuronal cells to treat neuronal defects

Traumas and deficits in the human CNS may have a permanent effect on the functionality of the patient, and in many cases the prognosis is poor. Healing with traditional medicine is insufficient because human CNS suffers from a low inbuilt regenerative capacity. Therefore, TE or more specifically regenerative medicine is considered a potential treatment method. [7] One such strategy is cell therapy combined with a supportive biomaterial scaffold, e.g., hydrogel. In this thesis, HA-PVA- and AL-PVA-based hydrogels were first tested as a growth surface for human pluripotent stem cell derived neuronal cells (Study III). All compositions supported cell growth with no detected cytotoxicity. The best compositions (HP1 and AP hydrogels) were chosen for further 3D culturing experiments (cells encapsulated in the hydrogel), where these hydrogels, including the softer versions of the HP1 hydrogel, were shown to be well tolerated as a culturing environment. With the HP1b and AP hydrogels, the cell outgrowth from the aggregates into the hydrogel was more robust.

Some material parameters were shown to affect cells. The most supportive hydrogels were composed of a high molecular weight HA-component and had brain-mimicking mechanical properties (stiffness) at low strains. The molecular weight of HA is known to alter cell behavior, such as adhesion and growth, in many cell types and tissues [191]. Especially in neural tissue, the high molecular weight HA is linked to decreasing glial scar formation [192]. The effect of the increasing DS% of HA-component was not as dramatic on the cells as the change in molecular weight. This might have been due to the mechanisms of HA recognition in the cell membrane [191]. Material stiffness (mechanical environment) is known to affect neural cell viability and behavior by directing neural cell lineage, proliferation, and growth [68, 92]. Moreover, when cultured on material with a similar stiffness to native ECM, the cultured cells have been shown to better retain their functional phenotype [98]. Our findings are in line with previously published studies that suggest softer materials are more favored by the neural cells [68, 137, 193]. By lowering the polymer concentration of the hydrogel, softer hydrogels with lower crosslinking density (more space inside the hydrogel) were achieved, and further, a positive effect on neuronal growth was seen. In addition, the stiffness of the material has previously been reported to have a connection to cell type: neurons prefer lower stiffness (0.1 kPa to 1 kPa), whereas astrocytes and oligodendrocytes prefer a slightly higher stiffness (0.5 kPa to 10 kPa) [68]. In our studies with human neuronal cells, the cultures contained a high number of neurons even though the mechanical properties of the hydrogels used in this thesis are described to favor a mixed population of neurons and glial cell or rather glial fate [68]. One explanation for the different result might be the different hydrogels used in the studies (stiffness is not the only parameter that affects cells).

7 Conclusion

The primary aim of thesis was to find optimal hydrazone crosslinked hydrogel materials for soft TE applications (Studies I-III), and especially for corneal (Study II) and neural (Study III) applications. A further aim was to investigate the detailed properties of hydrogels using suitable characterization methods (Studies I-IV).

The main findings and conclusions of each study are described briefly below:

Study I:

- Hydrazone crosslinking can be used as an alternative for the traditional crosslinking methods of GG. The fabrication of injectable hydrazone crosslinked GG-based hydrogels was successful. Compared with the traditional methods, this method improves the gelation conditions, as well as the properties of GG-hydrogels.
- GG can be combined with HA to create less inert hydrogels with improved stability and swelling ability. In addition, the mechanical and physical properties of GG-HA-based hydrogels can be tailored. An ionic nature of the deswelling properties of GG-HA-based hydrogels in the presence of cations is also shown. The stiffness of GG-HA-based hydrogels was similar to that of soft tissues at low strains. Based on the results, these hydrogels can be considered as suitable candidates for soft TE applications.
- An improved method was used to determine the stiffness of the hydrogels to avoid the use of linear fit for the stress-strain data because the elastic portion of the stress-strain curve is non-linear for hydrogels.

Study II:

- Two types of transparent hydrazone crosslinked HA-based hydrogels (HH1 and HH2) were fabricated from differently modified components. Biodegradability of the HA components and favorable characteristics of hydrazone crosslinking, such as short gelation time, lack of harmful reagents or side-products, and mild reaction conditions, make these hydrogels a potential material for hASC delivery in the treatment of corneal stromal defects.
- Human collagen I can be introduced into these hydrogels, although collagen was incorporated only into the more stable HH2 hydrogel. Even though all hydrogels showed good hASC survival directly after encapsulation, only the col I-containing HH2C hydrogel showed cells with elongated morphology and significantly higher cell metabolic activity compared with the HH2 gel.

- HH2-based hydrogels showed better stability and manageability compared with the HH1 hydrogel, which degraded *in vitro* in three days. The hydrogels also had good optical properties. The refractive indices were close to that of the native cornea, and all hydrogels were visually transparent.
- The corneal organ culture model suggests that these hydrogels could be used as injectable cell delivery vehicles to corneal stromal defects, allowing efficient cell integration to the stroma and the overgrowth of epithelial cells.

Study III:

- Injectable hydrazone crosslinked HA-PVA- and AL-PVA-based hydrogels were fabricated. To the best of our knowledge, the polymerization and the properties of hydrazone crosslinked AL-PVA-based hydrogel were reported for the first time. The favorable characteristics of hydrazone crosslinking and polymers support the use of these hydrogels as 3D supportive and biomimicking materials for neural cell culture.
- The properties of these hydrogels can be tailored. The degree of substitution and molecular weight of the polymer components as well as the polymer concentration of the hydrogels were shown to affect to the swelling, degradation, and mechanical properties of the hydrogels.
- The most supportive HA-PVA-based hydrogels for neural cells had brain-mimicking mechanical properties at low strains and were composed of a high molecular weight HA component. It was also shown that lowering the polymer concentration of hydrogels enhanced the neuronal growth. The AL-PVA-based hydrogel, with stiffness similar to that of brain tissue, was shown to be similarly supportive. Generally, neuronal spreading and 3D neural network formation were enhanced inside the softest hydrogels. Based on the results, these hydrogels can be considered potential 3D supportive materials for neural cell culture.

Study IV:

- The microstructures of the hydrazone crosslinked HA-, GG-, and AL-based hydrogels were successfully evaluated using rheology- and FRAP-based methods. With these methods, the microstructure can be evaluated from wet samples, which gives more reliable results than by imaging dried samples. These methods not only allowed the determination of the viscoelastic and diffusion properties of these hydrogels, but they also enabled the evaluation of their structural parameters, e.g., mesh size, M_c, and crosslinking density. The results obtained from both experiments supported each other.
- The diffusivity decreased when larger dextran sizes (500 kDa and 2000 kDa) where used. These molecule sizes are equivalent to the average mesh sizes of hydrogels (15 nm to 47 nm) determined by the rheological method. This size range is comparable with many other hydrogels, and it allows the transportation of small molecules, peptides, and most of the proteins. The results also showed the expected outcome that when the G' was increased, the mesh size and M_c decreased, whereas the crosslinking density increased. Overall, the results showed that hydrazone crosslinking offers an easy way to produce hydrogels with variable microstructures as well as variable viscoelastic and diffusion properties.

- Material parameters, e.g., polymer components, the degree of substitution (DS%), molecular weight, the ratio of gel components, and the polymer concentration of the hydrogels were shown to affect the viscoelastic and diffusion properties in addition to the structural parameters of the hydrogels.

In summary, hydrazone crosslinked HA- (Studies II-III), GG- (Study I), and AL- (Study III) based hydrogels have shown their potential as materials for soft TE applications (Studies I-IV), and especially for corneal stroma (Study II) and neural (Study III) applications. The favorable characteristics of this crosslinking method and the studied polymers, and further, the tunable properties and injectability of the materials support their potential use (Studies I-IV). The addition of signaling effects, such as peptides, may further favor their suitability.

Bibliography

[1] J. Guan, J. J. Stankus, and W. R. Wagner, "Soft tissue scaffolds," *Wiley Encyclopedia of Biomedical Engineering*, 2006.

[2] J. A. Burdick and R. L. Mauck, *Biomaterials for Tissue Engineering Applications – A Review of the Past and Future Trends*. Springer, 2011.

[3] J. Zhu and R. E. Marchant, "Design properties of hydrogel tissue-engineering scaffolds," *Expert review of medical devices*, vol. 8, no. 5, pp. 607–626, 2011.

[4] C. Cha, S. Y. Kim, L. Cao, and H. Kong, "Decoupled control of stiffness and permeability with a cell-encapsulating poly (ethylene glycol) dimethacrylate hydrogel," *Biomaterials*, vol. 31, no. 18, pp. 4864–4871, 2010.

[5] K. N. Nguyen, S. Bobba, A. Richardson, M. Park, S. L. Watson, D. Wakefield, and N. Di Girolamo, "Native and synthetic scaffolds for limbal epithelial stem cell transplantation," *Acta biomaterialia*, vol. 65, pp. 21–35, 2018.

[6] C. E. Ghezzi, J. Rnjak-Kovacina, and D. L. Kaplan, "Corneal tissue engineering: recent advances and future perspectives," *Tissue Engineering Part B: Reviews*, vol. 21, no. 3, pp. 278–287, 2015.

[7] P. Sensharma, G. Madhumathi, R. D. Jayant, and A. K. Jaiswal, "Biomaterials and cells for neural tissue engineering: Current choices," *Materials Science and Engineering: C*, vol. 77, pp. 1302–1315, 2017.

[8] A. M. Hopkins, E. DeSimone, K. Chwalek, and D. L. Kaplan, "3D in vitro modeling of the central nervous system," *Progress in neurobiology*, vol. 125, pp. 1–25, 2015.

[9] Y. Tang, J. Sun, H. Fan, and X. Zhang, "An improved complex gel of modified gellan gum and carboxymethyl chitosan for chondrocytes encapsulation," *Carbohydrate polymers*, vol. 88, no. 1, pp. 46–53, 2012.

[10] S. J. Buwalda, K. W. Boere, P. J. Dijkstra, J. Feijen, T. Vermonden, and W. E. Hennink, "Hydrogels in a historical perspective: From simple networks to smart materials," *Journal of controlled release*, vol. 190, pp. 254–273, 2014.

[11] J. Alemán, A. V. Chadwick, J. He, M. Hess, K. Horie, R. G. Jones, P. Kratochvíl, I. Meisel, I. Mita, G. Moad, S. Penczek, and R. Stepto, "Definitions of terms relating to the structure and processing of sols, gels, networks, and inorganic-organic hybrid materials (IUPAC recommendations 2007)," *Pure and Applied Chemistry*, vol. 79, no. 10, pp. 1801–1829, 2007.

[12] K. Park, "Superporous hydrogels for pharmaceutical and other applications," *Drug. Deliver. Technol*, vol. 38, pp. 40 – 44, 2002.

[13] A. M. Grillet, N. B. Wyatt, and L. M. Gloe, "Polymer gel rheology and adhesion," in *Rheology*. InTech, 2012.

[14] C. García-González, M. Alnaief, and I. Smirnova, "Polysaccharide-based aerogels—promising biodegradable carriers for drug delivery systems," *Carbohydrate Polymers*, vol. 86, no. 4, pp. 1425 – 1438, 2011.

[15] T. R. Hoare and D. S. Kohane, "Hydrogels in drug delivery: Progress and challenges," *Polymer*, vol. 49, no. 8, pp. 1993 – 2007, 2008.

[16] E. Caló and V. V. Khutoryanskiy, "Biomedical applications of hydrogels: A review of patents and commercial products," *European Polymer Journal*, vol. 65, pp. 252 – 267, 2015.

[17] L. Yahia, N. Chirani, L. Gritsch, F. L. Motta, and S. Fare, "History and applications of hydrogels," *Journal of biomedical sciences*, vol. 4, no. 2, 2015.

[18] J. Tavakoli and Y. Tang, "Hydrogel based sensors for biomedical applications: An updated review," *Polymers*, vol. 9, no. 8, p. 364, 2017.

[19] S.-B. Park, E. Lih, K.-S. Park, Y. K. Joung, and D. K. Han, "Biopolymer-based functional composites for medical applications," *Progress in Polymer Science*, vol. 68, pp. 77 – 105, 2017.

[20] D. Diekjürgen and D. W. Grainger, "Polysaccharide matrices used in 3D in vitro cell culture systems," *Biomaterials*, vol. 141, pp. 96 – 115, 2017.

[21] S. Gomes, I. B. Leonor, J. F. Mano, R. L. Reis, and D. L. Kaplan, "Natural and genetically engineered proteins for tissue engineering," *Progress in polymer science*, vol. 37, no. 1, pp. 1 – 17, 2012.

[22] A. D. Augst, H. J. Kong, and D. J. Mooney, "Alginate hydrogels as biomaterials," *Macromolecular bioscience*, vol. 6, no. 8, pp. 623 – 633, 2006.

[23] P. M. Kharkar, K. L. Kiick, and A. M. Kloxin, "Designing degradable hydrogels for orthogonal control of cell microenvironments," *Chemical Society Reviews*, vol. 42, no. 17, pp. 7335 – 7372, 2013.

[24] S. N. Pawar and K. J. Edgar, "Alginate derivatization: a review of chemistry, properties and applications," *Biomaterials*, vol. 33, no. 11, pp. 3279 – 3305, 2012.

[25] S. Van Vlierberghe, P. Dubruel, and E. Schacht, "Biopolymer-based hydrogels as scaffolds for tissue engineering applications: a review," *Biomacromolecules*, vol. 12, no. 5, pp. 1387 – 1408, 2011.

[26] J. Dahlmann, A. Krause, L. Möller, G. Kensah, M. Möwes, A. Diekmann, U. Martin, A. Kirschning, I. Gruh, and G. Dräger, "Fully defined in situ cross-linkable alginate and hyaluronic acid hydrogels for myocardial tissue engineering," *Biomaterials*, vol. 34, no. 4, pp. 940 – 951, 2013.

[27] S. J. Bidarra, C. C. Barrias, and P. L. Granja, "Injectable alginate hydrogels for cell delivery in tissue engineering," *Acta biomaterialia*, vol. 10, no. 4, pp. 1646 – 1662, 2014.

[28] M. J. Rah, "A review of hyaluronan and its ophthalmic applications," *Optometry-Journal of the American Optometric Association*, vol. 82, no. 1, pp. 38–43, 2011.

[29] S. Khunmanee, Y. Jeong, and H. Park, "Crosslinking method of hyaluronic-based hydrogel for biomedical applications," *Journal of tissue engineering*, vol. 8, p. 2041731417726464, 2017.

[30] C. J. Ferris, K. J. Gilmore, G. G. Wallace, and M. in het Panhuis, "Modified gellan gum hydrogels for tissue engineering applications," *Soft Matter*, vol. 9, no. 14, pp. 3705–3711, 2013.

[31] R. López-Cebral, P. Paolicelli, V. Romero-Caamaño, B. Seijo, M. A. Casadei, and A. Sanchez, "Spermidine-cross-linked hydrogels as novel potential platforms for pharmaceutical applications," *Journal of pharmaceutical sciences*, vol. 102, no. 8, pp. 2632–2643, 2013.

[32] A. M. Soto, J. T. Koivisto, J. E. Parraga, J. Silva-Correia, J. M. Oliveira, R. L. Reis, M. Kellomäki, J. Hyttinen, and E. Figueiras, "Optical projection tomography technique for image texture and mass transport studies in hydrogels based on gellan gum," *Langmuir*, vol. 32, no. 20, pp. 5173–5182, 2016.

[33] D. F. Coutinho, S. V. Sant, H. Shin, J. T. Oliveira, M. E. Gomes, N. M. Neves, A. Khademhosseini, and R. L. Reis, "Modified gellan gum hydrogels with tunable physical and mechanical properties," *Biomaterials*, vol. 31, no. 29, pp. 7494–7502, 2010.

[34] I. Giavasis, L. M. Harvey, and B. McNeil, "Gellan gum," *Critical reviews in biotechnology*, vol. 20, no. 3, pp. 177–211, 2000.

[35] N. J. Whiteside, G. G. Wallace, and M. in het Panhuis, "Preparation and characterisation of graphene composite hydrogels," *Synthetic Metals*, vol. 168, pp. 36–42, 2013.

[36] C. Ferris, L. Stevens, K. J. Gilmore, E. Mume, I. Greguric, D. Kirchmajer, G. G. Wallace, and M. in het Panhuis, "Peptide modification of purified gellan gum," *Journal of Materials Chemistry B*, vol. 3, no. 6, pp. 1106–1115, 2015.

[37] S. Naahidi, M. Jafari, M. Logan, Y. Wang, Y. Yuan, H. Bae, B. Dixon, and P. Chen, "Biocompatibility of hydrogel-based scaffolds for tissue engineering applications," *Biotechnology Advances*, vol. 35, pp. 530–544, 2017.

[38] W. Friess, "Collagen–biomaterial for drug delivery," *European Journal of Pharmaceutics and Biopharmaceutics*, vol. 45, no. 2, pp. 113–136, 1998.

[39] B. Wright, S. Mi, and C. J. Connon, "Towards the use of hydrogels in the treatment of limbal stem cell deficiency," *Drug discovery today*, vol. 18, no. 1, pp. 79–86, 2013.

[40] B. D. Walters and J. P. Stegemann, "Strategies for directing the structure and function of three-dimensional collagen biomaterials across length scales," *Acta biomaterialia*, vol. 10, no. 4, pp. 1488–1501, 2014.

[41] D. A. Ossipov, K. Brännvall, K. Forsberg-Nilsson, and J. Hilborn, "Formation of the first injectable poly (vinyl alcohol) hydrogel by mixing of functional PVA precursors," *Journal of applied polymer science*, vol. 106, no. 1, pp. 60–70, 2007.

[42] J. M. Ino, P. Chevallier, D. Letourneur, D. Mantovani, and C. Le Visage, "Plasma functionalization of poly (vinyl alcohol) hydrogel for cell adhesion enhancement," *Biomatter*, vol. 3, no. 4, p. e25414, 2013.

[43] R. H. Schmedlen, K. S. Masters, and J. L. West, "Photocrosslinkable polyvinyl alcohol hydrogels that can be modified with cell adhesion peptides for use in tissue engineering," *Biomaterials*, vol. 23, no. 22, pp. 4325–4332, 2002.

[44] F. Ullah, M. B. H. Othman, F. Javed, Z. Ahmad, and H. M. Akil, "Classification, processing and application of hydrogels: A review," *Materials Science and Engineering: C*, vol. 57, pp. 414–433, 2015.

[45] M. Oyen, "Mechanical characterisation of hydrogel materials," *International Materials Reviews*, vol. 59, no. 1, pp. 44–59, 2014.

[46] D. Y. Ko, U. P. Shinde, B. Yeon, and B. Jeong, "Recent progress of in situ formed gels for biomedical applications," *Progress in polymer science*, vol. 38, no. 3, pp. 672–701, 2013.

[47] E. M. Sletten and C. R. Bertozzi, "Bioorthogonal chemistry: fishing for selectivity in a sea of functionality," *Angewandte Chemie International Edition*, vol. 48, no. 38, pp. 6974–6998, 2009.

[48] Y. Jiang, J. Chen, C. Deng, E. J. Suuronen, and Z. Zhong, "Click hydrogels, microgels and nanogels: emerging platforms for drug delivery and tissue engineering," *Biomaterials*, vol. 35, no. 18, pp. 4969–4985, 2014.

[49] D. K. Kölmel and E. T. Kool, "Oximes and hydrazones in bioconjugation: Mechanism and catalysis," *Chemical reviews*, vol. 117, no. 15, pp. 10 358–10 376, 2017.

[50] G. T. Hermanson, *Bioconjugate techniques*. Academic press, 2013.

[51] X. Jia, Y. Yeo, R. J. Clifton, T. Jiao, D. S. Kohane, J. B. Kobler, S. M. Zeitels, and R. Langer, "Hyaluronic acid-based microgels and microgel networks for vocal fold regeneration," *Biomacromolecules*, vol. 7, no. 12, pp. 3336–3344, 2006.

[52] E. Martínez-Sanz, D. A. Ossipov, J. Hilborn, S. Larsson, K. B. Jonsson, and O. P. Varghese, "Bone reservoir: injectable hyaluronic acid hydrogel for minimal invasive bone augmentation," *Journal of controlled release*, vol. 152, no. 2, pp. 232–240, 2011.

[53] P. Bulpitt and D. Aeschlimann, "New strategy for chemical modification of hyaluronic acid: preparation of functionalized derivatives and their use in the formation of novel biocompatible hydrogels," *Journal of biomedical materials research*, vol. 47, no. 2, pp. 152–169, 1999.

[54] O. P. Oommen, S. Wang, M. Kisiel, M. Sloff, J. Hilborn, and O. P. Varghese, "Smart design of stable extracellular matrix mimetic hydrogel: synthesis, characterization, and in vitro and in vivo evaluation for tissue engineering," *Advanced Functional Materials*, vol. 23, no. 10, pp. 1273–1280, 2013.

[55] D. A. Ossipov, S. Piskounova, and J. Hilborn, "Poly (vinyl alcohol) cross-linkers for in vivo injectable hydrogels," *Macromolecules*, vol. 41, no. 11, pp. 3971–3982, 2008.

[56] C. Aulin, K. Bergman, M. Jensen-Waern, P. Hedenqvist, J. Hilborn, and T. Engstrand, "In situ cross-linkable hyaluronan hydrogel enhances chondrogenesis," *Journal of tissue engineering and regenerative medicine*, vol. 5, no. 8, pp. e188–e196, 2011.

[57] K. R. Kirker, Y. Luo, J. H. Nielson, J. Shelby, and G. D. Prestwich, "Glycosaminoglycan hydrogel films as bio-interactive dressings for wound healing," *Biomaterials*, vol. 23, no. 17, pp. 3661–3671, 2002.

[58] A. Borzacchiello and L. Ambrosio, "Structure-property relationships in hydrogels," in *Hydrogels: Biological Properties and Applications*. Springer, 2009, pp. 9–20.

[59] A. Göpferich, "Mechanisms of polymer degradation and erosion," *Biomaterials*, vol. 17, no. 2, pp. 103–114, 1996.

[60] J. Anderson, *Encyclopedia of Materials: Science and Technology*. Elsevier, 2001.

[61] N. A. Peppas, *Biomedical applications of hydrogels handbook*. Springer Science & Business Media, 2010.

[62] "ASTM Standard F2900:2011, Standard Guide for Characterization of Hydrogels used in Regenerative Medicine." West Conshohocken, PA, USA: ASTM International, 2011.

[63] R. Barbucci, *Hydrogels: Biological Properties and Applications*. Springer, 2009.

[64] A. S. Hoffman, "Hydrogels for biomedical applications," *Advanced drug delivery reviews*, vol. 64, pp. 18–23, 2012.

[65] G. M. Kavanagh and S. B. Ross-Murphy, "Rheological characterisation of polymer gels," *Progress in Polymer Science*, vol. 23, no. 3, pp. 533–562, 1998.

[66] S. Bajpai, "Swelling studies on hydrogel networks—a review," *Journal of Scientific and Industrial Research*, vol. 60, pp. 451–462, 2001.

[67] P. B. Welzel, S. Prokoph, A. Zieris, M. Grimmer, S. Zschoche, U. Freudenberg, and C. Werner, "Modulating biofunctional starpeg heparin hydrogels by varying size and ratio of the constituents," *Polymers*, vol. 3, no. 1, pp. 602–620, 2011.

[68] E. R. Aurand, K. J. Lampe, and K. B. Bjugstad, "Defining and designing polymers and hydrogels for neural tissue engineering," *Neuroscience research*, vol. 72, no. 3, pp. 199–213, 2012.

[69] M. C. LaPlaca, V. N. Vernekar, J. T. Shoemaker, and D. K. Cullen, "Three-dimensional neuronal cultures," *Methods in bioengineering: 3D tissue engineering. Norwood, MA: Artech House*, pp. 187–204, 2010.

[70] B. V. Slaughter, S. S. Khurshid, O. Z. Fisher, A. Khademhosseini, and N. A. Peppas, "Hydrogels in regenerative medicine," *Advanced Materials*, vol. 21, no. 32-33, pp. 3307–3329, 2009.

[71] D. J. Mooney and R. S. Langer, "Engineering biomaterials for tissue engineering: the 10–100 micron size scale," *Tissue Engineering*, 2000.

[72] S. T. Ho and D. W. Hutmacher, "A comparison of micro CT with other techniques used in the characterization of scaffolds," *Biomaterials*, vol. 27, no. 8, pp. 1362–1376, 2006.

[73] S. Lin, N. Sangaj, T. Razafiarison, C. Zhang, and S. Varghese, "Influence of physical properties of biomaterials on cellular behavior," *Pharmaceutical research*, vol. 28, no. 6, pp. 1422–1430, 2011.

[74] E. Santos, R. M. Hernández, J. L. Pedraz, and G. Orive, "Novel advances in the design of three-dimensional bio-scaffolds to control cell fate: translation from 2D to 3D," *Trends in biotechnology*, vol. 30, no. 6, pp. 331–341, 2012.

[75] T. Canal and N. A. Peppas, "Correlation between mesh size and equilibrium degree of swelling of polymeric networks," *Journal of Biomedical Materials Research Part A*, vol. 23, no. 10, pp. 1183–1193, 1989.

[76] V. Hagel, T. Haraszti, and H. Boehm, "Diffusion and interaction in PEG-DA hydrogels," *Biointerphases*, vol. 8, no. 1, p. 36, 2013.

[77] J. L. Drury and D. J. Mooney, "Hydrogels for tissue engineering: scaffold design variables and applications," *Biomaterials*, vol. 24, no. 24, pp. 4337–4351, 2003.

[78] M. Golmohamadi, "Quantifying diffusion in biofilms: from model hydrogels to living biofilms," Ph.D. dissertation, Universite de Montreal (Canada), 2012.

[79] A. M. Kloxin, C. J. Kloxin, C. N. Bowman, and K. S. Anseth, "Mechanical properties of cellularly responsive hydrogels and their experimental determination," *Advanced materials*, vol. 22, no. 31, pp. 3484–3494, 2010.

[80] B. Amsden, "Solute diffusion within hydrogels. mechanisms and models," *Macromolecules*, vol. 31, no. 23, pp. 8382–8395, 1998.

[81] T. K. Meyvis, S. C. De Smedt, P. Van Oostveldt, and J. Demeester, "Fluorescence recovery after photobleaching: a versatile tool for mobility and interaction measurements in pharmaceutical research," *Pharmaceutical research*, vol. 16, no. 8, pp. 1153–1162, 1999.

[82] H. Deschout, J. Hagman, S. Fransson, J. Jonasson, M. Rudemo, N. Lorén, and K. Braeckmans, "Straightforward frap for quantitative diffusion measurements with a laser scanning microscope," *Optics express*, vol. 18, no. 22, pp. 22 886–22 905, 2010.

[83] C. Klein and F. Waharte, "Analysis of molecular mobility by fluorescence recovery after photobleaching in living cells," in *Microscopy: Science, Technology, Applications and Education, Formatex Research Center*. Formatex Research Center, 2010, pp. 772–783.

[84] J. M. Zuidema, C. J. Rivet, R. J. Gilbert, and F. A. Morrison, "A protocol for rheological characterization of hydrogels for tissue engineering strategies," *Journal of Biomedical Materials Research Part B: Applied Biomaterials*, vol. 102, no. 5, pp. 1063–1073, 2014.

[85] T. G. Mezger, *The rheology handbook: for users of rotational and oscillatory rheometers*. Vincentz Network GmbH & Co KG, 2006.

[86] M. J. Moura, M. M. Figueiredo, and M. H. Gil, "Rheological study of genipin cross-linked chitosan hydrogels," *Biomacromolecules*, vol. 8, no. 12, pp. 3823–3829, 2007.

[87] M. Rubinstein and R. H. Colby, *Polymer physics*. Oxford university press New York, 2003, vol. 23.

[88] R. Suriano, G. Griffini, M. Chiari, M. Levi, and S. Turri, "Rheological and mechanical behavior of polyacrylamide hydrogels chemically crosslinked with allyl agarose for two-dimensional gel electrophoresis," *Journal of the mechanical behavior of biomedical materials*, vol. 30, pp. 339–346, 2014.

[89] S. Piskounova, R. Rojas, K. Bergman, and J. Hilborn, "The effect of mixing on the mechanical properties of hyaluronan-based injectable hydrogels," *Macromolecular Materials and Engineering*, vol. 296, no. 10, pp. 944–951, 2011.

[90] A. Vedadghavami, F. Minooei, M. H. Mohammadi, S. Khetani, A. R. Kolahchi, S. Mashayekhan, and A. Sanati-Nezhad, "Manufacturing of hydrogel biomaterials with controlled mechanical properties for tissue engineering applications," *Acta Biomaterialia*, vol. 62, pp. 42–63, 2017.

[91] M. Ahearne, Y. Yang, and K. Liu, "Mechanical characterisation of hydrogels for tissue engineering applications," *Topics in tissue Engineering*, vol. 4, no. 12, pp. 1–16, 2008.

[92] F. Brandl, F. Sommer, and A. Goepferich, "Rational design of hydrogels for tissue engineering: impact of physical factors on cell behavior," *Biomaterials*, vol. 28, no. 2, pp. 134–146, 2007.

[93] W. D. Callister and D. G. Rethwisch, *Materials science and engineering: an introduction*. Wiley New York, 2007, vol. 7.

[94] J. F. Nye, *Physical properties of crystals: their representation by tensors and matrices*. Oxford university press, 1985.

[95] K. Brugger, "Thermodynamic definition of higher order elastic coefficients," *Physical Review*, vol. 133, no. 6A, p. A1611, 1964.

[96] J. O. Rawlings, S. G. Pantula, and D. A. Dickey, *Applied regression analysis: a research tool*. Springer Science & Business Media, 1998.

[97] J. D. Kretlow, L. Klouda, and A. G. Mikos, "Injectable matrices and scaffolds for drug delivery in tissue engineering," *Advanced drug delivery reviews*, vol. 59, no. 4, pp. 263–273, 2007.

[98] W. L. K. Chen and C. A. Simmons, "Lessons from (patho) physiological tissue stiffness and their implications for drug screening, drug delivery and regenerative medicine," *Advanced drug delivery reviews*, vol. 63, no. 4, pp. 269–276, 2011.

[99] R. Uibo, I. Laidmäe, E. S. Sawyer, L. A. Flanagan, P. C. Georges, J. P. Winer, and P. A. Janmey, "Soft materials to treat central nervous system injuries: evaluation of the suitability of non-mammalian fibrin gels," *Biochimica et Biophysica Acta (BBA)-Molecular Cell Research*, vol. 1793, no. 5, pp. 924–930, 2009.

[100] H. Park, K. Park, and W. S. Shalaby, *Biodegradable hydrogels for drug delivery*. CRC Press, 2011.

[101] G. Swift, "Requirements for biodegradable water-soluble polymers," *Polymer degradation and stability*, vol. 59, no. 1, pp. 19–24, 1998.

[102] M. Timmins and A. Liebmann-Vinson, *Biodegradable Polymers: Degradation Mechanisms Part I*. Citus Books: London, UK, 2003, vol. 2.

[103] L. S. Nair and C. T. Laurencin, "Biodegradable polymers as biomaterials," *Progress in polymer science*, vol. 32, no. 8, pp. 762–798, 2007.

[104] J. C. Middleton and A. J. Tipton, "Synthetic biodegradable polymers as orthopedic devices," *Biomaterials*, vol. 21, no. 23, pp. 2335–2346, 2000.

[105] H. Tan and K. G. Marra, "Injectable, biodegradable hydrogels for tissue engineering applications," *Materials*, vol. 3, no. 3, pp. 1746–1767, 2010.

[106] J. P. Maranchi, M. M. Trexler, Q. Guo, and J. H. Elisseeff, "Fibre-reinforced hydrogels with high optical transparency," *International Materials Reviews*, vol. 59, no. 5, pp. 264–296, 2014.

[107] N. Efron, *Contact Lens Practice E-Book*. Elsevier Health Sciences, 2016.

[108] S. Hayes, P. Lewis, M. M. Islam, J. Doutch, T. Sorensen, T. White, M. Griffith, and K. M. Meek, "The structural and optical properties of type III human collagen biosynthetic corneal substitutes," *Acta biomaterialia*, vol. 25, pp. 121–130, 2015.

[109] R. Fuentes, E. Fernández, I. Pascual, and C. García, "UV–visible transmittance of silicone–hydrogel contact lenses measured with a fiber optic spectrometer," in *Proceedings of SPIE*, vol. 8785, 2013, pp. 8785AZ–1.

[110] M. Gonzalez-Andrades, J. de la Cruz Cardona, A. M. Ionescu, C. A. Mosse, and R. A. Brown, "Photographic-based optical evaluation of tissues and biomaterials used for corneal surface repair: A new easy-applied method," *PloS one*, vol. 10, no. 11, p. e0142099, 2015.

[111] K. M. Meek, S. Dennis, and S. Khan, "Changes in the refractive index of the stroma and its extrafibrillar matrix when the cornea swells," *Biophysical journal*, vol. 85, no. 4, pp. 2205–2212, 2003.

[112] P. Ducheyne, K. Healy, D. E. Hutmacher, D. W. Grainger, and C. J. Kirkpatrick, *Comprehensive biomaterials*. Newnes, 2015, vol. 1.

[113] M. Born and E. Wolf, *Principles of optics: electromagnetic theory of propagation, interference and diffraction of light*. Elsevier, 2013.

[114] J. M. González-Méijome, M. Lira, A. López-Alemany, J. B. Almeida, M. A. Parafita, and M. F. Refojo, "Refractive index and equilibrium water content of conventional and silicone hydrogel contact lenses," *Ophthalmic and Physiological Optics*, vol. 26, no. 1, pp. 57–64, 2006.

[115] O. Zhernovaya, O. Sydoruk, V. Tuchin, and A. Douplik, "The refractive index of human hemoglobin in the visible range," *Physics in Medicine & Biology*, vol. 56, no. 13, p. 4013, 2011.

[116] D. F. Williams, *Definitions in biomaterials: proceedings of a consensus conference of the European Society for Biomaterials, Chester, England, March 3-5, 1986*. Elsevier Science Limited, 1987, vol. 4.

[117] D. S. Kohane and R. Langer, "Biocompatibility and drug delivery systems," *Chemical Science*, vol. 1, no. 4, pp. 441 – 446, 2010.

[118] D. Williams, "On the mechanisms of biocompatibility," *Biomaterials*, vol. 29, no. 20, pp. 2941 – 2953, 2008.

[119] H.-W. Chien, W.-B. Tsai, and S. Jiang, "Direct cell encapsulation in biodegradable and functionalizable carboxybetaine hydrogels," *Biomaterials*, vol. 33, no. 23, pp. 5706 – 5712, 2012.

[120] K. S. Straley, C. W. P. Foo, and S. C. Heilshorn, "Biomaterial design strategies for the treatment of spinal cord injuries," *Journal of neurotrauma*, vol. 27, no. 1, pp. 1 – 19, 2010.

[121] WHO, *Priority eye diseases*, 2016.

[122] J. Y. Oh, M. K. Kim, M. S. Shin, H. J. Lee, J. H. Ko, W. R. Wee, and J. H. Lee, "The anti-inflammatory and anti-angiogenic role of mesenchymal stem cells in corneal wound healing following chemical injury," *Stem cells*, vol. 26, no. 4, pp. 1047 – 1055, 2008.

[123] S. K. Mittal, M. Omoto, A. Amouzegar, A. Sahu, A. Rezazadeh, K. R. Katikireddy, D. I. Shah, S. K. Sahu, and S. K. Chauhan, "Restoration of corneal transparency by mesenchymal stem cells," *Stem cell reports*, vol. 7, no. 4, pp. 583 – 590, 2016.

[124] B. Kong, W. Sun, G. Chen, S. Tang, M. Li, Z. Shao, and S. Mi, "Tissue-engineered cornea constructed with compressed collagen and laser-perforated electrospun mat," *Scientific Reports*, vol. 7, 2017.

[125] J. J. Doutch, A. J. Quantock, N. C. Joyce, and K. M. Meek, "Ultraviolet light transmission through the human corneal stroma is reduced in the periphery," *Biophysical journal*, vol. 102, no. 6, pp. 1258 – 1264, 2012.

[126] W. J. Dupps and S. E. Wilson, "Biomechanics and wound healing in the cornea," *Experimental eye research*, vol. 83, no. 4, pp. 709 – 720, 2006.

[127] W. Liu, C. Deng, C. R. McLaughlin, P. Fagerholm, N. S. Lagali, B. Heyne, J. C. Scaiano, M. A. Watsky, Y. Kato, R. Munger, N. Shinozaki, F. Li, and M. Griffith, "Collagen – phosphorylcholine interpenetrating network hydrogels as corneal substitutes," *Biomaterials*, vol. 30, no. 8, pp. 1551 – 1559, 2009.

[128] I. Brunette, C. J. Roberts, F. Vidal, M. Harissi-Dagher, J. Lachaine, H. Sheardown, G. M. Durr, S. Proulx, and M. Griffith, "Alternatives to eye bank native tissue for corneal stromal replacement," *Progress in retinal and eye research*, vol. 59, pp. 97 – 130, 2017.

[129] D. G. Harkin, K. A. George, P. W. Madden, I. R. Schwab, D. W. Hutmacher, and T. V. Chirila, "Silk fibroin in ocular tissue reconstruction," *Biomaterials*, vol. 32, no. 10, pp. 2445 – 2458, 2011.

[130] K. M. Meek and C. Knupp, "Corneal structure and transparency," *Progress in retinal and eye research*, vol. 49, pp. 1–16, 2015.

[131] M. Mannis and E. Holland, *Cornea: Fundamentals, diagnosis, and management*. Elsevier, 2016.

[132] M. Koulikovska, M. Rafat, G. Petrovski, Z. Veréb, S. Akhtar, P. Fagerholm, and N. Lagali, "Enhanced regeneration of corneal tissue via a bioengineered collagen construct implanted by a nondisruptive surgical technique," *Tissue Engineering Part A*, vol. 21, no. 5-6, pp. 1116–1130, 2015.

[133] A. Tidu, D. Ghoubay-Benallaoua, B. Lynch, B. Haye, C. Illoul, J.-M. Allain, V. M. Borderie, and G. Mosser, "Development of human corneal epithelium on organized fibrillated transparent collagen matrices synthesized at high concentration," *Acta biomaterialia*, vol. 22, pp. 50–58, 2015.

[134] L. Espandar, B. Bunnell, G. Y. Wang, P. Gregory, C. McBride, and M. Moshirfar, "Adipose-derived stem cells on hyaluronic acid–derived scaffold: A new horizon in bioengineered cornea," *Archives of ophthalmology*, vol. 130, no. 2, pp. 202–208, 2012.

[135] T. I. Zarembinski, N. J. Doty, I. E. Erickson, R. Srinivas, B. M. Wirostko, and W. P. Tew, "Thiolated hyaluronan-based hydrogels crosslinked using oxidized glutathione: An injectable matrix designed for ophthalmic applications," *Acta biomaterialia*, vol. 10, no. 1, pp. 94–103, 2014.

[136] D. Chen, Y. Qu, X. Hua, L. Zhang, Z. Liu, S. Pflugfelder, and D. Li, "A hyaluronan hydrogel scaffold-based xeno-free culture system for ex vivo expansion of human corneal epithelial stem cells," *Eye*, vol. 31, pp. 962–971, 2017.

[137] S. K. Seidlits, Z. Z. Khaing, R. R. Petersen, J. D. Nickels, J. E. Vanscoy, J. B. Shear, and C. E. Schmidt, "The effects of hyaluronic acid hydrogels with tunable mechanical properties on neural progenitor cell differentiation," *Biomaterials*, vol. 31, no. 14, pp. 3930–3940, 2010.

[138] Z.-N. Zhang, B. C. Freitas, H. Qian, J. Lux, A. Acab, C. A. Trujillo, R. H. Herai, V. A. N. Huu, J. H. Wen, S. Joshi-Barr, J. V. Karpiak, A. J. Engler, X.-D. Fu, A. R. Muotri, and A. Almutairi, "Layered hydrogels accelerate iPSC-derived neuronal maturation and reveal migration defects caused by MeCP2 dysfunction," *Proceedings of the National Academy of Sciences*, vol. 113, no. 12, pp. 3185–3190, 2016.

[139] S. Wu, R. Xu, B. Duan, and P. Jiang, "Three-dimensional hyaluronic acid hydrogel-based models for in vitro human iPSC-derived NPC culture and differentiation," *Journal of Materials Chemistry B*, vol. 5, pp. 3870–3878, 2017.

[140] M. M. Adil, T. Vazin, B. Ananthanarayanan, G. M. Rodrigues, A. T. Rao, R. U. Kulkarni, E. W. Miller, S. Kumar, and D. V. Schaffer, "Engineered hydrogels increase the post-transplantation survival of encapsulated hesc-derived midbrain dopaminergic neurons," *Biomaterials*, vol. 136, pp. 1–11, 2017.

[141] A. Banerjee, M. Arha, S. Choudhary, R. S. Ashton, S. R. Bhatia, D. V. Schaffer, and R. S. Kane, "The influence of hydrogel modulus on the proliferation and differentiation of encapsulated neural stem cells," *Biomaterials*, vol. 30, no. 27, pp. 4695–4699, 2009.

[142] G. Palazzolo, N. Broguiere, O. Cenciarelli, H. Dermutz, and M. Zenobi-Wong, "Ultrasoft alginate hydrogels support long-term three-dimensional functional neuronal networks," *Tissue Engineering Part A*, vol. 21, no. 15-16, pp. 2177–2185, 2015.

[143] Z. Wei, J. Zhao, Y. M. Chen, P. Zhang, and Q. Zhang, "Self-healing polysaccharide-based hydrogels as injectable carriers for neural stem cells," *Scientific reports*, vol. 6, p. 37841, 2016.

[144] P. Brodal, *The central nervous system: structure and function*. Oxford University Press, 2016.

[145] R. Y. Tam, T. Fuehrmann, N. Mitrousis, and M. S. Shoichet, "Regenerative therapies for central nervous system diseases: a biomaterials approach," *Neuropsychopharmacology*, vol. 39, no. 1, pp. 169–188, 2014.

[146] Z. Z. Khaing, R. C. Thomas, S. A. Geissler, and C. E. Schmidt, "Advanced biomaterials for repairing the nervous system: what can hydrogels do for the brain?" *Materials Today*, vol. 17, no. 7, pp. 332–340, 2014.

[147] "Neuron," https://upload.wikimedia.org/wikipedia/commons/thumb/b/bc/Neuron_Hand-tuned.svg/400px-Neuron_Hand-tuned.svg.png, accessed: 23.1.2018.

[148] X. Wang, J. He, Y. Wang, and F.-Z. Cui, "Hyaluronic acid-based scaffold for central neural tissue engineering," *Interface focus*, p. rsfs20120016, 2012.

[149] A. R. Murphy, A. Laslett, C. M. O'Brien, and N. R. Cameron, "Scaffolds for 3D in vitro culture of neural lineage cells," *Acta Biomaterialia*, vol. 54, pp. 1–20, 2017.

[150] N. A. Hadjiev and B. G. Amsden, "An assessment of the ability of the obstruction-scaling model to estimate solute diffusion coefficients in hydrogels," *Journal of Controlled Release*, vol. 199, pp. 10–16, 2015.

[151] K. H. Bouhadir, D. S. Hausman, and D. J. Mooney, "Synthesis of cross-linked poly (aldehyde guluronate) hydrogels," *Polymer*, vol. 40, no. 12, pp. 3575–3584, 1999.

[152] Y. Gong, C. Wang, R. C. Lai, K. Su, F. Zhang, and D.-a. Wang, "An improved injectable polysaccharide hydrogel: modified gellan gum for long-term cartilage regeneration in vitro," *Journal of Materials Chemistry*, vol. 19, no. 14, pp. 1968–1977, 2009.

[153] T. Kühn, T. O. Ihalainen, J. Hyväluoma, N. Dross, S. F. Willman, J. Langowski, M. Vihinen-Ranta, and J. Timonen, "Protein diffusion in mammalian cell cytoplasm," *PLoS One*, vol. 6, no. 8, p. e22962, 2011.

[154] B. M. Slepchenko and L. M. Loew, "Chapter one-use of virtual cell in studies of cellular dynamics," *International review of cell and molecular biology*, vol. 283, pp. 1–56, 2010.

[155] H. Nakajima, *Optical Design Using Excel: Practical Calculations for Laser Optical Systems*. John Wiley & Sons, 2015.

[156] L. Ylä-Outinen, T. Joki, M. Varjola, H. Skottman, and S. Narkilahti, "Three-dimensional growth matrix for human embryonic stem cell-derived neuronal cells," *Journal of tissue engineering and regenerative medicine*, vol. 8, no. 3, pp. 186–194, 2014.

[157] J. Koivisto, T. Joki, J. Parraga, R. Pääkkönen, L. Ylä-Outinen, L. Salonen, I. Jonkkari, M. Peltola, T. Ihalainen, S. Narkilahti, and M. Kellomäki, "Bioamine-crosslinked gellan gum hydrogel for neural tissue engineering," *Biomedical materials*, vol. 12, no. 2, p. 025014, 2017.

[158] D. A. Ossipov, S. Piskounova, O. P. Varghese, and J. Hilborn, "Functionalization of hyaluronic acid with chemoselective groups via a disulfide-based protection strategy for in situ formation of mechanically stable hydrogels," *Biomacromolecules*, vol. 11, no. 9, pp. 2247–2254, 2010.

[159] F. Brandl, F. Kastner, R. M. Gschwind, T. Blunk, J. Teßmar, and A. Göpferich, "Hydrogel-based drug delivery systems: comparison of drug diffusivity and release kinetics," *Journal of Controlled Release*, vol. 142, no. 2, pp. 221–228, 2010.

[160] S. Nesrinne and A. Djamel, "Synthesis, characterization and rheological behavior of pH sensitive poly (acrylamide-co-acrylic acid) hydrogels," *Arabian Journal of Chemistry*, vol. 10, no. 4, pp. 539–547, 2017.

[161] C. K. Kuo and P. X. Ma, "Maintaining dimensions and mechanical properties of ionically crosslinked alginate hydrogel scaffolds in vitro," *Journal of Biomedical Materials Research Part A*, vol. 84, no. 4, pp. 899–907, 2008.

[162] J. Li and D. J. Mooney, "Designing hydrogels for controlled drug delivery," *Nature Reviews Materials*, vol. 1, p. 16071, 2016.

[163] R. Kocen, M. Gasik, A. Gantar, and S. Novak, "Viscoelastic behaviour of hydrogel-based composites for tissue engineering under mechanical load," *Biomedical Materials*, vol. 12, no. 2, p. 025004, 2017.

[164] E. R. Morris, K. Nishinari, and M. Rinaudo, "Gelation of gellan – a review," *Food Hydrocolloids*, vol. 28, no. 2, pp. 373–411, 2012.

[165] A.-M. Ionescu, M. Alaminos, J. de la Cruz Cardona, J. de Dios García-López Durán, M. González-Andrades, R. Ghinea, A. Campos, E. Hita, and M. del Mar Pérez, "Investigating a novel nanostructured fibrin–agarose biomaterial for human cornea tissue engineering: Rheological properties," *Journal of the mechanical behavior of biomedical materials*, vol. 4, no. 8, pp. 1963–1973, 2011.

[166] S. J. Petsche, D. Chernyak, J. Martiz, M. E. Levenston, and P. M. Pinsky, "Depth-dependent transverse shear properties of the human corneal stroma," *Investigative ophthalmology & visual science*, vol. 53, no. 2, pp. 873–880, 2012.

[167] H. Hatami-Marbini, "Viscoelastic shear properties of the corneal stroma," *Journal of biomechanics*, vol. 47, no. 3, pp. 723–728, 2014.

[168] S. Cheng, E. C. Clarke, and L. E. Bilston, "Rheological properties of the tissues of the central nervous system: a review," *Medical engineering & physics*, vol. 30, no. 10, pp. 1318–1337, 2008.

[169] G. Lamouche, B. F. Kennedy, K. M. Kennedy, C.-E. Bisaillon, A. Curatolo, G. Campbell, V. Pazos, and D. D. Sampson, "Review of tissue simulating phantoms with controllable optical, mechanical and structural properties for use in optical coherence tomography," *Biomedical optics express*, vol. 3, no. 6, pp. 1381–1398, 2012.

[170] K. J. Lampe, R. G. Mooney, K. B. Bjugstad, and M. J. Mahoney, "Effect of macromer weight percent on neural cell growth in 2D and 3D nondegradable PEG hydrogel culture," *Journal of Biomedical Materials Research Part A*, vol. 94, no. 4, pp. 1162–1171, 2010.

[171] B. Bhana, R. K. Iyer, W. L. K. Chen, R. Zhao, K. L. Sider, M. Likhitpanichkul, C. A. Simmons, and M. Radisic, "Influence of substrate stiffness on the phenotype of heart cells," *Biotechnology and Bioengineering*, vol. 105, no. 6, pp. 1148–1160, 2010.

[172] N. Garcia-Porta, P. Fernandes, A. Queiros, J. Salgado-Borges, M. Parafita-Mato, and J. M. González-Méijome, "Corneal biomechanical properties in different ocular conditions and new measurement techniques," *ISRN ophthalmology*, vol. 2014, 2014.

[173] J.-P. Karam, C. Muscari, and C. N. Montero-Menei, "Combining adult stem cells and polymeric devices for tissue engineering in infarcted myocardium," *Biomaterials*, vol. 33, no. 23, pp. 5683–5695, 2012.

[174] J. Y. Wong, J. B. Leach, and X. Q. Brown, "Balance of chemistry, topography, and mechanics at the cell–biomaterial interface: Issues and challenges for assessing the role of substrate mechanics on cell response," *Surface Science*, vol. 570, no. 1, pp. 119–133, 2004.

[175] N. S. El-Safory, A. E. Fazary, and C.-K. Lee, "Hyaluronidases, a group of glycosidases: current and future perspectives," *Carbohydrate Polymers*, vol. 81, no. 2, pp. 165–181, 2010.

[176] I. Sall and G. Férard, "Comparison of the sensitivity of 11 crosslinked hyaluronic acid gels to bovine testis hyaluronidase," *Polymer degradation and stability*, vol. 92, no. 5, pp. 915–919, 2007.

[177] M. Patenaude and T. Hoare, "Injectable, mixed natural-synthetic polymer hydrogels with modular properties," *Biomacromolecules*, vol. 13, no. 2, pp. 369–378, 2012.

[178] J. Kim, I. S. Kim, T. H. Cho, K. B. Lee, S. J. Hwang, G. Tae, I. Noh, S. H. Lee, Y. Park, and K. Sun, "Bone regeneration using hyaluronic acid-based hydrogel with bone morphogenic protein-2 and human mesenchymal stem cells," *Biomaterials*, vol. 28, no. 10, pp. 1830–1837, 2007.

[179] R. Stern, G. Kogan, M. J. Jedrzejas, and L. Šoltés, "The many ways to cleave hyaluronan," *Biotechnology advances*, vol. 25, no. 6, pp. 537–557, 2007.

[180] J. Fraser, T. Laurent, and U. Laurent, "Hyaluronan: its nature, distribution, functions and turnover," *Journal of internal medicine*, vol. 242, no. 1, pp. 27–33, 1997.

[181] S. L. Wilson, A. J. El Haj, and Y. Yang, "Control of scar tissue formation in the cornea: strategies in clinical and corneal tissue engineering," *Journal of functional biomaterials*, vol. 3, no. 3, pp. 642–687, 2012.

[182] A. Fakhari and C. Berkland, "Applications and emerging trends of hyaluronic acid in tissue engineering, as a dermal filler and in osteoarthritis treatment," *Acta biomaterialia*, vol. 9, no. 7, pp. 7081–7092, 2013.

[183] K. Y. Lee and D. J. Mooney, "Alginate: properties and biomedical applications," *Progress in polymer science*, vol. 37, no. 1, pp. 106–126, 2012.

[184] B. Lindroos, R. Suuronen, and S. Miettinen, "The potential of adipose stem cells in regenerative medicine," *Stem Cell Reviews and Reports*, vol. 7, no. 2, pp. 269–291, 2011.

[185] F. Arnalich-Montiel, S. Pastor, A. Blazquez-Martinez, J. Fernandez-Delgado, M. Nistal, J. L. Alio, and M. P. De Miguel, "Adipose-derived stem cells are a source for cell therapy of the corneal stroma," *Stem Cells*, vol. 26, no. 2, pp. 570–579, 2008.

[186] S. Suri and C. E. Schmidt, "Cell-laden hydrogel constructs of hyaluronic acid, collagen, and laminin for neural tissue engineering," *Tissue Engineering Part A*, vol. 16, no. 5, pp. 1703–1716, 2010.

[187] J. Gomes, R. Amankwah, A. Powell-Richards, and H. Dua, "Sodium hyaluronate (hyaluronic acid) promotes migration of human corneal epithelial cells in vitro," *British journal of ophthalmology*, vol. 88, no. 6, pp. 821–825, 2004.

[188] M. D. Evans, G. A. McFarland, R. Z. Xie, S. Taylor, J. S. Wilkie, and H. Chaouk, "The use of corneal organ culture in biocompatibility studies," *Biomaterials*, vol. 23, no. 5, pp. 1359–1367, 2002.

[189] S. Sandeman, A. Lloyd, B. Tighe, V. Franklin, J. Li, F. Lydon, C. Liu, D. Mann, S. James, and R. Martin, "A model for the preliminary biological screening of potential keratoprosthetic biomaterials," *Biomaterials*, vol. 24, no. 26, pp. 4729–4739, 2003.

[190] M. Notara, S. Schrader, and J. T. Daniels, "The porcine limbal epithelial stem cell niche as a new model for the study of transplanted tissue-engineered human limbal epithelial cells," *Tissue Engineering Part A*, vol. 17, no. 5-6, pp. 741–750, 2011.

[191] J. M. Cyphert, C. S. Trempus, and S. Garantziotis, "Size matters: molecular weight specificity of hyaluronan effects in cell biology," *International journal of cell biology*, vol. 2015, pp. 1–8, 2015.

[192] S. Hou, Q. Xu, W. Tian, F. Cui, Q. Cai, J. Ma, and I.-S. Lee, "The repair of brain lesion by implantation of hyaluronic acid hydrogels modified with laminin," *Journal of neuroscience methods*, vol. 148, no. 1, pp. 60–70, 2005.

[193] L. A. Flanagan, Y.-E. Ju, B. Marg, M. Osterfield, and P. A. Janmey, "Neurite branching on deformable substrates," *Neuroreport*, vol. 13, no. 18, p. 2411, 2002.

APPENDIX I.

Table 1: Statistical analysis of the mechanical properties (second-order elastic constants) of hydrazone crosslinked HA-PVA-, AL-PVA-, GG-HA-, and HA-HA-based hydrogels. p-values < 0.05 (statistically significant difference between the hydrogels) are shown in black and p-values $= 0.0571$ in light gray. The p-values larger than 0.05 are marked only with the symbol >.

	HP1a	HP1b	HP2	HP3	HP4	AP	GH1	GH2	GH3	GH4	HH1	HH2	HH2C	brain	heart	GG-Ca
HP1	>	0.0043	>	>	0.0079	0.0159	>	>	>	0.0357	0.0079	0.0357	0.0357	>	0.0159	
HP1a		0.0095	0.0571	>	0.0159	0.0571	>	>	>	0.0571	0.0159	0.0571	0.0571	>	0.0286	
HP1b			0.0095	0.0095	0.0043	>	0.0238	0.0238	0.0043	0.0238	0.0043	0.0238	0.0238	>	0.0095	
HP2				>	>	0.0286	0.0571	>	0.0317	>	>	>	0.0571	0.0571	0.0286	
HP3					0.0317	0.0286	>	>	>	>	0.0159	0.0571	0.0571	>	0.0286	
HP4						0.0159	0.0357	0.0357	0.0079	>	>	0.0357	0.0357	0.0357	0.0159	
AP							0.0571	0.0571	>	0.0571	0.0159	0.0571	0.0571	>	0.0286	
GH1								>	>	>	0.0357	>	>	>	0.0571	>
GH2									>	>	0.0357	>	>	>	0.0571	>
GH3										0.0357	0.0357	0.0357	0.0357	>	0.0159	0.0357
GH4											>	>	>	>	>	>
HH1												>	0.0357	0.0357	0.0159	
HH2													>	>	>	
HH2C														>	>	
brain															0.0571	>
heart																0.0571

Publications

Publication I

Karvinen J., Koivisto J.T., Jönkkäri I., Kellomäki M.

"The production of injectable hydrazone crosslinked gellan gum-hyaluronan-hydrogels with tunable mechanical and physical properties"

Journal of the Mechanical Behavior of Biomedical Materials, 71 (2017) 383-391.

Journal of the Mechanical Behavior of Biomedical Materials 71 (2017) 383–391

Contents lists available at ScienceDirect

Journal of the Mechanical Behavior of Biomedical Materials

journal homepage: www.elsevier.com/locate/jmbbm

The production of injectable hydrazone crosslinked gellan gum-hyaluronan-hydrogels with tunable mechanical and physical properties

Jennika Karvinen[a,*], Janne T. Koivisto[a,c], Ilari Jönkkäri[b], Minna Kellomäki[a,c]

[a] BioMediTech Institute and Faculty of Biomedical Sciences and Engineering, Tampere University of Technology, Korkeakoulunkatu 3, FI-33101 Tampere, Finland
[b] Faculty of Engineering Sciences, Tampere University of Technology, FI-33101, Tampere, Finland, Korkeakoulunkatu 6, FI-33101 Tampere, Finland
[c] BioMediTech Institute and Faculty of Medicine and Life Sciences, University of Tampere, Lääkärinkatu 1, FI-33520 Tampere, Finland

ARTICLE INFO

Keywords:
Gellan gum
Hyaluronan
Hydrogel
Hydrazone
Stiffness

ABSTRACT

Gellan gum (GG) has been proposed for use in tissue engineering (TE) due to its structural and functional similarities with alginate. The most traditional crosslinking methods of GG, ionical and photocrosslinking, have downsides such as loss of stability or phototoxicity, which can limit their use in certain applications. In this study, an alternative hydrazone crosslinking method is introduced. Hydrazone crosslinking is a simple method that produces no toxic reagents or side-products. The method enables the fabrication of injectable hydrogels. GG was combined with hyaluronan (HA) to improve some properties such as cell attachment. The mechanical and physical properties of GG-HA hydrogels were controlled by changing the molecular weight, the degree of modification, and the ratio of polymer components. GG-HA hydrogels showed ionic nature of deswelling in the presence of cations enabling the control of physical properties in different solution environments. Due to the non-linear elastic behavior of hydrogels and tissues, the stiffness as a function of strain was represented instead of solely giving the second-order elastic constants. The stiffness of GG-HA hydrogels was similar to that of soft tissues at small strains.

1. Introduction

A thorough knowledge of the different properties of materials is important when materials are designed for use in applications such as tissue engineering (TE). The basic principle behind the design of materials for TE is that the material mimics the features of native tissue (Brandl et al., 2007). Hydrogels are materials of particular interest due to their favorable biomimicking properties.

Gellan gum (GG) is an anionic extracellular polysaccharide composed of tetrasaccharide repeating units of 1,3-β-D-glucose, 1,4-β-D-glucuronic acid, 1,4-β-D-glucose and 1,4-$\alpha\beta$-L-rhamnose, containing one carboxyl side group. GG is produced by *Sphingomonas elodea* bacteria (Ferris et al., 2013). In the US, GG has been approved by the Food and Drug Administration (FDA) and by the European Medicines Agency (EMA) in the EU for use in food and medical products as a gelling, stabilizing, and suspending agent (Giavasis et al., 2000; Whiteside and Wallace, 2013). Due to structural and functional similarities with widely used alginate, GG has also been proposed as a scaffold material for TE (Ferris et al., 2015).

At higher temperatures (≥ 40 °C) GG exists as a disordered coil, but on cooling it forms a double-helix structure. This structure is not a true gel, although it has weak gel characteristics. A true gel is formed through the cation-mediated association of helices. Either monovalent or divalent cations can be used. A stronger gel is formed by using divalent cations such as Ca^{2+} and Mg^{2+}, due to bridge formation between pairs of carboxyl groups. Monovalent cations, such as K^{+} or Na^{+}, suppress electrostatic repulsions inducing an aggregation that leads to weaker gels (Ferris et al., 2013). The downside of this crosslinking method is a loss of stability and a weakening of the mechanical properties caused by the exchange of divalent cations with monovalent ones, for example in the physiological environment. An alternative way of producing ionically crosslinked GG hydrogels is by using polyamines such as spermine (SPM^{4+}) and spermidine (SPD^{3+}) (López-Cebral et al., 2013; Soto et al., 2016). In addition, GG hydrogels can also be chemically crosslinked using methacrylate derivatives followed by photocrosslinking with UV-light (Coutinho et al., 2010). The drawbacks of this method are the phototoxicity of UV-light and the reactivity of the photoinitiator.

In order to produce more stable GG hydrogels with an improved gelation environment, a chemical crosslinking method, hydrazone crosslinking, can be used. It is an aldehyde-hydrazide coupling reaction, which belongs to the group of pseudo click chemistry reactions (pseudo

* Corresponding author.
E-mail address: jennika.karvinen@tut.fi (J. Karvinen).

http://dx.doi.org/10.1016/j.jmbbm.2017.04.006
Received 10 December 2016; Received in revised form 26 March 2017; Accepted 4 April 2017
Available online 07 April 2017
1751-6161/

is characterized by moderate orthogonality). These reactions are versatile, simple and reversible and there are no toxic reagents or side-products. The reactions also have high reactivity and yield (Jiang et al., 2014) The properties of hydrazone crosslinked hydrogels can be controlled by altering the number of crosslinkable groups available, the molecular weight of the polymer, the ratio of gel components, and water content. The fabrication of injectable hydrogels is also possible. The injectability of hydrogels would be especially beneficial for TE or drug delivery applications.

Like many other polysaccharides, GG is a relatively inert biomaterial. In order to make GG less inert, hyaluronan (HA) can be added. HA is a naturally occurring anionic polysaccharide composed of β-1,4-linked D-glucuronic acid and β-1,3 N-acetyl-D-glucosamine disaccharide units. HA is a major glucosaminoglucan component of the extracellular matrix (ECM) found in different mammalian tissues. It can be enzymatically degraded with hyaluronidase enzyme. HA has a fairly simple repetitive chemical structure with groups suitable for specific modification (Burdick and Prestwich, 2011).

GG and HA can be modified with complementary reactive aldehyde and hydrazide groups to enable hydrazone crosslinking using, for example, oxidation and adipic acid dihydrazide (ADH) coupling reactions. To date, there have only been a few studies carried out on GG-HA hydrogels (Cencetti et al., 2011; Cerqueira et al., 2014), and no studies were found on using hydrazone crosslinking.

In this study, we have modified GG and HA polymers using aldehyde and hydrazide groups and produced injectable hydrazone crosslinked GG-HA-hydrogels with controllable swelling, biodegradation, rheological and mechanical properties. The aim of the study was to replace the traditional crosslinking methods with hydrazone crosslinking in order to produce GG-HA hydrogels with tunable mechanical and physical properties suitable, for example, for soft tissue applications.

2. Materials and methods

2.1. Materials

Hyaluronic acid sodium salt from streptococcus equi (HA, $M_w = 1.5–1.8 \times 10^6$ g/mol), 1-hydroxybentzotriazole (HOBt), adipic acid dihydrazide (ADH), hydroxylamine hydrochloride, sodium periodate, 1-Ethyl-3-[3-(dimethylamino) propyl]carbodiimide (EDC), hyaluronidase from bovine testes (Type I-S, 400-1000 units/mg solid), sucrose, gellan gum (GG, Gelzan^{TM}, $M_w = 1$ kg/mol), ethylene glycol, dimethyl sulphoxide (DMSO) and deuterium oxide (99.9 atom % D, contains 0.05 wt. % 3-(trimethylsilyl)-propionic-2,2,3,3-d4 acid, sodium salt) were purchased from Sigma-Aldrich (St. Louis, MO, USA). Hyaluronic acid sodium salt (HA, $M_w = 1.5 \times 10^5$ g/mol) was purchased from Lifecore (Chaska, MN, USA). All solvents used were of analytical quality. Milli-Q water was used in synthesis and determinations. Dialysis membranes (Spectra/Por® cut-off 1000 and 12-14,000 g/mol) were purchased from Spectrum Laboratories, Inc. (Rancho Dominguez, CA, USA).

2.2. Synthesis of aldehyde-modified gellan gum

GG was modified with aldehyde groups using periodate oxidation according to a previously reported method (Gong et al., 2009) that was slightly modified. The reaction scheme is shown in Fig. 1. Briefly, GG (0.500 g) was dissolved in deionized water (50 mL) in 60 °C for a few hours. Sodium periodate (0.05 M; 0.022, 0.038, 0.044 or 0.048 g) was added dropwise and stirred for 4 h at room temperature under nitrogen. Ethylene glycol (4 equivalents) was added to inactivate any unreacted periodate and the reaction was stirred for 1 h. Derivatized GG was dialyzed with MW cutoff 1000 membranes against deionized water for a few days. Purified polymers were lyophilized to obtain white cotton-like products (GGALD1, 2, 3 and 4).

All Nuclear Magnetic Resonance (NMR) spectroscopy experiments were measured with a Varian Mercury 300 MHz NMR Spectrometer (Palo Alto, USA). Samples (5 mg) were dissolved in deuterium oxide (600 µL) containing an internal standard (0.05 wt.% 3-(trimethylsilyl)-propionic-2,2,3,3-d4 acid, sodium salt). ^{1}H NMR 300 MHz (D_2O, ppm, Fig. 1): δ 5.15 (s, 1H, CH-1 of rhamnose unit), 4.72 (s, 1H, CH-1 of glucose unit), 4.56 (s, 1H, CH-1 of glucuronic acid unit), 4.07-3.43 (m, 5H, CH-2-5 of units), 1.3 (s, 3H, CH_3 of rhamnose unit).

All Fourier Transform Infrared (FTIR) spectroscopy experiments were collected on a Perkin Elmer Spectrum One FT-IR Spectrometer (Waltham, MA, USA) in the spectral range of 400 cm^{-1} to 4000 cm^{-1}. Samples (1 mg to 2 mg) were pressed into KBr (200 mg) tablets. FTIR (KBr, cm^{-1}, Fig. 2): 1733 (ν(C=O) of –C(O)H), 1615 (ν(C=O) of –C(O)OH).

The degree of substitution (DS%) of GGALD was determined using a previously reported method (Tang et al., 2012). Briefly, GGALD (0.1 g) was dissolved in deionized water (20 mL) and the pH was adjusted to 5 by using 0.1 M HCl. The pH of 0.1 M hydroxylamine hydrochloride solution was also adjusted to 5 by using 0.5 M NaOH. These solutions were mixed together and allowed to react for 15 min. The reacted solution was titrated with 0.5 M NaOH to pH 5. A blank titration was done to serve as a control. The DS% was calculated from

$$DS\% = \frac{645(V_1 - V_2) \times c \times 10^{-3}}{2\,M} \quad (1)$$

where V_1 is the volume (mL) of NAOH reacted with GGALD, V_2 is the volume (mL) of NAOH reacted with a blank sample, c is the concentration (mol/L) of NAOH, M is the mass (g) of the sample, and 645 is the monomer M_w of GG residues.

2.3. Synthesis of hydrazide-modified hyaluronic acid

HA was modified with hydrazide groups (Fig. 1) according to a previously reported method (Bulpitt and Aeschlimann, 1999; Jia et al., 2006). Briefly, HA (200 mg, high $M_w = 1.5–1.8 \times 10^6$ Da or low $M_w = 1.5 \times 10^5$ Da) was dissolved in deionized water (66.66 mL) in a three-necked flask. A 30-fold molar excess of ADH (2.614 g) was added, and the pH was adjusted to 6.8 with 0.1 M HCl or 0.1 M NaOH. EDC (387 mg) and HOBt (271 mg) were dissolved in 2 mL of DMSO/H_2O (vol 1:1) and little by little, this mixture was added to the flask using a dropping funnel. The pH was maintained at 6.8 by adding 0.1 M NaOH or 0.1 M HCl. The reaction was allowed to proceed overnight. Next day, the pH was adjusted to 7 with 0.1 M NaOH. Derivatized HA was dialyzed with MW cutoff 12–14,000 membranes against deionized water for few days. The solution was taken out from dialyzing membrane and NaCl was added to obtain a 5% w/v solution. Derivatized HA was precipitated by adding ethanol (3 vol equivalents). The precipitate was weighted, dissolved in deionized water (5 mg/mL) and dialyzed against deionized water. Purified polymers were lyophilized to obtain white cotton-like products (high molecular weight HAADH1 and low molecular weight HAADH2).

^{1}H NMR 300 MHz (D_2O, ppm, Fig. 1): δ 2.42 (m, 2H, $NHNHCOCH_2$), 2.26 (m, 2H, $CH_2CONHNH_2$), 1.66(m, 4H, $CH_2CH_2CH_2CH_2$).

FTIR (KBr, cm^{-1}, Fig. 2): 1706 (ν(C=O) of sec. amide), 1652 (d(N–H) of prim. amine and amide), 1559 (d(N-H) of sec. amine and amide), 1410 (d(CH_2–C=O) of –CH_2), 1078 (ν(C–N) of amine).

The DS% of HAADH components were determined from integration of the ^{1}H-NMR peaks (Oh et al., 2008). The methyl resonance (δ=2.03 ppm) of the acetamido moiety of the N-acetyl-D-glucosamine was used as an internal standard. The degree of ADH modification of HA at the carboxyl group was determined by the peak area of methylenes of ADH.

2.4. Formation of hydrazone crosslinked gellan gum-hyaluronan hydrogels

GG-HA hydrogels were prepared by combining two complementary

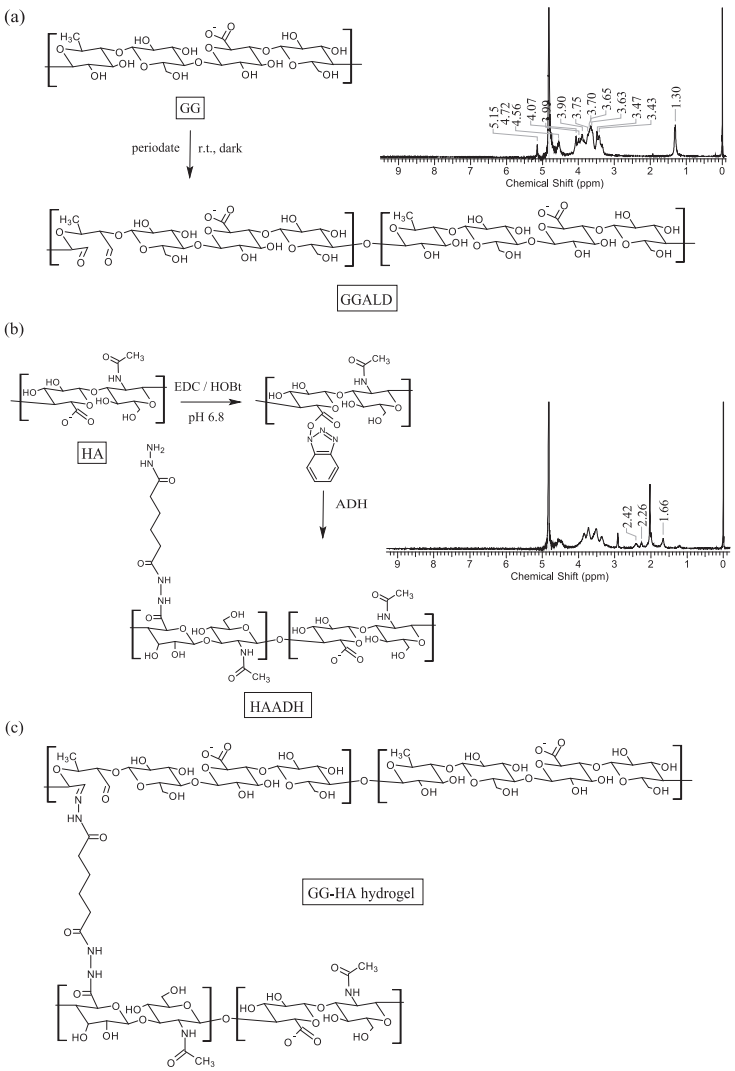

Fig. 1. Reaction schemes of (a) aldehyde-modification of GG (GGALD) and (b) hydrazide-modification of HA (HAADH). The ^{1}H-NMR spectra of GGALD and HAADH components are presented next to the structures. (c) The chemical structure of hydrazone crosslinked GG-HA hydrogels.

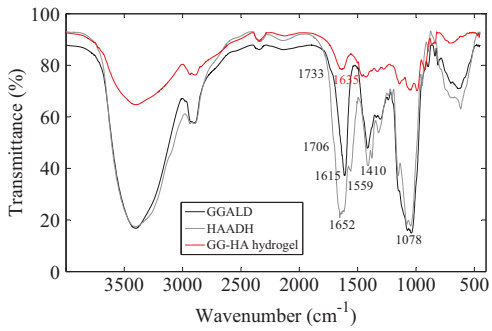

Fig. 2. FTIR spectra of (a) GGALD component, (b) HAADH component, and (c) hydrazone crosslinked GG-HA hydrogel.

reactive polymer components. Freeze dried GGALD components were dissolved in a 10% sucrose solution at 50 °C, whereas HAADH components were dissolved in 10% sucrose solution at room temperature. Polymer solutions were sterilized prior to gelation using Whatman FP 30/0.2 CA-s 0.2 µm (Whatman plc, Little Chalfont, UK) filters. Equal volumes of these solutions were mixed together at room temperature. A dual syringe system was used to improve the mixing. The final polymer concentration of the hydrogels was 1.5%. Different sized cut syringes were used as a mold to ease the pulling out of the sample. The effect of the DS%, concentration, molecular weight and ratio of polymer components on gelation was tested. The compositions of all tested GG-HA hydrogels are shown in Table 1. Only well gelated samples, coded as G1H1, G1H2, G2H1 and G2H2, were chosen for further characterization.

Ionically crosslinked gellan gum gel was used as a control in the characterizations. Ca-crosslinked GG gel (GG-Ca) was prepared by dissolving GG (0.5 % w/v) and $CaCl_2$ (10 mM) in 10% sucrose. The

Table 1
Compositions of tested hydrazone crosslinked GG-HA hydrogels. Terms describing the gelation: Good = fully gelated gel with clear shape, Moderate = nearly gelated gel with almost clear shape, Poor = liquid with some gel structure, No gelation = liquid with no gel structure. Hydrogels with a specific code were chosen for further characterization.

Gel #	Component A	DS %	Concentration mg/mL	Component B	DS %	Concentration mg/mL	Ratio A:B	Gelation	Code
1	GGALD1	7	15	HAADH1	30	15	1:1	Poor	–
2	GGALD1	7	20	HAADH1	30	10	2:1	Poor	–
3	GGALD1	7	15	HAADH2	50	15	1:1	No gelation	–
4	GGALD1	7	20	HAADH2	50	10	2:1	No gelation	–
5	GGALD2	15	15	HAADH1	30	15	1:1	Poor	–
6	GGALD2	15	20	HAADH1	30	10	2:1	Poor	–
7	GGALD2	15	15	HAADH2	50	15	1:1	Poor	–
8	GGALD2	15	20	HAADH2	50	10	2:1	Poor	–
9	GGALD3	20	15	HAADH1	30	15	1:1	Moderate	–
10	GGALD3	20	20	HAADH1	30	10	2:1	Good	G1H1
11	GGALD3	20	15	HAADH2	50	15	1:1	Moderate	–
12	GGALD3	20	20	HAADH2	50	10	2:1	Good	G1H2
13	GGALD4	25	15	HAADH1	30	15	1:1	Good	G2H1
14	GGALD4	25	20	HAADH1	30	10	2:1	Moderate	–
15	GGALD4	25	15	HAADH2	50	15	1:1	Good	G2H2
16	GGALD4	25	20	HAADH2	50	10	2:1	Moderate	–

solutions were heated in a water bath to 37 °C before gelation. The components were mixed together at a volume ratio of 3:1 (GG:$CaCl_2$) with a final crosslinker concentration of 2.5 mM.

2.5. Gelation time

The gelation time was determined with a tube tilt test (ASTM Standard F2900, 2011). The gel point is determined by tilting a tube containing the solution and is considered to be the point where the system stops to flow (transition from fluid to gel state).

2.6. Chemical structure analysis

The chemical structure of the hydrogels was determined using Fourier transform infrared spectroscopy (FTIR). Freeze dried hydrogel samples were pressed into KBr tablets and measured with a FT-IR spectrometer (a Perkin Elmer Spectrum One FT-IR Spectrometer, Waltham, MA, USA) in the spectral range of 400–4000 cm^{-1}.

2.7. Swelling kinetics

The swelling behavior of the GG-HA and GG-Ca hydrogels was studied in deionized water and PBS. Freshly made wet hydrogel samples (3 × 100 µL) were weighed and placed into different media at 37 °C. The hydrogels were weighed at different time points to determine the swelling ratio (SR). The SR was calculated from

$$SR = \frac{W_{swollen} - W_{initial}}{W_{initial}} \times 100\% \quad (2)$$

where $W_{swollen}$ is the mass of swollen hydrogel and $W_{initial}$ is the mass of freshly made wet hydrogel. Equilibrium was considered to be achieved when hydrogel mass no longer increased but remained constant.

The ionic nature of hydrogel shrinking was tested similarly to Coutinho et al. (2010). The hydrogel was first immersed in water for 30 min, then in PBS for 20 h and again immersed in water for 30 min. Variation of hydrogel mass (%) was illustrated at different timepoints.

2.8. Enzymatic degradation

Hyaluronidase-enzyme (HAse) was used to study the enzymatic degradation of the GG-HA hydrogels. Hydrogel samples (3 × 100 µL) were weighed, placed into HAse solution (20–50 U/mL, in PBS) and incubated at 37 °C until the hydrogels were completely degraded. The hydrogels were weighed at different time points to determine the residual mass (%) of hydrogel, and this data was plotted as mass loss curves. The hydrogel was considered to be degraded when there was visually no gel left to weigh.

2.9. Rheological measurements of hydrogels

Rheological measurements of the GG-HA hydrogels were performed using a rotational Haake RheoStress RS150 rheometer equipped with Rheowizard 4.3 software (ThermoHaake, Germany) with cone-plate geometry (20 mm diameter) and a gap of 0.8 mm. Hydrogel samples (500 µL) were prepared into 20 mL cut syringes covered with Parafilm and allowed to stand for 24 h to obtain uniform hydrogels. All rheological experiments were performed at 37 °C in the oscillatory mode. Amplitude sweep ($\gamma = 0.01–10$, $\omega = 1$ Hz) and frequency sweep ($\omega = 0.1–10$ Hz, $\gamma = 0.1$ chosen from the linear viscoelastic region based on the amplitude sweep measurement) were used. Each test was performed three times and each sample was used only once. Storage modulus (G', elastic response)

$$G' = \frac{\sigma_0}{\gamma_0}\cos(\delta) \quad (3)$$

and loss modulus (G", viscous response)

$$G'' = \frac{\sigma_0}{\gamma_0}\sin(\delta) \quad (4)$$

where σ_0 is the stress, γ_0 is the strain amplitude and δ is the phase angle between stress and strain, were determined from the linear viscoelastic region (LVR). Complex modulus

$$G^* = \sqrt{(G')^2 + (G'')^2} \quad (5)$$

resulting from storage and loss modulus and describing the overall viscoelastic behavior of hydrogel was also determined (Mezger, 2006). Also, the loss tangent

$$\tan\delta = \frac{G''}{G'} \quad (6)$$

indicating the overall viscoelasticity of material ($\tan\delta < 0.1$ = a strong gel structure or $\tan\delta > 0.1$ = weak gel structure), was determined (Borzacchiello and Ambrosio, 2009).

2.10. Mechanical measurements of hydrogels and rabbit tissues

Compression measurements were performed using a BOSE Electroforce Biodynamic 5100 machine equipped with a 225 N load sensor and Wintest 4.1 software (Bose Corporation, Eden Prairie, Minnesota, USA). GG-HA and GG-Ca hydrogel samples (875 µL) were

prepared into 5 mL cut syringes covered with Parafilm and allowed to stand for 24 h to obtain uniform hydrogels. Similar sized New Zealand white rabbit (age 10 weeks, male) midbrain and heart samples (obtained from the animal experiments conducted at Tampere University Medical School, University of Tampere) were tested as a reference. The surface of the platens was covered with Parafilm to avoid slipping of the sample. Samples were compressed using unconfined compression at a rate of 10 mm/min to at least 65% strain in the air at room temperature. Five parallel samples were measured.

The measuring data was imported to MS Excel and plotted as stress-strain curves. The data obtained from a stress-strain curve can be used to estimate the so-called stiffness of the material. Here, the stiffness τ, is defined as the derivative of stress σ with respect to strain ϵ (or second derivative of energy density with respect to strain). Therefore, if the measured stress-strain data is represented by a polynomial

$$\sigma(\epsilon) = \sum_{k=0}^{n} c_k \epsilon^k, \tag{7}$$

the stiffness may be defined as

$$\frac{d\sigma}{d\epsilon} \equiv \tau(\epsilon) = \sum_{k=1}^{n} k c_k \epsilon^{k-1}, \tag{8}$$

where the coefficients of the polynomial c_k are the so-called elastic constants (Brugger, 1964; Nye, 1985). For example, c_1 in Eq. (8) is the second-order elastic constant (sometimes called elastic constant, Young's modulus or elastic stiffness constant) (Brugger, 1964; Nye, 1985; Callister and Rethwisch, 2007), while the coefficient c_{k-1} is the kth-order elastic constant. At relatively small strains, the so-called Hooke's law is usually expected to hold (Nye, 1985) and in this case one puts $n=1$ and writes for Eq. (7) $\sigma(\epsilon) \approx c_1\epsilon$, where it was assumed that $c_0 = 0$, that is, $\sigma(0) = 0$ (stress vanishes at zero strain). Due to a characteristic non-linear elastic behavior of hydrogels and tissues, the stress-strain curve cannot be described appropriately by Hooke's law, except at low strains. Therefore, 6th-order polynomials [in Eq. (7) $n=6$] were used in all cases to represent the measured stress-strain data and the coefficients were obtained by using least square fitting optimizing the correlation coefficient R^2. The stiffness describes the same quantity as the second-order elastic constant, the latter being the stiffness at zero strain $\tau(0) = c_1$. The stress polynomial was fitted at strains between 0 and 60%. To compare the $\tau(\epsilon)$ values for different hydrogels and tissues, the stiffness [Eq. (8)] values as a function of strain obtained from the polynomials were plotted.

As is customary, estimates for the second-order elastic constants are given. One way to obtain the second-order elastic constant is to use a linear fit at the small strains of the stress-strain data, the second-order elastic constant being the slope of this linear fit. However, the result may depend rather strongly on the strain interval chosen for the fit, which was also verified in the present work. As previously mentioned, the elastic constants of different order can be obtained, in principle, from the polynomial coefficients. However, the polynomial coefficients, when fitting such experimental data, can behave in a rather unpredictable way, even when the polynomial fit itself describes the measured data quite accurately when measured with R^2. Such instability of the polynomial coefficients can follow from the problem of collinearity (Rawlings et al., 1998) and this was found to be the case in the present work. In order to give some estimates for the second-order elastic constants, the following method was used. The mean and standard deviation of stiffness polynomials for parallel samples were taken at 0 to 0.15 strain. Within this interval, estimates for the second-order elastic constants were chosen to be the mean values for which the standard deviations have their minimum. By using the preceding procedure, the exclusion of initial measurement disruption is enabled. The upper limit for the strain (0.15) was a compromise in that the initial disruption (toe region) is taken into account and that the non-linear elasticity of the materials at this strain is rather weak. The preceding procedure gives only a rather rough estimate for the second-order elastic constants and it is probably more beneficial to study the elasticity in these materials by considering the stiffness as a function of strain.

2.11. Statistical data analysis

Statistical data analyses were performed with MATLAB (Statistics and Machine Learning Toolbox^{TM}). All the quantitative data are presented as mean and standard deviation. A non-parametric Kruskal-Wallis test was used to determine whether there were statistically significant differences within a mechanical and rheological data set. A Wilcoxon rank sum test (equivalent to Mann-Whitney U test) was used to analyze the specific sample pairs for statistically significant differences. Due to a relatively low n, the assumption of normally distributed data would be unjustifiable and therefore non-parametric testing was chosen. When more than two groups were compared, the resulting p values were multiplied by the number of comparisons performed (Bonferroni correction). A p-value of < 0.05 was considered significant.

3. Results and discussion

3.1. Modification of gellan gum and hyaluronan with complementary reactive groups

Gellan gum and hyaluronan were modified with complementary reactive groups to enable hydrazone crosslinking. GG was periodate oxidized by cleaving the C2-C3 bond from the polysaccharide chain to obtain an aldehyde-group containing GGALD components with variable DS% (Table 1, Fig. 1). The success of the modifications was confirmed with ^{1}H-NMR and FTIR structure analysis. In the ^{1}H-NMR spectrum (Fig. 1), the aldehyde peak (9–10 ppm) was not observed. The explanation could be that, in water, aldehydes exist in equilibrium with their hydrated forms. However, aldehydes can also react with some OH-groups of GG and form reversible hemiacetals (Ossipov et al., 2010). In addition, the DS% of the GGALD components were rather low. In the FTIR spectrum (Fig. 2), the aldehyde shoulder (1733 cm^{-1}) was observed, though the signal partly overlaps with carboxyl C=O stretching (1615 cm^{-1}).

Hyaluronan was modified with hydrazide-groups by reacting carboxyl groups of HA with homobifunctional ADH. When using ADH, it should be noted that it can act as a crosslinker if both hydrazide groups manage to react. Despite using a large excess of ADH, the crosslinking effect can be considerable (Ossipov et al., 2010). Two HAADH components with different DS% and molecular weight were obtained (Fig. 1). In the ^{1}H-NMR spectrum (Fig. 1), new CH_2 peaks (2.42, 2.26 and 1.66 ppm) of the modified hydrazide unit were observed, whereas in the FTIR spectrum (Fig. 2), strong amide C=O stretching (1706 cm^{-1}) and amine/amide N-H deformation (1652 and 1559 cm^{-1}) signals from the hydrazide unit were observed.

3.2. Formation of hydrazone crosslinked gellan gum-hyaluronan hydrogels

In order to find the best hydrogel formulations, several gelation tests were made by changing the ratio of the polymer components, the DS% of polymers and the molecular weight of the HAADH component. The compositions of the tested GG-HA hydrogels are shown in Table 1. The gelation was poor or there was no gelation with lower DS% GGALD1-2 components. With higher DS%, the gelation was more successful. Well gelated hydrogels were obtained by using a 2:1 ratio for G1H1 and G1H2 hydrogels, and a 1:1 ratio for G2H1 and G2H2 hydrogels. This could be explained by the availability of crosslinkable groups. It should be noted that due to the high viscosity of the HAADH1 component solution it is more difficult to handle and filter. The four GG-HA hydrogels chosen for characterization were clear and transparent, looking similar to ionically crosslinked GG-Ca gel. GG-HA hydrogels

were found to have stickiness to plastic and glass surfaces, unlike GG-Ca gel. This could be explained by the sticky nature of hyaluronan component added.

The gelation time was estimated using a tube tilt test, which is a simple method, but only gives estimated results. All GG-HA hydrogels gelated in around 5 min with no clear difference between them. The GG-Ca gel also started to gelate in a few minutes, but the full gelation took longer than with the GG-HA hydrogels. Due to a reasonable gelation time, it was possible to prepare the GG-HA hydrogels by using a double syringe system. This also enhances the mixing of gel components and can lead to a more homogeneous gel structure.

3.3. Chemical structure analysis

The chemical structure of the GG-HA hydrogels was determined using FTIR spectroscopy. The FTIR spectrum of the GG-HA hydrogel (Fig. 2) showed that the aldehyde signal at 1733 cm^{-1} disappeared and a new signal at 1635 cm^{-1} appeared, indicating hydrazone crosslinking (C=N stretching). The change of this signal is not so easily verified, because the amide signal at 1652 cm^{-1} overlaps with the hydrazone signal.

3.4. Swelling and deswelling kinetics

The swelling ratio of hydrogels is generally estimated by quantifying the water content as a function of time. Here, the swelling ratio was determined from fresh samples instead of using dried ones. The drying process can damage the network structure and lead to false results. Moreover, the use of fresh samples can better describe the swelling or deswelling behavior in studied conditions. The swelling kinetics of the GG-HA hydrogels in water and PBS are presented in Fig. 3. The results show that in water hydrogels containing a low molecular weight HAADH2 component slightly swelled, leading quickly to the degradation of the structure, whereas hydrogels with a high molecular weight HAADH1 component swelled more without degrading. In PBS, the HAADH1 component-containing hydrogels shrank instead of swelling. Hydrogels containing a low molecular weight HAADH2 component slightly swelled instead of shrinking. There was no significant difference between GGALD3 and GGALD4 components in water or PBS. A control GG-Ca hydrogel hardly swelled in water, whereas in PBS it shrank the most.

In water, the higher swelling ratio of hydrogels containing a high molecular weight HAADH1 component can be explained by the lower crosslinking ratio of those gels. The structure of the hydrogels containing a low molecular weight HAADH2 component is more compact in terms of crosslinking, and therefore prevents further swelling. In PBS, the shrinking of hydrogels can be explained by the ions of PBS. Hydrogels lose their hydrophilic-hydrophobic internal network balance in the presence of ions due to ex-osmosis. At high concentrations, counter ions condense around the fixed carboxylate ion ($-COO^-$) charges leading to a decrease in the repulsive forces among the carboxylate groups, which is why the internal network collapses.

PBS contains cations that can form ionical crosslinks with gellan gum. The ions increase the double helix formation and the establishment of junction zones leading to a more crosslinked structure (Coutinho et al., 2010). The ionic nature of GG-HA hydrogel shrinking was confirmed by first immersing the hydrogel in water for 30 min and then in PBS for 20 h to enable the supposed crosslinking with ions. The shrunken hydrogel was then again immersed in water for 30 min to swell back to its original shape. The results (Fig. 3) showed that all the hydrogels first swelled in water, then deswelled in PBS and swelled again in water. This not only confirmed the ionic nature of the GG-HA

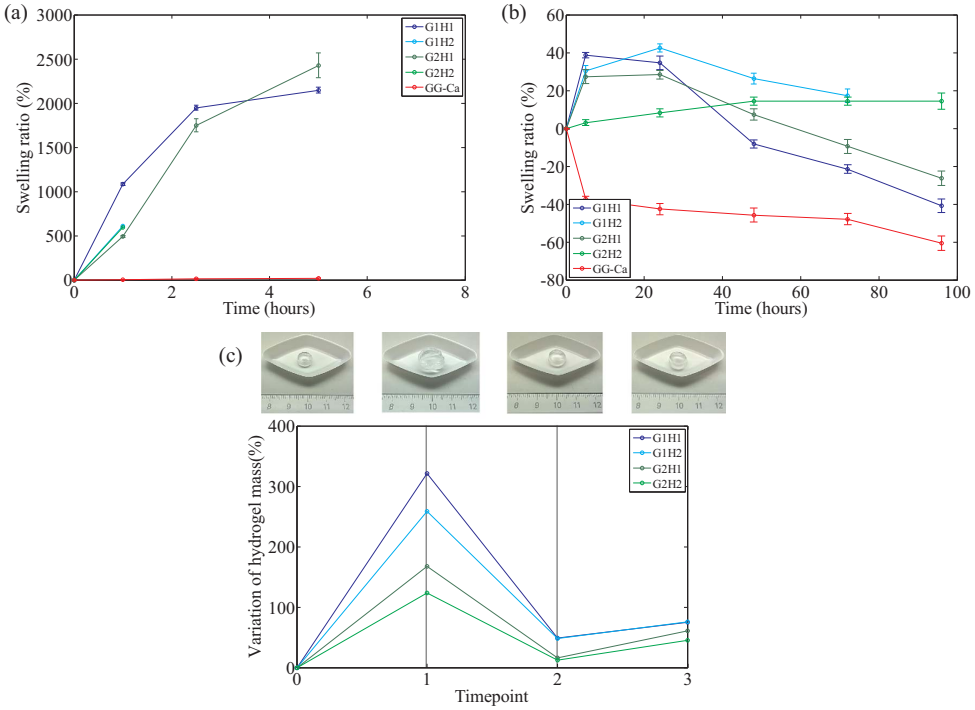

Fig. 3. Swelling ratios of GG-HA hydrogels in (a) deionized water and in (b) PBS. (c) The confirmation of the ionic nature of the GG-HA hydrogel shrinking. Timepoint 1 was taken after swelling in water for 30 min, timepoint 2 after shrinking in PBS for 20 h and timepoint 3 after swelling in water for 30 min. The G1H1 hydrogel is shown as an example. The mean (n=3) and standard deviation bars are shown.

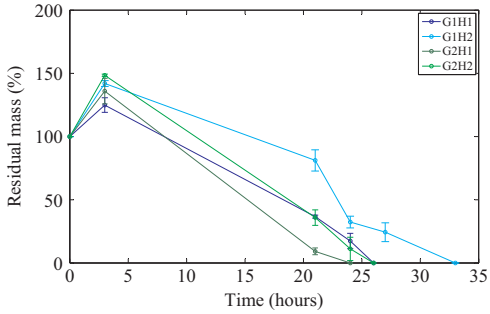

Fig. 4. Enzymatic degradation profiles of GG-HA hydrogels in HAse enzyme (20–50 U/mL). The mean (n = 3) and standard deviation bars are shown.

hydrogels, but also could make the controlling of the physical properties of GG-HA hydrogels possible by changing the solution environment. A similar procedure was used for the Ca-crosslinked GG hydrogel. However, because it degraded between timepoints 2 and 3, it is not included in Fig. 3(c).

3.5. Enzymatic biodegradation

Due to a modified hyaluronan component of hydrogel, hyaluronidase (HAse) was used to study the biodegradation of the GG-HA hydrogels. The degradation residual mass curves of the GG-HA hydrogels are presented in Fig. 4. Results showed that all hydrogels first swelled before any degradation could be detected due to a HAADH component. Hydrogels containing a low molecular weight HAADH2 component degraded slower than hydrogels with a high molecular weight HAADH1 component. On the other hand, hydrogels containing a GGALD3 component degraded slower than hydrogels with a GGALD4 component. Altogether, the degradation studies showed that HAse can recognize the crosslinked hydrazide-modified HA, which indicates that hydrogels could also be degraded *in vivo*. GG can also be degraded with a number of human enzymes such as trypsin, lysozyme and amylase (Ferris et al., 2013), but they were not, however, tested in this work.

3.6. Rheological properties of hydrogels

The viscoelastic properties of the GG-HA hydrogels were studied using rheological measurements. The LVR of the GG-HA hydrogels was determined from amplitude sweep measurements using variable amplitudes, while keeping the frequency constant. The amplitude dependence of modulus is presented in Fig. 5(a). All GG-HA hydrogels showed linear behavior of G' up to about 10% strain. Outside the LVR, G' decreases indicating structure breakdown due to large deformations.

The frequency sweep measurements were performed at variable frequencies at the LVR strain amplitude. The frequency dependence of modulus is presented in Fig. 5(b). For all GG-HA hydrogels, the G′ was parallel to G″ indicating a true gel structure. G′ was higher than G″ and independent of frequency, which is typical for ideal gels (Morris et al., 2012) Results also showed that G′ slightly increased at higher frequencies. As the frequency increases, there is less time for greater movement of the polymer chains. Polymer chains fail to rearrange at a given time scale and this will lead to stiffening and more solid-like behavior (Moura et al., 2007).

The G′ and G″ values are presented in Fig. 5(c). The values show that hydrogels containing a low molecular weight HAADH2 component had slightly higher G′ (and G″) indicating a more stiffer structure and higher resistance to deformation. Hydrogels containing a GGALD4 component had slightly higher G′ than hydrogels containing GGALD3. Complex modulus (G*) was equal to G′ (results not shown) indicating that the properties of hydrogels were dominated by the elastic response over the viscous response. The loss tangent (G1H1, G1H2 and G2H1: $\tan\delta = 0.03$, G2H2: $\tan\delta = 0.02$) was lower than 0.1 for all GG-HA hydrogels, and therefore they were considered as strong gels. It was not possible to perform the rheological measurement of the GG-Ca hydrogel due to measuring problems caused by a water layer existing near the solid boundaries.

3.7. Mechanical properties of hydrogels and rabbit tissues

The mechanical properties of GG-HA and GG-Ca hydrogels and rabbit brain and heart tissues were studied using compression testing. Hydrogels and tissues show non-linear elastic behavior. Therefore, the stiffness as a function of strain was represented for each case instead of solely giving the second-order elastic constants.

Fig. 6(a) shows the representative stress-strain curves for GG-HA and GG-Ca hydrogels and rabbit brain and heart tissues. The GG-HA hydrogels, like many others, were shown to be initially resistant to deformation, and then became progressively stiffer as the load was increased. This finally led to fracture due to permanent deformation, a phenomenon known as strain hardening (Lamouche et al., 2012). The GG-Ca hydrogel showed fracture at a lower strain than the GG-HA hydrogels. When comparing the stress-strain curves of hydrogels and tissues, the GG-HA hydrogels showed a similar elastic behavior to brain tissue at smaller strains.

Fig. 6(b) presents how the stiffness changes with respect to increasing strain. Overall, it can be seen that stiffness is strain dependent with all GG-HA hydrogels and both tissues. With G1H2 and G2H2 hydrogels stiffness is quite constant up to 20% to 30% strain, after which it increases rapidly. This indicates the non-linear deformation characteristics of the hydrogels under compression. At a certain point the stiffness starts to drop, indicating some structural changes, which eventually lead to hydrogel fracture. G1H1 and G2H1 hydrogels show quite constant stiffness until 40% strain. Both hydrogels start to fracture at around 60% strain. The drop in stiffness value, indicating fracture, happens at different strain values for different hydrogels. For G1H2 and GG-Ca hydrogels, this was sooner than for other hydrogels, indicating that they can withstand less deformation before the fracture. Generally, GG-HA hydrogels can be considered more elastic when compared with GG-Ca hydrogel. Brain tissue, on the other hand, showed constant stiffness until 20% strain, after which it increased with no clear fracture. The constant area of heart tissue was even shorter, after which the stiffness increased rapidly with no clear fracture. Based on Fig. 6(b), G1H1, G1H2 and G2H1 hydrogels behaved in a quite similar way to brain tissue from 0% to 15% strain. After that, the stiffness of brain tissue increased more steeply with no sign of fracture, whereas hydrogel stiffness slowly increased and dropped leading finally to fracture. A comparison with heart tissue shows that the stiffness of the hydrogels is too low at low strains to mimic heart tissue. However, some studies have shown that myoblasts or cardiomyocytes differentiate and beat synchronously on a matrix with an intermediate stiffness of 8 kPa to 11 kPa (Karam et al., 2012). This could mean that the G2H2 hydrogel would be close to that range.

The second-order elastic constants of the GG-HA and GG-Ca hydrogels and brain and heart tissues are shown in Fig. 6 (c). The second-order elastic constants of the tissues were found to be similar to previously measured values (Seidlits et al., 2010; Lampe et al., 2010; Bhana et al., 2010). G2H1 hydrogels showed significant difference ($p < 0.05$) with respect to G2H2 and GG-Ca hydrogels and heart tissue. Heart tissue showed a relatively significant difference ($p = 0.0571$) with respect to G1H1, G1H2, GG-Ca and midbrain tissue. Otherwise, there were no statistically significant differences detected between the studied materials.

4. Conclusions

In summary, the fabrication of hydrazone crosslinked gellan gum

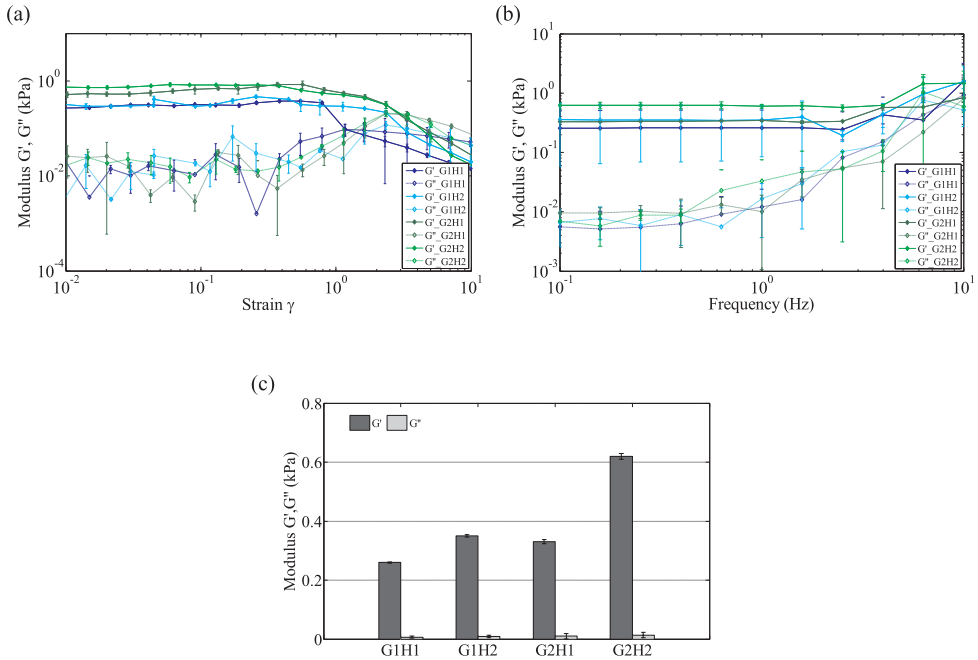

Fig. 5. (a) Amplitude dependence and (b) frequency dependence of modulus of GG-HA-hydrogels. (c) Storage (G′) and loss (G″) modulus of GG-HA hydrogels. The mean (n = 3) and standard deviation are shown. There were no statistically significant differences found between gel types.

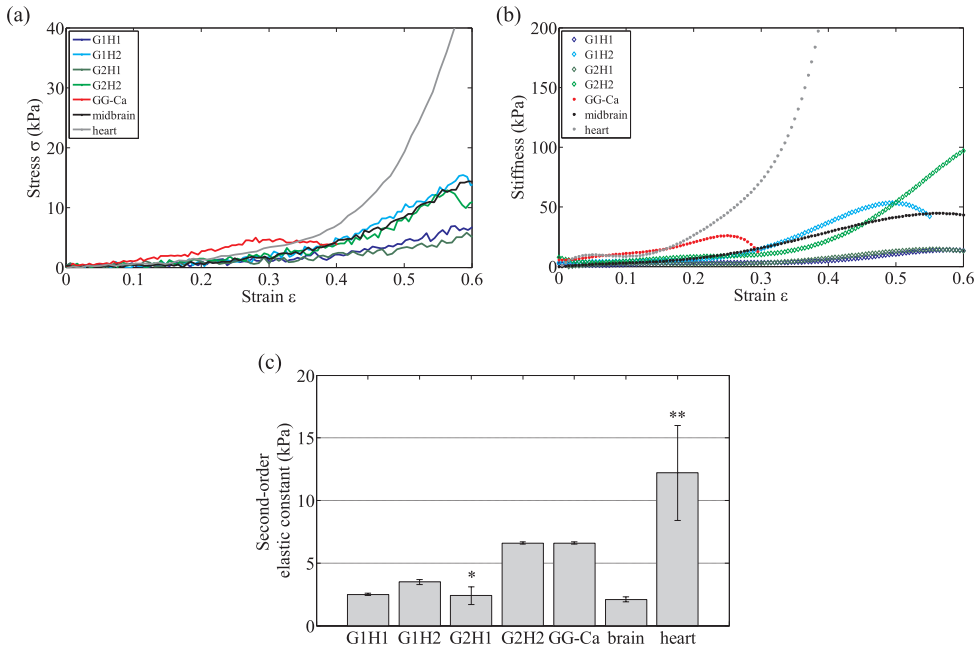

Fig. 6. (a) Stress as a function of strain (representative), and (b) stiffness as a function of strain (average) for GG-HA and GG-Ca hydrogels and rabbit midbrain and heart tissues. (c) Second-order elastic constants determined from the stiffness polynomials by using the method described in Section 2.10. The mean (n = 3-5) and standard deviation bars are shown. *$p < 0.05$ with respect to G2H2, GG-Ca and heart. **$p = 0.0571$ with respect to G1H1, G1H2, GG-Ca and midbrain.

(GG)-based hydrogels was successful. The gelation method described here can be used as an alternative to traditional gelation methods. Moreover, when compared with traditional methods, our method improves the gelation conditions and properties of GG hydrogels. Gellan gum can be combined with hyaluronan (HA) to make the hydrogels less inert, and more swelling and stable. The mechanical and physical properties of GG-HA hydrogels were controlled by changing the degree of modification and the molecular weight of the polymers and the ratio of the gel components. The ionic nature of the deswelling properties of GG-HA hydrogels in the presence of cations was shown. Rheological results confirmed typical gel behavior. Mechanical compressive tests showed that GG-HA hydrogels had similar stiffness to soft tissues at small strains.

Acknowledgements

This work was supported by TEKES (the Finnish Funding Agency for Innovation). The authors would like to thank Ph.D. Mari Hämäläinen (University of Tampere Medical School, Tampere, Finland) for providing the rabbit tissue samples. The authors would also like to thank Ph.D. Alexandre Efimov and Laboratory Attendant Anne-Maarit Tikkanen (Faculty of Natural Sciences, Laboratory of Chemistry and Bioengineering, Tampere University of Technology, Tampere, Finland) for their help related to the NMR- and FTIR-measurements, and Ph.D. Ville Härkönen (University of Jyväskylä, Department of Chemistry, Jyväskylä, Finland) for his help related to the mechanical properties.

References

ASTM Standard F2900: 2011. Standard Guide for Characterization of Hydrogels used in Regenerative Medicine, ASTM International, West Conshohocken, PA, USA.

Bhana, B., Iyer, R.K., Chen, W.L.K., Zhao, R., Sider, K.L., Likhitpanichkul, M., Simmons, C.A., Radisic, M., 2010. Influence of substrate stiffness on the phenotype of heart cells. Biotechnol. Bioeng. 105 (6), 1148–1160.

Borzacchiello, A., Ambrosio, L. 2009. Structure-property relationships in hydrogels, in: Hydrogels, Springer, 2009, pp. 9–20.

Brandl, F., Sommer, F., Goepferich, A., 2007. Rational design of hydrogels for tissue engineering: impact of physical factors on cell behavior. Biomaterials 28 (2), 134–146.

Brugger, K., 1964. Thermodynamic definition of higher order elastic coefficients. Phys. Rev. 133 (6A), A1611.

Bulpitt, P., Aeschlimann, D., 1999. New strategy for chemical modification of hyaluronic acid: preparation of functionalized derivatives and their use in the formation of novel biocompatible hydrogels. J. Biomed. Mater. Res. 47 (2), 152–169.

Burdick, J.A., Prestwich, G.D., 2011. Hyaluronic acid hydrogels for biomedical applications. Adv. Mater. 23 (12).

Callister, W.D., Rethwisch, D.G., 2007. Materials Science and Engineering: An Introduction. 7 Wiley, New York.

Cencetti, C., Bellini, D., Longinotti, C., Martinelli, A., Matricardi, P., 2011. Preparation and characterization of a new gellan gum and sulphated hyaluronic acid hydrogel designed for epidural scar prevention. J. Mater. Sci.: Mater. Med. 22 (2), 263–271.

Cerqueira, M.T., da Silva, L.P., Santos, T.C., Pirraco, R.P., Correlo, V.M., Reis, R.L., Marques, A.P., 2014. Gellan gum-hyaluronic acid spongy-like hydrogels and cells from adipose tissue synergize promoting neoskin vascularization. ACS Appl. Mater. interfaces 6 (22), 19668–19679.

Coutinho, D.F., Sant, S.V., Shin, H., Oliveira, J.T., Gomes, M.E., Neves, N.M., Khademhosseini, A., Reis, R.L., 2010. Modified gellan gum hydrogels with tunable physical and mechanical properties. Biomaterials 31 (29), 7494–7502.

Ferris, C.J., Gilmore, K.J., Wallace, G.G., et al., 2013. Modified gellan gum hydrogels for tissue engineering applications. Soft Matter 9 (14), 3705–3711.

Ferris, C., Stevens, L., Gilmore, K.J., Mume, E., Greguric, I., Kirchmajer, D., Wallace, G.G., et al., 2015. Peptide modification of purified gellan gum. J. Mater. Chem. B 3 (6), 1106–1115.

Giavasis, I., Harvey, L.M., McNeil, B., 2000. Gellan gum. Crit. Rev. Biotechnol. 20 (3), 177–211.

Gong, Y., Wang, C., Lai, R.C., Su, K., Zhang, F., Wang, D.-a, 2009. An improved injectable polysaccharide hydrogel: modified gellan gum for long-term cartilage regeneration in vitro. J. Mater. Chem. 19 (14), 1968–1977.

Jia, X., Yeo, Y., Clifton, R.J., Jiao, T., Kohane, D.S., Kobler, J.B., Zeitels, S.M., Langer, R., 2006. Hyaluronic acid-based microgels and microgel networks for vocal fold regeneration. Biomacromolecules 7 (12), 3336–3344.

Jiang, Y., Chen, J., Deng, C., Suuronen, E.J., Zhong, Z., 2014. Click hydrogels, microgels and nanogels: emerging platforms for drug delivery and tissue engineering. Biomaterials 35 (18), 4969–4985.

Karam, J.-P., Muscari, C., Montero-Menei, C.N., 2012. Combining adult stem cells and polymeric devices for tissue engineering in infarcted myocardium. Biomaterials 33 (23), 5683–5695.

López-Cebral, R., Paolicelli, P., Romero-Caamaño, V., Seijo, B., Casadei, M.A, Sanchez, A., 2013. Spermidine-cross-linked hydrogels as novel potential platforms for pharmaceutical applications. J. Pharm. Sci. 102 (8), 2632–2643.

Lamouche, G., Kennedy, B.F., Kennedy, K.M., Bisaillon, C.-E., Curatolo, A., Campbell, G., Pazos, V., Sampson, D.D., 2012. Review of tissue simulating phantoms with controllable optical, mechanical and structural properties for use in optical coherence tomography. Biomed. Opt. express 3 (6), 1381–1398.

Lampe, K.J., Mooney, R.G., Bjugstad, K.B., Mahoney, M.J., 2010. Effect of macromer weight percent on neural cell growth in 2D and 3D nondegradable PEG hydrogel culture. J. Biomed. Mater. Res. Part A 94 (4), 1162–1171.

Mezger, T.G., 2006. The Rheology Handbook: For Users Of Rotational And Oscillatory Rheometers, Vincentz Network GmbH & Co KG.

Morris, E.R., Nishinari, K., Rinaudo, M., 2012. Gelation of gellan-a review. Food Hydrocoll. 28 (2), 373–411.

Moura, M.J., Figueiredo, M.M., Gil, M.H., 2007. Rheological study of genipin cross-linked chitosan hydrogels. Biomacromolecules 8 (12), 3823–3829.

Nye, J.F., 1985. Physical properties of crystalstheir representation by tensors and matrices. Oxford University Press, New York.

Oh, E.J., Kang, S.-W., Kim, B.-S., Jiang, G., Cho, I.H., Hahn, S.K., 2008. Control of the molecular degradation of hyaluronic acid hydrogels for tissue augmentation. J. Biomed. Mater. Res. Part A 86 (3), 685–693.

Ossipov, D.A., Piskounova, S., Varghese, O.P., Hilborn, J., 2010. Functionalization of hyaluronic acid with chemoselective groups via a disulfide-based protection strategy for in situ formation of mechanically stable hydrogels. Biomacromolecules 11 (9), 2247–2254.

Rawlings, J.O., Pantula, S.G., Dickey, D.A., 1998. Applied Regression Analysis: A Research Tool. Springer Science & Business Media, New York.

Seidlits, S.K., Khaing, Z.Z., Petersen, R.R., Nickels, J.D., Vanscoy, J.E., Shear, J.B., Schmidt, C.E., 2010. The effects of hyaluronic acid hydrogels with tunable mechanical properties on neural progenitor cell differentiation. Biomaterials 31 (14), 3930–3940.

Soto, A.M., Koivisto, J.T., Parraga, J.E., Silva-Correia, J., Oliveira, J.M., Reis, R.L., Kellomäki, M., Hyttinen, J., Figueiras, E., 2016. Optical projection tomography technique for image texture and mass transport studies in hydrogels based on gellan gum. Langmuir 32 (20), 5173–5182.

Tang, Y., Sun, J., Fan, H., Zhang, X., 2012. An improved complex gel of modified gellan gum and carboxymethyl chitosan for chondrocytes encapsulation. Carbohydr. Polym. 88 (1), 46–53.

Whiteside, N.J., Wallace, G.G., 2013. M. in het Panhuis, Preparation and characterisation of graphene composite hydrogels. Synth. Met. 168, 36–42.

Publication II

Koivusalo L.*, Karvinen J.*, Sorsa E., Jönkkäri I., Väliaho J., Kallio P., Ilmarinen T., Miettinen S., Skottman H., Kellomäki M.

"Hydrazone crosslinked hyaluronan-based hydrogels for therapeutic delivery of adipose stem cells to treat corneal defects"

Materials Science and Engineering C: Materials for Biological Applications, 85 (2018), 68-78.

* Authors contributed equally.

Materials Science & Engineering C 85 (2018) 68–78

Contents lists available at ScienceDirect

Materials Science & Engineering C

journal homepage: www.elsevier.com/locate/msec

Hydrazone crosslinked hyaluronan-based hydrogels for therapeutic delivery of adipose stem cells to treat corneal defects

Laura Koivusalo[a,*,1], Jennika Karvinen[b,1], Eetu Sorsa[b], Ilari Jönkkäri[c], Jari Väliaho[b], Pasi Kallio[b], Tanja Ilmarinen[a], Susanna Miettinen[a], Heli Skottman[a], Minna Kellomäki[a,b]

[a] BioMediTech Institute and Faculty of Medicine and Life Sciences, University of Tampere, Arvo Ylpön katu 34, FI-33520 Tampere, Finland
[b] BioMediTech Institute and Faculty of Biomedical Sciences and Engineering, Tampere University of Technology, Korkeakoulunkatu 3, FI-33101 Tampere, Finland
[c] Faculty of Engineering Sciences, Tampere University of Technology, Korkeakoulunkatu 6, FI-33101 Tampere, Finland

ARTICLE INFO

Keywords:
Hyaluronan
Hydrogel
Collagen I
Adipose stem cells
Cell delivery
Corneal stroma

ABSTRACT

Corneal blindness is a worldwide problem, plagued by insufficient amount of high-quality donor tissue. Cell therapy using human adipose stem cells (hASCs) has risen as an alternative to regenerate damaged corneal stromal tissue, the main structural and refractive layer of the cornea. Herein we propose a method to deliver hASCs into corneal defects in hyaluronan (HA)-based hydrogels, which form rapidly *in situ* by hydrazone crosslinking. We fabricated two different HA-based hydrazone-crosslinked hydrogels (HALD1-HACDH and HALD2-HAADH), and characterized their swelling, degradation, mechanical, rheological and optical properties and their ability to support hASC survival. To promote hASC attachment and survival, we incorporated collagen I (col I) to the more stable HALD1-HACDH hydrogel, since the HALD2-HAADH hydrogel suffered swift degradation in culture conditions. We then used an organ culture model with excised porcine corneas to study the delivery of hASCs in these three hydrogels for stromal defect repair. Although all hydrogels showed good hASC survival directly after encapsulation, only the collagen-containing HALD1-HACDH-col I hydrogel showed cells with elongated morphology, and significantly higher cell metabolic activity than the HALD1-HACDH gel. The addition of col I also increased the stiffness and reduced the swelling ratio of the resulting hydrogel. Most importantly, the corneal organ culture model demonstrated these hydrogels as clinically feasible cell delivery vehicles to corneal defects, allowing efficient hASC integration to the corneal stroma and overgrowth of corneal epithelial cells.

1. Introduction

Corneal blindness due to trauma, burns and various inherited or acquired diseases is a worldwide problem, with estimated 1.5 to 2 million new cases annually [1]. Currently these cases are only treatable by transplantation of a donor cornea; a procedure restricted by immune reactions and graft failure, as well as a continuous shortage of suitable donor tissue [2]. The limitations of corneal transplants have driven the search for alternative treatment options, particularly by means of tissue engineering and stem cell therapy. Mesenchymal stem cells (MSCs) have gained great interest in corneal regeneration due to their immunomodulatory and antiangiogenic properties [3], as well as for their capability to inhibit corneal scarring [4]. Human adipose stem cells (hASCs) are an abundant and accessible source of adult MSCs [5], which have also been shown to differentiate towards corneal stromal keratocytes *in vivo* when delivered to the corneal stroma [6,7]. However, simple stromal injection of hASCs in saline solution results in only low amount of integrated cells and insufficient new collagen production [6,8], whereas hydrogel delivery increases the survival of hASCs in the corneal stroma [7].

Collagen I (col I) and hyaluronan (HA) are natural extracellular matrix (ECM) components, present in varying abundance in different tissues. Col I is the main component of ECM in the corneal stroma, where it exists as highly regular fibrils for combined mechanical strength and high transparency [9]. HA is a high molecular weight polysaccharide, which has a high capacity to retain water and is degraded *in vivo* by hyaluronidase enzymes [10,11]. Rather than use HA in its native form, it can be modified through the carboxyl acid and hydroxyl groups in the D-glucuronic acid and *N*-acetyl-D-glucosamine sugar residues. HA-based hydrogels have also been previously suggested for corneal stromal repair, but to date they have required external crosslinkers and need to be preformed prior to implantation [7].

* Corresponding author.
E-mail address: laura.koivusalo@uta.fi (L. Koivusalo).
[1] Authors contributed equally.

https://doi.org/10.1016/j.msec.2017.12.013
Received 3 July 2017; Received in revised form 22 August 2017; Accepted 7 December 2017
Available online 18 December 2017
0928-4931/

Hydrogel components, which gel upon mixing without external crosslinking agents, have the added advantage that they can be injected directly to the defect site where they are able to fill even irregularly shaped defects.

Hydrazone crosslinking has been widely used to prepare hydrogels for tissue engineering applications. Hydrazone crosslinking is a reaction between aldehyde- and hydrazide-groups and belongs to the group of pseudo click reactions (pseudo refers to moderate orthogonality). These reactions have many favorable properties, i.a. high reactivity, simple reaction conditions, no toxic reagents or side products, and high yields [12]. HA can be modified with complementary reactive aldehyde and hydrazide groups to enable this crosslinking. Aldehyde groups can be generated from vicinal diol groups of HA using periodate oxidation [13], or by incorporating an amino-glycerol side chain *via* an amidation reaction and selective oxidation of the pendent group of HA [14]. The latter method provides a less invasive way to modify the polymer. Hydrazide groups can be produced *via* reaction with either adipic acid dihydrazide [15,16] or carbodihydrazide [17]. The polyanionic behavior of HA at physiological pH hinders the adhesion of proteins and cells, which can be overcome by addition of other ECM binding sites, such as collagen [18]. Collagen can be incorporated to the previously described hydrogels, for example through imine formation, although it should be noted, that neutralized collagen can also form a gel on its own at 37 °C.

The aim of the study was to create transparent HA-based hydrogels for the delivery of hASCs for regeneration of the corneal stroma. In this study, we fabricated two HA-based hydrazone crosslinked hydrogels, and characterized their swelling, degradation, mechanical, rheological and optical properties and their ability to support hASC survival. We then further incorporated human col I into the more stable hydrogel, with the aim to promote hASC attachment and survival. In order to demonstrate proof-of-concept, we used an organ culture model with excised porcine corneas to evaluate the clinical relevance of the HA-based hydrogels for hASC delivery to stromal defects.

2. Materials and methods

2.1. Materials and general methods

Hyaluronic acid sodium salt (M_w = 1.5 × 10^5 g/mol) was purchased from Lifecore (Chaska, MN, USA). Adipic acid dihydrazide (ADH), hyaluronidase from bovine testes (Type I–S, 400–1000 units/mg solid), hydroxylamine hydrochloride, acetic acid, sucrose, 1-hydroxybentzotriazole (HOBt), carbodihydrazide (CDH), 3-amino-1,2-propanediol, t-butyl carbazate (TBC), picrylsulfonic acid solution (5% (*w/v*) in H_2O, TNBS), sodium cyanoborohydride, sodium periodate, sodium acetate, ethylene glycol, 1-Ethyl-3-[3-(dimethylamino)propyl] carbodiimide (EDC), dimethyl sulphoxide (DMSO), and deuterium oxide (99.9 atom% D, contains 0.05 wt% 3-(trimethylsilyl)-propionic-2,2,3,3-d4 acid, sodium salt) and collagen type I from human placenta were purchased from Sigma-Aldrich (St. Louis, MO, USA). Sodium chloride was purchased from J.T. Baker (Holland). All solvents used were of analytical quality. Milli-Q water was used in synthesis and determinations. Dialysis membranes (Spectra/Por®cut-off 3500, 12–14,000 and 25,000 g/mol) were purchased from Spectrum Laboratories, Inc. (Rancho Dominguez, CA, USA).

NMR-spectra were measured with Varian Mercury 300 MHz NMR Spectrometer (Palo Alto, USA). Samples (5 mg) were dissolved in deuterium oxide (600 μL) containing internal standard (0.05 wt% 3-(trimethylsilyl)-propionic-2,2,3,3-d4 acid, sodium salt). FTIR-spectra from hyaluronan components and formed hydrogels were measured on a Perkin Elmer Spectrum One ATR-FTIR Spectrometer (Waltham, MA, USA) in the spectral range of 400 to 4000 cm^{-1}.

2.2. Synthesis of aldehyde-modified hyaluronans

Aldehyde groups were introduced to HA according to previously reported method [14]. Reaction scheme is shown in Fig. S1 (a). Briefly, HA (400 mg) was dissolved in deionized water (60 mL). 3-amino-1,2-propanediol (182 mg), and HOBt (153 mg) pre-dissolved in 1:1 (*v/v*) mixture of acetonitrile-water (2 mL) were added, and pH of the solution was adjusted to 6 (1 M HCl). EDC (58 mg) was added to the mixture under nitrogen and stirred overnight. Derivatized polymer was dialyzed with MW cutoff 3500 membrane against dilute HCl (pH 3) containing 0.1 M NaCl for 48 h and against dilute HCl (pH 3) for 24 h. Purified polymer was lyophilized to obtain a white cotton-like product (2,3-dihydroxypropyl amide derivative of HA). This product (200 mg) was dissolved in deionized water (25 mL). Sodium periodate (107 mg) pre-dissolved in deionized water (0.5 mL) was added to the solution in the dark at room temperature (RT) and stirred for 5 min. Ethylene glycol (0.06 mL) was added to inactivate unreacted periodate and solution was stirred for 2 h. Derivatized polymer was dialyzed with MW cutoff 3500 membrane against deionized water for 24 h. Purified polymer was lyophilized to obtain a white cotton-like product, HALD1. ^{1}H NMR (D_2O, 300 MHz) 2,3-dihydroxypropyl amide derivative of HA: δ 4.53 (br s, 1H), 3.83–3.34 (m, 10H), 2.00 (s, 3H). HALD1 (Fig. S3 (a), D_2O, 300 MHz): δ 9.57 (s, 1H), 4.53 (br s, 1H), 3.65 (sharp s, 1H), 3.83–3.34 (m, 10H), 2.01 (s, 3H). FTIR (Fig. 1 (a), cm^{-1}): 1732 (ν(C═O) of −C(O)H), 1643 (ν(C═O) of *sec*. amide), 1617 (d(N−H) of −NHC(O)−), 1558 (d(N−H) of sec. amide).

Alternatively, a periodate oxidation was used to generate aldehyde groups from vicinal diol groups of HA according to previously reported method [13] with small modifications. Reaction scheme is shown in Fig. S1 (b). Briefly, sodium hyaluronate (0.500 g) was dissolved in deionized water (100 mL). Sodium periodate (0.30 g) was dissolved in deionized water (2.7 mL), added dropwise and stirred for 4 h in the dark at RT under nitrogen. Ethylene glycol (4 equivalents) was added to inactivate any unreacted periodate and the solution was then stirred for 1 h. Derivatized polymer was dialyzed with MW cutoff 25,000 membrane against deionized water for three days. Purified polymers were lyophilized to obtain white cotton-like product, HALD2. ^{1}H NMR (Fig. S3 (b), D_2O, 300 MHz): HALD2: *δ* 4.47 (m, 1H, H1 of glucose unit), 3.84–3.34 (m, 5H, H2–5 of glucose unit), 2.02 (s, 3H, −NHC(O)CH3). FTIR (Fig. 1 (b), cm^{-1}): HALD2: 1721 (ν(C═O) of −C(O)H), 1633 (ν(C═O) of −NHC(O)− and −C(O)OH), 1618 (d(N−H) of −NHC(O)−).

Degree of substitution (DS%) of HALD components were determined with TNBS method similarly to [19,20]. Briefly, HALD (20 mg) was dissolved in acetate buffer (2 mL, 0.1 M, pH 5.2) and added to TBC solution in acetate buffer (1 mL, 0.0348 g, 10-fold excess per molar amount of sodium periodate used). The mixture was allowed to react for 1 h at RT. Sodium cyanoborohydride (1 mL, 0.0166 g, equimolar amount to TBC) in acetate buffer was added and allowed to react for 24 h at room temperature under nitrogen. The polymer was dialyzed with MW cutoff 25,000 membrane against 0.1 M NaCl for 24 h and for a further 24 h in deionized water. Purified polymer was lyophilized to obtain a white cotton-like product. The ^{1}H NMR spectrum was measured and the DS% was determined from the integration of ^{1}H NMR peaks. ^{1}H NMR (D_2O, 300 MHz): δ 2.0 (3H, $NHCOCH_3$) and 1.4 (9H, t-Boc).

2.3. Synthesis of hydrazide-modified hyaluronans

Hydrazide groups were introduced to HA according to previously reported method [17]. Reaction scheme is shown in Fig. S1 (c). Briefly, HA (408 mg) was dissolved in deionized water (100 mL). Carbodihydrazide (90 mg) and HOBt (153 mg) were added to the solution and pH was adjusted to 4.7 (0.1 M NaOH). EDC (19.17 mg) was added under nitrogen and stirred for overnight. Derivatized polymer was dialyzed with MW cutoff 3500 membrane against dilute HCl (pH 3.5) containing 0.1 M NaCl for 48 h and against deionized water for 24 h. Purified

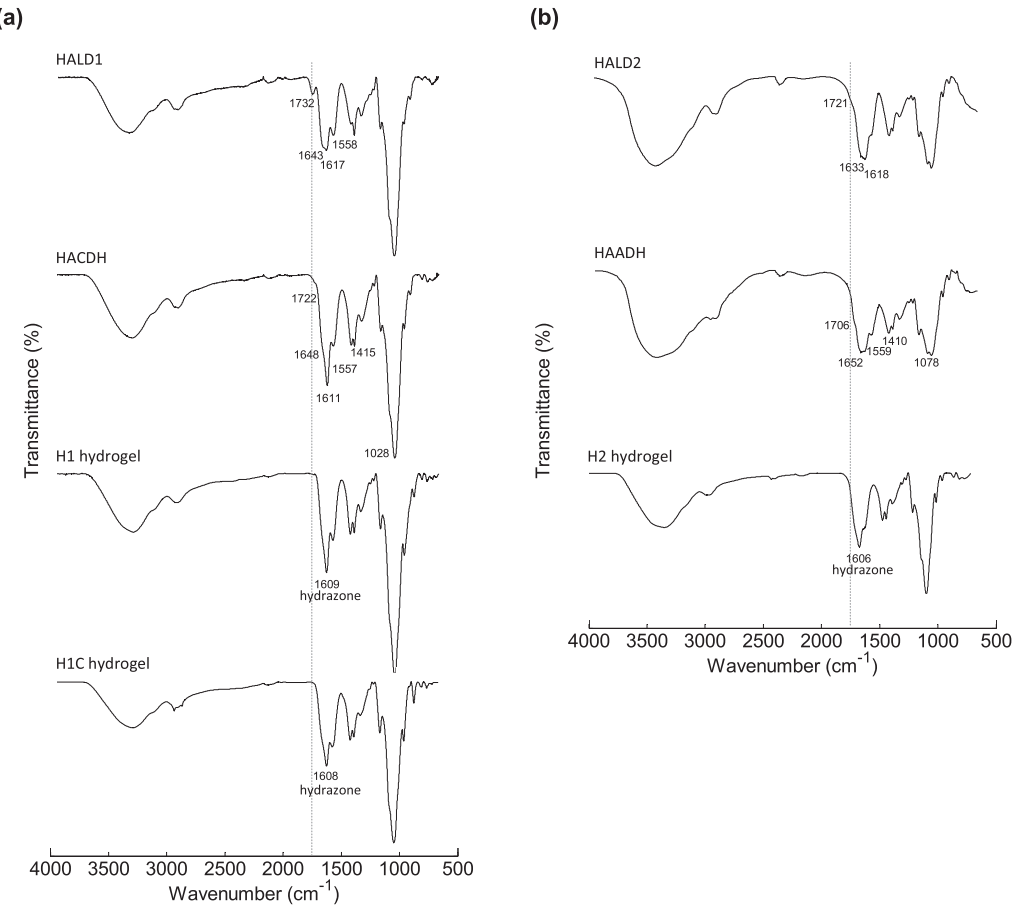

Fig. 1. Chemical structure analysis of polymer components and HA-based hydrogels. (a) FTIR spectra of HALD1 and HACDH components and hydrazone crosslinked HALD1-HACDH (− col I) hydrogels (H1 and H1C). (b) FTIR spectra of HALD2 and HAADH components and hydrazone crosslinked HALD2-HAADH (H2) hydrogel. The appearance of a hydrazone C═N stretching signal at 1609, 1608 and 1606 cm^{-1} for H1, H1C and H2 hydrogels (respectively) and the disappearance of an aldehyde signal at 1732 cm^{-1} for H1 and H1C hydrogels, and at 1721 cm^{-1} for H2 hydrogel confirmed the presence of hydrazone crosslinking.

polymer was lyophilized to obtain a white cotton-like product, HACDH. ^{1}H NMR (Fig. S4, D_2O, 300 MHz): δ 4.54 (br s, 1H), 3.84–3.34 (m, 10H), 2.02 (s, 3H). FTIR (Fig. 1 (a), cm^{-1}): 1722 and 1648 (ν*C═O*) of *sec*. amide), 1611 (d(N−H) of prim. amine), 1557 (d(N−H) of prim. amide), 1415 (d(N−H) of sec. amide), 1028 (ν(C−N) of amine).

DS% of HACDH was determined with TNBS assay as described in [17].

Alternatively, HA was modified with hydrazide groups *via* reaction with adipic acid dihydrazide. The fabrication of the polymer product, HAADH, has been previously reported in [16]. ^{1}H NMR and FTIR spectra are reported in the same article.

2.4. Formation of hydrazone crosslinked hyaluronan-based hydrogels

Hydrogels were fabricated according to Table 1 and Fig. S2. HALD1-HACDH hydrogel (H1) was prepared by dissolving the freeze-dried HALD1 and HACDH components in PBS (pH 7.4) and mixing them in equal volumes. The gelation was shown to occur at RT and at 37 °C; in this case the components were allowed to gel at 37 °C for at least 30 min. HALD2-HAADH hydrogel (H2) was prepared similarly, with the freeze dried HALD2 and HAADH components dissolved in 10% sucrose. For different characterizations, cut syringes were used as molds to ease pushing the sample out. For cell culture, circular polydimethyl siloxane (PDMS) molds with 10 mm inner diameter were used. Solutions were sterilized prior to gelation using Whatman FP 30/0.2 CA-s 0.2 μm (Whatman plc, Little Chalfont, UK) filters.

Additionally, human col I was introduced as a third gel component in H1-based hydrogel (H1C). Briefly, col. I solution (5 mg/mL in acetic acid, pH ≈ 3) was sonicated and then neutralized using 1 M NaOH. After neutralization, col I was mixed with HALD1 component followed by mixing with HACDH component.

The gelation time of hydrogels was determined using a tube tilt test [21], where the gel point can be determined simply by tilting a tube

Table 1
Compositions of hydrazone crosslinked HA-based hydrogels.

Code	Gel components A-B-C	DS% A/B	Conc. mg/mL A/B/C	Volume ratio A:B:C
H1	HALD1-HACDH	15/17	30/30	1:1
H1C	HALD1-HACDH-col I	15/17	30/30/5	2:2:1
H2	HALD2-HAADH	9/50	20/10	1:1

with gel solution and observing the time point where the system stops flowing.

2.5. Swelling kinetics

The swelling kinetics of the hydrogels were studied in cell culture medium (DMEM/F-12, Thermo Fisher Scientific, Waltham, MA, USA). Three parallel freshly made hydrogel samples (100 μL) were weighed and placed into medium at 37 °C. At different time points, the hydrogels were weighed and the swelling ratio (SR) was calculated from the following equation:

$$SR = \frac{W_{swollen} - W_{initial}}{W_{initial}} \times 100\%$$

where $W_{swollen}$ is the mass of swollen hydrogel and $W_{initial}$ is the mass of freshly made wet hydrogel.

2.6. Enzymatic degradation

The enzymatic degradation of the hydrogels was studied by incubating three parallel freshly made hydrogel samples (100 μL) in hyaluronidase (HAse)-solution (20–50 U/mL in PBS) at 37 °C until they were completely degraded. At specific time points, the samples were weighed and the residual mass (%) was calculated. Control samples, without hyaluronidase, were used to show that the degradation was not only due to hydrolysis.

2.7. Rheological measurements

The rheological measurements were performed using a rotational Haake RheoStress RS150 rheometer equipped with Rheowizard 4.3 software (ThermoHaake, Germany) with cone-plate geometry (20 mm diameter) and a gap of 0.8 mm. Three parallel hydrogel samples (500 μL, height 1 mm x diameter 20 mm) were prepared 24 h before measurements into molds and covered with Parafilm. All rheological experiments were performed at 37 °C in the oscillatory mode. Amplitude sweep (γ = 0.01–10, ω = 1 Hz) and frequency sweep (ω = 0.1–10 Hz, γ = 0.1) were used. Storage (G′), loss (G″) and complex moduli (G*) as well as the loss tangent (tan δ = G″/G′) indicating the overall viscoelasticity of material were determined [16].

2.8. Mechanical measurements

The compression measurements were conducted using a BOSE Electroforce Biodynamic 5100 machine equipped with a 225 N load sensor and Wintest 4.1 software (Bose Corporation, Eden Prairie, MN, USA). Five parallel hydrogel samples (875 μL, height 7 mm x diameter 12 mm) were prepared 24 h before measurements into molds and covered with Parafilm. To keep the sample from slipping, the platen surfaces were covered with Parafilm. Samples were compressed using unconfined compression at a rate of 10 mm/min to at least 65% strain in air at RT.

The stiffness of the materials was estimated based on the data obtained from a stress-strain curve. The determination was done similarly to [16]. Briefly, if the measured data is represented by a polynomial (6th order), the stiffness (Γ) may be defined as a derivative of stress (σ) with respect to strain (ε) according to the equation:

$$\frac{d\sigma}{d\varepsilon} \equiv \Gamma(\varepsilon) = \sum_{k=1}^{n} k c_k \varepsilon^{k-1}$$

where the coefficients of the polynomial c_k are the so-called elastic constants. Here, c_1 is the second-order elastic constant, which is sometimes also called the elastic constant, Young's modulus or elastic stiffness constant [22–24]. Second-order elastic constants were estimated based on the means of stiffness polynomials of the five parallel samples at 0–0.15 strain with minimum standard deviations. It should be noted that the stiffness describes the same quantity as the second-order elastic constant, the latter being the stiffness at zero strain $\Gamma(0) = c_1$.

2.9. Optical measurements – refractive index and transparency

Refractive indices of the hydrogels were determined using surface plasmon resonance equipment Navi 210A (BioNavis, Tampere, Finland). The device's goniometer and light source were used to scan the critical angle of total internal reflection between glass and hydrogel. A glass slide (BK7 glass) with a known refractive index was used for device calibration and measurements. After calibration, the flow cell of the device was filled with a hydrogel sample. A curve showing the reflection coefficient as a function of the angle of incidence was obtained from the measurement. The refractive indices of the hydrogels were determined from the curves utilizing Snell's law with the critical angle condition:

$$n_{gel} = n_{glass} \sin(\alpha)$$

where n_{gel} and n_{glass} are the refractive indices of hydrogel and glass slide (n_{glass} = 1.514, [25]), and α is the angle of incidence determined from the curve.

The optical transparency of hydrogels was evaluated using a spectrophotometer (UV–VIS–NIR Spectrophotometer UV-3600Plus, Shimadzu, Kyoto, Japan) operating at the visible wavelength range (400–700 nm). Hydrogel samples (900 μL, thickness 10 mm) were prepared directly into the 1.5 mL semi-micro cuvettes. The hydrogel films (diameter 10 mm × thickness 1 mm) were also photographed to show their optical clarity and transparency.

2.10. Cell experiments in hyaluronan-based hydrogels

2.10.1. Cell encapsulation in hydrogels and in vitro cell culture

This study was conducted under approval of the Ethics Committee of the Pirkanmaa Hospital District (Tampere, Finland, approval number R15161). The hASCs were isolated from adipose tissue samples from a female donor undergoing elective plastic surgery at Tampere University Hospital (Tampere, Finland) with patient's written consent. hASCs were isolated mechanically and enzymatically from subcutaneous adipose tissue as described previously [26,27] and characterized for their surface marker expression by flow cytometry (FACSAria; BD Biosciences, Erembodegem, Belgium) as described in [27]. The cell characterization profile is shown in Table S1.

The hASCs were cultured in a medium containing Dulbecco's modified Eagle's medium/Ham's nutrient mixture F-12 (DMEM/F-12 1:1, Thermo Fisher Scientific, Waltham, MA, USA) supplemented with 5% human serum (type AB male, HIV tested from BioWest, Nuaillé, France), 1% L-glutamine (GlutaMAX™, Thermo Fisher Scientific) and 1% antibiotics (100 U/mL penicillin, 100 μg/mL streptomycin, Lonza, Basel, Switzerland). The cells were maintained in T175 cell culture flasks at 37 °C in 5% CO_2, and passaged at approximately 80% confluence using TrypLE™ Select (Thermo Fisher Scientific).

Cells were encapsulated in hydrogels at passages 4–6. Prior to encapsulation, hASCs were detached from cell culture flasks and collected by centrifugation. Cells were resuspended in cell culture medium, counted and the appropriate number of cells required for each hydrogel were centrifuged to a pellet. Supernatant was removed and cell pellets were mixed by thorough pipetting into the aldehyde-modified HA component at a concentration of 4 × 10^6 cells/mL, with final hydrogel volume of 100 μL. The hydrogels were then formed in PDMS molds as described in Section 2.3. The cell-laden hydrogels were transferred onto tissue culture plates for further *in vitro* culture, with fresh hASC medium changed three times a week.

2.10.2. Cell viability measurements

The viability of hydrogel-encapsulated hASCs was assessed at time points 1 day, 3 days, 7 days and 10 days after encapsulation. Resazurin-based measurement of metabolic activity was performed using PrestoBlue® Cell Viability Reagent and qualitative analysis of viable cells using LIVE/DEAD® viability/cytotoxicity kit for mammalian cells (both from Thermo Fisher Scientific).

For PrestoBlue® analysis, three samples of each hydrogel containing hASCs and one sample without cells were washed once with DPBS (Lonza) and PrestoBlue® reagent diluted 1:10 (*v*/v) in hASC medium was added to the samples. After a 4-h incubation at 37 °C, 100 μL aliquots of PrestoBlue® medium were collected in triplicate from each sample on a 96-well plate and their fluorescence was measured using Viktor 1420 Multilabel Counter (Wallac, Turku, Finland) at excitation and emission wavelengths of 544 nm and 590 nm, respectively.

For qualitative analysis of cell viability, hydrogel samples were incubated with Live/Dead staining solution containing 2 μM Calcein AM and 1 μM Ethidium homodimer diluted in DPBS in 37 °C for 45 min. The samples were washed with DPBS to reduce background fluorescence, and subsequently imaged using an Olympus IX51 fluorescence microscope equipped with a DP71 camera (Olympus Corporation, Tokyo, Japan).

2.10.3. Cornea organ culture

Whole porcine eyes were obtained from a local abattoir and kept on ice in AMES buffer (Sigma–Aldrich) containing 10 mM HEPES and 2% antibiotics for up to 4 h. Excess tissue was removed and the eyes were disinfected as described in [28]. The corneas were excised, moved to tissue culture plates, and cultured partially submerged in serum-free co-culture medium (CnT-Prime-CC, CellnTech, Bern, Switzerland) with 1% antibiotics, 0.25 μg/mL amphotericin B (Thermo Fisher Scientific) and 5 μg/mL Plasmocin (InvivoGen, Toulouse, France) at 37 °C in 5% CO_2 for up to two weeks. The culture medium was changed three times a week, with dropwise addition of new medium to wet the central cornea.

For implantation of hydrogels to porcine corneas, they were mounted on a Barron artificial anterior chamber (Katena products Inc., Denville, NJ, USA) where the operation was performed. First, the corneal epithelium was scraped off using the flat edge of a scalpel (Feather Safety Razor co,. ltd, Osaka, Japan). Then, a 5-mm trephine (Robbins Instruments, Chatham, NJ, USA) was used to make a partial depth incision in the center of the cornea, from which the stroma was removed with a crescent knife (Bausch&Lomb Inc., Rochester, NY, USA). In the formed stromal cavities, hydrogels with hASCs ($n = 5$) and without any cells ($n = 2$) were cast as described in Sections 2.3. and 2.10.1. with final hydrogel volume of 50 μL. After gelation, the corneas were removed from the artificial anterior chamber, placed back into culture plates and covered with silicone contact lenses (EyeQ One-Day Premium, Cooper Vision, Hamble, UK). The culture medium was changed to hASC medium, with the corneas partially submerged. The porcine corneas were cultured for 7 days with the hydrogels and subsequently fixed for 4 h in RT with either 4% PFA or acid-formalin/EtOH –fixative (10% formaldehyde in 70% ethanol and 5% glacial acetic acid, all *v*/v), as the acid-formalin/EtOH should preserve HA better than the standard formalin fixation [29]. The samples were dehydrated in an automated tissue processor (Tissue-Tek VIP, Sakura Finetek Europe) and embedded in paraffin.

To evaluate hASC incorporation into the corneal stroma, immunohistochemical staining for the pan-human marker TRA-1-85 was performed. 5-μm-thick sections of samples were mounted onto SuperFrost glass slides, conventionally deparaffinated and hydrated. Antigen retrieval was performed by placing slides in hot 0.01 M citrate buffer (pH 6.0) for 10 min. After cooling to RT, samples were washed with PBS, endogenic tissue peroxidases were inactivated with 3% H_2O_2 for 5 min, and unspecific binding sites were blocked by incubation with 2.5% normal horse serum (Vector ImmPress reagent, Vector Laboratories) at 37 °C for 45 min. Samples were subsequently incubated with anti-TRA-1-85 mouse IgG antibody (courtesy of Peter Andrews, University of Sheffield) in a 1:50 (*v*/v) dilution in 0.5% BSA at 37 °C for 60 min, and washed with PBS. Secondary labeling with the reporter enzyme was done by incubating samples with Vector ImmPress HRP Reagent (Vector Laboratories, Inc., Burlingame, CA, USA) for 30 min at RT. After subsequent washes in PBS, peroxidation was performed for 5 min at RT with Dako liquid DAB+ chromogen system (Dako North America, Inc., Carpinteria, CA, USA). Finally, samples were counterstained with Harris hematoxylin (Millipore, Billerica, MA, USA) and mounted with Pertex (Histolab, Askim, Sweden). Samples were imaged with a Nikon Eclipse TE2000-S microscope equipped with a DS-Fi1 camera (Nikon Instruments, Amsterdam, Netherlands).

2.11. Statistical data analysis

Statistical data analyses were performed with MATLAB (Statistics and Machine Learning Toolbox™). All the quantitative data are presented as mean and standard deviation. A non-parametric Kruskal-Wallis test and a Wilcoxon rank sum test were used to determine whether there were statistically significant differences within the mechanical and rheological data set, and to analyze specific sample pairs, respectively. Due to a relatively low *n*, a non-parametric testing was chosen. Bonferroni correction was used when more than two groups were compared. A p-value < 0.05 was considered significant.

3. Results and discussion

3.1. Synthesis of complementary reactive hyaluronan components

Hyaluronans were modified with aldehyde groups either through periodate oxidation or through selective oxidation of diol-modified HA. The modifications were confirmed with ^{1}H NMR and FTIR analysis. In the ^{1}H NMR spectrum (Fig. S3 (a)) of HALD1, a barely observable aldehyde peak (9.57 ppm) was detected, whereas with HALD2 it was not visible (Fig. S3 (b)). The reason why the aldehyde peak is not usually observed, is due to a reversible hemiacetal formation [30]. The presence of aldehyde-groups was confirmed based on the FTIR-spectrum (Fig. 1), where the typical aldehyde shoulder (HALD1: 1732 cm^{-1}, HALD2: 1721 cm^{-1}) was detected. The benefit of using selective oxidation of diol-modified HA instead of periodate oxidation is that it keeps the ring-structure of HA intact and therefore HA is more easily recognized by the cells. Hyaluronans were also modified with hydrazide-groups using either CDH or ADH as a source of the hydrazide unit. The ^{1}H NMR spectrum (Fig. S4) of HACDH hardly differed from that of non-modified HA (spectrum not shown), whereas in the FTIR-spectrum (Fig. 1 (a)) signals from the hydrazide unit were detected, including strong amide C=O stretching (1722 cm^{-1}) and amide N−H deformation (1611 and 1557 cm^{-1}) signals. The benefit of using CDH instead of ADH is discussed more deeply in the next section. The DS% of HALD1 and HACDH components were kept relatively low not to lose the favorable properties of original polymer (Table 1).

3.2. Formation of hydrazone crosslinked hydrogels

HA-based hydrazone crosslinked hydrogels were formed from complementary reactive HA components according to Table 1 and Fig. S2. Different aldehyde- and hydrazide-modified components were used for the two hydrogel types, H1 and H2. H1 hydrogel was composed of the HALD1 component formed by selective oxidation of diol-modified HA, and the HACDH component formed by reacting the carboxylic groups in HA with an excess of CDH in the presence of EDC and HOBt. H2 hydrogel, on the other hand, was composed of the periodate oxidized HALD2 component and the HAADH component formed by reacting the carboxylic groups in HA with an excess of ADH in the presence of EDC and HOBt. H1 hydrogel was considered more stable due to a resonance stabilization effect of CDH [17]. CDH has a neighboring

heteroatom (N^3) providing resonance stabilization to the developing N^2 positive charge. This type of linker (C^1=N^1–N^2H–(C=O)N^3H) allows the delocalization of N^2 positive charge due to its urea-type structure. There is no stabilization effect with ADH [17]. H1 hydrogel was preferred due to the more stable structure and the less invasive modification of HALD1 component, thus the effect of col I addition was only tested with the H1 hydrogel. The gelation of H1 hydrogels was successful only when PBS or cell culture medium solutions were used, whereas H2 hydrogel gelated only in deionized water or in 10% sucrose. Sucrose was used to make the osmotic pressure more suitable for the cells in cell culture experiments, therefore it was used in other experiments as well.

The hydrogels gelated in 3–5 min, therefore it was possible to mix the components, for example by pipetting the gel solution few times back and forth in the tip. Alternatively, a double syringe system could be used, making the hydrogel injectable. The gelation time is appropriate for clinical applications of the hydrogels as a cell delivery vehicle, as the gels can flow to fill the wound site, but gelate rapidly enough for a fast and simple implantation.

The chemical structure of the hydrogels was determined with FTIR. The FTIR spectra (Fig. 1) of hydrogels showed the appearance of a hydrazone C=N stretching signal at 1609, 1608 and 1606 cm^{-1} for H1, H1C and H2 hydrogels and the disappearance of an aldehyde signal at 1732 cm^{-1} for H1 and H1C hydrogels, and at 1721 cm^{-1} for H2 hydrogel.

3.3. Swelling kinetics

The swelling tests were conducted in cell culture medium (DMEM/F-12) to determine hydrogel swelling behavior in the cell culture environment. The swelling ratios (SR, %) of the hydrogels are shown in Fig. 2 (a). The results revealed a difference in the stability of hydrogels. Both H1 and H1C hydrogels were stable even after 48 h, whereas H2 hydrogel degraded in hours, and after 24 h there was no gel left to weigh. Both H1 and H1C hydrogels swell considerably. After 48 h, the SR of H1 hydrogel was over 200%, whereas that of H1C hydrogel was approximately 150%. Although the SRs are quite high considering the final application, it is notable that the addition of col I lowered the SR approximately 20% at each data point. One possible explanation for this is that the imine formation between amino groups of collagen and the aldehyde groups of HA makes the structure of H1C hydrogel more crosslinked. Higher degree of crosslinking reduces the swelling ratio. There is also a marked difference in the swelling behavior of the components themselves; HA is susceptible to swelling whereas collagen is not. As expected, replacing some of the HA with collagen led to a lower swelling ratio.

Usually the swelling ratio is determined by studying the water uptake of dry hydrogels. In this case, it was more informative to study the swelling of freshly made wet hydrogels, because this form of gel was used in the cell culture experiments. It is also known that the drying methods, for example freeze-drying, affect the hydrogel structure [31] and therefore can distort the swelling results. We have also noticed this in our studies (data not shown).

3.4. Enzymatic degradation

Enzymatic degradation of the hydrogels was studied using HAse enzyme (20–50 U/mL in PBS). The degradation curves are shown in Fig. 2 (b). The results showed that the degradation behavior of H1 and H2 hydrogels was very different. H1 and H1C hydrogels remained relatively stable for 28 h, after which they were completely degraded by the enzyme by the 48-h time point. H1C hydrogel was slightly more stable than H1, but not significantly. The H1 and H1C control hydrogels did not exhibit significant degradation during the 48 h, indicating that the observed degradation is truly enzymatic rather than caused by simple hydrolysis. On the other hand, H2 hydrogel degraded in a matter of hours. After 24 h, there was no gel left to weigh. Even the control hydrogel started to degrade at the same time, which refers to its tendency to simple hydrolysis caused by the solution environment. Similar behavior was observed in the swelling tests. Different stability behavior between the H1, H1C and H2 hydrogels can be explained by the resonance stabilization effect of CDH described earlier (Section 3.2.).

Based on the results, HAse which degrades HA in biological systems, can recognize the modified HA components and therefore indicates that these hydrogels should be degradable also *in vivo*. HA degradation products are mainly metabolized in the lymph nodes and liver, or locally in alymphatic, densely structured tissues, such as the cornea [10]. As cultured tissue finally replaces the hydrogel scaffold material, the degradation rate of these hydrogels should be tested more thoroughly in actual conditions in order to see if it matches the regeneration rate of the receiving native tissue, as the true HAse enzyme concentration in the cornea may vary from the amount of enzyme used here. It should be noted that the remodeling process of the injured stroma can take months or even years to complete [32].

3.5. Rheological properties

The viscoelastic properties of the hydrogels were determined using rheological tests. The amplitude dependence of modulus for hydrogels is presented in Fig. 3 (a). The linear viscoelastic region (LVR) was

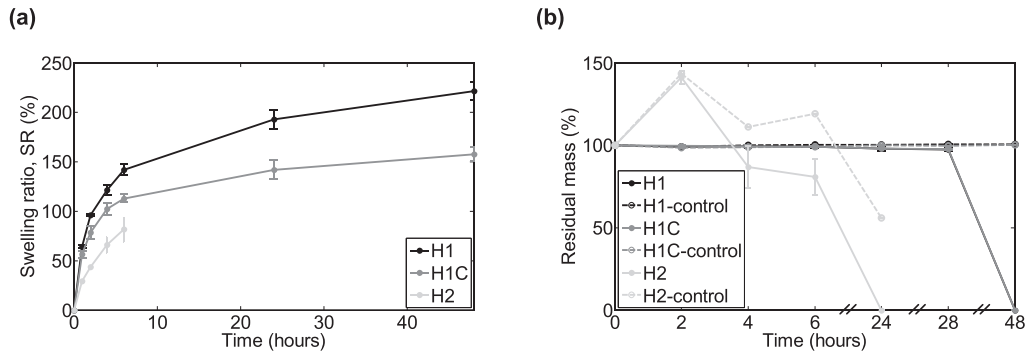

Fig. 2. Swelling kinetics and enzymatic degradability of HA-based hydrogels. (a) Swelling ratio (SR, %) as a function of time (hours) curves of HALD1-HACDH (H1), HALD1-HACDH-col I (H1C) and HAL2-HAADH (H2) hydrogels in cell culture medium (DMEM/F-12). (b) Enzymatic degradation profiles of H1, H1C and H2 hydrogels in HAse enzyme (20–50 U/mL in PBS). Both experiments showed the instability of H2 hydrogel, whereas H1 and H1C were shown to be more stable. The mean (n = 3) and standard deviation bars are shown.

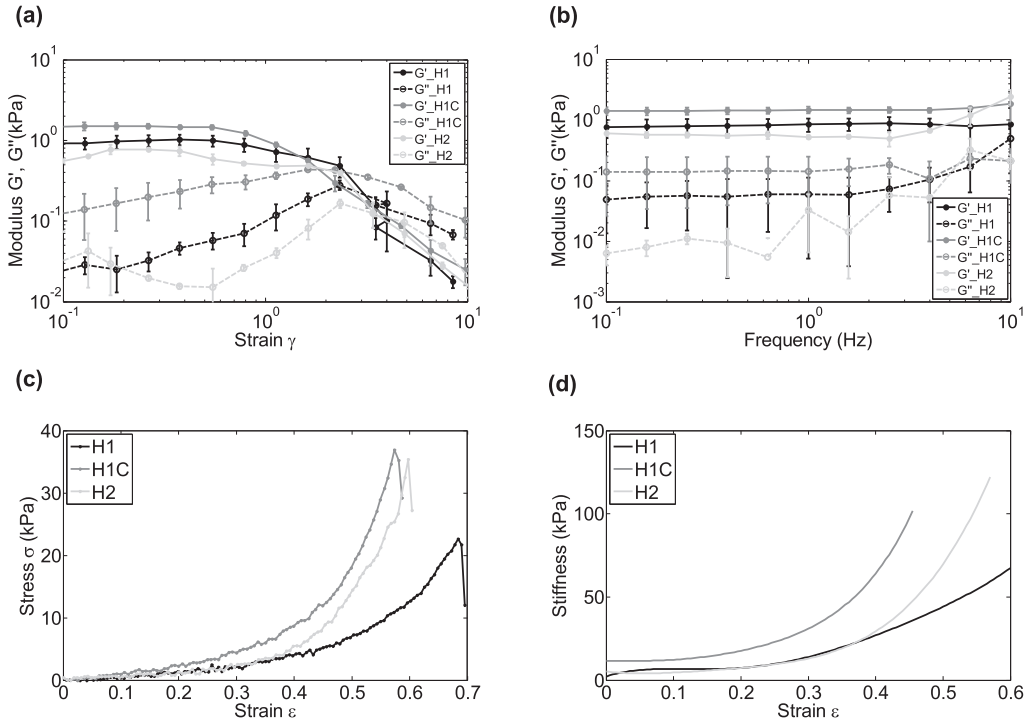

Fig. 3. Rheological and mechanical properties of HA-based hydrogels. (a) Amplitude dependence and (b) frequency dependence of modulus of HALD1-HACDH (H1), HALD1-HACDH-col I (H1C) and HALD2-HAADH (H2) hydrogels (measured with Haake RheoStress RS150 rheometer). The mean (n = 3) and standard deviation are shown. (c) Stress as a function of strain (representative curves, measured with BOSE Electroforce Biodynamic 5100 machine equipped with a 225 N load sensor), and (d) stiffness as a function of strain (average curves, calculated similarly to [16]) curves of H1, H1C and H2 hydrogels.

determined for all the hydrogels. The hydrogels showed linear behavior of G′ up to about 10% strain. Outside this region, G′ dropped indicating a structure breakdown.

The frequency sweep measurements were performed based on the LVR. The frequency dependence of modulus is presented in Fig. 3 (b). A true gel structure was discovered, meaning that G′ was parallel to G″. Moreover, G′ was higher than G″ and independent of frequency, which is typical for ideal gels [33]. The H1 and H1C hydrogels showed more linear behavior of G′ and G″ than the H2 hydrogel. Especially, G″ of the H2 hydrogel was more non-linear, indicating possible non-homogeneity of the structure. This can cause changes in the structure during the measurement. For the H2 hydrogel, the G″ increased at higher strains. This means that there is less time for greater movement of the polymer chains and polymer chains fail to rearrange at a given time scale. This will lead to stiffening and more solid-like behavior [34].

The complex modulus (G*) values of the hydrogels are presented in Table 2. The G* of the H1 and H1C hydrogels were higher than with the H2 hydrogel, although there were no statistically significant differences between the gels. Higher G* indicates stiffer structure and higher resistance to deformation. It is also known that if the loss tangent is lower than 0.1, the hydrogels are considered as strong gels [35]. This was true for all the tested hydrogels (H1:tan δ = 0.084, H1C: tan δ = 0.096 and H2: tan δ = 0.014).

Table 2
The complex modulus, second-order elastic constant, and refractive index values of HALD1-HACDH (H1), HALD1-HACDH-col I (H1C) and HALD2-HAADH (H2) hydrogels. * p < 0.05 H1C with respect to H2. There were no statistically significant differences found between the complex modulus of hydrogels.

Gel	Complex modulus, G* kPa	Second-order elastic constant kPa	Refractive index
H1	0.81 ± 0.23	6.7 ± 1.0	1.337
H1C	1.42 ± 0.16	11.6 ± 1.7*	1.334
H2	0.57 ± 0.06	5.4 ± 1.1	1.332

Rheological properties of the cornea have been studied previously by, for example, Ionescu et al. [36], Petsche et al. [37] and Hatami–Marbini [38]. Due to the differences in the testing conditions, experimental procedures and samples, the results are not directly comparable with each other or with our results.

3.6. Mechanical properties

For tissues and hydrogels, the stress-strain curve is non-linear in the elastic portion even at small strains. For this reason, a polynomial fit, instead of a linear fit, was used for the data. Moreover, the stiffness as a function of strain was represented to illustrate the material behavior in a wider strain range. The representative compressive stress as a function of the deformation strain curves are shown in Fig. 3 (c). The results showed that the hydrogels were initially resistant to deformation, but became progressively stiffer as load increased. Finally, the hydrogels fractured at 55% to 70% strain range. Due to a higher fracture strain, the H1 hydrogel was considered to be more elastic compared to the H1C and H2 hydrogels, whereas the col I-containing H1C hydrogel was the least elastic.

The curves of average stiffness as a function of increasing strain are shown in Fig. 3 (d). The stiffness was shown to be strain dependent. At low strains (0% to 20%) the stiffness was quite constant, but increased after that more or less depending on the sample. This phenomenon is

called strain hardening and it indicates a non-linear deformation characteristic of hydrogels under compression [39].

The second-order elastic constants (stiffness at zero strain) of the hydrogels are shown in Table 2. The H1C hydrogel with highest second-order elastic constant showed significant difference ($p < 0.05$) with respect to the H2 hydrogel. Otherwise, there were no statistically significant differences between the hydrogels.

In the cornea, the predominant component for its mechanical strength is the stroma [40]. Although, the mechanical properties of the studied hydrogels were not close to the native tissue (0.1 to 57 MPa [41]), the hydrogel films were still fairly easy to handle during the cell culturing. This was also one of the main requirements for the material, more than just replicate the mechanical properties, which might be redundant for cell delivery applications.

3.7. Optical properties

The refractive index data of hydrogels was presented as the reflection coefficient, and it was plotted as a function of angle of incidence curves, which are shown in Fig. S5. The angle value was derived by drawing tangent lines on the vertical and horizontal parts of the curve and determining the angle at their intersection point. The calculated refractive indices are shown in Table 2. The refractive indices of all hydrogels were close to that of water ($n = 1.333$). The H1 hydrogel had the highest refractive index of the three, bringing it closest to that of the native corneal stroma ($n = 1.376$ [42]). The rays pass from the cornea into the aqueous humor having a lower refractive index ($n = 1.336$), so most of the reflection occurs at the cornea-air interface.

Although cornea represents the strongest part of the refracting power of the eye, the exact replication of its refractive capacity may not be necessary for clinically viable corneal biomaterials. As refractive errors can be easily adjusted with spectacles, the transparency of the material is more important than its correct refractive properties. This is especially true for degradable materials, which should promote the healing of healthy stromal tissue to ultimately regain the refraction power of the cornea.

The visible light transmission spectra of hydrogels are shown in Fig. 4 (a). The light transmittances for H1, H1C and H2 hydrogels were 85 ± 1, 82 ± 1 and 90 ± 1%, respectively in the 400–700 nm wavelength range. The transparency of the hydrogels was close to the native cornea (> 87%) [43]. The results showed that H2 hydrogel was slightly more transparent than H1-based hydrogels. Also, the addition of col I slightly lowered the transparency. The visible inspection of the samples (inside the cuvettes) also supported these findings. While H2 hydrogel looked visibly clear, the crosslinking was clearly seen inside the H1-based hydrogels. This can be explained with the higher polymer concentration and higher crosslinking density of H1-based hydrogels. The sample thickness used in the transparency measurements was significantly higher than the one intended for the final application. Therefore, thinner hydrogel films were photographed in order to show their optical clarity and transparency. As the photographic images presented in Fig. 4 (b) (and (c)) show, all hydrogels were visibly transparent, even with the addition of col. I.

We measured the optical properties from the hydrogel delivery vehicle alone. However, we note that encapsulating cells in the hydrogels causes light scattering, thus affecting their optical properties. Furthermore, both the refractive index and the transparency may change after implantation due to swelling and degradation, as well as the proliferation and differentiation of encapsulated cells.

3.8. In vitro cell culture

Human ASCs were encapsulated into the three HA-based hydrogels and their viability was assessed qualitatively using Live/Dead staining and the relative metabolic activity in different hydrogels was analyzed with PrestoBlue®. Both the Live/Dead staining (Fig. 5 (a)) and the PrestoBlue® results (Fig. 5 (b)) show that all HA-based hydrogels were capable of sustaining short-term cell survival. However, the more unstable H2 hydrogel samples degraded during the first three days of culture, making their handling for imaging and PrestoBlue® analysis difficult. For this reason, no images could be obtained after the first time point.

Live/Dead staining showed that the number of live cells seemed to decrease from the first time point onwards, although the number of dead cells did not increase. The major cause for this cell loss seems to be cell movement away from the hydrogels, which was observed during culture (Fig. 5 (c)). Additionally, hydrogel swelling, which pulls the cells further away from each other, and possible wash-out of unattached cells may contribute to apparent cell loss from the hydrogels. The col I-containing H1C hydrogel seemed to support hASC attachment better than the purely HA-based H1 hydrogel, based on the presence of more cells with elongated morphology in the Live/Dead images. Previous research has also shown, that the addition of ECM components, such as col I and laminin to hyaluronan hydrogels is required to support cellular attachment and elongated morphology for cardiomyocytes [44], vocal fold fibroblasts [13] and neural cells [18].

Cell metabolic activity seemed to decrease in all hydrogels after the first time point (Fig. 5 (b)). The trend was similar in all hydrogels, but

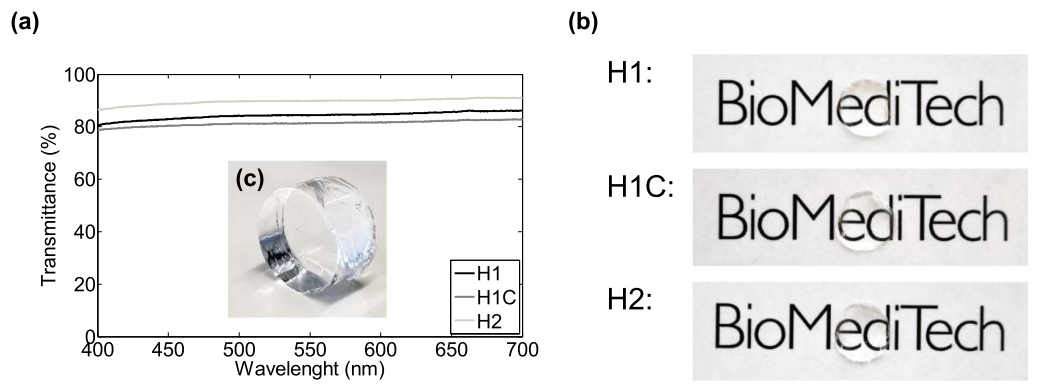

Fig. 4. Transparency of HA-based hydrogels. (a) Light transmission spectra of HALD1-HACDH (H1), HALD1-HACDH-col I (H1C) and HAL2-HAADH (H2) hydrogels. (b) Photographic images of H1, H1C and H2 hydrogels (diameter 10 mm × thickness 1 mm) showing their transparency. (c) Photographic image of H1-based hydrogel (diameter 12 mm × thickness 7 mm) prepared for the compression testing.

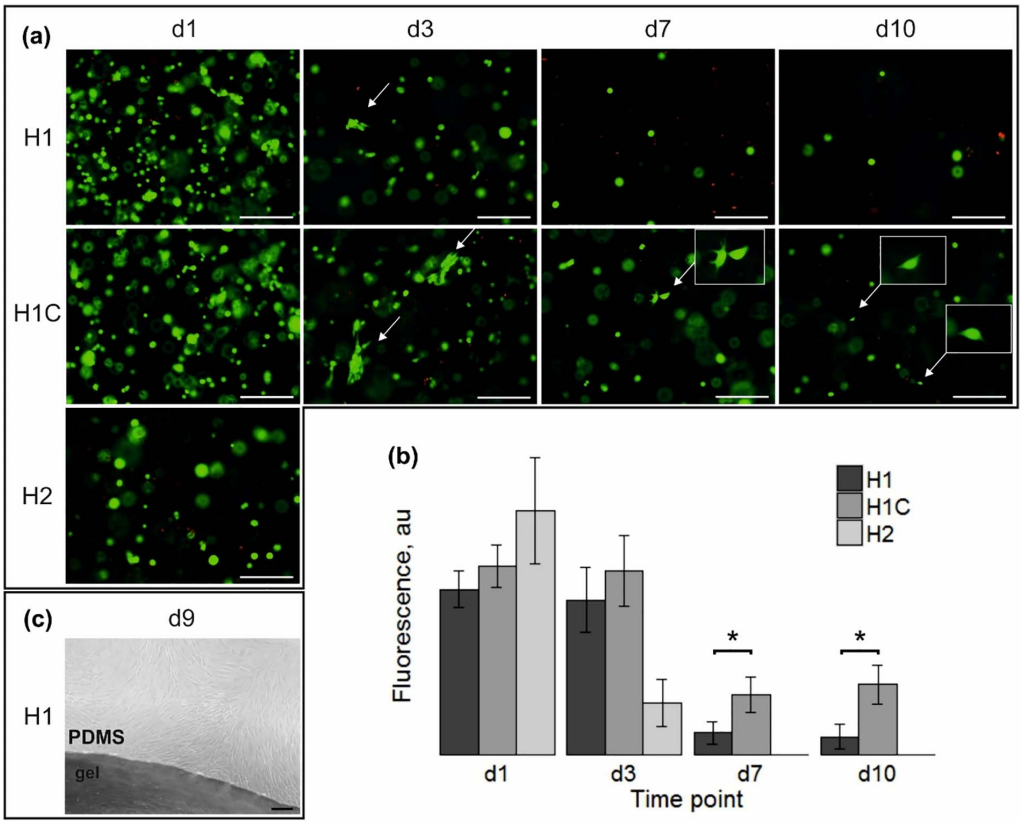

Fig. 5. Cell viability and metabolic activity in HA-based hydrogels. (a) Live-dead staining of hASCs encapsulated in HALD1-HACDH (H1), HALD1-HACDH-col I (H1C) and HALD2-HAADH (H2) hydrogels at different time points. Live cells are shown in green and dead cells in red, with arrows pointing at elongated cells. (b) Metabolic activity of hydrogel-encapsulated hASCs during *in vitro* culture as measured by PrestoBlue® analysis. The bars show the relative fluorescence values of cell-laden hydrogel samples with mean and standard deviation. The H2 hydrogel could not be handled for imaging any more at day 3, and the PrestoBlue® analysis could not be performed after that time point. *significant difference at $p < 0.05$ (c) Representative image of the observed cell growth out of the hydrogels and under the PDMS mold at day 9. Scale bars in the images are 200 μm. (For interpretation of the references to colour in this figure legend, the reader is referred to the web version of this article.)

the onset of the steep decline in metabolic activity varied; for the H2 hydrogel, the drop occurred between day 1 and day 3, whereas for H1 and H1C it occurred between day 3 and day 7. The decline in cell metabolic activity correlated with the observed decrease of cells in the Live/Dead images, also indicating that cells escaped from the hydrogels. However, the remaining cells maintained their metabolic activity at a steady level for the rest of the culture period. Importantly, the H1C hydrogel-encapsulated hASCs had significantly higher metabolic activity than those in the H1 hydrogel in the two last time points, which indicates that addition of col I has a significant effect on promoting active cell metabolism and survival.

The Live/Dead and PrestoBlue® results indicate that hASCs survive encapsulation into all of the HA-hydrogels, but the addition of col I is required for cell attachment to the hydrogel matrix. The efficient loss of cells from the hydrogels consisting of purely HA-components, suggests they could be suitable cell delivery vehicles, with either a rapid (H2) or more delayed delivery (H1) of hASCs to stromal defects. However, for long-term tissue integration of the hydrogel matrix, cell attachment may be required for efficient cell proliferation and ECM synthesis [45].

3.9. Implantation to corneal organ culture model

The corneal organ culture model is an excellent method to study cellular interactions at the organ level and to evaluate the clinical feasibility of biomaterials for corneal applications [46,47]. The corneal organ culture model has been previously used mainly to study re-epithelialization, since the organ-cultured corneas retain their capability for epithelial regeneration for as long as two months in culture [28]. Although the results obtained from the corneal organ culture model always require validation in an *in vivo* animal model, its use in fast and low-cost preliminary screening of corneal biomaterials can significantly reduce unnecessary animal testing.

We used excised porcine corneas to model the delivery of hASCs in the HA-based hydrogels into stromal defects. As a proof-of-concept, we inflicted large stromal wounds, into which the hydrogels were implanted with and without hASCs. The immunohistological evaluation of the porcine corneas with hydrogel-delivered hASCs revealed cell migration into the corneal stroma, after just one week of culture (Fig. 6). Successful integration of hASCs into the stroma was observed for all of the hydrogels, although H1C hydrogel samples seemed to show slightly less migrated hASCs in the stroma than H1 and H2. Possibly, collagen's effect on improving hASC attachment may have delayed their migration to the stroma from the H1C hydrogel. The integration of hASCs to the corneal stroma in the organ culture model demonstrates the clinical feasibility of the hydrogels for stromal delivery of hASCs.

Despite the predominant loss of the hydrogels themselves during

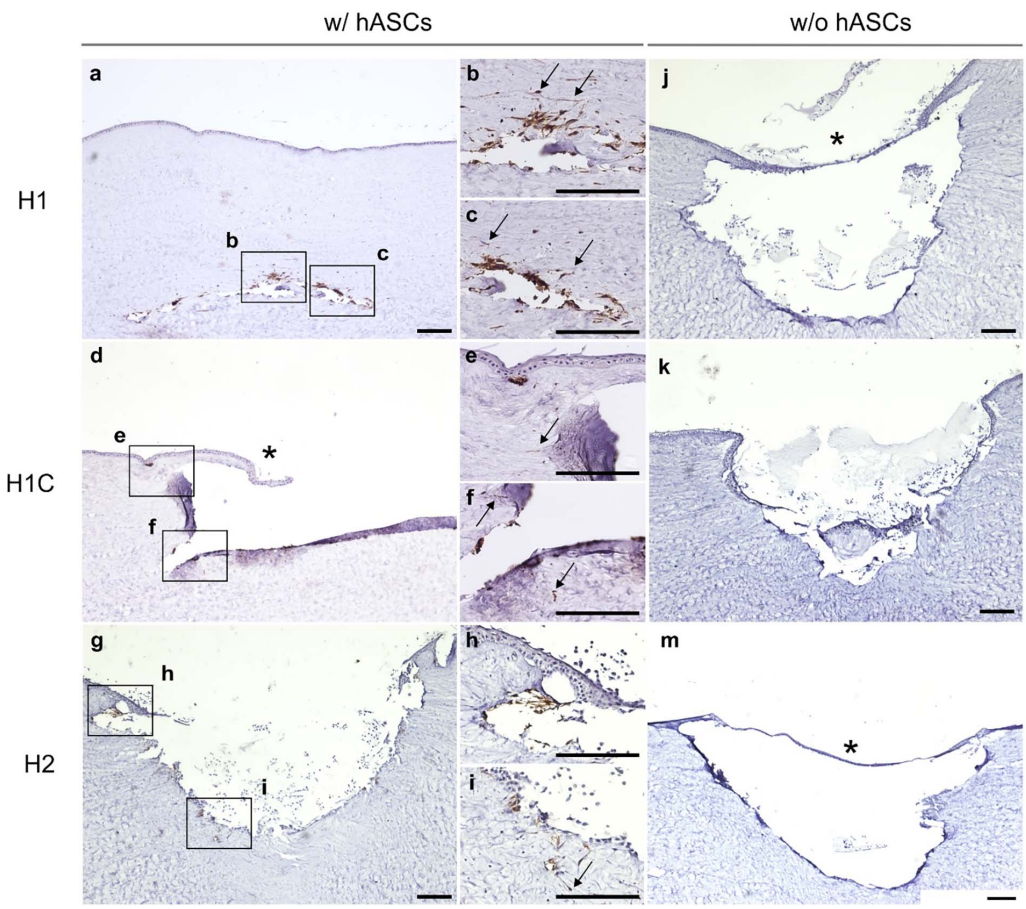

Fig. 6. Immunohistochemical detection of hydrogel-delivered hASCs after seven days in porcine corneal organ culture model using human cell marker TRA-1-85. Images on the left panel (a–i) describe hydrogels HALD1-HACDH (H1), HALD1-HACDH-col I (H1C) and HALD2-HAADH (H2) with encapsulated hASCs, and the images on the right (j–m) depict delivery of each gel vehicle only. All other sections depict the central wound area, except that of H1 w/hASCs, which was sectioned near the wound edge. Successful hASC integration into the corneal stroma was seen for all hydrogels (examples marked with arrows), and epithelium growth on top of the transplanted gels was observed with all gels, even without hASCs (denoted by * in images e, j and m). However, epithelial overgrowth could not be verified for all samples, as the gels were lost during histological processing. Scale bars in the images are 200 μm.

histological processing, re-epithelialization of the corneal surface was evident from the tissue sections. This was clearly seen in the vehicle-only controls of H1 and H2 in Fig. 6 (j) and (m), respectively. Fig. 6 (d) also implies epithelial outgrowth over the H1C hydrogel sample, although the complete epithelium is not visible in the section. Previous research has also reported that HA can support corneal epithelial cell growth [48], which further validates its use in the repair of the underlying stroma. However, some sections showed epithelial growth at the edges of the wound rather than on top of the hydrogel (shown in Fig. 6 (k)), indicating that the gels were not always in good contact with the underlying tissue.

The organ culture model also revealed that the degradation rate of the hydrogels on the corneal surface is not directly comparable to the dilute medium environment of the swelling tests or *in vitro* culture. For example, the complete re-epithelialization and shape retention of the corneal surface in Fig. 6 (m) indicates that the H2 hydrogel remained stable for the entire culture period of seven days, whereas during *in vitro* culture, the hydrogel could no longer be observed after three days.

4. Conclusions

In this study, we fabricated two types of hydrazone crosslinked HA-based hydrogels, with the addition of human collagen I. We characterized the physical and mechanical properties of these hydrogels and evaluated their potential as cell delivery vehicles to the corneal stroma. Based on the results, HALD1-HACDH hydrogels showed better stability and manageability compared to the HALD2-HAADH hydrogel, which degraded *in vitro* in three days. These hydrogels had also good optical properties, the refractive indices were close to the native cornea and they were visually transparent. Although all hydrogels showed good hASC survival directly after encapsulation, only the col I-containing HALD1-HACDH-col I hydrogel showed cells with elongated morphology, and significantly higher cell metabolic activity than the HALD1-HACDH gel. Corneal organ culture model suggests that these hydrogels could be used as injectable cell delivery vehicles to corneal stromal defects, allowing efficient cell integration to the stroma and overgrowth of epithelial cells. Biodegradability of the HA components and favorable properties of hydrazone crosslinking, such as short gelation time, lack of harmful reagents or side-products and mild reaction conditions, together with the results make these hydrogels a potential

material for hASC delivery to treat corneal stromal defects.

Supplementary data to this article can be found online at https://doi.org/10.1016/j.msec.2017.12.013.

Acknowledgements

This work was funded by the Finnish Funding Agency for Innovation's (TEKES) Human Spare Parts project and the European COST Action BM-1302 (Joining forces in corneal regeneration research). The funding sources were not involved in conduction if the research or interpretation of the results. The authors would like to thank Ph.D. Alexandre Efimov and Laboratory Attendant Anne-Maarit Tikkanen (Faculty of Natural Sciences, Laboratory of Chemistry and Bioengineering, Tampere University of Technology, Tampere, Finland) for their help related to the NMR- and FTIR-measurements. We would also like to thank Ph.D. Maria Notara (University Hospital Cologne, Cologne, Germany) for expertise in the corneal organ culture method, Marja-Leena Koskinen for aiding with the histological analysis and Miia Juntunen for technical assistance and theTampere Imaging Facility, BioMediTech and Institute of Medicine and Life Sciences, University of Tampere for the tools and expertise in cell imaging.

References

[1] WHO, Priority eye diseases, http://www.who.int/blindness/causes/priority/en/index8.html, (2016) (accessed 03.07.2017).
[2] C.E. Ghezzi, J. Rnjak-Kovacina, D.L. Kaplan, Corneal tissue engineering: recent advances and future perspectives, Tissue Eng. B Rev. 21 (2015) 278–287.
[3] Oh. JY, M.S. MK Kim, H.J. Shin, J.H. Lee, W.R. Ko, Wee, et al., The anti-inflammatory and anti-angiogenic role of mesenchymal stem cells in corneal wound healing following chemical injury, Stem Cells 26 (2008) 1047–1055.
[4] M. SK Mittal, A. Omoto, A. Amouzegar, A. Sahu, K.R. Rezazadeh, Katikireddy, et al., Restoration of corneal transparency by mesenchymal stem cells, Stem Cell Rep. 7 (2016) 583–590.
[5] B. Lindroos, R. Suuronen, S. Miettinen, The potential of adipose stem cells in regenerative medicine, Stem Cell Rev. Rep. 7 (2011) 269–291.
[6] F. Arnalich-Montiel, S. Pastor, A. Blazquez-Martinez, J. Fernandez-Delgado, M. Nistal, J.L. Alio del Barrio, et al., Adipose-derived stem cells are a source for cell therapy of the corneal stroma, Stem Cells 26 (2008) 570–579.
[7] L. Espandar, B. Bunnell, G.Y. Wang, P. Gregory, C. McBride, M. Moshirfar, Adipose-derived stem cells on hyaluronic acid–derived scaffold: a new horizon in bioengineered cornea, Arch.Ophthalmol. 130 (2012) 202–208.
[8] J. Alio del Barrio, M. Chiesa, N. Garagorri, N. Garcia-Urquia, J. Fernandez-Delgado, L. Bataille, et al., A cellular human corneal matrix sheets seeded with human adipose-derived mesenchymal stem cells integrate functionally in an experimental animal model, Exp.Eye Res 132 (2015) 91–100.
[9] K.M. Meek, C. Knupp, Corneal structure and transparency, Prog.Retin.Eye Res. 49 (2015) 1–16.
[10] J. Fraser, T. Laurent, U. Laurent, Hyaluronan: its nature, distribution, functions and turnover, J.Intern.Med. 242 (1997) 27–33.
[11] X. Xu, D.A. AK Jha, M.C. Harrington, X. Farach-Carson, Jia. Hyaluronic acid-based hydrogels: from a natural polysaccharide to complex networks, Soft Matter 8 (2012) 3280–3294.
[12] Y. Jiang, J. Chen, C. Deng, E.J. Suuronen, Z. Zhong, Click hydrogels, microgels and nanogels: emerging platforms for drug delivery and tissue engineering, Biomaterials 35 (2014) 4969–4985.
[13] X. Jia, Y. Yeo, R.J. Clifton, T. Jiao, D.S. Kohane, J.B. Kobler, et al., Hyaluronic acid-based microgels and microgel networks for vocal fold regeneration, Biomacromolecules 7 (2006) 3336–3344.
[14] E. Martínez-Sanz, D.A. Ossipov, J. Hilborn, S. Larsson, K.B. Jonsson, O.P. Varghese, Bone reservoir: injectable hyaluronic acid hydrogel for minimal invasive bone augmentation, J. Control. Release 152 (2011) 232–240.
[15] P. Bulpitt, D. Aeschlimann, New strategy for chemical modification of hyaluronic acid: preparation of functionalized derivatives and their use in the formation of novel biocompatible hydrogels, J. Biomed. Mater. Res. A 47 (1999) 152–169.
[16] J. Karvinen, J.T. Koivisto, I. Jönkkäri, M. Kellomäki, The production of injectable hydrazone crosslinked gellan gum-hyaluronan-hydrogels with tunable mechanical and physical properties, J. Mech. Behav. Biomed. Mater. 71 (2017) 383–391.
[17] O.P. Oommen, S. Wang, M. Kisiel, M. Sloff, J. Hilborn, O.P. Varghese, Smart design of stable extracellular matrix mimetic hydrogel: synthesis, characterization, and in vitro and in vivo evaluation for tissue engineering, Adv. Funct. Mater. 23 (2013) 1273–1280.
[18] S. Suri, C.E. Schmidt, Cell-laden hydrogel constructs of hyaluronic acid, collagen, and laminin for neural tissue engineering, Tissue Eng. A 16 (2010) 1703–1716.
[19] D.A. Ossipov, S. Piskounova, J. Hilborn, Poly (vinyl alcohol) cross-linkers for in vivo injectable hydrogels, Macromolecules 41 (2008) 3971–3982.
[20] K.H. Bouhadir, D.S. Hausman, D.J. Mooney, Synthesis of cross-linked poly (aldehyde guluronate) hydrogels, Polymer 40 (1999) 3575–3584.
[21] ASTM Standard F2900, Standard Guide for Characterization of Hydrogels used in Regenerative Medicine, ASTM International, West Conchoken, PA, USA, 2011, pp. 1–10.
[22] K. Brugger, Thermodynamic definition of higher order elastic coefficients, Phys. Rev. 133 (1964) A1611.
[23] J.F. Nye, Physical Properties of Crystals: Their Representation by Tensors and Matrices, Oxford University Press, 1985.
[24] W.D. Callister, D.G. Rethwich, Materials Science and Engineering: An Introduction, 7th ed., Wiley, New York, 2007.
[25] H. Nakajima, APPENDIX B: Table of Refractive Indices for BK7, Optical Design Using Excel: Practical Calculations for Laser Optical Systems, 1st ed., John Wiley & Sons Singapore Pte Ltd, 2015, pp. 277–278.
[26] J.M. Gimble, F. Guilak, Adipose-derived adult stem cells: isolation, characterization, and differentiation potential, Cytotherapy 5 (2003) 362–369.
[27] B. Lindroos, S. Boucher, L. Chase, H. Kuokkanen, H. Huhtala, R. Haataja, et al., Serum-free, xeno-free culture media maintain the proliferation rate and multipotentiality of adipose stem cells in vitro, Cytotherapy 11 (2009) 958–972.
[28] M. Notara, S. Schrader, J.T. Daniels, The porcine limbal epithelial stem cell niche as a new model for the study of transplanted tissue-engineered human limbal epithelial cells, Tissue Eng. A 17 (2011) 741–750.
[29] W. Lin, S. Shuster, H.I. Maibach, R. Stern, Patterns of hyaluronan staining are modified by fixation techniques, J. Histochem. Cytochem. 45 (1997) 1157–1163.
[30] D.A. Ossipov, S. Piskounova, O.P. Varghese, J. Hilborn, Functionalization of hyaluronic acid with chemoselective groups via a disulfide-based protection strategy for in situ formation of mechanically stable hydrogels, Biomacromolecules 11 (2010) 2247–2254.
[31] C. García-González, M. Alnaief, I. Smirnova, Polysaccharide-based aerogels—promising biodegradable carriers for drug delivery systems, Carbohydr. Polym. 86 (2011) 1425–1438.
[32] S.L. Wilson, A.J. El Haj, Y. Yang, Control of scar tissue formation in the cornea: strategies in clinical and corneal tissue engineering, J. Funct. Biomat. 3 (2012) 642–687.
[33] E.R. Morris, K. Nishinari, M. Rinaudo, Gelation of gellan–a review, Food Hydrocoll. 28 (2012) 373–411.
[34] M.J. Moura, M.M. Figueiredo, M.H. Gil, Rheological study of genipin cross-linked chitosan hydrogels, Biomacromolecules 8 (2007) 3823–3829.
[35] A. Borzacchiello, L. Ambrosio, Structure-Property Relationships in Hydrogels, Hydrogels, Springer, 2009, pp. 9–20.
[36] A. Ionescu, M. Alaminos, Juan de la Cruz Cardona, Durán, Juan de Dios García-López, M. González-Andrades, R. Ghinea, et al., Investigating a novel nanostructured fibrin–agarose biomaterial for human cornea tissue engineering: Rheological properties, J. Mech. Behav. Biomed. Mater. 4 (2011) 1963–1973.
[37] S.J. Petsche, D. Chernyak, J. Martiz, M.E. Levenston, P.M. Pinsky, Depth-dependent transverse shear properties of the human corneal stroma, Invest. Ophthalmol. Vis. Sci. 53 (2012) 873–880.
[38] H. Hatami-Marbini, Viscoelastic shear properties of the corneal stroma, J. Biochem. 47 (2014) 723–728.
[39] G. Lamouche, B.F. Kennedy, K.M. Kennedy, C. Bisaillon, A. Curatolo, G. Campbell, et al., Review of tissue simulating phantoms with controllable optical, mechanical and structural properties for use in optical coherence tomography, Biomed. Opt. Express 3 (2012) 1381–1398.
[40] W.J. Dupps, S.E. Wilson, Biomechanics and wound healing in the cornea, Exp. Eye Res. 83 (2006) 709–720.
[41] N. Garcia-Porta, P. Fernandes, A. Queiros, J. Salgado-Borges, M. Parafita-Mato, J.M. González-Méijome, Corneal biomechanical properties in different ocular conditions and new measurement techniques, ISRN Ophthalmol. 2014 (2014).
[42] K.M. Meek, S. Dennis, S. Khan, Changes in the refractive index of the stroma and its extrafibrillar matrix when the cornea swells, Biophys. J. 85 (2003) 2205–2212.
[43] W. Liu, C. Deng, C.R. McLaughlin, P. Fagerholm, N.S. Lagali, B. Heyne, et al., Collagen–phosphorylcholine interpenetrating network hydrogels as corneal substitutes, Biomaterials 30 (2009) 1551–1559.
[44] J. Dahlmann, A. Krause, L. Möller, G. Kensah, M. Möwes, A. Diekmann, et al., Fully defined in situ cross-linkable alginate and hyaluronic acid hydrogels for myocardial tissue engineering, Biomaterials 34 (2013) 940–951.
[45] J. Zhu, R.E. Marchant, Design properties of hydrogel tissue-engineering scaffolds, Expert Rev. Med. Devices 8 (2011) 607–626.
[46] M.D.M. Evans, G.A. McFarland, R.Z. Xie, S. Taylor, J.S. Wilkie, H. Chaouk, The use of corneal organ culture in biocompatibility studies, Biomaterials 23 (2002) 1359–1367.
[47] S. Sandeman, A. Lloyd, B. Tighe, V. Franklin, J. Li, F. Lydon, et al., A model for the preliminary biological screening of potential keratoprosthetic biomaterials, Biomaterials 24 (2003) 4729–4739.
[48] J.A. Gomes, R. Amankwah, A. Powell-Richards, H.S. Dua, Sodium hyaluronate (hyaluronic acid) promotes migration of human corneal epithelial cells in vitro, Br. J. Ophthalmol. 88 (2004) 821–825.

APPENDIX A: Supplementary Material

Hydrazone crosslinked hyaluronan-based hydrogels for therapeutic delivery of adipose stem cells to treat corneal defects

Laura Koivusalo[†], Jennika Karvinen[†], Eetu Sorsa, Ilari Jönkkäri, Jari Väliaho, Pasi Kallio, Tanja Ilmarinen, Susanna Miettinen, Heli Skottman and Minna Kellomäki

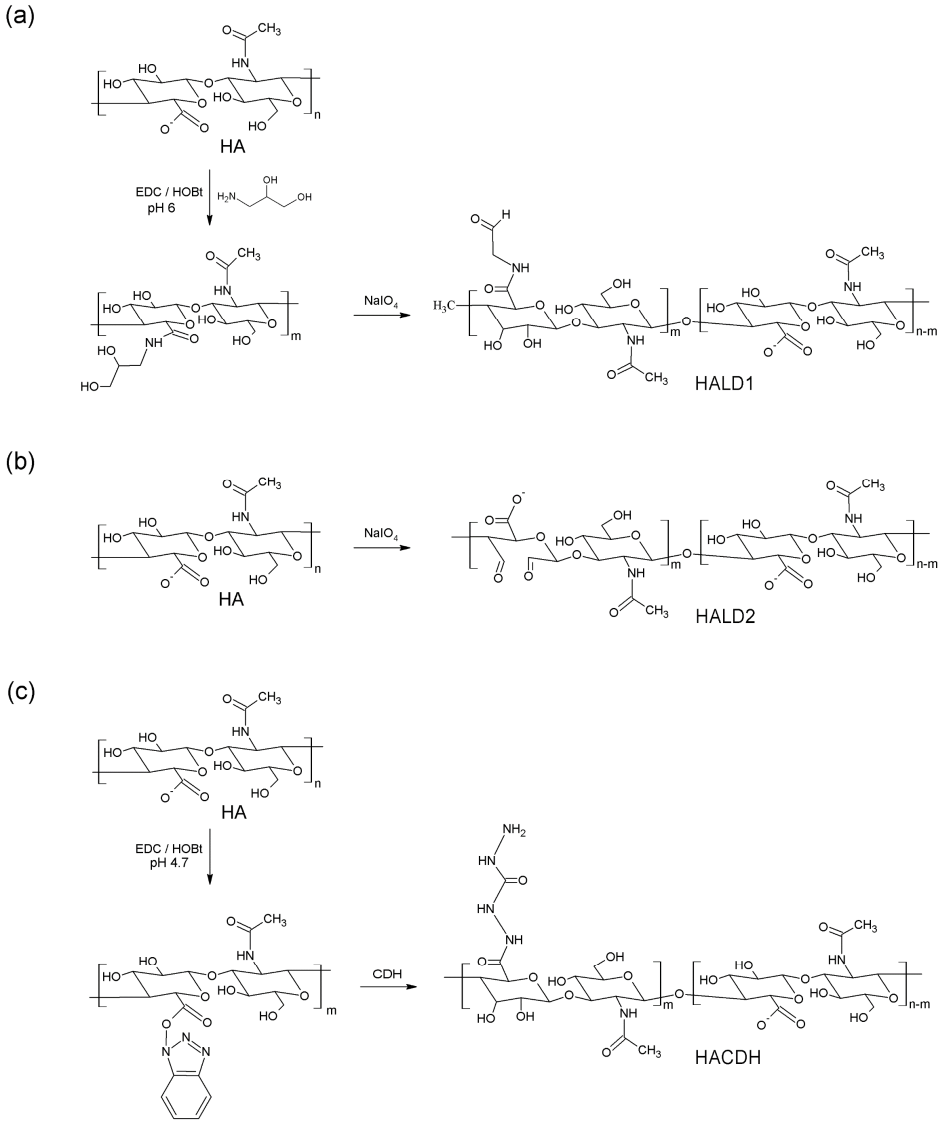

Fig. S1. Reaction schemes of (a) selective oxidation of diol-modified HA (HALD1), (b) periodate oxidation of HA (HALD2) and (c) hydrazide-modification of HA (HACDH). The reaction scheme of HAADH modification is shown in (Karvinen, Koivisto et al. 2017).

APPENDIX A: Supplementary Material

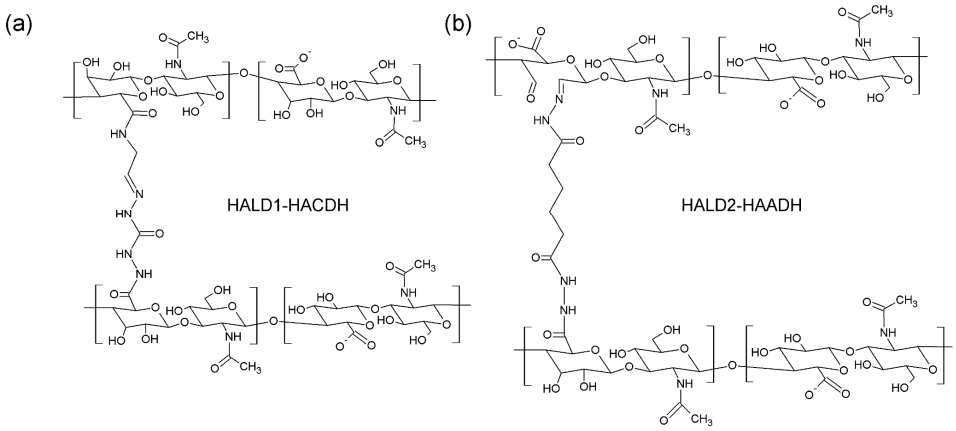

Fig. S2. The chemical structures of hydrazone crosslinked (c) HALD1-HACDH (H1) and (d) HALD2-HAADH (H2) hydrogels.

APPENDIX A: Supplementary Material

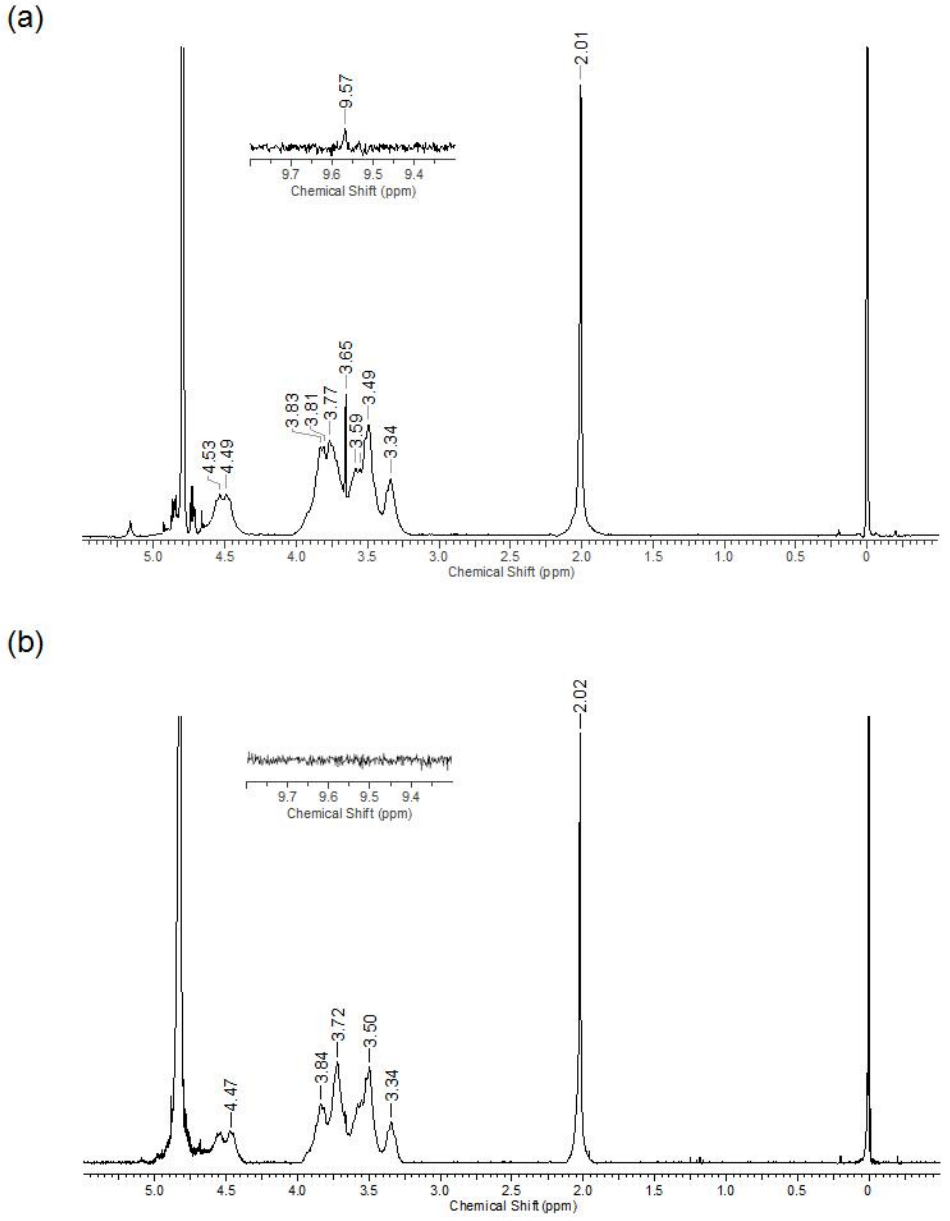

Fig. S3. ^{1}H-NMR spectra of hydrogel components (a) HALD1 and (b) HALD2.

APPENDIX A: Supplementary Material

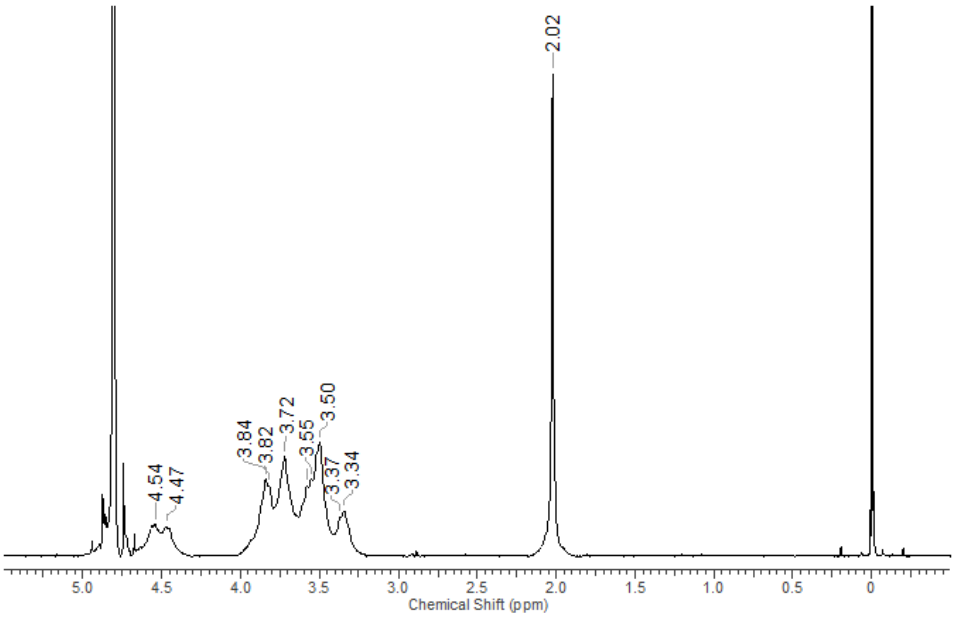

Fig. S4. ^{1}H-NMR spectra of hydrogel component HACDH.

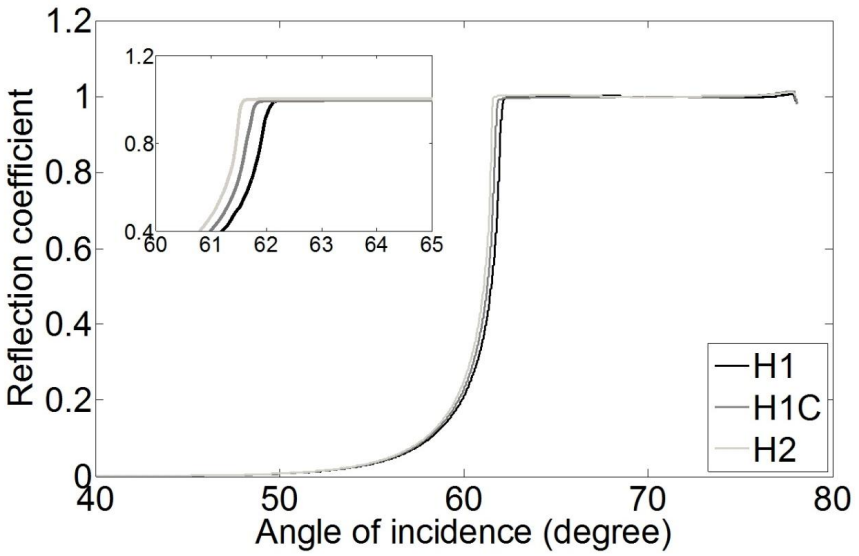

Fig. S5. Reflection coefficient as a function of angle of incidence curves of HALD1-HACDH (H1), HALD1-HACDH-colI (H1C) and HALD2-HAADH (H2) hydrogels.

APPENDIX A: Supplementary Material

Table S1. Cell surface marker profile of hASCs determined by flow cytometry.

Marker	Amount of positive cells (%)
CD73	95.8
CD90	99.2
CD105	98.7
CD14	0.7
CD19	0.9
CD45	2.0
HLA-DR	1.1
CD34	47.5

Publication III

Karvinen J., Joki T., Ylä-Outinen L., Koivisto J.T., Narkilahti S., Kellomäki M.

"Soft hydrazone crosslinked hyaluronan- and alginate-based hydrogels as 3D supportive matrices for human pluripotent stem cell-derived neuronal cells"

Reactive and Functional Polymers, 124 (2018), 29-39.

Reactive and Functional Polymers 124 (2018) 29–39

Contents lists available at ScienceDirect

Reactive and Functional Polymers

journal homepage: www.elsevier.com/locate/react

Soft hydrazone crosslinked hyaluronan- and alginate-based hydrogels as 3D supportive matrices for human pluripotent stem cell-derived neuronal cells

Jennika Karvinen[a,*], Tiina Joki[b], Laura Ylä-Outinen[b], Janne T. Koivisto[a,b], Susanna Narkilahti[b], Minna Kellomäki[a,b]

[a] BioMediTech Institute and Faculty of Biomedical Sciences and Engineering, Tampere University of Technology, Korkeakoulunkatu 3, Tampere FI-33101, Finland
[b] BioMediTech Institute and Faculty of Medicine and Life Sciences, University of Tampere, Arvo Ylpön katu 34, Tampere FI-33520, Finland

ARTICLE INFO

Keywords:
Hyaluronan
Alginate
Hydrazone
Hydrogel
3D neuronal culture

ABSTRACT

Regenerative medicine, especially cell therapy combined with a supportive biomaterial scaffold, is considered to be a potential treatment for various deficits in humans. Here, we have produced and investigated the detailed properties of injectable hydrazone crosslinked hyaluronan-polyvinyl alcohol (HA-PVA) and alginate-polyvinyl alcohol (AL-PVA) hydrogels to be used as a supportive biomaterial for 3D neural cell cultures. To the best of our knowledge, this is the first time the polymerization and properties of hydrazone crosslinked AL-PVA hydrogel have been reported. The effect of the degree of substitution and molecular weight of the polymer components as well as the polymer concentration of the hydrogel on the swelling, degradation and mechanical properties of the hydrogels is reported. Furthermore, we studied the effect of the above parameters on the growth of human pluripotent stem cell-derived neuronal cells. The most neural cell supportive HA-PVA hydrogel was composed of high molecular weight HA component with brain-mimicking mechanical properties and decreased polymer concentration. AL-PVA hydrogel, with stiffness quite similar to brain tissue, was also shown to be similarly supportive. Neuronal spreading and 3D network formation was enhanced inside the softest hydrogels.

1. Introduction

Traumas and deficits in the human central nervous system (CNS) may have a permanent effect on the functionality of the patient and the prognosis in many cases is poor. Moreover, human CNS, as an organ, suffers from low inbuilt regenerative capacity, which makes healing with traditional medicine (drugs and surgical operations) insufficient. As a result, regenerative medicine is considered to be a potential treatment for CNS deficits. Regenerative medicine aims to restore normal functionality by enhancing the regeneration of tissue or by replacing the damaged parts with engineered biological transplants. One such strategy is cell therapy combined with a supportive biomaterial scaffold.

Biomaterial scaffold should fulfill specific criteria when they are used for neural tissue engineering with the aim of neuronal network regeneration. For example, the scaffolds should have similar mechanical properties to those of the brain or spinal cord, they should allow the infiltration of cells and axons, they should allow the transportation of nutrients and metabolites, they should integrate with the host tissue, they should exhibit a suitable degradation rate without any harmful degradation products, and they should not induce inflammatory and glial scar formation [1]. Based on these requirements, polymer-based hydrogels can be considered to be suitable biomaterial candidates for neural tissue engineering. A soft, hydrated form of three-dimensional crosslinked hydrogels resembles that of naturally occurring living tissue. The porous nature of hydrogels enables the transportation of waste, oxygen and nutrients. The mechanical and physical properties of hydrogels are tunable making it easier to mimic the living tissue [2]. Most hydrogels are also considered to be cyto- and biocompatible materials.

When designing hydrogels for this kind of application, a thorough knowledge of their various properties is important. Hydrogels have variable mechanical, physical and degradation properties that can be controlled, for example, by altering the molecular weight (M_w), the chemical structure and the number of available crosslinkable groups in the polymer, the ratio of gel components, the amount of water, and the crosslinking method. It is well known that, for example, crosslinking density can affect mechanical, swelling and degradation properties and the functionality of hydrogels. The difficulty lies in the altering of properties individually when needed without affecting the others [3]. Further modification of hydrogels can be carried out by incorporating extracellular matrix (ECM) molecules (collagen, laminin, *etc.*) or

* Corresponding author.
E-mail address: jennika.karvinen@tut.fi (J. Karvinen).

https://doi.org/10.1016/j.reactfunctpolym.2017.12.019
Received 7 August 2017; Received in revised form 1 December 2017; Accepted 30 December 2017
Available online 04 January 2018
1381-5148/

peptides to provide more anchoring sites for the cells [4,5].

Numerous natural and synthetic polymer-based hydrogels have been used as scaffolds for the 3D culture of neural lineage cells as reviewed by, for example, Murphy et al. [2]. Two widely used polysaccharide polymers used in neural research are hyaluronan (HA) [6,7] and alginate [8,9]. HA is an anionic and hydrophilic polysaccharide composed of β-1, 4-D-glucuronic acid and β-1, 3-N-acetyl-D-glycosamine residues that is a major glycosaminoglycan component in the ECM of the brain. HA plays a vital role in the development of the CNS, and it is particularly abundant in the fetal brain and the surrounding immature neurons during differentiation in the spinal cord [10]. HA is produced by almost all the members of the animal kingdom as well as certain members of the streptococci species. It has a relatively simple repetitive chemical structure. The carboxyl and hydroxyl groups allow specific modification and the introduction of functional groups for crosslinking. Alginate (AL) is an anionic and hydrophilic polysaccharide composed of 1,4-linked β -D-mannuronic acid (M) and α -L-guluronic acid (G) residues that is obtained from brown algae. It is structurally similar to ECM. AL is inherently non-biodegradable, but it can be made degradable, for example, by replacing the divalent cations with monovalent cations or by oxidation [11]. The properties of natural polymer-based hydrogels can be improved and widened by combining them with a synthetic polymer such as polyvinyl alcohol (PVA). PVA is a hydrophilic polymer with good chemical, thermal and mechanical stability. Hydroxyl groups in the structure provide chemical versatility that enables further modification and functionalization [12]. Biocompatible PVA hydrogels have been used quite widely in several biomedical applications [13]. PVA has also been approved by the Food and Drug Administration (FDA) and Conformité Européenne (CE) for clinical use in humans [14].

HA-PVA and AL-PVA hydrogels can be fabricated by using hydrazone crosslinking, which is an aldehyde-hydrazide coupling reaction. Hydrazone crosslinking belongs to the group of pseudo click chemistry reactions together with the Michael addition reaction (pseudo is usually characterized by moderate orthogonality). The reactions are versatile, simple and reversible, and they have high reactivity and yield. Furthermore, no toxic reagents or side-products are produced [15]. This crosslinking method also enables the fabrication of injectable hydrogels. The injectability of the hydrogels is desirable for when the hydrogels are eventually transplanted into the injury site. To date, there have been several studies carried out on hydrazone crosslinked HA-PVA hydrogels [16,17]. The focus of these studies has, however, been on other areas of soft tissue engineering. To the best of our knowledge, this is the first time the polymerization and properties of the hydrazone crosslinked AL-PVA hydrogel have been reported.

In this study, we have produced injectable hydrazone crosslinked HA-PVA and AL-PVA hydrogels with variable properties. We studied the effect of the degree of substitution (DS%), the molecular weight of the polymer components and the polymer concentration of the hydrogel on swelling, degradation and the mechanical properties of the hydrogels. We also studied the effects of the above parameters on the growth of human pluripotent stem cell-derived neuronal cells.

2. Materials and methods

2.1. Materials and general methods

Hyaluronic acid sodium salt ($M_w = 1.5 \times 10^5$ g/mol) was purchased from Lifecore (Chaska, MN, USA). Hyaluronic acid sodium salt from streptococcus equi ($M_w = 1.5 - 1.8 \times 10^6$ g/mol), polyvinyl alcohol (M_w = 27000 g/mol, 98.0 –98.8 % hydrolyzed), t-butyl carbazate (TBC), 1,1 ′ - carbonyldiimidazole (CDI), glycine ethyl ester hydrochloride, hydrazine solution (35 wt % in H_2O), 1-hydroxybenzotriazole (HOBt), alginic acid sodium salt from brown algae (low viscosity), picrylsulfonic acid solution (5-% (w/v) in H_2O, TNBS), hyaluronidase from bovine testes (Type I-S, 400-1000 units/mg solid), ethylene glycol, dimethyl sulfoxide (DMSO), deuterium oxide (99.9 atom% D, contains 0.05 wt % 3-(trimethylsilyl)-propionic-2,2,3,3-d4 acid, sodium salt), sodium cyanoborohydride ($NaBH_3CN$), sucrose, sodium periodate, sodium acetate, acetic acid, sodium tetraborate decahydrate and boric acid were purchased from Sigma-Aldrich (St. Louis, MO, USA). Triethylamine was purchased from J.T. Baker (The Netherlands). Acetate buffer was prepared from sodium acetate and acetic acid, and borate buffer was prepared from sodium tetraborate decahydrate and boric acid. All solvents used were of analytical quality. Milli-Q water was used in synthesis and determinations. Dialysis membranes (Spectra/Por® cut-off 1000 and 25,000 g/mol) were purchased from Spectrum Laboratories, Inc. (Rancho Dominguez, CA, USA).

Cell culture reagents DMEM/F12, Neurobasal, GlutaMax, B27, N2 and penicillin/streptomycin were purchased from Thermo Fisher Scientific (Waltham, MA, USA), and basic fibroblast growth factor (FGF2) from Bio-Techne (Minneapolis, MN, USA). Rabbit anti-microtubule associated protein 2 (MAP-2, AB5622) was purchased from Merck Millipore (Darmstadt, Germany), monoclonal mouse anti-B-tubulin III (T8660) was purchased from Sigma-Aldrich (St. Louis, MO, USA) and Alexa Fluor 488 or 568 conjugated secondary antibodies (1:400) from Thermo Fisher Scientific. VECTASHIELD mounting media containing 4 ′,6-diamidino-2-phenylindole (DAPI) was purchased from Vector Laboratories (Peterborough, United Kingdom).

Nuclear Magnetic Resonance (NMR) spectroscopy experiments were measured with a Varian Mercury 300 MHz NMR Spectrometer (Palo Alto, USA). Polymer samples (5 mg) were dissolved deuterium oxide (600 μL) containing internal standard (0.05 wt % 3-(trimethylsilyl)-propionic-2,2,3,3-d4 acid, sodium salt). Fourier Transform Infrared (FTIR) spectroscopy experiments were collected on a Perkin Elmer Spectrum One FT-IR Spectrometer (Waltham, MA, USA) in the spectral range of 400 to 4000 cm^{-1}. Freeze-dried polymer and hydrogel samples (1–2 mg) were pressed into KBr (200 mg) tablets.

2.2. Synthesis of aldehyde-modified hyaluronan and alginate

Aldehyde groups were generated from the vicinal diol groups of HA and AL by using periodate oxidation (Fig. 1 (a), (b)) according to the previously reported method [18] that was slightly modified. Briefly, sodium hyaluronate or alginate (0.500 g) was dissolved in deionized water (100 mL). Sodium periodate (Table S1.) was dissolved in deionized water (2.7 mL), added dropwise and stirred for 2 h to 4 h (Table S1.) in the dark at room temperature under nitrogen. Ethylene glycol (4 equivalents) was added to inactivate any unreacted periodate and the solution was then stirred for 1 h. Derivatized polymers were dialyzed with MW cutoff 25,000 membrane against deionized water for three days. Purified polymers were lyophilized to obtain white cotton-like products (HAALD and ALALD). ^{1}H NMR (Fig. 1, D_2O, 300 MHz): HAALD: δ 4.47 (m, 1H, H1 of glucose unit), 3.82 –3.35(m, 5H, H2–5 of glucose unit), 2.03 (s, 3H, -NHC(O)CH_3). ALALD: 5.72 (s, 1H, H4-G), 5.26 and 5.18 (s, 1H, hemiacetal protons), 5.00 (s, 1H, H1-G), 4.59 (s, 1H, H1-M and H5-GM), 4.39 (s, 1H, H5-GG). FTIR (Fig. 2, KBr pellet): HAALD: 1720 (ν(C=O) of –C(O)H), 1618 (ν(C=O) of –NHC(O) – and –C(O)OH). ALALD: 1732 (ν(C=O) of –C(O)H)), 1634 (ν(C=O) of –C(O)OH).

The DS% of HAALD was determined using a TNBS method [16,19]. Briefly, HAALD (20 mg) was dissolved in acetate buffer (2 mL, 0.1 M, pH 5.2) and added to TBC solution in acetate buffer (1 mL, 0.0348 g, 10-fold excess per molar amount of sodium periodate used). The mixture was allowed to react for 1 h at room temperature. $NaBH_3CN$ (1 mL, 0.0166 g, equimolar amount to TBC) in acetate buffer was added and allowed to react for 24 h at room temperature under nitrogen. The polymer was dialyzed with MW cutoff 25,000 membrane against 0.1 M NaCl for 24 h and for a further 24 h in deionized water. Purified polymer was lyophilized to obtain a white cotton-like product. The ^{1}H-NMR spectrum was measured and the DS% was determined from the integration of the ^{1}H-NMR peaks. ^{1}H NMR (D_2O, 300 MHz): δ 1.9 (3H,

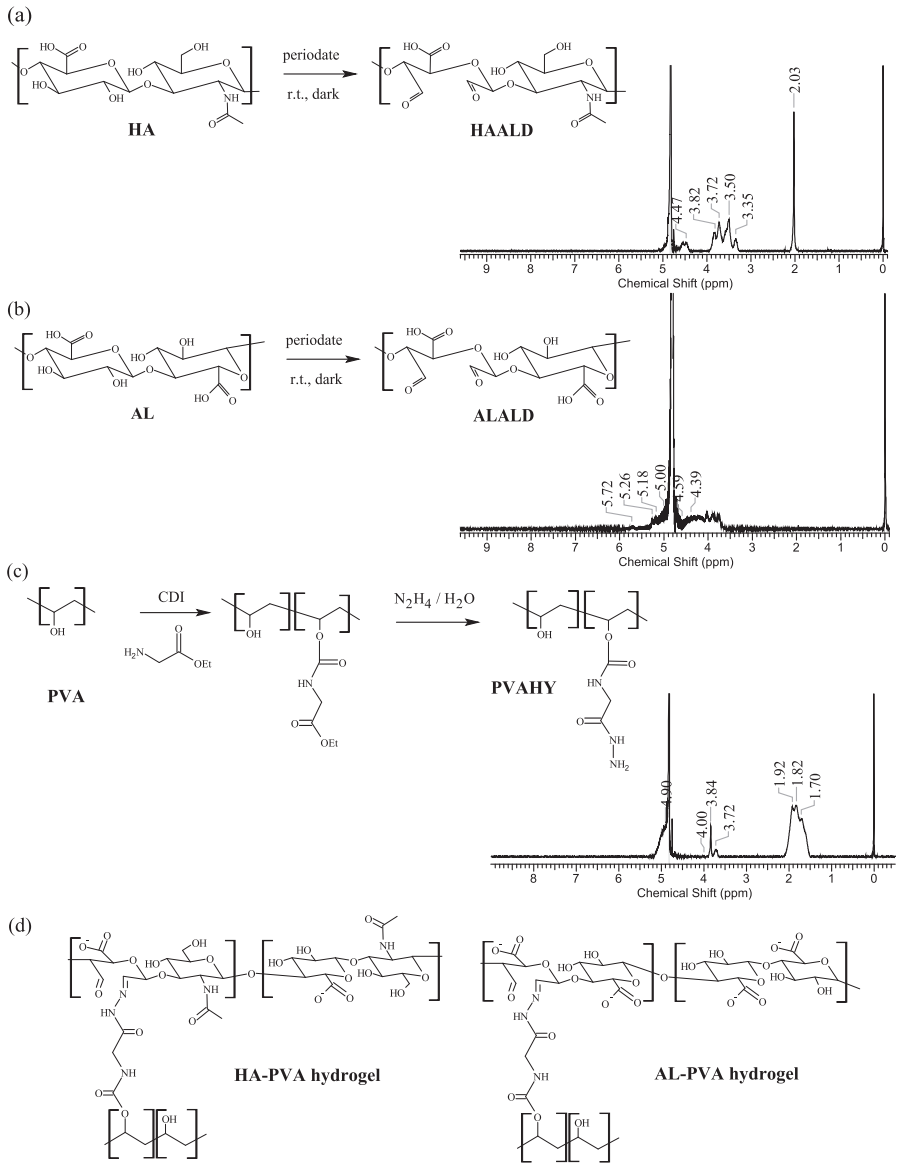

Fig. 1. Reaction schemes of the oxidation of (a) HA (HAALD) and (b) AL (ALALD), and (c) the hydrazide-modification of PVA (PVAHY). The ^{1}H-NMR spectra of hydrogel components are presented next to the structures. (d) The chemical structures of HA-PVA and AL-PVA hydrogels formed by hydrazone crosslinking.

$NHCOCH_3$) and 1.3 (9H, t-Boc).

The DS% of ALALD was determined using an aldehyde assay [19]. Briefly, aqueous ALALD solution (0.5 mL, 10 mM) was mixed with TBC solution (0.5 mL, 24.75 mM) in aqueous trichloroacetic acid (1%) and allowed to react for 24 h at room temperature. A portion of this solution (200 µL) was mixed with aqueous TNBS solution (2 mL, 4 mM, 0.1 mM borate buffer, pH 8) and allowed to react for 30 min at room temperature. After this, it was diluted with aqueous hydrochloric acid (0.5 M) and the absorbance was measured at 334 nm. TBC was used as a standard to obtain a calibration curve. The blank sample was composed of deionized water (0.5 mL) and aqueous trichloroacetic acid (0.5 mL, 1%).

2.3. Synthesis of hydrazide-modified polyvinyl alcohol

PVA was modified with hydrazide groups (Fig. 1 (c)) according to the previously reported method [12]. Briefly, PVA (400 mg) was dissolved in dry DMSO (8 mL). CDI (730 mg) was added under nitrogen at room temperature and the solution was mixed for 3 h. Glysine ethyl ester hydrochloride (126 mg) and triethylamine (125 µL) were added and stirring was continued overnight under nitrogen. Finally, hydrazine 35 w-% aqueous solution (8.6 mL) was added. After 24 h of stirring at room temperature, the solution was mixed with water (50 mL) and reduced to about 8 mL of volume. The PVA derivative was precipitated from DMSO by using 10-fold excess of mixture of diethyl ether/ethanol

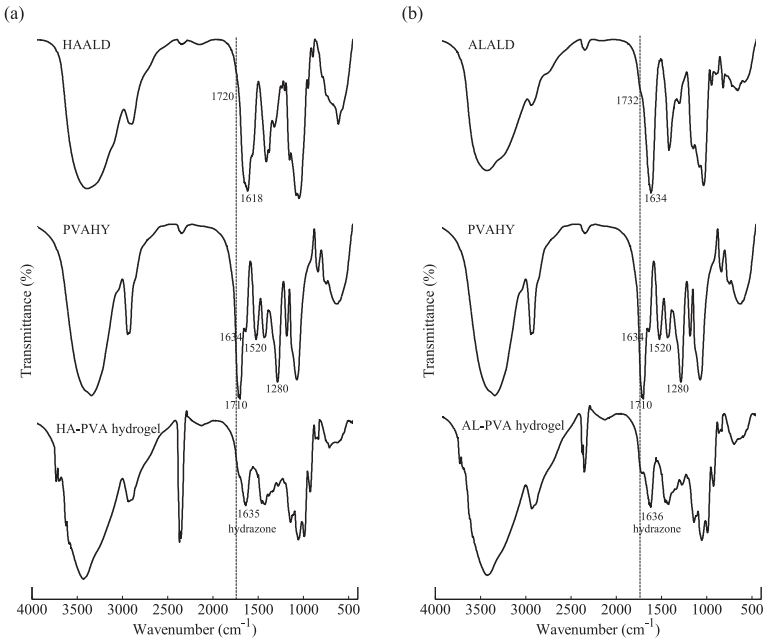

Fig. 2. FTIR spectra of (a) HA-PVA, and (b) AL-PVA hydrogels, including their components. The peak of 2300 cm^{-1} is caused by the CO_2 problem of the Spectrometer and is not related to the samples.

(80/20 mL). The precipitate was dissolved in a small amount of deionized water and dialyzed with MW cutoff 1000 membranes against deionized water for 3 days. Purified polymer was lyophilized to obtain a white cotton-like product (PVAHY). ^{11}H NMR (Fig. 1, D_2O, 300 MHz): δ 4.90 (m, 1H, polymer backbone CH of the modified unit), 4.00 –3.72(m, 3H, polymer backbone CH of the unmodified unit + $CH_2CONHNH_2$), 1.92 –1.60(m, 2H, polymer backbone CH_2). FTIR (Fig. 2, KBr pellet): 1710 (ν(C=O) of –C(O) O–), 1634 (d(N–H) of prim. amine), 1520 (d (N–H) of sec. amine), 1280 (ν(C–O) of –C(O) O–).

The DS% of PVAHY was determined using a spectrophotometric method [12] based on the reaction between TNBS and the primary amines of PVAHY. Briefly, PVA (0.8 mg) was dissolved in borate buffer (2 mL, 0.1 M, pH 9.3). A sample (0.1 mL) was taken and diluted with borate buffer (2.8 mL). TNBS solution (75 μL, 0.025 M) was added and the solution was vigorously mixed. The mixture was allowed to stand for 30 min at room temperature to obtain a red color indicating primary amine groups. The absorbance was read at 505 nm. A mixture of borate buffer (2.9 mL) and TNBS solution (75 μL, 0.025 M) was used as a blank reference. TBC was used as a standard to obtain a calibration curve.

2.4. Formation of hydrogels

Freeze-dried HAALD, ALALD and PVAHY components were dissolved in a 10% sucrose solution according to Table 1. Sucrose was used to make the osmotic pressure more suitable for cells in the cell culture experiments. Equal volumes of components A and B were mixed together in a mold by using a dual syringe system to form HA-PVA and AL-PVA hydrogels (Table 1, Fig. 1 (d)). Cut syringes were used as a mold to ease pushing the sample out.

The gelation time was determined using a tube tilt test [20], where the gel point is determined by tilting a tube containing the hydrogel solution. The gel point is the transition point from fluid to gel state, in other words, where the system stops flowing.

2.5. Structural homogeneity

The structural homogeneity of the hydrogels was studied using a dry to wet weight ratio test [21]. Three parallel cylinder shaped hydrogels were formed and slices of equal size were cut (A–D, diameter × height = 5 mm × 5 mm). The mass of the freshly made wet hydrogel slices (W_{wet}) was weighed prior to freeze-drying. The slices were weighed again after drying to obtain the mass of the dry hydrogel (W_{dry}). The dry to wet ratios were calculated from the following:

$$\text{dry to wet ratio} = \frac{W_{dry}}{W_{wet}} \quad (1)$$

Table 1
Compositions and gelation time of hydrazone crosslinked HA-PVA and AL-PVA hydrogels. At the end of the name of component A, H denotes high M_w ($1.5 - 1.8 \times 10^6$ g/mol) and L denotes low M_w (1.5×10^5 g/mol).

Gel code	Component A	DS %	Concentration mg/mL	Component B	DS %	Concentration mg/mL	Polymer conc. %	Gelation time
HP1	HAALD1H	5	20	PVAHY	13	10	1.5	Seconds
HP1a	HAALD1H	5	10	PVAHY	13	5	0.75	1–5 min
HP1b	HAALD1H	5	5	PVAHY	13	2.5	0.375	5 min
HP2	HAALD2H	9	25	PVAHY	13	5	1.5	Seconds
HP3	HAALD1L	5	20	PVAHY	13	10	1.5	Seconds
HP4	HAALD2L	9	20	PVAHY	13	10	1.5	Seconds
AP	ALALD	7	20	PVAHY	13	10	1.5	30 s

2.6. Swelling kinetics

The swelling kinetics of the hydrogels were studied in cell culture medium (DMEM/F12) and in deionized water. Three parallel, freshly made wet hydrogel samples (100 μL) were weighed ($W_{initial}$) and placed into deionized water or cell culture medium and incubated at 37 °C. Samples were weighed at specific time points to obtain the mass of a swollen hydrogel ($W_{swollen}$). Swelling ratio (SR,%) was calculated from the following:

$$SR(\%) = \frac{W_{swollen} - W_{initial}}{W_{initial}} \times 100 \quad (2)$$

Equilibrium was considered to have been achieved when the mass of the sample no longer changed but remained constant.

2.7. Enzymatic biodegradation

The enzymatic degradation of hydrogels was studied using a hyaluronidase-enzyme (HAse). Three parallel hydrogel samples (100 μL) were weighed, placed into HAse solution (20–50 U/mL, in PBS) and incubated at 37 °C until the samples were completely degraded. The samples were weighed at different time points. The sample was considered to be degraded when there was visually no sample left to weigh. The residual mass (%) was determined at each point and plotted as a mass loss curve.

2.8. Mechanical properties of hydrogels and rabbit midbrain tissue

The compression tests were performed using a BOSE Electroforce Biodynamic 5100 machine equipped with a 225 N load sensor and Wintest 4.1 software (Bose Corporation, Eden Prairie, Minnesota, USA). Five parallel hydrogel samples (875 μL) were prepared into 5 mL cut syringes to ease pushing the sample out. The samples were left to stand for 24 h to obtain uniform hydrogels. The surface of the platens was covered with Parafilm to avoid slipping of the sample. Samples were compressed using unconfined compression at a rate of 10 mm/min to at least 65% to 70% strain. The measurements were conducted in the air at room temperature. The test data obtained from the measurement of New Zealand white rabbit midbrain samples (obtained from the animal experiments conducted at Tampere University Medical School, University of Tampere) were used as a reference [22].

The measuring data were imported to MS Excel, where stress and strain were plotted as graphs. The so-called stiffness of the material can be estimated based on the data and it was done similarly to Karvinen et al. [23]. Briefly, due to the characteristic non-linear elastic behavior of the hydrogels and tissues, the stress-strain curve cannot be described appropriately by Hooke's law (except at low strains). Therefore, the data were fitted to a 6th-order polynomial. Stiffness, τ, can be defined as the derivative of stress σ with respect to strain ϵ. When the measured stress-strain data is represented by a polynomial, stiffness may be defined as follows:

$$\frac{d\sigma}{d\epsilon} \equiv \tau(\epsilon) = \sum_{k=1}^{n} k c_k \epsilon^{k-1}, \quad (3)$$

where the coefficients of the polynomial c_k are the so-called elastic constants [24,25]. Here, c_1 is the second-order elastic constant, which is sometimes also called the elastic constant, Young's modulus or elastic stiffness constant [24–26]. The stiffness values obtained from the polynomial were plotted as a function of strain to be able to compare the behavior of materials at different strains. The second-order elastic constants were estimated based on the mean of stiffness polynomials of parallel samples at 0% to 15% strain with minimum standard deviations. It should be noted that the stiffness describes the same quantity as the second-order elastic constant, the latter being the stiffness at zero strain $\tau(0) = c_1$.

2.9. Cell culture

The cell culture experiments were performed using human pluripotent stem cell derived neuronal cells. Human embryonic stem cell (hESC) lines Regea08/023 and Regea11/013, and human induced pluripotent stem cell (iPCS) lines HEL 24.3 (kindly donated by Prof. Timo Otonkoski, University of Helsinki, Finland) and 04511.WT were used. BioMediTech has been granted ethical approval to derivate, culture and differentiate hESCs (Skottman, R05116) by the Pirkanmaa Hospital District. Moreover, permission has been granted by the National Authority for Medicolegal Affairs (FIMEA 1426/32/300/05) to conduct human stem cell research. Additionally, approval has been obtained to use hiPSC lines produced by other laboratories for neuronal research (R14023). The stem cell line derivation, culturing and characterization for all lines has been previously published [27–29]. The used stem cell lines are under constant quality control with frequent gene and protein expression analysis, karyotype and mycoplasma assays. Neuronal differentiation was performed using a suspension culture method [30]. Briefly, undifferentiated colonies were mechanically cut into small cell aggregates and transferred into the neural differentiation medium (NDM), containing 1:1 DMEM/F12: Neurobasal supplemented with GlutaMax (2 mM), B, N, penicillin/streptomycin (25 U/mL) and FGF2 (20 ng/mL). During the culture, cell aggregates formed round, freely floating neurospheres. During the differentiation, the neurospheres were kept small (diameter ~ 500 μm) by cutting mechanically once a week. Half of the medium was changed three times a week.

The cells were plated as previously described [22,31]. Briefly, predifferentiated neuronal cell aggregates were mechanically cut into small cell clusters. These freshly cut small clusters were then plated either on top of the hydrogel surface or encapsulated inside the hydrogel. 2D growth controls were plated on top of mouse laminin (10 μg/mL) coated cell culture plastic. When culturing cells on top of the hydrogel surfaces, the gelation was performed directly into the cell culture well by combining equal volumes of components A and B similarly as described in Section 2.4 and mixed using a pipette tip. After complete gelation, the cells were plated on top of the hydrogel. When preparing 3D cultures with cells encapsulated inside the hydrogel, the cell clusters were mixed into PVAHY component just before performing the gelation. The cells were then cultured for two weeks either on top of or encapsulated inside the hydrogel. Cell culture media (NDM without FGF) was changed three times a week and cells were monitored during the culturing.

2.10. Molecular biology analysis

After two weeks in culture, the cells underwent viability analysis and immunocytochemical analysis as previously described [22]. Briefly, viability was analyzed with fluorescence-based LIVE/DEAD® viability/cytotoxicity assay (Thermo Fisher Scientific). The labels, Calcein-AM (0.1 μM) that stains intact cells and ethidium homodimer-1 (0.4 μM) that stains dead cells, were incubated for 30 min at +37 °C on the cells. After staining, the cells were imaged using an Olympus IX51 microscope (Olympus IX51 inverted microscope, PlanFLN 10×, and 20× objectives, Olympus DP30BW CCD camera). For immunocytochemistry, the cultures were fixed with 4% paraformaldehyde at room temperature for 30 min. After a brief wash in phosphate buffered saline (PBS), the cultures were incubated for 1 h with blocking solution containing 10% normal donkey serum (NDS), 0.1% Triton X-100, and 1% bovine serum albumin (BSA) in PBS at room temperature, followed by another wash in 1% NDS, 0.1 % Triton X-100 and 1% BSA in PBS. Then, the cultures were incubated with primary antibody solution in 1% NDS, 0.1% Triton X-100, and 1% BSA in PBS at +4°C for 3 days. The antibodies used were MAP-2 (1:400) and B-tubulin (1:1000). After primary antibody incubation, the samples were washed three times in 1% BSA in PBS (the first time only briefly followed by

2 × 1 h washes) and then incubated overnight at +4 °C with secondary antibodies (1:400). After secondary antibody incubation, the samples were again washed three times (the first time only briefly followed by 2 × 1 h washes) in PBS and then mounted with VECTASHIELD mounting media. The cultures were imaged using an Olympus IX51 microscope.

2.11. Statistical data analysis

Statistical data analyses were performed with MATLAB (Statistics and Machine Learning Toolbox™). All the quantitative data are presented as mean and standard deviation. A non-parametric Kruskal-Wallis test was used to determine whether there were statistically significant differences within the mechanical test data set. A Wilcoxon rank sum test was used to analyze the specific sample pairs for statistically significant differences. Non-parametric testing was chosen because the assumption of normally distributed data would be unjustifiable due to a relatively low *n*. When more than two groups were compared, the resulting p values were multiplied by the number of comparisons performed (Bonferroni correction). A p-value of < 0.05 was considered significant.

3. Results and discussion

3.1. Modification of hyaluronan, alginate and polyvinyl alcohol with complementary reactive groups

The polymers were modified with complementary reactive groups to attain aldehyde-modified HA (HAALD) and alginate (ALALD), and hydrazide-modified PVA (PVAHY) with relatively low DS%, in order to not lose the characteristic properties of the polymers. Hyaluronan and alginate were periodate oxidized to obtain one ALALD component and four HAALD components with variable DS% (Table 1). The modification was confirmed with ^{1}H-NMR and FTIR analysis. In the ^{1}H-NMR spectrum of HAALD (Fig. 1), the aldehyde peak (9 ppm to 10 ppm) was invisible. One explanation for this can be that, in water, aldehydes exist in equilibrium with their hydrated forms. They may also form reversible hemiacetals when reacting with some hydroxyl groups of HA [32]. In the FTIR spectrum (Fig. 2), the aldehyde shoulder (1720 cm^{-1}) was observed. The signal partly overlaps with the carboxyl and amide C=O stretching (1633 cm^{-1}) signal, which makes observation more difficult. The success of ALALD modification was confirmed from the ^{1}H-NMR spectrum (Fig. 1), where two new signals at 5.26 ppm and 5.19 ppm can be found. Those correspond to a hemiacetalic proton that is formed when aldehyde reacts with the neighboring hydroxyl groups of alginate. In the FTIR spectrum of ALALD (Fig. 2), a new peak appeared at 1147 cm^{-1} (C–O–C), whereas the peaks at 879 and 818 cm^{-1} (C–O–C) weakened. The aldehyde shoulder at 1732 cm^{-1} was also found. Modifications were successful, although there are some things to be considered with regard to the reaction used. For example, periodate oxidation can lead to the loss of native backbone structure and a reduction in molecular weight, which might have an effect on the cells' ability to recognize HA molecule.

PVA was modified with hydrazide groups (PVAHY, DS% = 13). The ^{1}H-NMR spectrum (Fig. 2) showed new CH peaks of the polymer backbone and the CH_2 of the modified hydrazide unit around 4.90 ppm and 4 ppm to 3.72 ppm. In the FTIR spectrum (Fig. 2), the carbonyl C=O and C–O stretching signals (1710 and 1280 cm^{-1}) and the amine N–H deformation signals (1634 and 1520 cm^{-1}) of the modified unit were observed. There was also a C=O stretching signal in the spectrum of the unmodified PVA, but this was due to the acetate groups left over from the manufacturing process.

3.2. Formation of fast gelling hydrazone crosslinked hydrogels

When choosing a fabrication method for a scaffold comprising living cells, biocompatibility should be considered. For example, extreme temperatures, toxic components, free radicals and organic solvents should all be avoided, whereas mild reaction conditions such as water-based methods are preferable [33,34]. Injectable hydrogels can provide an alternative to physical implants due to their less invasive implantation process. An ideal implantation strategy would be to premix the cells with liquid gel precursors followed by injection and gelation *in situ*. To meet these requirements, hydrazone crosslinking was chosen as a fabrication method for our hydrogels.

Hydrazone crosslinked HA-PVA and AL-PVA hydrogels (Table 1) were prepared from modified polymer components by varying the DS% and the molecular weight of the HA component and the polymer concentration of the hydrogel. HP1 and HP2 hydrogels contain a high molecular weight HAALD component, whereas HP3 and HP4 hydrogels contain a low molecular weight HAALD component. Additionally, the polymer concentration of the HP1 hydrogel was decreased, while keeping the other parameters within the group the same. Due to a higher water content and a lower number of crosslinkable groups, the decrease in the concentration led to softer hydrogels and a less constant shape. The other hydrogels had a stronger gel structure with better shape constancy that was presumably due to a higher crosslinking ratio. HP3 and HP4 hydrogels looked more crystalline and fragile when compared to HP1 and HP2 hydrogels. A stickiness to different surfaces such as plastic or glass, and a clear and transparent appearance were common for all the HA-PVA hydrogels. The AP hydrogel had a slightly yellowish appearance, but otherwise was similar to the HP1 and HP2 hydrogels. The presented hydrogels were chosen based on a preliminary study (data not shown), where it was shown, for example, that HA-PVA and AL-PVA hydrogels containing PVAHY component with lower DS%, or ALALD component with higher DS% did not gelate well.

The gelation time of hydrogels (Table 1) was determined using a tube tilt test (gives only estimated results). Mild chemoselective reaction produced soft hydrazone crosslinked HA-PVA and AL-PVA hydrogels with a gelation time ranging from seconds to minutes. The gelation time depended on the polymer concentration and the properties of the gel components. The gelation time of the HP1-based hydrogels increased from seconds to minutes when polymer concentration was decreased. The gelation time of the AP hydrogel was around 30 s. The gelation time of these hydrogels should be long enough for the proper mixing and injection of the cell-polymer solutions, although, it should be noted that injecting a large amount of fast-gelling material has a potential to damage the surrounding tissue. Injecting smaller amounts of gel over a longer period of time could be one option.

The chemical structure of the hydrogels was determined using a FTIR. The FTIR spectra (Fig. 2) showed the disappearance of an aldehyde signal (HAALD: 1720, ALALD: 1732 cm^{-1}) and the appearance of a hydrazone C=N stretching signal at 1635 cm^{-1} for the HA-PVA hydrogels and 1636 cm^{-1} for AP hydrogel. The change in the amine/amide signal (PVAHY: 1634 cm^{-1}) is not easily detected because it overlaps with the hydrazone signal.

3.3. Structural homogeneity

In the ideal hydrogel, there exists a homogeneous distribution of crosslinks, but this is not the case in real hydrogels where spatial concentration fluctuations are common. This spatial gel inhomogeneity can negatively affect the hydrogel properties and functionality or cause uneven cell distribution if cells are involved. Commonly used methods to study the inhomogeneity are based on light scattering [35]. A simpler way to study the structural homogeneity is to determine the dry to wet ratios of the hydrogels. The dry to wet ratios of the hydrogels are presented in Fig. 3. The ratios were lower when the polymer concentration of the hydrogels was lowered. The HP1 hydrogel and the AP hydrogel showed the most linear (homogeneous) behavior between the slices. Hydrogels with higher DS% (higher crosslinking density) and a lower molecular weight and polymer concentration showed more

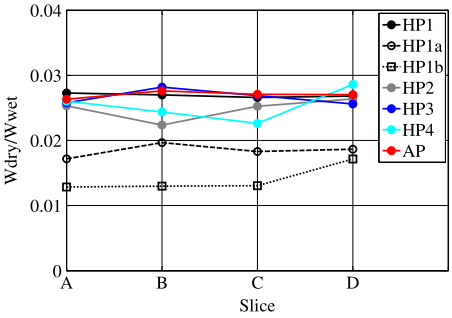

Fig. 3. Homogeneity of the hydrogels based on the calculated average values of dry to wet ratios (n = 3). Homogeneity is connected to the linearity of dry to wet ratios between different slices (A to D) of the same gel sample.

inhomogeneity. Based on the results, the inhomogeneity increased with the crosslinking density as was expected based on the literature [35]. This increase in inhomogeneity is caused by the simultaneous increase of the extent of network imperfections, which lead to regions with a different number of crosslinks.

3.4. Swelling and deswelling kinetics

The primary method for the estimation of hydrogel swelling rate is the quantifying of water content as a function of time. Therefore, swelling is not only a thermodynamic but also a kinetic process. The swelling ratio (SR, %) of hydrogels is generally determined by studying either the water uptake of dry hydrogels or the water uptake of wet hydrogels which are dried after the swelling. The drawback of the first method is that the drying process can be harmful to the hydrogel structure and cause distortions to the swelling results. Moreover, these methods do not describe how initially wet hydrogel behaves, for example, during the cell culture experiment. For these reasons, the swelling kinetics of the wet hydrogels in deionized water and cell culture medium (DMEM/F12) were studied without drying the samples at any stage of the measurement. The SRs of the hydrogels are collected in Fig. 4. Results showed that in cell culture medium some hydrogels started to shrink in the presence of divalent ions. The HP1 and HP3 hydrogels (DS% = 5 HAALD) slightly swelled in cell culture medium, whereas other hydrogels shrank. The lower the polymer concentrations of the hydrogel were, the more the hydrogels shrank. The SR was higher with hydrogels containing a lower molecular weight HAALD component when compared with similar gels containing a higher molecular weight HAALD component. The AP hydrogel shrank the most. Similar behavior was also observed during the cell culture experiments.

In deionized water, with no ions present, all the hydrogels swelled. The HA-PVA hydrogels containing a higher DS% HAALD component (higher crosslinking) swelled less compared with the HA-PVA hydrogel containing a lower DS% HAALD component. Moreover, a lower polymer concentration of the hydrogel led to a lower SR and to hydrogels that degraded faster during the experiment. Comparing hydrogels with similar polymer concentration and DS% of the HAALD component, hydrogels with the lower molecular weight HAALD component swelled less. The swelling ratio for the AP hydrogel in water could not be determined because it was not stable in water.

The swelling was shown to be dependent on the solvent and its ionic strength (Fig. 4). In cell culture medium, most hydrogels did not swell, but instead they shrank. This was expected because in the presence of salts hydrogel networks lose their hydrophilic-hydrophobic balance and shrink due to ex-osmosis. Counter ions (Na^+) condense around the fixed carboxylate ion charges of hyaluronan or alginate and cause a decrease in repulsive forces among the carboxylate groups. This leads to a decrease in swelling. The cell culture medium and body fluids also

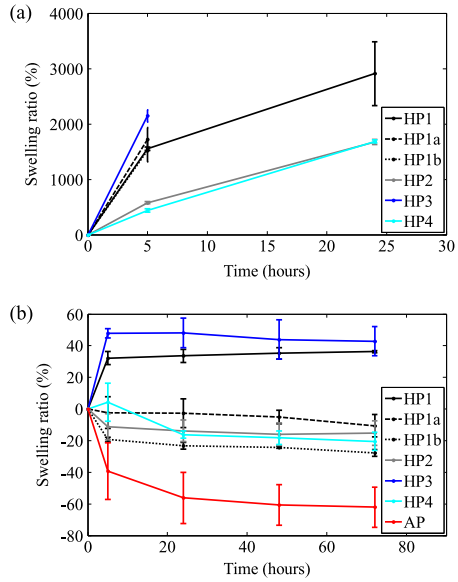

Fig. 4. Swelling ratios (SR,%) of the initially wet hydrogels in (a) deionized water and in (b) cell culture medium (DMEM/F12). AP hydrogel was not stable in water and degraded in a few hours. The mean (n = 3) and standard deviation bars are shown.

contain divalent cations. Therefore, it can be expected that when placed into such media or fluids, the AP hydrogel may also form ionic crosslinks leading to a more crosslinked structure and swelling will be reduced, as was also reported by Kuo and Ma [36]. The adsorption of water was many times that of cell culture medium. The degree to which the volume increases depends on the degree of crosslinking and the degree to which the polymer chains like to have solvent molecules around them. Due to the many hydrophilic groups of HA-PVA hydrogels, they swelled more in water. The more hydrophilic the structure, the stronger the polymer-water interaction becomes [37]. The swelling ratio will be lower when the degree of crosslinking is higher due to the tighter gel structure and less mobile polymer chains. This was seen with the HA-PVA hydrogels.

3.5. Enzymatically biodegradable hyaluronan-based hydrogels

In biological systems, hyaluronan is degraded by hyaluronidase (HAse) enzyme, which cleaves the β-1,4-glycosidic linkage. Hyaluronan itself is degraded sufficiently fast, whereas crosslinking makes it more resistant to degradation. Here, the enzymatic biodegradation of the HA-PVA hydrogels was determined using a higher amount of HAse (20–50 U/mL) than in physiological conditions, and the degradation was followed by monitoring the bulk mass loss. The degradation curves are shown in Fig. 5. It was notable that almost all the gels swelled first before any mass loss could be detected. The hydrogels were completely degraded in 21 to 25 h. Degradation was faster when the polymer concentration of the hydrogels decreased, and when both the molecular weight and DS% of the HAALD component were lower. Higher crosslinking density delayed the degradation. Overall, the results showed that HAse can recognize the crosslinked oxidized hyaluronan, which indicates that these hydrogels could also be degraded *in vivo*, as has also been shown in the literature [16,32,38-40]. Degradation products, rather than the polymer itself, may have a critical influence on the biocompatibility. Degradation products of HA, N-acetylglucosamine at the reducing terminus and glucuronic acid at the nonreducing end, are cleared from the body, but they have also been found to modulate

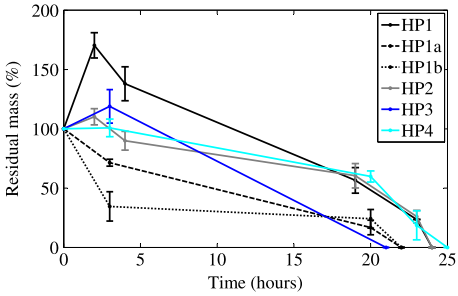

Fig. 5. Enzymatic degradation profiles of the HA-PVA hydrogels in HAse enzyme (20–50 U/mL). The mean (n = 3) and standard deviation bars are shown.

wound healing [41]. Here, only the degradation of HA-PVA hydrogels was studied. Alginate is inherently non-degradable in mammals because they lack the enzyme (*i.e.*, alginase) that can cleave the polymer chains. However, it is said that alginate can be made degradable in physiological conditions by partial oxidation [42], which was also used in our study.

3.6. Brain mimicking mechanical properties of hydrogels

Stiffness is a constant over the range of strain for many materials. Such materials are called linear. For tissues and hydrogels, the stress-strain curve is non-linear in the elastic portion, even at small strains. Therefore, a polynomial fit was used for the data and the stiffness of materials was determined similar to Karvinen et al. [23]. Moreover, instead of giving only the second-order elastic constants for the materials, the stiffness as a function of strain was shown in order to represent the material behavior in a wider strain range. The representative compressive stress as a function of the deformation strain curves, and the stiffness as a function of the strain curves of the HA-PVA and AL-PVA hydrogels and midbrain tissue are shown in Fig. 6.

The deformation of the hydrogel depends on the structure of the hydrogel. The shape of the stress-strain curves (Fig. 6 (a)) showed that when the stress was increased, the polymer chains in the structure reorientate at the beginning before the hydrogels start to resist the applied force. All the hydrogels were initially resistant to deformation and became progressively stiffer when the load was increased leading finally to the fracture of the hydrogels. The HP2 and AP hydrogels had the lowest fracture strains (50% to 57%) compared with the others (over 60%). The stress-strain curves of the hydrogels behaved similarly to midbrain tissue at lower strains, but at higher strains the curve of the midbrain tissue became steeper showing no clear fracture. In addition, it was noted that at lower strain values, HP4 hydrogel was stiffer than midbrain tissue, but at higher strains (over 20% strain) the opposite was the case. This would mean that for midbrain tissue a greater force is required to fracture it. Altogether, the stress-strain curves of the brain tissue and the hydrogels were in the same range at lower strains and showed similar elastic behavior, whereas at higher strains in the fracture area the difference was clearer.

Stiffness was also plotted as a function of strain. The stiffness-strain curves (Fig. 6 (b)) showed that the hydrogels were initially resistant to deformation, but became progressively stiffer with increasing strain (also known as strain hardening [43]) indicating a non-linear deformation characteristic of hydrogels under compression. At certain strain the stiffness started to decrease, which indicated some irreversible changes in the hydrogel structure. When the drop happens sooner, it indicates that the material can withstand less deformation before the final fracture caused by a permanent deformation. Hydrogels with higher fracture strain are considered to be more elastic. The stiffness-strain curves showed that the stiffness was strain dependent and quite

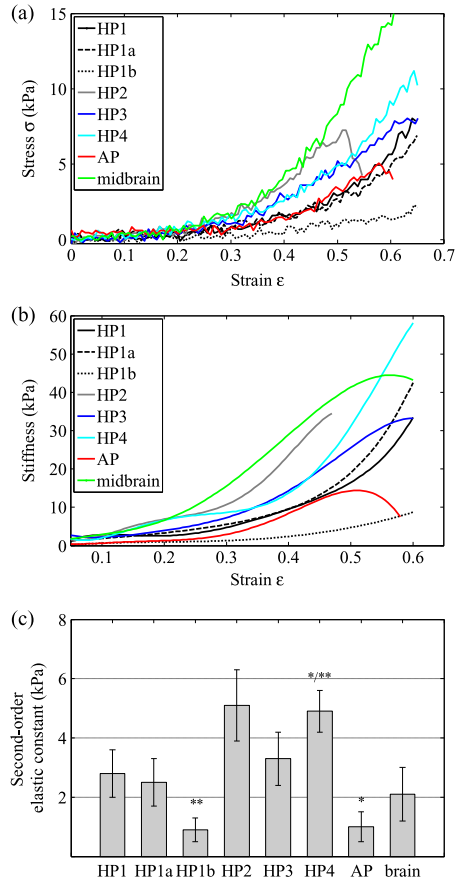

Fig. 6. (a) Stress as a function of strain (representative), and (b) stiffness as a function of strain curves (average), and (c) second-order elastic constants of HA-PVA and AL-PVA hydrogels and rabbit midbrain tissue. The mean (n = 3 to 5) and standard deviation bars are shown. *p < 0.05 HP4 with respect to HP1a, HP3, AP and brain, and AP with respect to HP1, HP2, HP3 and HP4. **p < 0.01 HP1b with respect to HP1, HP1a, HP2, HP3 and HP4, and HP4 with respect to HP1 and HP1b.

constant at around 20% strain with all the hydrogels. After that, the stiffness increased more or less depending on the sample and at a specific point started to drop. This drop occurred sooner for the HP2 and AP hydrogels when compared with the others. The stiffness decreased when the polymer concentration of the hydrogel decreased. At low strain values, hydrogels containing a low molecular weight HAALD component or a higher DS% had higher stiffness. In addition, the stiffness of the AP hydrogel was similar to the lowest HP1b hydrogel. At lower strain values, the stiffness of the HP1 hydrogel was the most similar to midbrain tissue.

The second-order elastic constants for the hydrogels and midbrain tissue are presented in Fig. 6 (c). The HP1b hydrogel showed a statistically significant difference $p < 0.01$ with respect to the HP1, HP1a, HP2, HP3 and HP4 hydrogels. The HP4 hydrogel showed significant difference $p < 0.05$ with respect to the HP1a, HP3 and AP hydrogels and midbrain, and $p < 0.01$ with respect to the HP1 and HP1b hydrogels. Whereas, the AP hydrogel showed significant difference $p < 0.05$ with respect to the HP1, HP2, HP3 and HP4 hydrogels. No statistically significant differences were detected between other materials. Overall, the second-order elastic constants of hydrogels were relatively low (0.9 kPa to 5.1 kPa) and similar to midbrain tissue, which

could indicate their suitability for neural application. In particular, the HP1 hydrogel showed the most similar elastic behavior (and second-order elastic constant) compared with midbrain tissue at lower strains. The second-order elastic constant of brain tissue was in the same range as reported in previous studies [10,44]. This was true, even though the same data of brain tissue had been previously analyzed by Koivisto et al. [22] showing that the constant, or as they call it, the compressive modulus was slightly higher, and thus deviated from the literature.

In this study, the bulk properties of hydrogels were tested. In biological tissues, there are local regions with variable stiffness due to the composite character and ongoing remodeling of the ECM [45,46]. Because cells respond to these spatial variations, the local mechanical properties should be crucial for hydrogel design and should also be measured, for example, with atomic-force microscopy (AFM) [46]. The drawback of this method is that it only measures the surface of the material (2D), but does not really tell anything about the 3D environment.

3.7. High molecular weight HA-PVA hydrogels and AL-PVA hydrogels supported human neuronal cells

Hydrogel compositions were first tested as a growth surface for the cells. The human neuronal cells were cultured on top of the hydrogel surfaces and analyzed after two weeks of culturing. All tested hydrogel compositions supported cell growth and no cytotoxicity was observed (data not shown). The best compositions were the HA-PVA hydrogels containing a high molecular weight HAALD component (HP1, HP2) as well as the AP hydrogel. These both supported cell growth and neurite outgrowth along the hydrogel surface (Fig. 7 (a), (c), (e)), whereas the HP3 and HP4 hydrogels containing a low molecular weight HAALD component were less-supportive (Fig. 7 (b), (d)). The molecular weight of HA is known to alter cell behavior, such as adhesion and growth, in many cell types and tissues reviewed by Cyphert et al. [47]. Especially in neural tissue, the high molecular weight HA is linked to decreasing glial scar formation [48]. Neurite outgrowth from cell aggregates was the highest in the HP1 hydrogel. The increase of the DS% of the HAALD component in HA-PVA hydrogels had a negative effect on neurite outgrowth when the HP1 and HP2 hydrogels were compared (Fig. 7 (f)). The effect of increasing the DS% was not as dramatic on the cells as the change in molecular weight. This might be due to the mechanisms of HA recognition in the cell membrane [47]. The most prominent compositions, HP1 and AL, had the lowest stiffness of all the tested hydrogels. Overall, material stiffness (mechanical environment) is known to affect neural cell viability and behavior by directing neural cell lineage, proliferation and growth [4,46]. Moreover, cultured cells have been shown to better retain their functional phenotype when cultured on material with a similar stiffness to native ECM [49]. Our findings are in line with previously published studies that suggest softer materials are more favored by the neural cells [4,50].

3.8. Human neuronal cells preferred low stiffness hydrogels

The best hydrogel compositions, HP1 and AP, were selected for further 3D culturing experiments. Here, the cells were cultured encapsulated in the hydrogel. First, the viability of neuronal cells inside the HP1 and AP hydrogels was analyzed after two weeks in culture. The cell viability in 3D was at a similar level as viability in 2D control cultures on top of laminin (Fig. 8 (a–c)). This indicates that the hydrogel was well tolerated as a culturing environment. Next, the effect of the decreased polymer concentration of the HP1 hydrogel was studied in order to see how the cells behaved in even softer hydrogels. Neuronal cells were cultured for two weeks encapsulated inside the four soft hydrogel compositions (HP1, HP1a, HP1b and AP). Cell growth was seen inside all the studied compositions and the cells were positive for the neuronal markers MAP-2 and B-tubulin III (Fig. 8 (d–g)). The stiffness of the material has been previously reported to be related to cell type: neurons prefer lower compressive modulus (0.1 kPa to 1 kPa), whereas astrocytes and oligodendrocytes prefer slightly higher (0.5 kPa to 10 kPa) [4]. In our studies with human neuronal cells, the cultures contained a high number of neurons even though the mechanical properties of the hydrogels used in this study are reported to favor a mixed population of neurons and glial cells or rather glial fate [4]. One explanation for the different result might be in the different hydrogels used in the studies. Slight differences were seen in the cell growth, for example, in the HP1 and HP1a hydrogels more cells stayed in clusters (Fig. 8 (d), (e)), whereas inside the softest HP1b and AP hydrogels the cell outgrowth from the aggregates into the hydrogel was more robust (Fig. 8 (f), (g)). From our results with HA-based hydrogels, we can conclude that lowering the polymer concentration of the hydrogel had a positive effect on neuronal growth. Lower concentration hydrogels were softer and had a lower crosslinking density leaving more space inside the hydrogel. Nevertheless, it is not known how these changes caused the positive effect on cell growth.

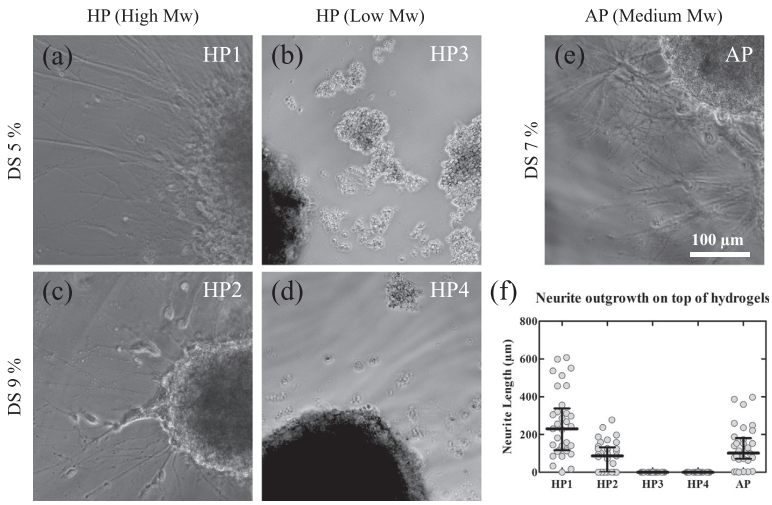

Fig. 7. Representative images of neural cells growing on top of hydrogel surfaces: the high molecular weight HA hydrogels (a) HP1 and (b) HP2, the low molecular weight HA hydrogels (c) HP3 and (d) HP4 and (e) the alginate hydrogel AP. (f) Neurite outgrowth measured from cultures on top of the hydrogels. Median with inter-quartile range of the measured neurites is shown as line and whiskers whereas individual values are presented as grey dots. The scale bar in all images is 100 µm.

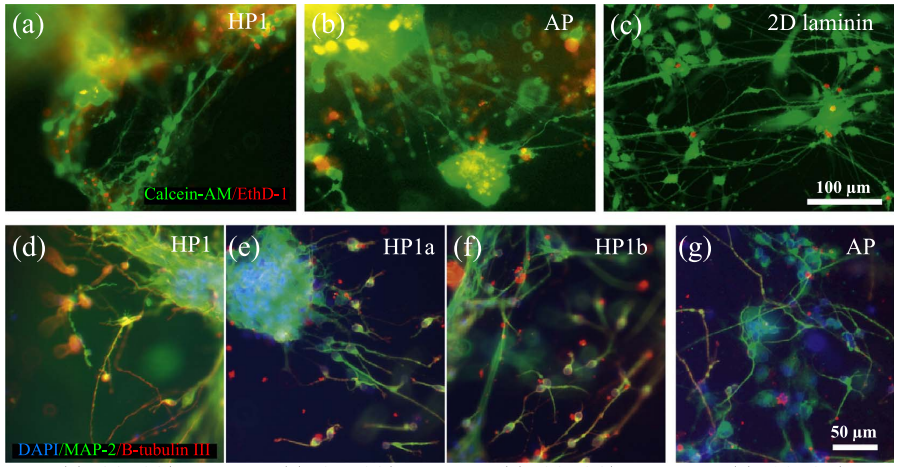

Fig. 8. Live/dead labeling of the neurons cultured two weeks inside HP1 (a) and AP (b) hydrogels, and on top of laminin coated plastic (c). Living cells are labeled with Calcein-AM (green) and dead cells with EthD-1 (red). Neurons grown for two weeks encapsulated inside the HP1 (d), HP1a (e), HP1b (f) and AP (g) hydrogels labeled with neuron specific immunocytochemical markers MAP-2 (green) and B-tubulin III (red), co-labeled with nuclear marker DAPI (blue). The second-order elastic constants of each hydrogel are shown under the images. The scale bars in images (a–c) is 100 µm and in (d–g) is 50 µm. (For interpretation of the references to color in this figure legend, the reader is referred to the web version of this article.)

4. Conclusions

In summary, injectable hydrazone crosslinked HA-PVA and AL-PVA hydrogels were produced and their detailed properties were investigated. To the best of our knowledge, the polymerization and properties of hydrazone crosslinked AL-PVA hydrogel are reported for the first time. The degree of substitution and molecular weight of the polymer components as well as the polymer concentration of the hydrogel were shown to affect to the swelling, degradation and mechanical properties of the hydrogels. Furthermore, the suitability of these hydrogels to be used as a supportive biomaterial for 3D neuronal cell culture was studied. The effect of the above parameters on the growth of human pluripotent stem cell-derived neuronal cells was studied. The most supportive HA-PVA and AL-PVA hydrogels for neural cells had brain-mimicking mechanical properties and were composed of a high molecular weight HA component. It was also shown that lowering the polymer concentration of hydrogel enhanced the neuronal growth. In this study, it was shown that neuronal spreading and 3D neural network formation were enhanced inside the softest hydrogels.

Acknowledgments

This work was funded by TEKES (the Finnish Funding Agency for Innovation) Human Spare Parts project, the Finnish Cultural Foundation grant numbers 00140325 and 00150312, and by the Academy of Finland grant number 286990. The authors would like to thank Ph.D. Mari Hämäläinen (University of Tampere Medical School) for providing the rabbit tissue samples. The authors would also like to thank Ph.D. Alexandre Efimov and Laboratory Attendant Anne-Maarit Tikkanen (Faculty of Natural Sciences, Laboratory of Chemistry and Bioengineering, Tampere University of Technology, Tampere, Finland) for their help related to the NMR- and FTIR-measurements.

Appendix A. Supplementary data

Supplementary data to this article can be found online at https://doi.org/10.1016/j.reactfunctpolym.2017.12.019.

References

[1] X. Wang, J. He, Y. Wang, F.-Z. Cui, Hyaluronic acid-based scaffold for central neural tissue engineering, Interface Focus (2012) rsfs20120016.
[2] A.R. Murphy, A. Laslett, C.M. O'Brien, N.R. Cameron, Scaffolds for 3D in vitro culture of neural lineage cells, Acta Biomater. 54 (2017) 1–20.
[3] C. Cha, S.Y. Kim, L. Cao, H. Kong, Decoupled control of stiffness and permeability with a cell-encapsulating poly (ethylene glycol) dimethacrylate hydrogel, Biomaterials 31 (18) (2010) 4864–4871.
[4] E.R. Aurand, K.J. Lampe, K.B. Bjugstad, Defining and designing polymers and hydrogels for neural tissue engineering, Neurosci. Res. 72 (3) (2012) 199–213.
[5] D.R. Nisbet, K.E. Crompton, M.K. Horne, D.I. Finkelstein, J.S. Forsythe, Neural tissue engineering of the CNS using hydrogels, J. Biomed. Mater. Res. B Appl. Biomater. 87 (1) (2008) 251–263.
[6] S. Wu, R. Xu, B. Duan, P. Jiang, Three-dimensional hyaluronic acid hydrogel-based models for in vitro human iPSC-derived NPC culture and differentiation, J. Mater. Chem. B 5 (2017) 3870–3878.
[7] M.M. Adil, T. Vazin, B. Ananthanarayanan, G.M. Rodrigues, A.T. Rao, R.U. Kulkarni, E.W. Miller, S. Kumar, D.V. Schaffer, Engineered hydrogels increase the post-transplantation survival of encapsulated hESC-derived midbrain dopaminergic neurons, Biomaterials 136 (2017) 1–11.
[8] Z. Wei, J. Zhao, Y.M. Chen, P. Zhang, Q. Zhang, Self-healing polysaccharide-based hydrogels as injectable carriers for neural stem cells, Sci. Rep. 6 (2016) 37841.
[9] G. Palazzolo, N. Broguiere, O. Cenciarelli, H. Dermutz, M. Zenobi-Wong, Ultrasoft alginate hydrogels support long-term three-dimensional functional neuronal networks, Tissue Eng. A 21 (15-16) (2015) 2177–2185.
[10] S.K. Seidlits, Z.Z. Khaing, R.R. Petersen, J.D. Nickels, J.E. Vanscoy, J.B. Shear, C.E. Schmidt, The effects of hyaluronic acid hydrogels with tunable mechanical properties on neural progenitor cell differentiation, Biomaterials 31 (14) (2010) 3930–3940.
[11] A.D. Augst, H.J. Kong, D.J. Mooney, Alginate hydrogels as biomaterials, Macromol. Biosci. 6 (8) (2006) 623–633.
[12] D.A. Ossipov, K. Brännvall, K. Forsberg-Nilsson, J. Hilborn, Formation of the first injectable poly (vinyl alcohol) hydrogel by mixing of functional PVA precursors, J. Appl. Polym. Sci. 106 (1) (2007) 60–70.
[13] R.H. Schmedlen, K.S. Masters, J.L. West, Photocrosslinkable polyvinyl alcohol hydrogels that can be modified with cell adhesion peptides for use in tissue engineering, Biomaterials 23 (22) (2002) 4325–4332.
[14] J.M. Ino, P. Chevallier, D. Letourneur, D. Mantovani, C. Le Visage, Plasma functionalization of poly (vinyl alcohol) hydrogel for cell adhesion enhancement, Biomatter 3 (4) (2013) e25414.
[15] Y. Jiang, J. Chen, C. Deng, E.J. Suuronen, Z. Zhong, Click hydrogels, microgels and nanogels: emerging platforms for drug delivery and tissue engineering, Biomaterials 35 (18) (2014) 4969–4985.
[16] D.A. Ossipov, S. Piskounova, J. Hilborn, Poly (vinyl alcohol) cross-linkers for in vivo injectable hydrogels, Macromolecules 41 (11) (2008) 3971–3982.
[17] C. Aulin, K. Bergman, M. Jensen-Waern, P. Hedenqvist, J. Hilborn, T. Engstrand, In situ cross-linkable hyaluronan hydrogel enhances chondrogenesis, J. Tissue Eng. Regen. Med. 5 (8) (2011) e188–e196.
[18] X. Jia, Y. Yeo, R.J. Clifton, T. Jiao, D.S. Kohane, J.B. Kobler, S.M. Zeitels, R. Langer,

Hyaluronic acid-based microgels and microgel networks for vocal fold regeneration, Biomacromolecules 7 (12) (2006) 3336–3344.
[19] K.H. Bouhadir, D.S. Hausman, D.J. Mooney, Synthesis of cross-linked poly (aldehyde guluronate) hydrogels, Polymer 40 (12) (1999) 3575–3584.
[20] ASTM Standard F2900:2011, Standard Guide for Characterization of Hydrogels Used in Regenerative Medicine, ASTM International, West Conshohocken, PA, USA, 2011.
[21] C.K. Kuo, P.X. Ma, Ionically crosslinked alginate hydrogels as scaffolds for tissue engineering: part 1. Structure, gelation rate and mechanical properties, Biomaterials 22 (6) (2001) 511–521.
[22] J. Koivisto, T. Joki, J. Parraga, R. Pääkkönen, L. Ylä-Outinen, L. Salonen, I. Jonkkari, M. Peltola, T. Ihalainen, S. Narkilahti, et al., Bioamine-crosslinked gellan gum hydrogel for neural tissue engineering, Biomed. Mater. 12 (2) (2017) 025014.
[23] J. Karvinen, J.T. Koivisto, I. Jönkkäri, M. Kellomäki, The production of injectable hydrazone crosslinked gellan gum-hyaluronan-hydrogels with tunable mechanical and physical properties, J. Mech. Behav. Biomed. Mater. 71 (2017) 383–391.
[24] K. Brugger, Thermodynamic definition of higher order elastic coefficients, Phys. Rev. 133 (6A) (1964) A1611.
[25] J.F. Nye, Physical Properties of Crystals: Their Representation by Tensors and Matrices, Oxford university press, 1985.
[26] W.D. Callister, D.G. Rethwisch, Materials Science and Engineering: An Introduction, vol. 7, Wiley New York, 2007.
[27] M. Ojala, C. Prajapati, R.-P. Pölönen, K. Rajala, M. Pekkanen-Mattila, J. Rasku, K. Larsson, K. Aalto-Setälä, Mutation-specific phenotypes in hiPSC-derived cardiomyocytes carrying either myosin-binding protein C or α-Tropomyosin mutation for hypertrophic cardiomyopathy, Stem Cells Int. 2016 (ID 1684792) (2016) 1–16.
[28] K. Rajala, H. Hakala, S. Panula, S. Aivio, H. Pihlajamäki, R. Suuronen, O. Hovatta, H. Skottman, Testing of nine different xeno-free culture media for human embryonic stem cell cultures, Hum. Reprod. 22 (5) (2007) 1231–1238.
[29] S. Toivonen, M. Ojala, A. Hyysalo, T. Ilmarinen, K. Rajala, M. Pekkanen-Mattila, R. Äänismaa, K. Lundin, J. Palgi, J. Weltner, et al., Comparative analysis of targeted differentiation of human induced pluripotent stem cells (hiPSCs) and human embryonic stem cells reveals variability associated with incomplete transgene silencing in retrovirally derived hiPSC lines, Stem Cells Transl. Med. 2 (2) (2013) 83–93.
[30] R.S. Lappalainen, M. Salomäki, L. Ylä-Outinen, T.J. Heikkilä, J.A. Hyttinen, H. Pihlajamäki, R. Suuronen, H. Skottman, S. Narkilahti, Similarly derived and cultured hESC lines show variation in their developmental potential towards neuronal cells in long-term culture, Regen. Med. 5 (5) (2010) 749–762.
[31] L. Ylä-Outinen, T. Joki, M. Varjola, H. Skottman, S. Narkilahti, Three-dimensional growth matrix for human embryonic stem cell-derived neuronal cells, J. Tissue Eng. Regen. Med. 8 (3) (2014) 186–194.
[32] D.A. Ossipov, S. Piskounova, O.P. Varghese, J. Hilborn, Functionalization of hyaluronic acid with chemoselective groups via a disulfide-based protection strategy for in situ formation of mechanically stable hydrogels, Biomacromolecules 11 (9) (2010) 2247–2254.
[33] H.-W. Chien, W.-B. Tsai, S. Jiang, Direct cell encapsulation in biodegradable and functionalizable carboxybetaine hydrogels, Biomaterials 33 (23) (2012) 5706–5712.
[34] M.C. LaPlaca, V.N. Vernekar, J.T. Shoemaker, D.K. Cullen, Three-dimensional neuronal cultures, Methods in bioengineering: 3D tissue engineering, Artech House, Norwood, MA, 2010, pp. 187–204.
[35] G. Gerlach, K.-F. Arndt, Hydrogel Sensors and Actuators: Engineering and Technology, vol. 6, Springer Science & Business Media, 2009.
[36] C.K. Kuo, P.X. Ma, Maintaining dimensions and mechanical properties of ionically crosslinked alginate hydrogel scaffolds in vitro, J. Biomed. Mater. Res. A 84 (4) (2008) 899–907.
[37] N.A. Peppas, R.M. Ottenbrite, K. Park, T. Okano, Biomedical Applications of Hydrogels Handbook, Springer Science & Business Media, 2010.
[38] M. Patenaude, T. Hoare, Injectable, mixed natural-synthetic polymer hydrogels with modular properties, Biomacromolecules 13 (2) (2012) 369–378.
[39] J. Kim, I.S. Kim, T.H. Cho, K.B. Lee, S.J. Hwang, G. Tae, I. Noh, S.H. Lee, Y. Park, K. Sun, Bone regeneration using hyaluronic acid-based hydrogel with bone morphogenic protein-2 and human mesenchymal stem cells, Biomaterials 28 (10) (2007) 1830–1837.
[40] R. Stern, G. Kogan, M.J. Jedrzejas, L. Šoltés, The many ways to cleave hyaluronan, Biotechnol. Adv. 25 (6) (2007) 537–557.
[41] A. Fakhari, C. Berkland, Applications and emerging trends of hyaluronic acid in tissue engineering, as a dermal filler and in osteoarthritis treatment, Acta Biomater. 9 (7) (2013) 7081–7092.
[42] K.Y. Lee, D.J. Mooney, Alginate: properties and biomedical applications, Prog. Polym. Sci. 37 (1) (2012) 106–126.
[43] G. Lamouche, B.F. Kennedy, K.M. Kennedy, C.-E. Bisaillon, A. Curatolo, G. Campbell, V. Pazos, D.D. Sampson, Review of tissue simulating phantoms with controllable optical, mechanical and structural properties for use in optical coherence tomography, Biomed. Opt. Express 3 (6) (2012) 1381–1398.
[44] K.J. Lampe, R.G. Mooney, K.B. Bjugstad, M.J. Mahoney, Effect of macromer weight percent on neural cell growth in 2D and 3D nondegradable PEG hydrogel culture, J. Biomed. Mater. Res. A 94 (4) (2010) 1162–1171.
[45] J.Y. Wong, J.B. Leach, X.Q. Brown, Balance of chemistry, topography, and mechanics at the cell-biomaterial interface: issues and challenges for assessing the role of substrate mechanics on cell response, Sur. Sci. 570 (1) (2004) 119–133.
[46] F. Brandl, F. Sommer, A. Goepferich, Rational design of hydrogels for tissue engineering: impact of physical factors on cell behavior, Biomaterials 28 (2) (2007) 134–146.
[47] J.M. Cyphert, C.S. Trempus, S. Garantziotis, Size matters: molecular weight specificity of hyaluronan effects in cell biology, Int. J. Cell Biol. 2015 (2015) 1–8.
[48] S. Hou, Q. Xu, W. Tian, F. Cui, Q. Cai, J. Ma, I.-S. Lee, The repair of brain lesion by implantation of hyaluronic acid hydrogels modified with laminin, J. Neurosci. Methods 148 (1) (2005) 60–70.
[49] W.L.K. Chen, C.A. Simmons, Lessons from (patho) physiological tissue stiffness and their implications for drug screening, drug delivery and regenerative medicine, Adv. Drug Deliv. Rev. 63 (4) (2011) 269–276.
[50] L.A. Flanagan, Y.-E. Ju, B. Marg, M. Osterfield, P.A. Janmey, Neurite branching on deformable substrates, Neuroreport 13 (18) (2002) 2411.

APPENDIX A. Supplementary material

Soft hydrazone crosslinked hyaluronan- and alginate-based hydrogels as 3D supportive matrices for human pluripotent stem cell-derived neuronal cells

Jennika Karvinen[1, *], Tiina Joki[2], Laura Ylä-Outinen[2], Janne T. Koivisto[1,2], Susanna Narkilahti[2], Minna Kellomäki[1,2]

[1]BioMediTech Institute and Faculty of Biomedical Sciences and Engineering, Tampere University of Technology, Korkeakoulunkatu 3, FI-33101 Tampere, Finland

[2]BioMediTech Institute and Faculty of Medicine and Life Sciences, University of Tampere, Lääkärinkatu 1, FI-33520 Tampere, Finland

[*] Corresponding author: E-mail: Jennika.karvinen@tut.fi, Tel.: +358 408490988

Table S1. Oxidation of hyaluronan and alginate. At the end of the component names, H denotes high M_w and L denotes low M_w.

Component	Mw (Da)	Sodium periodate (g)	Reaction time (hours)
HAALD1H	1.5-1.8 x 10^6	0.26	2
HAALD1L	1.5 x 10^5	0.30	4
HAALD2H	1.5-1.8 x 10^6	0.26	2
HAALD2L	1.5 x 10^5	0.30	4
ALALD	-	0.30	3

Unpublished manuscript IV

Karvinen J., Ihalainen T., Calejo T., Jönkkäri I., Kellomäki M.

"Characterization of the microstructure of hydrazone crosslinked polysaccharide-based hydrogels through rheological and diffusion studies"

submitted on 22.01.2018.

Tampereen teknillinen yliopisto
PL 527
33101 Tampere

Tampere University of Technology
P.O.B. 527
FI-33101 Tampere, Finland

ISBN 978-952-15-4208-4
ISSN 1459-2045